THE UNIVERSITY *of* EDINBURGH

Performance Analysis of Relay-Aided Wireless Communication Systems

Yunhan Zhang

A thesis submitted for the degree of Doctor of Philosophy.
The University of Edinburgh.
2018

Abstract

Relay-aided networks have been proved to be cost-efficient solutions for wireless communications in respect of high data rates, enhanced spectrum efficiency and improved signal coverage. In the past decade, relaying techniques have been written into standards of modern wireless communications and significantly improve the quality of service (QoS) in wireless communications.

In order to satisfy exponentially increased demands for data rates and wireless connectivities, various novel techniques for wireless communications have been proposed in recent years, which have brought significant challenges for the performance analysis of relaying networks. For the purpose of more practical investigations into relaying systems, researchers should not only analyse the relays employing novel techniques but also attach more importance to complex environments of wireless communications. With these objectives in mind, in this thesis, in-depth investigations into system performance for relay-assisted wireless communications are detailed.

Firstly, the theoretic reliability of dual-hop amplify-and-forward (AF) systems over generalised η-μ and κ-μ fading channels are investigated using Gallager's error exponents. These two versatile channel models can encompass a number of popular fading channels such as Rayleigh, Rician, Nakagami-m, Hoyt and one-sided Gaussian fading channels. We derive new analytical expressions for the probability distribution function (pdf) of the end-to-end signal-to-noise-ratio (SNR) of the system. These analytical expressions are then applied to analyse the system performance through the study of Gallager's exponents, which are classical tight bounds of error exponents and present the trade-off between the practical information rate and the reliability of communication. Two types of Gallager's exponents, namely the random coding error exponent (RCEE) and the expurgated error exponent, are studied. Based on the newly derived analytical expressions, we provide an efficient method to compute the required codeword length to achieve a predefined upper bound of error probability. In addition, the analytical expressions are derived for the cut-off rate and ergodic capacity of the system. Moreover, simplified expressions are presented at the high SNR regime.

Secondly, the performance of a dual-hop amplify-and-forward (AF) multi-antenna relaying system over complex Gaussian channels is investigated. Three classical receiving strategies, i.e. the maximal-ratio combining (MRC), zero-forcing (ZF) and minimum mean square error (MMSE) are employed in the relay to mitigate the impact of co-channel interference (CCI), which follows the Poisson point process (PPP). We derive the exact analytical expressions of the capacities for this system in the infinite-area interference environment and the asymptotic analytical expressions for the lower bounds of capacities in the limited-area interference scenario. By computing the numerical results and the Monte Carlo simulation, we can observe the effect of relay processing schemes under different interference regimes.

In the end, the non-orthogonal multiple access (NOMA) technique is introduced to relaying systems, which exploits multiplexing in the power domain. Order statistics are applied in this

part to analyse the performances of ordered users. The randomness of both channel fading and path loss are taken into consideration. In addition to the exact analytical expressions, asymptotic expressions at high-SNR regimes are provided, which clearly show the effects of NOMA techniques using at relaying systems.

Lay summary

The next generation of wireless communication networks is supposed to provide extremely high data rates, massive connectivity and low power consumption. To meet these requirements, relay-aided wireless communication system has been proposed as a cost-efficient technique to enhance spectrum efficiency, improve data rates and optimize coverages. Therefore, the relaying network is considered as a competitive candidate for the future wireless communication. The fast development of techniques and complexity of electromagnetic environment result in great challenges of investigating relay-aided systems. To address these challenges, multiple relaying communication systems will be investigated in this thesis.

By investigating the relaying systems with generalized fading channel, the performance of random coding and expurgated error exponents will be analysed in Chapter 3. This investigation represents the balance between reliability and complexity for wireless communications with complicated scattering environments. Multiple popular channel models are considered, such as Rayleigh, Rician, Nakagami-m, Hoyt and one-sided Gaussian fading channels.

As a key limitation of system performance, co-channel interferences are drawing more and more attentions in wireless communications, because of the application of heterogeneous networks. The performance on ergodic capacity for a dual-hop relaying system with co-channel interference (CCI) is analysed in Chapter 4. Three different receiving strategies are implemented at relay to mitigate the effect of CCI. The interferers are modelled by using stochastic geometry.

In the fifth Chapter, the non-orthogonal multiple access (NOMA) technique is applied to the relay aided system, which exploits multiplexing in the power domain. The performance is studied by using the order, while the randomness of the system is also considered. In addition to the exact analytical expressions, asymptotic approximations are provided at high-SNR regimes, which clearly show the advantages of using NOMA at relaying systems.

Declaration of Originality

1. I declare that this thesis has been composed solely by myself and that it has not been submitted, in whole or in part, in any previous application for a degree. Except where states otherwise by reference or acknowledgment, the work presented is entirely my own.

2. I confirm that this thesis presented for the degree of PhD, has
   i been composed entirely by myself
   ii been solely the result of my own work
   iii not been submitted for any other degree or professional qualification

3. I declare that this thesis was composed by myself, that the work contained herein is my own except where explicitly stated otherwise in the text, and that this work has not been submitted for any other degree or processional qualification except as specified. Parts of this work have been published in

   1. Jiang Xue, Yunhan Zhang, et al. "Error exponents analysis for dual-hop η-μ fading channel with amplify-and-forward relaying." *IEEE. Wireless Communications and Networking Conference (WCNC)*, 2014.
   2. Yunhan Zhang, et al. "Error exponents analysis of dual-hop η-μ and κ-μ fading channel with amplify-and-forward relaying." *IET Communications* vol. 9, iss. 11, pp. 1367-1379, Jul. 2015.
   3. Yunhan Zhang, et al. "Capacity Analysis for Multi-Antenna Dual-Hop AF System with Random Co-channel Interference Using Different Transferring Schemes" *IET Communications* vol. 11, Mar. 2017.

   .

Yunhan Zhang

Acknowledgements

My deepest gratitude goes first and foremost to my supervisors Professor John Thompson, for their constant encouragement and guidance. Although he became my supervisor just after I submitted the draft of my thesis, I have received a lot of help through all stages of correcting this thesis. Without working with him in the past 9 months, I cannot become a certificated phD graduate.

I would like to express my heartfelt gratitude to Dr. Jiang Xue, who led me into the world of research, with his extraordinary patience and consistent encouragement. He gave me great help by providing me with necessary materials, advice of great value and inspiration for new ideas. It was his suggestions that drew my attention to a number of deficiencies and made many problems clearer. Gratitude also belongs to my colleagues, Huasen He, Yibo He, Lin Zhou and others, who shared their valuable technical experience with me.

I am also greatly indebted to the professors and teachers at the Institute for Digital Communications at the University of Edinburgh, who have instructed and helped me a lot in the past four years.

Last, my thanks go to my beloved family for their loving consideration and great confidence in me throughout these years. I also owe my sincere gratitude to my friends and fellow classmates who gave their help and time in listening to me and helping me to work out my problems during the difficult course of the thesis.

Contents

List of figures

List of tables

Acronyms and abbreviations

TLA Three letter acronym

4G fourth generation

QoS quality of service

AF amplify and forward

SNR signal to noise ration

PDF probability distribution function

RCEE random coding error exponent

MRC maximum ratio combination

ZF zero forcing

MMSE minimum mean square error

CCI co-channel interference

PPP Poisson point process

LTE long -term evolution

MAC media access control

WiMAX worldwide interoperability for microwave access

3GPP third -generation partnership project

CLT central limitation theory

UE user element

OFDM orthogonal frequency division multiplexing

MIMO multi-input and multi-output

SIC successive interference cancellation

SINR signal to interference plus noise ratio

OMA orthogonal multiple access

NOMA non-orthogonal multiple access

CSI channel state information

SDM space division multiplexing

FDM frequency division multiplexing

TDM time division multiplexing

CDM code division multiplexing

PSK phase shifting keying

FSK frequency shifting keying

ASK amplitude shifting keying

QAM quadrature amplitude modulation

MA multiple access

FDMA frequency division multiple access

OFDMA orthogonal frequency division multiple access

SISO single-input and single-output

AWGN added white Gaussian noise

i.i.d. independently and identically distributed

LOS line of sight

NLOS none line of sight

FD full duplex

HD half duplex

DH dual hop

SC superposition coding

Nomenclature

$\in$	Belongs to.
$\sim$	Follows certain distribution.
$\simeq$	Similar to.
$\triangleq$	Defined as.
$\mathbb{E}\{\cdot\}$	Expectation.
$\mathcal{A}$	A set notation.
$\mathcal{A}^c$	A complement set of set $\mathcal{A}$.
$\mathbf{h}$	A vector.
$\mathbf{H}$	A matrix.
$\mathbf{H}$	Inverse of matrix $\mathbf{H}$.
$\mathbf{H}^\dagger$	Conjugate transpose of matrix $\mathbf{H}$.
$\mathbf{H}_{i,j}$	(i,j)-th element of matrix $\mathbf{H}$.
$\mathbf{I}_n$	n $\times$ n Identity matrix.
$Re(a)$	Real part of complex number a.
$\mathbb{R}^m, \mathbb{C}^m$	Real and complex $m \times 1$ vector.
$\mathbb{R}^{m\times n}, \mathbb{C}^{m\times n}$	Real and complex $m \times n$ vector.
$\mathbb{E}\{\cdot\}$	Expectation.
$\mathcal{CN}(a,b)$	Complex Gaussian distribution with mean a and variance b.
$\exp(\cdot)$	Exponential function.
$\log_a(\cdot)$	Logarithm in base a.
$\ln(\cdot)$	Logarithm in base e.
$\max(\mathcal{A})$	Maximum of set $\mathcal{A}$.
$\lceil L \rceil$	The smallest integer which is greater than L.

Chapter 1
Introduction

1.1 Background

From the first generation (1G) to the fourth generation (4G), wireless communications have evolved so rapidly over recent decades, due to the growing demand for high data rates. So far, wireless communication has become a crucial part of modern society. On one hand, it connects people effectively, ignoring time and geographical limitations. As an extension of the internet, the cellular network constructs the links for the last meter between people and the internet. On the other hand, from remote education to cloud computing, it supports industry with data exchange at the basic layer. In the digital age, the concept of communication is far more than the transmission of voice or video, and the users of communication are not only humans, but also machines or sensors. In addition, with the rapid improvement of electronic and computing techniques, high performance in wireless communication is demanded all the time. In 4G wireless communications, many new network structures in the physical and media access control (MAC) layers have been proposed to provide more stable and high-speed services at lower cost. These evolutions and the upcoming next generation of wireless communications are inversely changing the working and living patterns of people and mobile devices. Overall, wireless communications have become an inevitable component in modern life and industry.

1.2 Relay-aided Network

The current wireless communication systems are facing challenges mainly in three domains. Firstly, the sparse spectrum imposes the further increase of data rates, because, in 4G wireless communications, the spectrum has already been applied in efficient ways. For example, from the Long-term-Evolution (LTE) systems to the LTE-Advance (LTE-A) systems, although the peak data rate of each user is enhanced, the total throughput for a cell remains the same. The second challenge is related to the hardware limitation. As the spectrum has been exploited efficiently in the frequency domain, engineers are looking for improvements in system performance through more dense spatial divisions, which enlarges the number of base stations.

Small-sized base stations with dense users result in significant interference, which demands high capabilities of signal processing at the transmitting and receiving sides. All of these aspects increase the cost of mobile devices and base stations. Thirdly, with more powerful portable devices, people require stable connections in various modern scenarios, such as crowded public environments, fast-moving vehicles, and complex indoor circumstances.

In the post-LTE time, improvements in spectrum efficiency are quite expensive, and researchers are focusing their attention on new network structures as attractive solutions to the problems involved in future wireless communications. Proved by abundant research, such as [1,2], relay-aided transmission can somewhat improve the performance of wireless communications in a cost-effective way. In more detail, relying nodes are able to enhance the signals for users with bad quality of service (QoS). Since the enhancement is achieved without the construction of new base stations, relaying networks could optimise coverage and improve data rates at little extra cost. So far, relaying techniques have been written into several general wireless communication standards, such as IEEE 802.16j for Worldwide Interoperability for Microwave Access (WiMAX) and LTE-A for the Third Generation Partnership Project (3GPP) [3]. Coinciding the working pattern , the protocols concerning relaying techniques are mainly for the MAC and physical layers. Similarly, the evaluation studies on system performance over such systems are commonly concentrating on the bottom layers as well.

1.3 Motivation

Due to the advantages of relaying networks, a great deal of studies have appeared in the literature analysing the performance of relaying systems. So far, the performances of relaying networks have, in general, been well understood for a number of popular fading channels, such as Rayleigh, Rician, Nakagami-m and Weibull, and for traditional network structures. However, these investigations are not proper, due to some complicated circumstances. On one hand, a major limitation of conventional investigations is that all of these works are based on channel models relying on the key assumption that the scatters in propagation environments are homogeneously distributed. Therefore, the results predicted by these previous studies may fail to give an accurate performance account of practical scenarios in which the scatters are non-homogeneous.

On the other hand, due to the employment of aggressive frequency reusing, researchers are

paying more attention to the CCI impact when analysing the performance of wireless networks. Most current studies evaluating the relaying system with CCI have been conducted without considering the randomness of interference sources, which indicates that they are less appropriate to analyse the performance of emerging heterogeneous communication systems. As early as the 1990s, researchers had worked on investigations of interference attended mobile networks. The stochastic geometry was initially introduced into wireless communication by [4]. Compared with traditional Gaussian interference models, which can only evaluate large amounts of weak interferences according to central limitation theory (CLT), the Poison point process (PPP) model has significant advantages in the following aspects: (i) the statistic model of the spatial distribution of interference; (ii) combined with the characters of user equipment (UE); (iii) cooperating with statistic models of channel propagations. Therefore, the PPP methods are commonly involved in modelling the spatial distributions of interferences.

In the current LTE or LTE-A wireless communication systems, frequency and spatial diversity multiplexing techniques are applied to enhance the spectral efficiency in terms of orthogonal frequency division multiplexing (OFDM) and multi-input and multi-output (MIMO). With the improved capability of signal processing in the terminal ports, some novel techniques have been proposed in recent years for future wireless communication systems. Non-orthogonal multiple access (NOMA) was introduced as a potential 5G standard in 2012 [5]. The principle concept behind the NOMA scheme is to make successive interference cancellation (SIC) at receivers; it achieves spectrum efficiency enhancement and multi-user division by applying power multiplexing. The key advantages of NOMA include higher spectral efficiency, lower transmission latency and more connectivity per cell.

1.4 Contributions and Outline of Thesis

An outline of the remainder of this thesis is given below.

Chapter 2 reviews the basic concepts of our research. Firstly, a concise summary of wireless communication systems is provided, including the typical methods of system evaluation. A specific introduction to the relay-assisted system is provided, subsequently. The fundamental concepts of the general channel coefficient, PPP and the NOMA techniques are demonstrated as well. In addition, we briefly interpret the mathematical tool applied in this thesis, which can help to understand the work in Chapters 3 to 5 more easily.

Chapter 3 evaluates a dual-hop relay-aided wireless communication system applying an amplify and forward (AF) relaying protocol. In order to model the heterogeneous distribution of channel scatter, the κ-μ and η-μ distributions are involved. For a noise-limited system model, first, the analytical expressions of the end-to-end SNR are developed. Subsequently, the error exponents of such a system are studied. As is known, in practical wireless communication systems, transmissions are classified as different sorts with corresponding priority levels in terms of service requirements, including stability, latency and data rate. Error exponent is an ideal criteria for the classification as it conveys the balance between error probability, transmission rate and code length, which indicates the coding complexity and system cost. In this chapter, new analytical expressions of RCEE, expurgated error exponent, cut-off rate and ergodic capacity are derived. Our generalised analytical results include the other previously popular fading channels as special cases. Also, simplified and insightful approximations are provided, which are shown to be tight at a high-SNR regime. Meanwhile, the required code length to achieve a certain upper bound of error probability are estimated based on our analytical expressions. The results show that a larger in-phase to quadrature components ratio, dominant components to scattered waves ratio and number of multipath clusters could reduce the required code length and improve the communication reliability of dual-hop AF channels.

Chapter 4 studies the end-to-end capacities of the dual-hop multi-antenna AF relaying systems, in which the relay implements MRC/MRT, ZF/MRT and MMSE/MRT signal processing schemes to eliminate co-channel interference. The locations of interferers are modelled with a Poisson Point Process (PPP). We consider both the infinite-area interference and limited-area interference environments in this chapter. For the infinite-area model, exact expressions of ergodic capacities are provided for each signal processing scheme; and for the limited-area scenario, the asymptotic expressions for the lower bounds on the ergodic capacities are provided, which can efficiently investigate the system performance, especially in dense-interferers environments. According to our numerical tests, the MMSE/MRT processing scheme performs the best in all interference scenarios and with all SNR values. The most attractive results come from the ZF/MRT processing scheme. In the infinite-area scenario, it performs much worse than the MRC/MRT scheme, whose performance is closer to the MMSE/MRT scheme. However, in limited-area interference regimes, it performs better than MRC/MRT, especially when the number of antennas at the relay is large enough, it performs nearly as well as MMSE/MRT.

Chapter 5 investigates a dual-hop AF relaying system over a complex Gaussian channel, the

non-orthogonal-multi-access (NOMA) technique is applied at the source nod. The path-loss attenuations for randomly located users are taken into consideration. Firstly, a single-antenna relaying system is evaluated, the exact expression of the end-to-end outage probability is given. In order to reduce the computational complexity, simplified upper and lower bounds are derived as well. Secondly, the multi-antenna relaying system is studied. A tractable integral method is involved to derive the analytical expressions of the outage probability and the corresponding upper and lower bounds. In addition, the diversity order of the system is studied.

Chapter 6 summarises the thesis and enumerates potential future works.

Chapter 2
Background

Wireless communication is a way of making an information transaction in free space with the aid of electromagnetic waves. Therefore, an elemental wireless communication system consists of a transmitter, a receiver and the transmission media (channel). However, as wireless communications are carried by a limited spectrum source and suffer a variety of influence, such as background noise, interference, channel fading, multipath fading and Doppler shift, a practical wireless communication system should be assisted by some other functional models to keep the transmission efficient and reliable.

2.1 Wireless Communication System

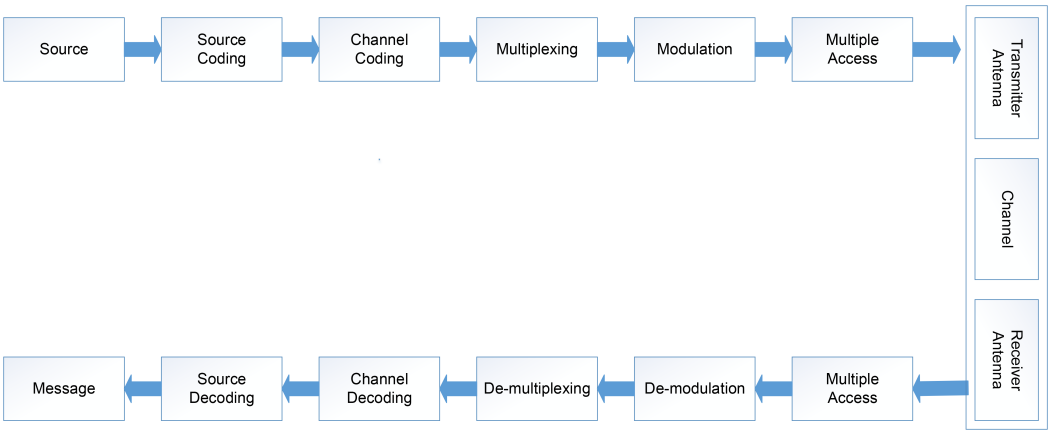

Figure 2.1: *Diagram of a basic wireless communication system.*

A typical transceiver link is illustrated by the diagram in Figure 2.1. The source coding is used to remove the redundancy of the message, which helps to improve the information entropy. Channel coding is the technique for enhancing the reliability of wireless communications. The principle behind channel coding techniques is to provide correlations amount adjacent code-words for information detections and/or corrections. Depending on the channel state, different coding schemes should be adopted, and the valid information rate is bound by the Shannon

theory. Note that, starting from the process of channel coding, the channel state information (CSI) is an important condition for the scheme selection. According to the method of channel division, the common multiplexing methods can be classified as space-division multiplexing (SDM), frequency-division multiplexing (FDM), time-division multiplexing (TDM), code-division multiplexing (CDM) and power-division multiplexing. Modulation is a process that conveys the digital signals to high-frequency analogue bandpass signals by modulating some of the properties of a periodic carrier signal. The family of modulated digital signals with a special signal property is known as keying. The fundamental modulation methods include phase-shifting keying (PSK), frequency-shifting keying (FSK), amplitude-shifting keying (ASK) and quadrature-amplitude modulation (QAM). In real-time application, different modulation methods and multiplexing schemes are frequently applied simultaneously. For example, the orthogonal frequency division multiple access (OFDMA) applies FDM between sub-carriers; it also utilises the TDM in the form of frequency shifting. In addition, the MIMO technique uses the SDM cooperating with any other sorts of multiplexing. Furthermore, some modulation processes can be achieved digitally in the multiplexing module, such as the OFDM. In the multiple access process, modulated signals are divided into small packs, and prefixes are fixed onto each pack to pilot connections. The packaged signals are then amplified and sent by the transmitter, pass through the wireless channel, and are received by the receiver. Information is extracted from the received signals through the reverse approach of the transmission chain shown in Figure 2.1. In this thesis, the investigations are concentrated on the channel fading between transmitter and receiver marked by the dashed block.

2.1.1 Wireless Channel Model

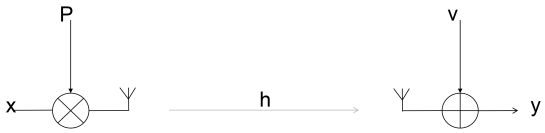

Figure 2.2: *SISO channel model*

The investigation on channel fading is to grab the statistical properties of received signals effected by system structure, channel fading, noise, and interference. To simplify the demonstration, a single-input and single-output (SISO) system is given here as an example. Since a single antenna is equipped at the transmitter and receiver, respectively, the channel is given as a scalar variable. Illustrated by Figure 2.2, the transmitted and received signals can be expressed as

$$y = hx + v, \tag{2.1}$$

where $y \in \mathbb{C}$ denotes the received signal. $x \in \mathbb{C}$ with $\mathbb{E}\{xx^* = P\}$ is the normalised transmitted signal. $h \in \mathbb{C}$ is the channel coefficient, which is denoted by a lot of aspects, such as channel fading, shadowing, and path-loss attenuation. Depending on their importance in different scenarios, the investigated h consists of one or several elements, and others are set to be constant. v denotes the system noise n and/or the interference $\sum I_i$, where $n \in \mathbb{C}$ with $\mathbb{E}\{nn^*\} = \sigma^2$ is frequently considered as the added white Gaussian noise (AWGN), which contains the least self-correlation and leads to the tightest upper bound of the data rate (Shannon capacity). The interference $I_i \in \mathbb{C}$ $(i = 1, \ldots, m)$ contains m independent interference coefficients.

2.1.2 Wireless Fading Channel

In long-distance transmissions, the signal accuracy is not only affected by the AWGN and interference but also depends on the channels. The channel that degrades the signal accuracy, either strength or phase, is the so-called fading channel. Fading is normally quantified in the form of channel coefficient, which varies over time and frequency. For single-user investigations, it is more important to observe the statistical properties of small-scale fading. Generally, the small-scale fading is referred to as fast fading and slow fading in terms of the coherence time of Doppler spreads. It is also classified as flat fading and frequency selected fading according to the coherence bandwidths of multi-path time intervals. When analysing the sum rate of multiple users, statistical properties of large-scale fading are sometimes taken into consideration, for example, when evaluating the total throughput in a cell.

1. Rayleigh fading

   The Rayleigh fading is one of the most elemental models of the flat fading. Mathematically, the Rayleigh distribution is used to characterise the sum of two identically and

independent distributed (i.i.d.) Gaussian variables, which indicate the real and imagined parts of a complex channel coefficient in wireless communications. It is used to model the summation of received signal powers consisting of abundant scatters, whose amplitude and phase are randomly distributed. This distribution is suitable for heavy built-up environments, such as a city centre. The pdf of a Rayleigh distribution is given in the following:

$$f^{Rayleigh}(x) = \frac{2x}{\Omega} \exp\{-\frac{x^2}{\Omega}\}, \qquad x \geq 0, \tag{2.2}$$

where $\Omega = \mathbb{E}\{x^2\}$ is the expectation of channel gain x^2.

2. Nakagami-m fading

   Nakagami distribution is more flexible to characterise the channel fading in place of the Rayleigh distribution. The pdf of a Nakagami-m distribution is given as

$$f^{\text{Nakagami}-m}(x) = \frac{2m^m x^{2m-1}}{\Omega^m \Gamma(m)}, \tag{2.3}$$

   where $\Omega = \mathbb{E}\{x^2\}$, the fading parameter $m \in [\frac{1}{2}, \infty)$ is determined by the propagation environment, and, correspondingly, a Nakagami-m distribution can be mapped to some other distributions as special cases. For $m \leq 1$, the Nakagami-m distribution can be changed to a Hoyt distribution, also called a Nakagami-q distribution, which is suitable for modelling long-distance communication disturbed by strong ionospheric scintillation. With m=1, the Nakagami-m distribution is equivalent to a Rayleigh distribution, which is suitable for the non-line-of-sight (NLOS) communication. When $m \geq 1$, the Nakagami-m distribution can be mapped to a Rician distribution (Nakagami-n). Mathematically, a Rician distribution is the statistics of the summation of a dominant Gaussian variable and some weak ones. Therefore, a Rician distribution is normally used to model the line-of-sight (LOS) wireless communications, such as in suburban areas.

3. κ-μ and η-μ distribution

   All fading distributions mentioned above assume that the transmission media is homogeneous, diffuse and scattering. In practice, due to spacial correlations between reflectors, received signals through different paths normally do not have i.i.d. real and imagined components. In order to characterise such channels more accurately, two general distri-

butions, namely, the κ-μ distribution and the η-μ distribution, are involved.

The κ-μ distribution is used to characterise the channel fading in small-scaled LOS communications. In more detail, the variable represents the total power gathered from multipath clusters. A cluster denotes a bundle of sub-channels whose paths are strongly correlated in space. Different clusters are assumed to have identical expected power but uniformly distributed delivery time. Within each cluster, there is a dominant multipath component with arbitrary power and the time spread for the scatter waves are identically distributed. According to [6], the pdf of normalised power subject to $\kappa-\mu$ channel fading is given by

$$f_{\gamma_{\kappa,\mu}}(\gamma) = \frac{\mu(1+\kappa)^{\frac{\mu+1}{2}}}{\kappa^{\frac{\mu-1}{2}} e^{\mu\kappa}} \gamma^{\frac{\mu-1}{2}} e^{-\mu(1+\kappa)\gamma} I_{\mu-1}\left(2\mu\sqrt{\kappa(1+\kappa)\gamma}\right), \tag{2.4}$$

where $I_\alpha(\cdot)$ denotes the modified Bessel function of the first kind. Parameter κ denotes the ratio between summation of the power of all dominant components and summation of the power of all scatter waves. Parameter μ synthesises some aspects, such as the correlation between in-phase and quadrature components, the correlations among clusters and some non-Gaussian natures in wireless channels. It should be noticeable that, γ is the normalized variable of power.

The η-μ distribution works better on modelling small-scale NLOS environments. The pdf of normalised power over η-μ channel is given by

$$f_{\gamma_{\eta-\mu}}(\gamma) = \frac{2\sqrt{\pi}\mu^{\mu+\frac{1}{2}}\phi^{\mu}\gamma^{\mu-\frac{1}{2}}\exp\left(-2\mu\gamma\phi\right)}{\Gamma(\mu)\psi^{\mu-\frac{1}{2}}} I_{\mu-\frac{1}{2}}\left(2\mu\gamma\psi\right). \tag{2.5}$$

The parameter μ has the same definition as in κ-μ distribution; however, the parameter η has different physical significances which will be introduced in the next chapter. Parameters ϕ and ψ are functions of η, defined in the next chapter.

2.1.3 Evaluations for the Performance of the Wireless Communications

The theoretical analysis of wireless communication systems is a crucial process before the practical constructions. On one hand, it indicates the potential of a given system structure, or a novel technique, which helps to evaluate new techniques before their development in industrial use. As tight bound of the performance expected, it is commonly used to access the achievement of a practical system. On the other hand, the theoretical performance in terms of the communica-

tion environment is a significant aspect of the system requirement for constructions in practice. For system design, engineers should comprehensively consider the user demands, the physical environments and the limitations of spectrum resources. The channel analysis theoretically reveals the ceiling of system performance in practice; some elemental indicators are introduced below.

2.1.3.1 Channel Capacity

The channel capacity is the theoretical upper bound of the reliable transmission over a communication channel. Defined by Shannon in 1948 [7], the channel capacity can be mathematically written as

$$C = \max_{\mathrm{p(x)}} I(x, y), \tag{2.6}$$

which denotes the maximum of the mutual information between transmitted signal x and received signal y. The channel capacity is independent from the source coding, but affected by channel coding schemes. Only when all codewords are uniformly distributed, the maximum can be obtained. Another definition of the information is based on the operation of channel coding. Setting a channel coding scheme totally contains M codewords in the coding index and each code requires n transmission; the data rate is then given by $R = \frac{\log_2(M)}{n}$ bits/transmission. If there is a code scheme to guarantee a randomly small error probability ϵ, when the code length n tends to infinity, the corresponding data rate is achievable. Proved by Shannon, the supremum of achievable rate equals the information channel rate, which is also known as the operational channel rate. According to [8], The information capacity of a Gaussian channel with AWGN, is given by

$$C = \log_2\left(1 + |h|^2 \frac{P}{\sigma^2}\right), \tag{2.7}$$

where h is the complex channel coefficient, $P = \mathbb{E}\{xx^\dagger\}$ is the power limitation and σ^2 denotes the average power of AWGN. Since channel coefficients vary with time, and the channel capacities can be achieved only with long codes, selections of coding schemes should be based on the long-time averaging of channel coefficients. In order to make faster decisions for the coding schemes, researchers can convert the averaging from time samples to spatial samples, i.e. statistics of CSI. This conversion performs with the aid of ergodic theory, and the corresponding channel capacity is referred to as the ergodic capacity.

$$C_{erg} = \mathbb{E}_h\left\{\log_2\left(1 + |h|^2 \frac{P}{\sigma^2}\right)\right\} \tag{2.8}$$

According to ergodic theory, time intervals should be long enough to avoid the effect of the initial state of the channel coefficient. Since the factors resulting in channel fading vary with different rates, the evaluation in this research refers to different lengths of period in terms of fading sorts. For example, for a noise-limited communication between a base station and an individual user moving slowly, the ergodic capacity is derived by averaging the small-scale fadings of the channel. However, if the mobile terminals move fast or the cells are tiny, the time intervals should be long enough to cover the variation of large-scale fadings.

2.1.3.2 SNR and SINR

Signal-to-noise ratio (SNR), the most fundamental parameter to reveal the system state, is the most basic parameter determining the system performance in wireless communications. Normally, it is measured in decibels (dB). Mathematically, the SNR is defined by the ratio of the power lever of the desired signal to the noise and can be written as

$$\gamma = \frac{\text{Power of received signal}}{\text{Power of AWGN}} = \frac{P|h|^2}{\sigma^2}. \tag{2.9}$$

In fading channels, the CSI acquired by the system should include the averaged SNR over time, which is denoted by $\bar{\gamma} = \mathbb{E}\{\gamma\}$. To model the communication system with interference, the power of interference is taken into consideration and regarded as the noise by the receiver. The parameter SNR is accordingly extended to the signal-to-interference-plus-noise ratio (SINR).

2.1.3.3 Outage Probability

Outage probability, normally denoted by P_{out}, is a crucial parameter evaluating the communication system. Physically, this indicator tells the probability that channel propagation or SNR falls under a threshold γ_{th}, which makes it difficult for the receiver to detect the information. Note that, this threshold does not exist when calculating the ergodic capacity. Mathematically, the outage probability can be calculated by

$$P_{out} = \int_0^{\gamma_{th}} f(x)dx, \tag{2.10}$$

where $f(x)$ denotes the pdf of channel coefficient or instantaneous SNR, and, consequently, $P_{out} = F(x)$. Therefore, the outage probability may be derived as an intermediate product when researchers are looking for channel capacities or some other indicators of system perfor-

mance.

2.1.3.4 Error exponent

2.1.3.5 Random Coding Error Exponent

In [9], the upper bound of average error probability for a discrete-time memoryless channel with maximum likelihood (ML) decoding is defined as

$$P_{e,m} \leq \left[\frac{2e^{r\delta}}{\xi}\right]^2 \exp\{-T_c N_b [E_r(\rho, p_{\mathbf{x}}(\mathbf{x}), r)]\}, \tag{2.11}$$

where T_c is the time interval that channel remains stable, N_b is the number of T_c to carry one code word, $p_{\mathbf{x}}(\mathbf{x})$ is the input source distribution and parameters ρ, r and δ are arbitrarily selected from regimes $0 \leq \rho \leq 1$, $r \geq 0$ and $\delta \geq 0$. Coefficients ξ and σ are defined as

$$\xi \approx \frac{\delta}{\sqrt{2\pi N_b \sigma_\xi^2}}, \tag{2.12}$$

$$\sigma_\xi^2 = \int_x [tr(\mathbf{x}^\dagger \mathbf{x}) - T_c \mathcal{P}] p_{\mathbf{x}}(\mathbf{x}) \mathrm{d}x, \tag{2.13}$$

where P is the power constraint. The RCEE [9, 5.6.16] of the SISO system is derived as

$$E_r(p_x(x), R, T_c) = \max_{0 \leq \rho \leq 1} \left\{ \max_{r \geq 0} E_0(p_{\mathbf{x}}(\mathbf{x}), \rho, r, T_c) - \rho R \right\}. \tag{2.14}$$

The element $E_0(p_{\mathbf{x}}(\mathbf{x}), \rho, r, T_c)$ is defined by

$$E_0(p_{\mathbf{x}}(\mathbf{x}), \rho, r, T_c) \triangleq$$
$$-\frac{1}{T_c} \ln \left(\int_h p_h(h) \int_{\mathbf{y}} \left(\int_{\mathbf{x}} p_{\mathbf{x}}(\mathbf{x}) e^{r[tr(\mathbf{x}\mathbf{x}^\dagger) - T_c \mathcal{P}]} p(\mathbf{y}|\mathbf{x}, h)^{\frac{1}{1+\rho}} d\mathbf{x} \right)^{1+\rho} \mathrm{d}\mathbf{y} \mathrm{d}h \right), \tag{2.15}$$

where $p_h(h)$ denotes the distribution of channel coefficient h. We denote $E_0(p_{\mathbf{x}}(\mathbf{x}), \rho, r, T_c)$ and $E_r(p_{\mathbf{x}}(\mathbf{x}), R, T_c)$ as $\tilde{E}_0(\rho, \beta, T_c)$ and $E_r(R, T_c)$, respectively. Therefore, $\tilde{E}_0(\rho, \beta, T_c)$ is given by [10]

$$\widetilde{E}_0(\rho, \beta, T_c) = \mathcal{A}(\rho, \beta) - \frac{1}{T_c} \ln \left\{ \mathbb{E}_\gamma \left[\left(1 + \frac{\gamma}{\beta(1+\rho)} \right)^{-T_c \rho} \right] \right\}, \tag{2.16}$$

where $\gamma = \bar{\gamma}|h|^2 = \frac{P|h|^2}{\sigma^2}$, $\mathcal{A}(\rho, \beta) = (1+\rho)(1-\beta) + (1+\rho)\ln(\beta)$. With the variance of Lagrange multiplier r, the parameter $\beta = 1 - rP$ is restricted to $0 \leq \beta \leq 1$. The RCEE can be rewritten as

$$E_r(R, T_c) = \max_{0 \leq \rho \leq 1} \left\{ \max_{0 \leq \beta \leq 1} \widetilde{E}_0(\rho, \beta, T_c) - \rho R \right\}. \tag{2.17}$$

2.1.3.6 Ergodic Capacity

According to [11], expression (2.16) is a convex function of β in range $0 \leq \beta \leq 1$. We know that there always exists $\beta = \hat{\beta}$ for $0 \leq \rho \leq 1$ to maximise $E_0(\rho, \beta, T_c)$, where $\hat{\beta}$ is the result of equation $\frac{\partial E_0(\rho,\beta,T_c)}{\partial \rho} = 0$. The information rate R in expression (2.17) can be derived as

$$R = \left. \frac{\partial E_0(\rho, \beta, T_c)}{\partial \rho} \right|_{\beta=\hat{\beta}}. \tag{2.18}$$

By setting $\rho = 0$ and the related $\hat{\beta}|_{\rho=0} = 1$ in (2.18), the ergodic capacity in nats is obtained as

$$\langle C \rangle = \left. \frac{\partial E_0(\rho, \beta, T_c)}{\partial \rho} \right|_{\rho=0,\beta=1}. \tag{2.19}$$

2.1.3.7 Cutoff rate

The cut off rate is an important parameter to evaluate channel capacity. As a lower bound of Shannon capacity, the cut off rate gives the practical limit of the symbol rate for sequential decodings. Due to the low complexity of calculation and the practicality in information rate evaluation, the cut off rate is frequently applied to analyse the system performance such as different coding and modulation schemes [12]. According to [10], the cut off rate can be derived as an extension of RCEE from (2.16) by setting $\rho = 1$ and $\hat{\beta} = 1$:

$$R_0 = E_0(p_{\mathbf{x}}(\mathbf{x}), 1, 1, T_c) = -\frac{1}{T_c} \ln \left\{ \mathbb{E}_\gamma \left[\left(1 + \frac{\gamma}{2} \right)^{-T_c} \right] \right\}. \tag{2.20}$$

2.1.3.8 Expurgated Error Exponent

In a random coding regime, good and bad codes are collected unbiasedly. Therefore, both contribute the dominant error probability. A compendious improvement is to expurgate the bad codewords from the codewords ensemble, which can improve the error exponent obviously at

low-rate regimes.

Developed by [9, 13], the expurgated error exponent is defined as

$$E_{ex}(R, T_c) = \max_{\rho \geq 1} \left\{ \max_{0 \leq \beta \leq 1} E_x(R, T_c) - \rho R \right\}, \tag{2.21}$$

in which

$$E_x(R, T_c) = \mathcal{A}'(\rho, \beta) - \frac{1}{T_c} \ln \left\{ \mathbb{E}_\gamma \left[\left(1 + \frac{\gamma}{2\beta\rho} \right)^{-T_c \rho} \right] \right\}, \tag{2.22}$$

where $\mathcal{A}'(\rho, \beta) = 2\rho(1 - \beta) + 2\rho \ln(\beta)$.

2.2 Relaying Network

As a proven technique, the relaying network is widely used in current wireless communication networks to efficiently extend the system coverage, improve the data rate in a unit area and to enhance spectrum efficiency without extra constructions of base stations, which may result in enormous hardware and administration costs. In the next generation of wireless communication, with the implementation of spectrums on higher frequency, the signal attenuation will become more significant. In order to guarantee users strong enough signals and to support more access, small cells will be constructed in future networks. Therefore, economical and power-saving solutions for the 5G techniques are urgently demanded. So far, the relaying network has been considered a key feature in the next generation of wireless communication.

2.2.1 Half-duplex(HD) Dual-hop(DH) Relaying

Originally proposed by [14], relays investigated in information theory works can transmit and receive signals simultaneously on the same frequency, which is defined as the full-duplex (FD) model. However, in the DF model, the relay is severely impacted by the self-interference, which makes the transmission impractical. Although some pioneer works have tremendously eliminated the self-interference through analogue methods; so far, the FD relaying still has difficulty transmitting signals with the same efficiency, compared to the HD model.

The large proportion of relaying-aided wireless communications work in the DH regime, where the information is transmitted from the source to relay via a single relay. The brief idea of DH

relaying is exhibited by Figure 2.3. As depicted in Figure 2.3, the transmission of an HD

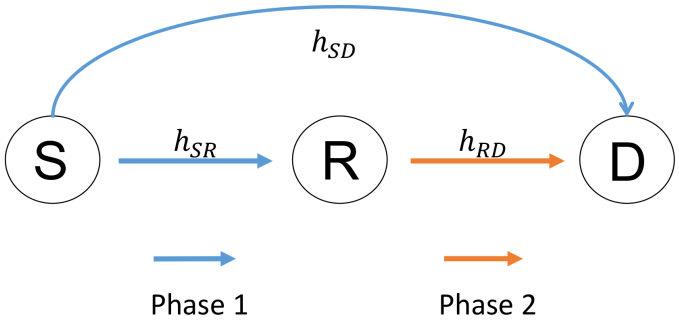

Figure 2.3: *Dual-hop relaying model*

relaying is constitutive of two steps, which happen in two orthogonal phases. In the first phase, the signal is transmitted from the source and received by the relay and destination. In the second phase, the relay transmits the processed signal to the destination. In scenarios in which the direct link from the base station to user is too weak to support a transmission, the channel coefficient h_{SD} shown in Figure 2.3 equals 0, and the system correspondingly becomes a DH relaying system. The DH relaying is a typical way to enlarge the coverage of base stations in wireless communications, which can efficiently enhance the signal strength with low extra cost. However, the DH relaying is not ideal when a direct transmission from the source to destination is feasible; in other words, DH relaying is not likely to improve data rates and spectrum efficiency when direct links are strong. Firstly, the relay cannot provide affluent diversity for the transmission because normally the source-destination channel is a one-path link. Secondly, although there is an improvement for path-loss attenuation, the time-efficiency for a DH relaying is only half of that for a direct transmission. To overcome these drawbacks of the DH scheme, cooperative relaying strategies have been proposed, where the destination combines or selects signals from both the relay and source. Due to the time interval between phases 1 and 2, the HD are responsible for a high cost with cooperative relaying strategies, especially on the mobile side.

2.2.2 AF Relay and Formulations

The basic relaying functions can be classified as Decode-and-Forward (DF), Compress-and-Forward (CF) and Amplify-and-Forward (AF). In the DF relaying system, the relay first decodes the information, and then encodes and forwards the information to the destination. The

relay of CF modes quantises the received signal, and then forwards them to the destination; sometimes it also compresses the quantised signals before transmission. In the AF strategy, the relay just amplifies the received signal, and forwards it in the second phase. Among these relay functions, the DF strategy normally presents the best system performance; however, the AF relay is applied more frequently in practice, because it strikes the balance between system performance and cost.

According to the power limitations at the relay, the AF strategy can be further sorted as fixed-gain AF relay and adapt-gain AF relay. The former amplifies the received signal in a fixed ratio based on the average channel gain coefficient over a long term; the latter adjusts the power magnification according to the instantaneous CSI of the source-relay channel. Without specific mention, the AF relaying in this thesis refers to the adjust-power one.

Using the model presented by Figure 2.3 and setting $h_{SD} = 0$, the signal received by the relay can be written as

$$y_R = \sqrt{P_S} h_{SR} x + n_R, \tag{2.23}$$

where x is the transmitted signal with $\mathbb{E}\{xx^\dagger\} = 1$, P_s is the averaged transmission power at base station, and n_R is the AWGN at relay with $\mathbb{E}\{n_R n_R^\dagger\} = 1$. Without consideration of the direct link, the signal received by the destination is given by

$$y_D = h_{RD} G(\sqrt{P_S} h_{SR} + n_R) + n_D, \tag{2.24}$$

where n_D denotes the AWGN in the destination node, scalar G is the power gain of the relay varying with the CSI to satisfy the power limit of the transmitter at the relay:

$$P_R = G^2 |\sqrt{P_S} h_{SR} + n_R|^2. \tag{2.25}$$

As the transmission of signals is not discarded by the AF relay, the performance of this system can be investigated through the statistics properties of the end-to-end channel. More details are given in the following chapters of this thesis.

2.3 Stochastic Geometric

Engineers have always fully considered the frequency assignment among base stations in the network constructions; therefore, the CCI happens only on the edges of cells in traditional wireless communications. However, in the past decade, emerging architectures for wireless communications have started to allow the frequency reuse without a central dispatch, such as ad hoc, relays and pico cells. In these networks, interference appears not only on the edges of communication cells, but is also likely to occur close to users in central areas of cells, because each user could be covered by different active cells. Stochastic geometry is involved to evaluate these more flexible and complex wireless systems statistically.

2.3.1 Stochastic Geometry in Wireless Communication

Mathematically, stochastic geometry is the study of the randomness of spatial patterns. The most dominant sub-field of stochastic geometry is the point process, which is also known as the random counting measure. With the aid of the point process, a variety of properties of system performance could be analytically characterised.

- To model a collection of points with uncertainty. The point process can calculate the expected number of random points, as well as their positions. These points could denote interference, users or relays in wireless communications.
- To formulate the distributions of points numbers and positions. Stochastic geometry enables the derivation of system properties concerning spatial realisations.
- To deal with the distance of points in order. In addition to survey properties of whole systems containing elements with randomness, stochastic geometric can be used to observe the statistics of ordered point/points.

2.3.2 Basic Point Process

The most basic and important point process is the PPP, which was well introduced by [15]. With a constant intensity λ, the PPP with dimension d is a point process with the following features:

- For each compact set B, the number of points falling into this set N_B has a Poisson

distribution and can be written as

$$\mathbb{P}(N_B = k) = e^{-\lambda B}\frac{(\lambda B)^k}{k!}. \tag{2.26}$$

- For disjoint sets $B_1, \ldots, B_m$, the counting $N_{B_1}, \ldots, N_{B_m}$ are independent variables.

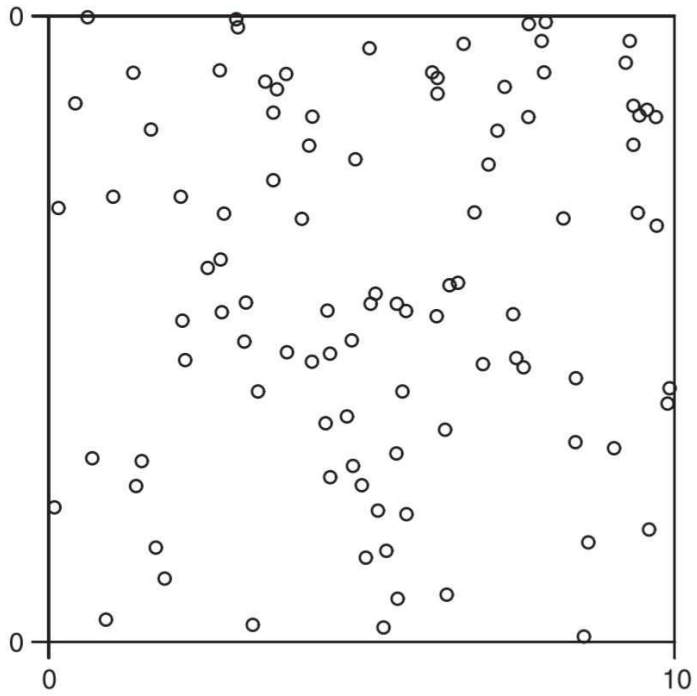

Figure 2.4: *A PPP process realisation.*

A realisation of the uniform PPP with $\lambda = 1$ in closed set $[0, 10]^2$ is presented in Figure 2.4. When the intensity is constant, the counting of points becomes a variable only determined by the area of the set. Based on this fact, the conditional property of PPP is generated:

- Considering a uniform PPP in $\mathbb{R}^d$ with intensity $\lambda > 0$. Given a compact set B with the number of points $N_B = n$ and a subset $W \subseteq B$, the distribution of N_W conditioned by $N_B = n$ is binomial and can be expressed as

$$\mathbb{P}(N_W = k | N_B = n) = \binom{n}{k} p^k (1-p)^{n-k}. \tag{2.27}$$

This equation is important to find out the statistics of ordered points in a homogeneous PPP.

2.3.2.1 Interference modelled by PPP

One of the most significant applications of PPP in wireless communications is to model the interference. Defining the path loss function as $l : \mathbb{R}^d \mapsto \mathbb{R}^+$, the expression of the total interference modelled by a point process can be expressed as

$$I_y = \sum_{x \in \Phi} l(y - x), \;\; y \in \mathbb{R}^d. \tag{2.28}$$

Specialising the point process as a homogeneous PPP in a 2-D round area, the distance $||y - x||$ could be replaced by a scalar variable r with centre y. By substituting the typical format of power law of path loss $l(x) = ||x||^{-\alpha}, x \in \mathbb{R}^d$, the expression of sum power of interference can be written as

$$I = \sum_{i \in \Phi} r_i^{-\alpha}. \tag{2.29}$$

Taking the channel fading into consideration, the sum of interference power at the receiver is given by

$$I = \sum_{i \in \Phi} |h_i|^2 r_i^{-\alpha} \tag{2.30}$$

2.4 Non-orthogonal Multiple Access

Radio access technologies are a principle aspect to decide the spectrum efficiency in cellular wireless communication. Reviewing the history of wireless communication technologies, multiple access (MA) techniques have been the key points to distinguish the systems of different generations. In the first generation, frequency division multiple access (FDMA) is applied for analogue signals, TDMA is adopted by the second generation for digital signals, CDMA is applied in 3G standards as the core MA technique, and OFDMA is currently applied in 4G techniques. In OFDMA, time division and frequency division have jointly worked for multiple access, which has already provided high spectrum efficiency. However, to accommodate the exponentially increased demands for system throughput in 5G wireless communications, a further boost of spectrum efficiency is still required. Therefore, NOMA approaches are proposed to afford better system-level throughput and a larger amount of connectivities. According to different division schemes, current NOMA solutions fall into two major catalogues, namely the power domain NOMA and the coding domain NOMA. In this work, we focus only on the power domain, a brief introduction of which is presented in the following.

2.4.1 Power Domain NOMA

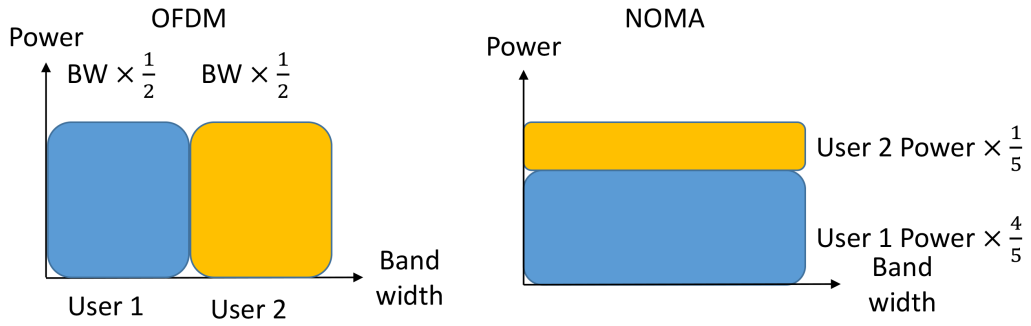

Figure 2.5: *Difference between OFDM and NOMA.*

Figure 2.5 illustrates a 2-user NOMA working in a power domain by comparing it with an OFDMA scheme. Users 1 and 2 are assigned different bandwidth and transmit power according to their priorities in transmission. The system throughput with the OMA approach can be expressed as $R = R_1 + R_2$, where

$$R_1 = \alpha \log_2 \left(1 + \frac{P_1 |h_1|^2}{\sigma_n^2}\right) \tag{2.31}$$

and

$$R_2 = (1 - \alpha) \log_2 \left(1 + \frac{P_2 |h|_2^2}{\sigma_n^2}\right), \tag{2.32}$$

where $P_1 = P_2 = P$.

Under the NOMA strategy, users 1 and 2 are served simultaneously, and the total transmit power is fixed. The achievable rate for users 1 and 2 can be expressed as

$$R_1 = \log_2 \left(1 + \frac{P_1 |h_1|^2}{P_2 |h_1|^2 + \sigma_n^2}\right), \tag{2.33}$$

$$R_2 = \log_2 \left(1 + \frac{P_2 |h|_2^2}{\sigma_n^2}\right), \tag{2.34}$$

where $P_1 + P_2 = P$. Setting P = 100, $|h_1|^2 = 0.01$, $|h_2|^2 = 1$, $\sigma^2 = 1$, the comparison of system throughput between the NOMA and OMA strategies is illustrated by Figure2.6.

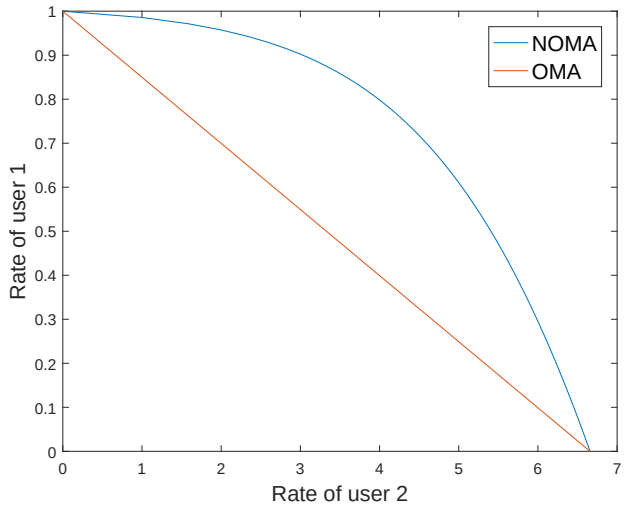

Figure 2.6: *Data rates of two users with NOMA and OMA strategies.*

2.4.2 Typical NOMA Strategy in Power Domain

NOMA in the power domain for the downlink is achieved by transmitting signals with superposition coding (SC) techniques at the base station and distinguishing signals with SIC techniques at mobile users [16]. A brief interpretation of SC for two users with QPSK modulation is given

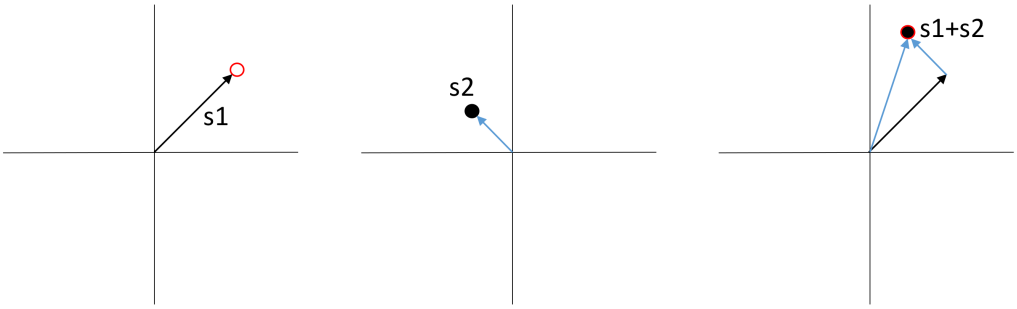

Figure 2.7: *An example of SC for two users.*

by Figure 2.7.

For multiple users, for example $N \geq 3$, the base station sends signals to all users simultaneously and the signal can be written as

$$x = \sqrt{P\beta_1}s_1(t) + \ldots + \sqrt{P\beta_N}s_N(t), \tag{2.35}$$

where $\beta_1 + \ldots + \beta_N = 1$ are the power coefficients, which are sorted in decreasing order

$\beta_1 > \ldots > \beta_N$.

In order to separate the required information from the SC signal, a SIC receiver should be applied to each user. The basic concept of SIC is expressed by Figure 2.8 for two-user NOMA with QPSK. It is noticeable that, even without noise or internal interference, user 1 can suc-

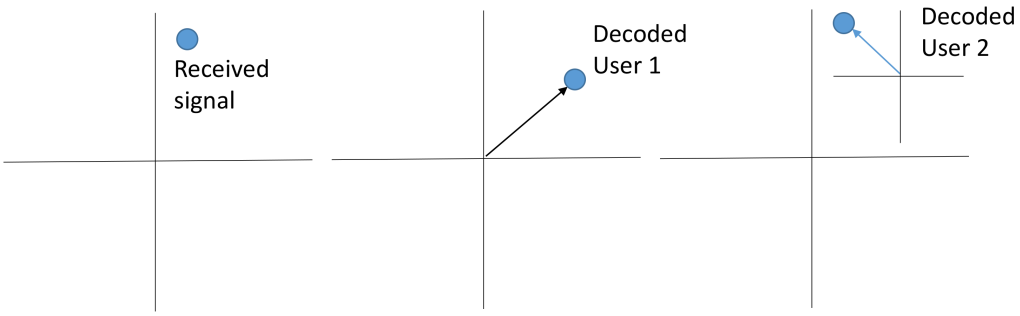

Figure 2.8: *An example of SIC for two users.*

cessively abstract the information only if the power assigned to user 2 is less than that to user 1. Extending this method to multi-user NOMA, the i-th user in a NOMA cluster receives the signal as

$$y_i = h_i \left(\sqrt{P\beta_1} s_1(t) + \ldots + \sqrt{P\beta_N} s_N(t) \right), \tag{2.36}$$

where $i = 1, \cdots, N$ is the user number, and these serial numbers are sorted in increasing order of channel gains $\left(|h|_1^2 \leq \cdots \leq |h|_N^2 \right)$ to guarantee the quality of service (QoS) for users on weak channels. To decode the desired signal, user i removes signals for other users as much as possible and treats the rest as noise. More specifically, user i first decodes the signal with the strongest power, i.e. β_1, and then removes it from the received signal. In the following, user i removes the current strongest signal of each round, until all the $(i-1)$ stronger signals are decoded and subtracted from the joint signal. Then, the processed signal can be expressed as

$$y_i' = h_i \left(\sqrt{P\beta_i} s_i(t) + \ldots + \sqrt{P\beta_N} s_N(t) \right), \tag{2.37}$$

and the corresponding SINR is given by

$$\gamma_i = \frac{P\beta_i |h|_i^2}{\sum\limits_{j=i+1}^{N} P\beta_j |h|_i^2 + \sigma^2}. \tag{2.38}$$

It is worth mentioning that (2.38) is achievable only if each SIC step runs successfully, i.e.

$\gamma_{k\to i} > \gamma_{th,k}$ is satisfied with any $0 < k < i$, where $\gamma_{th,k}$ denotes the threshold to demodulate and decode the signal for user k, $\gamma_{k\to i}$ is the SINR when user k trying to demodulate and decode the signals for user i.

2.5 Mathematical Preliminaries

2.5.1 Special Functions

In order to formulate the results of some integrals containing exponential functions, special functions are introduced in this thesis. The special functions are the general terms of some advanced transcendental functions. Transcendental functions are known as incomplete analytic terms of algebraic functions, and higher transcendental functions are transcendental functions whose components are not only elementary functions. Special functions are mostly defined to seek solutions to equations in physics, and are still becoming more multitudinous.

2.5.1.1 Gamma Function

The Gamma function $\Gamma(z)$ is the most frequently used special function in investigation works of wireless communication. Mathematically, it is motivated by finding a function to describe the curve-containing factorial series as the mappings of integer variables. In wireless communications, it is usually involved to analytically express the results of integrals containing power and exponential functions, which are closely related to the Gaussian process. For complex variable z with a positive real part, it can be defined through a convergent improper integral [17].

$$\Gamma(z) = \int_0^\infty t^{z-1}e^{-t}dt. \quad Rel(z) > 0 \tag{2.39}$$

Sometimes, definite integrals for such formulas are required, which conduces to the utility of upper and lower incomplete Gamma functions:

$$\Gamma(s,z) = \int_z^\infty t^{s-1}e^{-t}dt \quad Rel(s) > 0 \quad upper, \tag{2.40}$$

$$\gamma(s,z) = \int_0^z t^{s-1}e^{-t}dt \quad Rel(s) > 0 \quad lower. \tag{2.41}$$

2.5.1.2 Bessel Function

The Bessel function is wildly exploited in signal processing, electromagnet analysis and some physics domains. It can be defined by the solutions $y(x)$ of the differential equation which can be written as [17]:

$$x^2\frac{d^2y}{dx^2} + \frac{dy}{dx} + (x^2 - \alpha^2) = 0, \tag{2.42}$$

where the arbitrary complex number α is the order of the Bessel function. According to the multiformity of differential function (2.42), the Bessel function can be classified as the first kind $J_\alpha(x)$ and the second kind $Y_\alpha(x)$. As special cases, the modified Bessel function of the first and second kinds, $I_\alpha(z)$ and $K_\alpha(z)$ are defined by making the arguments of Bessel functions purely imaginary.

2.5.1.3 Hypergeometric Function

The hypergeometric function is defined by an infinite series of power functions [17], shown as

$${}_2F_1(a, b, ; c; z) = \sum_{n=0}^{\infty} \frac{(a)_n (b)_n}{(c)_n} \frac{z^n}{n!}, \quad |z| < 1, \tag{2.43}$$

where $(q)_n$ is given by

$$(q)_n = \begin{cases} 1 & n = 0 \\ q(q+1)\cdots(q+n-1) & n > 0 \end{cases}. \tag{2.44}$$

The arguments a, b and c refine the shape of the hypergeometric function. By adjusting the number of arguments, people can obtain generalised hypergeometric functions. As the limits of hypergeometric functions, confluent hypergeometric functions are utilised in this thesis as well.

2.5.1.4 Meijer's G-function

The general definition of the Meijer's G-function is given by an integral in the complex plane, which can be written as [17, 9.303]

$$\mathbf{G}_{p,q}^{m,n}\left(\left.\begin{matrix}a_1,\cdots,a_p\\ b_1,\cdots,b_q\end{matrix}\right|z\right)=\int_L\frac{1}{w\pi i}\int_L\frac{\sum_{j=1}^{m}\Gamma(b_j-s)\sum_{j=1}^{n}\Gamma(1-a_j+s)}{\sum_{j=m+1}^{q}\Gamma(1-b_j+s)\sum_{j=n+1}^{p}\Gamma(a_j-s)}z^s\mathrm{d}s. \tag{2.45}$$

In this thesis, all numerical examinations for expressions containing Meijer's G-function are operated with the help of the software Mathematica. It should be noticed that, the Meijer's G-function is a two-fold integral, which cannot be efficiently computed even by computers. Therefore, we find the simplification of the Meijer's G-function for the limit $z\to 0$ [18, Eq.07.34.06.0006.01], which consists of a series gamma functions. This simplification is applied several times in Chapter 3.

$$\begin{aligned}&G_{p,q}^{m,n}\left(z\left|\begin{smallmatrix}b_q,\ldots,a_n,a_{n+1},\ldots,a_p\\ b_1,\ldots,b_m,b_{m+1},\ldots,a_p\end{smallmatrix}\right.\right)=\\&\sum_{k=1}^{m}\frac{\prod\limits_{\substack{j=1\\ j\neq k}}^{m}\Gamma\left(b_j-b_k\right)\prod_{j=1}^{n}\Gamma\left(1-a_j+b_k\right)}{\prod_{j=n+1}^{p}\Gamma\left(a_j-b_k\right)\prod_{j=m+1}^{q}\Gamma\left(1-b_j+b_k\right)}z^{b_k}(1+\mathcal{O}(z))\\&\left(z\to 0\bigwedge p\le q\bigwedge\forall_{\{j,k\}\{j,k\}\in\mathbb{Z}\wedge j\neq k\wedge 1\le j\le m\wedge 1\le k\le m}\left(b_j-b_k\notin\mathbb{Z}\right)\right)\end{aligned} \tag{2.46}$$

Another important formula frequently used in this thesis is the definite integral containing two Meijer's G-functions, which is given by [18, Eq.07.34.21.0011.01]:

$$\begin{aligned}&\int_0^\infty x^{\alpha-1}\mathrm{G}_{u,v}^{s,t}\left(wx\left|\begin{smallmatrix}c_1,\ldots c_t,c_{t+1},\ldots,c_u\\ d_1,\ldots d_s,d_{s+1},\ldots,d_v\end{smallmatrix}\right.\right)\mathrm{G}_{p,q}^{m,n}\left(zx\left|\begin{smallmatrix}a_1,\ldots a_n,a_{n+1},\ldots,a_p\\ b_1,\ldots b_m,b_{m+1},\ldots,b_q\end{smallmatrix}\right.\right)\mathrm{d}x=\\&w^{-\alpha}\mathrm{G}_{v+p,u+q}^{m+t,n+s}\left(\frac{z}{w}\left|\begin{smallmatrix}a_1,\ldots,a_n,1-\alpha-d_1,\ldots,1-\alpha-d_s,1-\alpha-d_{s+1},\ldots,1-\alpha-d_v,a_{n+1},\ldots,a_p\\ b_1,\ldots,b_m,1-\alpha-c_1,\ldots,1-\alpha-c_t,1-\alpha-c_{t+1},\ldots,1-\alpha-c_u,b_{m+1},\ldots,b_q\end{smallmatrix}\right.\right).\end{aligned} \tag{2.47}$$

2.5.2 Order Statistics

In statistics, the k-th order statistic of a statistical sample is its k-th smallest value obtained from a group of samples following the same distribution. The pdf of the k-th smallest sample from a size n drawn from distribution X is given by [19]

$$f_{X_{(k)}}(x)=\frac{n!}{(k-1)!(n-k)!}[F_X(x)]^{k-1}[1-F_X(x)]^{n-k}f_X(x). \tag{2.48}$$

Chapter 3
Daul-hop κ-μ and η-μ Fading Channels

3.1 Introduction

3.1.1 Motivation

The dual-hop relaying technique [20, 21] has triggered enormous research interest in academia [22–24], because it can provide huge improvements in the throughput, coverage and energy consumption of wireless communication systems with little extra cost. Among various relaying protocols proposed in the literature, the AF protocol, in which an intermediate relay simply amplifies the received signal and forwards the scaled signal to the destination, has gained significant interest due to its simplicity and low implementation cost.

Many studies have appeared in the literature on the performance of dual-hop AF relaying systems. Thus far, the fundamental studies of system performance for AF relaying systems have been conducted in [25] and [26]. The performance of dual-hop AF relaying systems is in general well understood in widely used fading channels, such as Rayleigh, Rician, Nakagami-m and Weibull. For instance, the outage performance of AF relaying systems was studied in [22] for Rayleigh fading channels, and in [23] for Nakagami-m fading channels. While the bit error rate (BER) of dual-hop AF relaying transmission was analysed in [27] for the Rayleigh fading channel and in [28] for the Nakagami-m fading channel. The ergodic capacity of dual-hop AF relaying systems over Nakagami-m channels with different heuristic precoding schemes was also analysed in [29].

While these works have profoundly improved our understanding of the achievable performance of dual-hop AF relaying systems, a major limitation is that they are based on channel models that rely on the key assumption that the scatterers in the propagation environment are homogeneously distributed. Therefore, the results predicted by previous studies may fail to give an accurate performance account of practical scenarios in which the scatters are non-homogeneous.

Responding to these, versatile channel models, namely the generalised κ-μ and η-μ distributions were proposed in [6]. Since then, the performance of generalised κ-μ and η-μ fading models in various important communication systems has been examined (see [30] and references therein). Despite its importance, there are very few studies that have investigated the performance of dual-hop AF relaying systems over generalised κ-μ and η-μ fading channels. In [31] the moment-generating functions (MGF) of the dual-hop AF relaying systems over η-μ and κ-μ fading channels were derived, and the outage probabilities and average bit error probabilities were then obtained using the MGF. In a recent study by [32], the outage probability of dual-hop AF relaying systems over mixed κ-μ and η-μ fading channels was investigated. Therefore, there is intense demand to understand the important performance measures such as the ergodic capacity and error rate of dual-hop AF relaying systems in generalised κ-μ and η-μ fading channels.

Motivated by this, in this chapter, we present a thorough investigation of the error exponent of dual-hop AF systems in generalised κ-μ and η-μ fading channels. The error exponent was defined by [9]

$$E(R) := \limsup_{L\to\infty} \frac{-\ln P_e^{opt}(R,L)}{L}, \tag{3.1}$$

where $P_e^{opt}(R,L)$ is the average error probability of the optimal code of length L and rate R. It provides key insights into the tradeoff between information rate and the reliability of wireless communication systems, and can also help with the evaluation of the required codeword length given a predefined P_e. Due to the difficulty of deriving the exact expression for the error exponent, the author of [9] introduced the random coding error exponent (RCEE) and expurgated error exponents as computable tight upper bounds of the error exponents. Since then, Gallager's exponents, as a key performance indicator, have been widely studied [13, 33–38]. In the context of dual-hop AF relaying systems, the error exponents have been studied in [39] and [40] for Rayleigh and Nakagami-m fading channels, respectively.

3.1.2 Main Contributions

The main contribution of this chapter can be summarised as follows:

- We derive the exact analytical expressions of the pdf of end-to-end SNR for dual-hop AF relaying system over generalised η-μ and κ-μ fading channels.

- Based on the analytical pdf expression, numerical expressions are derived for the RCEE, cutoff rate, ergodic capacity and expurgated error exponent of dual-hop AF relaying systems. Simplified analytical expressions of the RCEE, cutoff rate and expurgated error exponent are obtained for high SNR regimes, which significantly reduces the computation time.

- With the help of the analytical expression of the RCEE, we characterise the required codeword length to achieve the predefined upper bound of error probability.

- It is shown that our analytical expressions include the previous results for the Rayleigh, Rician and Nakagami-m fading channels [40] as special cases. Also, the presented results can be extended to Hoyt and one-sided Gaussian fading channels as well which have not been reported elsewhere.

3.2 System Model

3.2.1 Dual-hop AF System

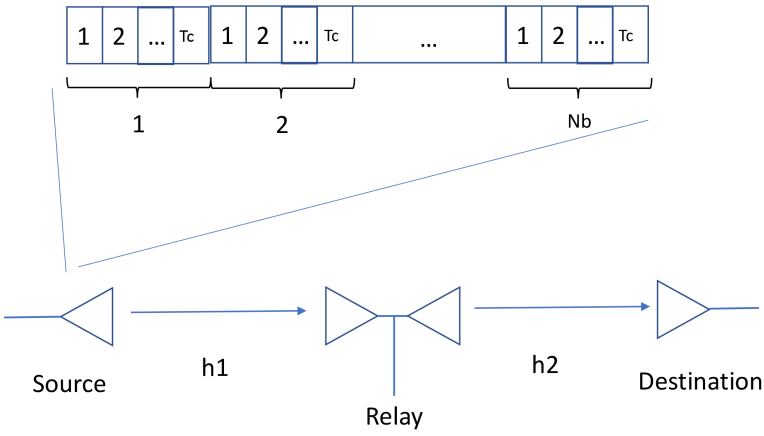

Figure 3.1: *A dual-hop AF relaying system transmitting block code sequence*

In this chapter, we consider a single antenna dual-hop AF relaying system. We assume block fading, such that the channel remains unchanged during T_c symbols. For N_b independent coherence intervals, the block codeword length is thus $N_b \times T_c$ symbol periods. Also, it is assumed that there is no direct communication link between the transmitter and receiver. Hence, the

received signal at the destination over the $T_c \times N_b$ symbol periods is given by

$$\mathbf{y}_k = h_2 G(h_1 \mathbf{x}_k + \mathbf{n}_{1,k}) + \mathbf{n}_{2,k}, \quad k = 1, 2, \ldots, N_b \tag{3.2}$$

where $\mathbf{x}_k \in \mathbb{C}^{1\times T_c}$ and $\mathbf{y}_k \in \mathbb{C}^{1\times T_c}$ denote the transmitted and received signal sequences, with $\mathbb{E}\{\mathbf{x}_{k,i}\mathbf{x}_{k,i}^{\dagger}\} = P$, $i = 1, \ldots, T_c$. Parameters h_1 and h_2 denote the fading coefficients of the first and second hops, respectively. Parameter G is the power gain of the relay. And $\mathbf{n}_i \sim \mathcal{CN}_{1,T_c}(0, \sigma^2)$ $(i = 1, 2)$ are the relay and destination AWGN vectors.

Therefore, the end-to-end SNR is given by

$$\gamma_{end} = \frac{\frac{P|h_1|^2}{\sigma^2}\frac{|h_2|^2}{\sigma^2}}{\frac{|h_2|^2}{\sigma^2} + \frac{1}{G^2\sigma^2}}. \tag{3.3}$$

Assuming the ideal relaying gain [1], i.e. $G^2 = \frac{1}{|h_1|^2}$, the end-to-end SNR at the destination is given by

$$\gamma_{end} = \frac{\gamma_1\gamma_2}{\gamma_1 + \gamma_2}, \tag{3.4}$$

where $\gamma_1 = \frac{P|h_1|^2}{\sigma^2} = \bar{\gamma}|h_1|^2$ and $\gamma_2 = \frac{P|h_2|^2}{\sigma^2} = \bar{\gamma}|h_2|^2$, $\bar{\gamma}$ is the average transmission SNR.

3.3 Gallager's Exponents of Dual-hop AF System over η-μ and κ-μ Fading Channels

This section presents a detailed performance investigation of the dual-hop AF relaying systems in generalised η-μ and κ-μ fading channels through the characterisation of the Gallager's exponents.

3.3.1 The η-μ channel and the $\kappa - \mu$ channel

The generalised η-μ distribution is normally used to analyse the performance of small-scale signals in a non-line-of-sight environment. According to [6], the pdf of the instantaneous SNR

[1] Please note, the adoption of the ideal relaying gain is mainly for analytical tractability. Nevertheless, it can serve as a tight upper bound for practical relaying gain such as $G^2 = \frac{P}{P|h_1|^2+\sigma^2}$, which also considers the added power caused by noise. Our model is widely used in the literature, for instance [22, 23, 40].

γ subject to η-μ fading can be expressed as:

$$f_{\gamma_{\eta-\mu}}(\gamma) = \frac{2\sqrt{\pi}\mu^{\mu+\frac{1}{2}}\phi^{\mu}\gamma^{\mu-\frac{1}{2}}\exp\left(-\frac{2\mu\gamma\phi}{\bar{\gamma}}\right)}{\Gamma(\mu)\psi^{\mu-\frac{1}{2}}\bar{\gamma}^{\mu+\frac{1}{2}}} I_{\mu-\frac{1}{2}}\left(\frac{2\mu\gamma\psi}{\bar{\gamma}}\right), \tag{3.5}$$

where $\bar{\gamma} = \mathbb{E}\{\gamma\}$, μ denotes the number of multipath clusters and $I_{\alpha}(\cdot)$ is the αth order modified Bessel function of the first kind. Parameters ψ and ϕ are defined differently in two formats:

Format 1: η denotes the scattered-wave power ratio between the in-phase and quadrature components in each multipath cluster and $0 < \eta < \infty$, then $\psi = \frac{\eta^{-1}-\eta}{4}$ and $\phi = \frac{2+\eta^{-1}+\eta}{4}$.

Format 2: η is the correlation coefficient between the in-phase and quadrature components in each multipath cluster and $-1 < \eta < 1$, then $\psi = \frac{1}{1-\eta^2}$ and $\phi = \frac{\eta}{1-\eta^2}$.

In this chapter, we use the definition of format 1. In addition, when coefficient $\eta = 1$ and replace μ with m, (3.5) becomes the Nakagami-m fading distribution.

Theorem 1. *The pdf of the end-to-end SNR of dual-hop AF relaying systems in η-μ fading channels is given by*

$$\begin{aligned} f_{\gamma}^{\eta-\mu}(\gamma) = &\sum_{m=0}^{\infty}\sum_{n=0}^{\infty}\sum_{a=0}^{2m}\sum_{b=0}^{2n} \frac{(-1)^b 2^{6-8\mu-4m-4n}\pi\bar{\gamma}^{-1}\mu\psi^{2m+2n}(m!n!)^{-1}\binom{2m}{a}\binom{2n}{b}}{\Gamma(\mu)^2\Gamma\left(m+\mu+\frac{1}{2}\right)\Gamma\left(n+\mu+\frac{1}{2}\right)\phi^{2\mu+2m+2n-1}} \\ &\times\Gamma\left(m+n-\frac{a}{2}-\frac{b}{2}+\frac{1}{2}\right) G_{1,2}^{2,0}\left(\frac{8\mu\phi\gamma}{\bar{\gamma}}\middle|\begin{matrix} 2\mu+m+n-\frac{a}{2}-\frac{b}{2}-\frac{1}{2} \\ 2\mu-1, 4\mu+2m+2n-1 \end{matrix}\right) \end{aligned} \tag{3.6}$$

where $G_{p,q}^{m,n}\left(x\middle|\begin{matrix} a_1,\cdots,a_p \\ b_1,\cdots,b_q \end{matrix}\right)$ is the Meijer's G-function [17], more details of which can be found in the background.

Proof. See Appendix A.1. □

Although this analytical expression involves infinite-term summations, the actual evaluation converges fairly quickly as shown in Figure 3.2, where 10^6-iteration Monte-Carlo simulations are provided. We can find the Figure behind Theorem 2. As can be observed in Figure 3.2, the infinite summation can converge quickly within $m = n = 5$, hence it can be efficiently evaluated. In addition, the analytical pdf expression is amenable to further mathematical ma-

nipulations, and enables the characterisation of key performance indicators, e.g. the Gallager's exponents. In the following, this pdf expression is used in the analysis of the error exponents.

The generalised κ-μ distribution has advantages in representing small-scale fading signal in line-of-sight environments [6]. The pdf of the instantaneous SNR γ with mean $\bar{\gamma}$ subject to κ-μ fading can be written as

$$f_{\gamma_{\kappa,\mu}}(\gamma) = \frac{\mu(1+\kappa)^{\frac{\mu+1}{2}}\gamma^{\frac{\mu-1}{2}}}{\kappa^{\frac{\mu-1}{2}}e^{\mu\kappa}\overline{\gamma}^{\frac{\mu+1}{2}}} e^{-\frac{\mu(1+\kappa)\gamma}{\overline{\gamma}}} I_{\mu-1}\left(2\mu\sqrt{\frac{\kappa(1+\kappa)\gamma}{\overline{\gamma}}}\right) \tag{3.7}$$

where $\kappa > 0$ is the power ratio between the dominant components and the scattered waves, and μ is linked to the number of multipath clusters. When $k \to 0$, expression (3.7) leads to the Nakagami-m distribution and it becomes a Rayleigh distribution by setting $k \to 0, \mu = 1$.

Theorem 2. *The pdf of the end-to-end SNR for the dual-hop AF κ-μ fading SISO channel is derived as:*

$$f_{\gamma}^{\kappa-\mu}(\gamma) = \sum_{m=0}^{\infty}\sum_{n=0}^{\infty}\sum_{a=0}^{m}\sum_{b=0}^{n} \frac{(-1)^{n-b}\Gamma\left(\frac{m}{2}+\frac{n}{2}-\frac{a}{2}-\frac{b}{2}+\frac{1}{2}\right)\binom{m}{a}\binom{n}{b}\mu^{1+m+n}(1+\kappa)}{2^{2\mu+m+n-3}\overline{\gamma}\mathrm{e}^{2\mu\kappa}m!n!\Gamma(m+\mu)\Gamma(n+\mu)\kappa^{-m-n}} \times G_{1,2}^{2,0}\left(\frac{4\mu(1+\kappa)\gamma}{\overline{\gamma}}\middle| \begin{matrix}\mu+\frac{m}{2}+\frac{n}{2}-\frac{a}{2}-\frac{b}{2}-\frac{1}{2}\\ \mu-1, 2\mu+m+n-1\end{matrix}\right). \tag{3.8}$$

Proof. See Appendix A.2 □

It can be observed that the series related to the pdf of dual-hop $\kappa-\mu$ fading converge slower than those for the dual-hop $\eta-\mu$ fading channel. According to our calculation, the difference between finite-term analytical results and simulation results with different η, μ and γ are quite small. When $m = n = 5$, $f_{sim}(\gamma) - f_{m=n=5}(\gamma) < 10^{-4}$ everywhere, and when $m = n = 10$, $f_{sim}(\gamma) - f_{m=n=10}(\gamma) < 10^{-6}$. Similarly for the dual-hop $\kappa-\mu$ fading channel, $f_{sim}(\gamma) - f_{m=n=10}(\gamma) < 10^{-4}$ and $f_{sim}(\gamma) - f_{m=n=15}(\gamma) < 10^{-6}$. It is clear that in Figure 3.2 that the whole curve of the finite-term analytical results match the simulation results well when $m = n \geq 5$ for $\eta-\mu$ distribution and $m = n \geq 10$ for $\kappa-\mu$ distribution.

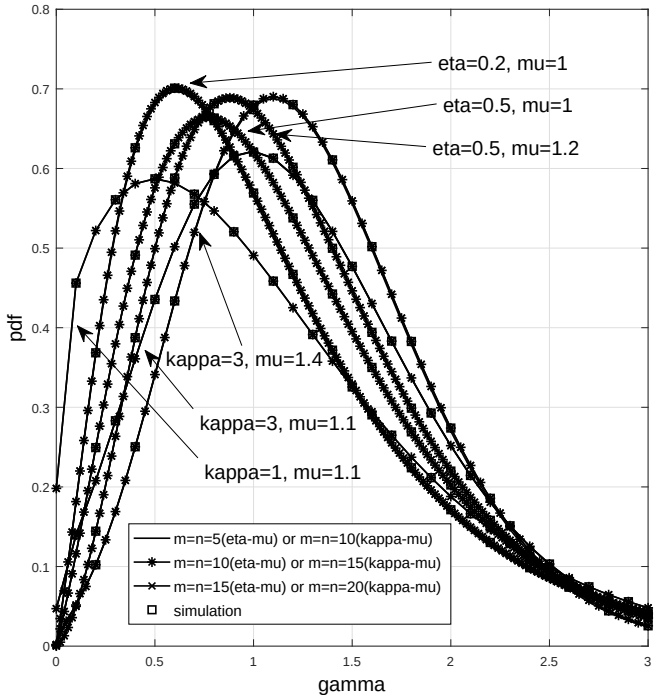

Figure 3.2: *The pdf of end-to-end SNR over η-μ and κ-μ fading with $\bar{\gamma} = 3$.*

3.3.2 Error exponents for the $\eta - \mu$ channel

3.3.2.1 Random Coding Error Exponent

Based on the definition and mathematical model of the RCEE given in the previous section, the analytical expression of the RCEE of the dual-hop AF relaying system over the η-μ fading channel is derived as follows.

Proposition 1. *The analytical expression of the RCEE of dual-hop AF relaying systems in the η-μ fading channels can be expressed as*

$$E_r(R,T_c) = \max_{0\le\rho\le 1}\left\{\max_{0\le\beta\le 1}\left\{\mathcal{A}(\rho,\beta) - \frac{1}{T_c}\ln\left\{\sum_{m=0}^{\infty}\sum_{n=0}^{\infty}\sum_{a=0}^{2m}\sum_{b=0}^{2n}\frac{(-1)^b\pi\mu\psi^{2m+2n}}{\phi^{2m+2n+2\mu-1}\overline{\gamma}}\right.\right.\right.$$
$$\times\frac{2^{6-8\mu-4m-4n}\binom{2m}{a}\binom{2n}{b}\beta\Gamma\left(m+n-\frac{a}{2}-\frac{b}{2}+\frac{1}{2}\right)}{(1+\rho)^{-1}\Gamma\left(n+\mu+\frac{1}{2}\right)m!n!\Gamma\left(m+\mu+\frac{1}{2}\right)\Gamma(\mu)^2\Gamma(T_c\rho)}$$
$$\left.\left.\left.\times\ G_{2,3}^{3,1}\left(\frac{8\mu\phi\beta(1+\rho)}{\overline{\gamma}}\middle|\begin{matrix}0, 2\mu+m+n-\frac{a}{2}-\frac{b}{2}-\frac{1}{2}\\ 2\mu-1, 4\mu+2m+2n-1, T_c\rho-1\end{matrix}\right)\right\}\right\} - \rho R\right\}. \tag{3.9}$$

Proof. Shown in Chapter 2, the RCEE can be written as

$$E_r(R,T_c)=\max_{0\le\rho\le1}\left\{\max_{0\le\beta\le1}\widetilde{E}_0(\rho,\beta,T_c)-\rho R\right\},\text{in which} \tag{3.10}$$

$$\widetilde{E}_0(\rho,\beta,T_c)=\mathcal{A}(\rho,\beta)-\frac{1}{T_c}\ln\left\{\mathbb{E}_\gamma\left[\left(1+\frac{\gamma}{\beta(1+\rho)}\right)^{-T_c\rho}\right]\right\}, \tag{3.11}$$

where $\mathcal{A}(\rho,\beta)=(1+\rho)(1-\beta)+(1+\rho)\ln(\beta)$. Because it is difficult to substitute (3.6) into (3.11) directly, we represent (3.11) in the form of the Meijer's G-function

$$\begin{aligned}\widetilde{E}_0(\rho,\beta,T_c)&=\mathcal{A}(\rho,\beta)-\frac{1}{T_c}\ln\left\{\mathbb{E}_\gamma\left(\left(1+\frac{\gamma}{\beta(1+\rho)}\right)^{-T_c\rho}\right)\right\}\\&=\mathcal{A}(\rho,\beta)-\frac{1}{T_c}\ln\left\{\mathbb{E}_\gamma\left(\Gamma(T_c\rho)^{-1}G_{1,1}^{1,1}\left(\frac{\gamma}{\beta(1+\rho)}\middle|\begin{matrix}1-T_c\rho\\0\end{matrix}\right)\right)\right\}.\end{aligned} \tag{3.12}$$

This transform is with the aid of [18, Eq.07.34.03.0271.01] given bellow.

$$\mathrm{G}_{1,1}^{1,1}\left(z\middle|\begin{smallmatrix}a\\b\end{smallmatrix}\right)=\Gamma(1-a+b)z^b(z+1)^{a-b-1}. \tag{3.13}$$

Then, we derive (3.9) by substituting (3.6) into (3.12):

$$\begin{aligned}\widetilde{E}_0(\rho,\beta,T_c)=&\mathcal{A}(\rho,\beta)-\frac{1}{T_c}\ln\left\{\int_0^\infty f_\gamma^{\eta-\mu}(x)\Gamma(T_c\rho)^{-1}G_{1,1}^{1,1}\left(\frac{x}{\beta(1+\rho)}\middle|\begin{matrix}1-T_c\rho\\0\end{matrix}\right)\mathrm{d}x\right\}\\
=&\mathcal{A}(\rho,\beta)-\frac{1}{T_c}\ln\left\{\sum_{m=0}^{\infty}\sum_{n=0}^{\infty}\sum_{a=0}^{2m}\sum_{b=0}^{2n}\frac{(-1)^b2^{6-8\mu-4m-4n}\pi\overline{\gamma}^{-1}\mu\psi^{2m+2n}}{m!n!\Gamma(\mu)^2\Gamma\left(m+\mu+\frac{1}{2}\right)\Gamma\left(n+\mu+\frac{1}{2}\right)}\right.\\
&\times\binom{2m}{a}\binom{2n}{b}\Gamma\left(m+n-\frac{a}{2}-\frac{b}{2}+\frac{1}{2}\right)\Gamma(T_c\rho)^{-1}\phi^{1-2\mu-2m-2n}\\
&\left.\times\int_0^\infty G_{1,2}^{2,0}\left(\frac{8\mu\phi x}{\overline{\gamma}}\middle|\begin{matrix}2\mu+m+n-\frac{a}{2}-\frac{b}{2}-\frac{1}{2}\\2\mu-1,4\mu+2m+2n-1\end{matrix}\right)G_{1,1}^{1,1}\left(\frac{x}{\beta(1+\rho)}\middle|\begin{matrix}1-T_c\rho\\0\end{matrix}\right)\mathrm{d}x\right\}\\
=&\mathcal{A}(\rho,\beta)-\frac{1}{T_c}\ln\left\{\sum_{m=0}^{\infty}\sum_{n=0}^{\infty}\sum_{a=0}^{2m}\sum_{b=0}^{2n}\frac{(-1)^b2^{6-8\mu-4m-4n}\pi\mu\psi^{2m+2n}}{\phi^{2m+2n+2\mu-1}\overline{\gamma}\Gamma(T_c\rho)\Gamma(\mu)^2}\right.\\
&\times\frac{\binom{2m}{a}\binom{2n}{b}\beta\Gamma\left(m+n-\frac{a}{2}-\frac{b}{2}+\frac{1}{2}\right)}{(1+\rho)^{-1}\Gamma\left(n+\mu+\frac{1}{2}\right)m!n!\Gamma\left(m+\mu+\frac{1}{2}\right)}\\
&\left.\times G_{2,3}^{3,1}\left(\frac{8\mu\phi\beta(1+\rho)}{\overline{\gamma}}\middle|\begin{matrix}0,2\mu+m+n-\frac{a}{2}-\frac{b}{2}-\frac{1}{2}\\2\mu-1,4\mu+2m+2n-1,T_c\rho-1\end{matrix}\right)\right\}\end{aligned} \tag{3.14}$$

The integration is according to [18, Eq.07.34.21.0011.01], which is also shown by (2.47).

Substituting the (3.14) into (3.10), equation (3.9) is finally obtained. □

To reduce the computation time of Meijer's G-functions, we look into the high SNR regime, and present an accurate approximation consisting of Gamma functions.

Corollary 1. *The RCEE of the dual-hop AF η-μ SISO fading channel at high SNR regime is given by*

$$
\begin{aligned}
&E_r^{\infty}(R,T_c) = \\
&\max_{0\le\rho\le 1}\left\{\max_{0\le\beta\le 1}\{\mathcal{A}(\rho,\beta) - \frac{1}{T_c}\ln\left\{\sum_{m=0}^{\infty}\sum_{n=0}^{\infty}\sum_{a=0}^{2m}\sum_{b=0}^{2n}\frac{(-1)^b 2^{6-8\mu-4m-4n}\pi\mu\psi^{2m+2n}}{\overline{\gamma}\phi^{2m+2n+2\mu-1}\Gamma(T_c\rho)\Gamma(\mu)^2}\right.\right. \\
&\times\frac{\binom{2m}{a}\binom{2n}{b}\beta(1+\rho)\Gamma\left(m+n-\frac{a}{2}-\frac{b}{2}+\frac{1}{2}\right)}{m!n!\Gamma\left(n+\mu+\frac{1}{2}\right)\Gamma\left(m+\mu+\frac{1}{2}\right)}\left(\frac{\Gamma(2\mu+2m+2n)\Gamma(T_c\rho-2\mu)Z_1^{2\mu-1}}{\Gamma(2\mu)^{-1}\Gamma\left(m+n-\frac{a}{2}-\frac{b}{2}+\frac{1}{2}\right)}\right. \\
&+\frac{\Gamma(-2\mu-2m-2n)\Gamma(4\mu+2m+2n)}{\Gamma(T_c\rho-4\mu-2m-2n)^{-1}\Gamma\left(-2\mu-m-n-\frac{a}{2}-\frac{b}{2}+\frac{1}{2}\right)}Z_1^{4\mu+2m-2n-1} \\
&\left.\left.\left.+\frac{\Gamma(2\mu-T_c\rho)\Gamma(4\mu+2m+2n-T_c\rho)\Gamma(T_c\rho)}{\Gamma\left(2\mu+m+n-\frac{a}{2}-\frac{b}{2}-T_c\rho+\frac{1}{2}\right)}Z_1^{T_c\rho-1}\right)\right\}\right\} - \rho R\Bigg\}, \qquad (3.15)
\end{aligned}
$$

where $Z_1 = \left(\frac{8\mu\phi\beta(1+\rho)}{\overline{\gamma}}\right)$.

Proof. In (3.9), we know $\frac{8\mu\phi\beta(1+\rho)}{\overline{\gamma}} \to 0$ when $\overline{\gamma}\to\infty$. Based on this condition, we derive the approximation at high SNR regimes in Corollary 1 with the help of [18, Eq.07.34.06.0006.01], shown in (2.46). □

The asymptotic expression (3.15) consisting of a group of Gamma functions consumes much less time for calculation than the analytical expression (3.9) containing Meijer's G-function. The Meijer's G-function is a general numeric integral result for a group of Gamma functions. That means, if a general numeric integral consists of K multiplication terms, the calculation of asymptotic expressions should require $\frac{1}{K}$ of time needed for the analytical expressions. The accuracy of the simplification (3.15) is presented in Figure 3.4.

3.3.2.2 Expurgated Error Exponent

Corollary 2. *For the expurgated error exponent of the dual-hop AF relaying systems in η-μ fading channels, the analytical expression and the simplified approximation at high-SNR regimes are given by*

$$
\begin{aligned}
&E_{ex}(R,T_c) = \\
&\max_{\rho\geq 1}\left\{\max_{0\leq\beta\leq 1}\left\{\mathcal{A}'(\rho,\beta) - \frac{1}{T_c}\ln\left\{\sum_{m=0}^{\infty}\sum_{n=0}^{\infty}\sum_{a=0}^{2m}\sum_{b=0}^{2n}\frac{(-1)^b 2^{7-8\mu-4m-4n}}{\overline{\gamma}\phi^{2m+2n+2\mu-1}}\right.\right.\right. \\
&\times\binom{2m}{a}\binom{2n}{b}\frac{\beta\rho\pi\mu\psi^{2m+2n}\Gamma\left(m+n-\frac{a}{2}-\frac{b}{2}+\frac{1}{2}\right)}{m!n!\Gamma\left(n+\mu+\frac{1}{2}\right)\Gamma\left(m+\mu+\frac{1}{2}\right)\Gamma(T_c\rho)\Gamma(\mu)^2} \\
&\left.\left.\left.\times G_{2,3}^{3,1}\left(\frac{16\mu\phi\beta\rho}{\overline{\gamma}}\middle|\begin{matrix}0, 2\mu+m+n-\frac{a}{2}-\frac{b}{2}-\frac{1}{2}\\ 2\mu-1, 4\mu+2m+2n-1, T_c\rho-1\end{matrix}\right)\right\}\right\} - \rho R\right\},
\end{aligned}
\tag{3.16}
$$

and

$$
\begin{aligned}
&E_{ex}^{\infty}(R,T_c) = \\
&\max_{\rho\geq 1}\left\{\max_{0\leq\beta\leq 1}\left\{\mathcal{A}'(\rho,\beta) - \frac{1}{T_c}\ln\left\{\sum_{m=0}^{\infty}\sum_{n=0}^{\infty}\sum_{a=0}^{2m}\sum_{b=0}^{2n}\frac{(-1)^b 2^{7-8\mu-4m-4n}\pi\mu\psi^{2m+2n}}{\overline{\gamma}\phi^{2m+2n+2\mu-1}\Gamma(T_c\rho)\Gamma(\mu)^2}\right.\right.\right. \\
&\times\frac{\binom{2m}{a}\binom{2n}{b}\rho\Gamma\left(m+n-\frac{a}{2}-\frac{b}{2}+\frac{1}{2}\right)}{m!n!\beta^{-1}\Gamma\left(m+\mu+\frac{1}{2}\right)\Gamma\left(n+\mu+\frac{1}{2}\right)}\left(\frac{\Gamma(2\mu+2m+2n)\Gamma(T_c\rho-2\mu)}{\Gamma\left(m+n-\frac{a}{2}-\frac{b}{2}+\frac{1}{2}\right)}Z_2^{2\mu-1}\right. \\
&+\frac{\Gamma(-2\mu-2m-2n)\Gamma(T_c\rho-4\mu-2m-2n)}{\left(\Gamma(4\mu+2m-2n)\right)^{-1}\Gamma\left(\frac{1}{2}-2\mu-m-n-\frac{a}{2}-\frac{b}{2}\right)}Z_2^{4\mu+2m+2n-1} \\
&\left.\left.\left.+\frac{\Gamma(2\mu-T_c\rho)\Gamma(4\mu+2m+2n-T_c\rho)\Gamma(T_c\rho)}{\Gamma\left(2\mu+m+n-\frac{a}{2}-\frac{b}{2}-T_c\rho+\frac{1}{2}\right)}Z_2^{T_c\rho-1}\right)\right\}\right\} - \rho R\right\},
\end{aligned}
\tag{3.17}
$$

respectively, where $Z_2 = \left(\frac{16\mu\phi\beta\rho}{\overline{\gamma}}\right)$.

Proof. The definition of expurgated error exponent is given by

$$
E_{ex}(R,T_c) = \max_{\rho\geq 1}\left\{\max_{0\leq\beta\leq 1}\tilde{E}_x(\rho,\beta,T_c) - \rho R\right\},
\tag{3.18}
$$

in which

$$
\tilde{E}_x(\rho,\beta,T_c) = \mathcal{A}'(\rho,\beta) - \frac{1}{T_c}\ln\left\{\mathbb{E}_\gamma\left[\left(1+\frac{\gamma}{2\beta\rho}\right)^{-T_c\rho}\right]\right\},
\tag{3.19}
$$

where $\mathcal{A}'(\rho,\beta) = 2\rho(1-\beta) + 2\rho\ln(\beta)$. For the convenience of the following integral, (3.19) is firstly rewritten in the form of Meijer's G-function with the aid of [18, Eq.07.34.03.0271.01], which is shown in (3.13):

$$\tilde{E}_x(\rho,\beta,T_c) = \mathcal{A}'(\rho,\beta) - \frac{1}{T_c}\ln\left\{\mathbb{E}_\gamma\left(\Gamma(T_c\rho)^{-1}G_{1,1}^{1,1}\left(\frac{\gamma}{2\rho\beta}\middle|\begin{matrix}1-T_c\rho\\0\end{matrix}\right)\right)\right\}. \quad (3.20)$$

The remaining derivation uses the same mathematical manipulations for Proposition 1 and Corollary 1. Substituting (3.6) into (3.20), equation (3.16) in Corollary 2 can be derived according to [18, Eq.07.34.21.0011.01], which is shown in (2.47). In high-SNR regime, with the help of [18, Eq.07.34.06.0006.01], which is shown by (2.46), and supposing $\frac{16\mu\phi\beta\rho}{\bar{\gamma}} \to 0$ in equation (3.16), the simplified approximation of expurgated error exponent at high SNR regime is obtained as (3.17). □

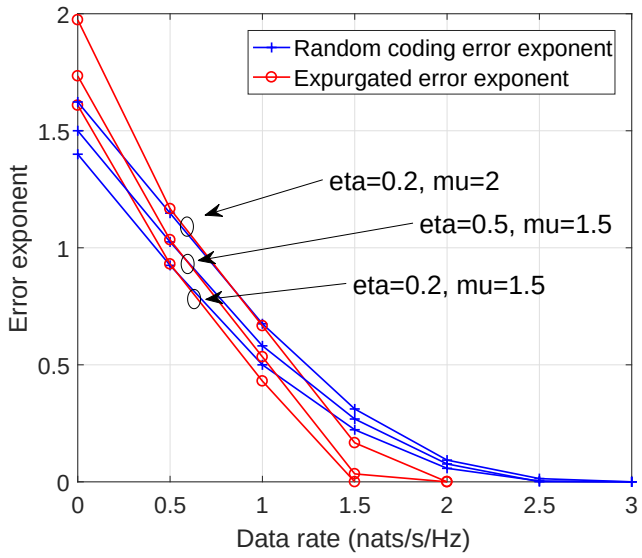

Figure 3.3: *The simulation and analytical results for the RCEE and expurgated error exponent of dual-hop AF η-μ fading SISO channel for selected value of η and μ with $\bar{\gamma} = 15dB$ and $T_c = 5$.*

Figure 3.3 compares the performance of RCEE $\left(E_r^{\eta-\mu}(R,T_c)\right)$ and the expurgated error exponent $\left(E_{ex}^{\eta-\mu}(R,T_c)\right)$ as a function of information rate R with different values of η and μ, where $\bar{\gamma} = 15$dB and $T_c = 5$. It is clear that both the RCEE and the expurgated error exponent reduce with increasing data rate R. With relatively small data rates, expurgated error exponents are greater than the corresponding RCEEs, and when data rates approach their limits (ergodic capacities), RCEEs are larger than the corresponding expurgated error exponents. Therefore,

we would better apply expurgated coding methods when making reliable communication, and apply random codding methods when making high-speed transmission. It should be noted that both parameters η and μ improve the error exponents performance when increasing, but the impact of μ on the error exponents is more significant than η.

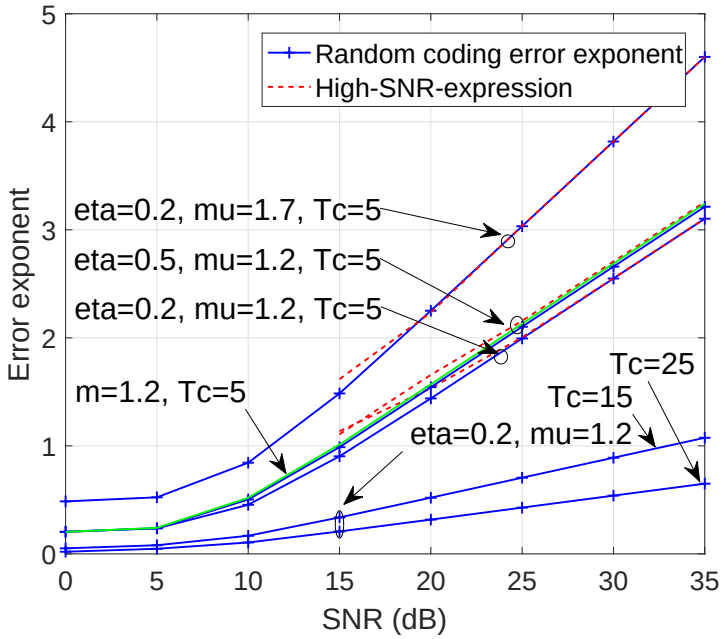

Figure 3.4: *Analytical results for the RCEE and high-SNR approximation of dual-hop AF η-μ fading SISO channel for selected value of η and μ with $R = 1$.*

Figure 3.4 illustrates the analytical results and approximation in the high SNR regime for the RCEE with selected parameters η and μ with $R = 1$ nats/s/Hz. As can be clearly seen, the RCEE increases with SNR, η (when $\eta < 1$) and μ as expected. Moreover, the simplified approximation results match very well at high SNR, when $\gamma \geq 20$dB. With the same value $Tc = 5$, it is obvious that parameter μ, which is related to the channel diversity, strongly impacts the RCEE, and η, which indicates the in-phase and quadrature power ratio, only slightly affects the RCEE. In addition, we present the effect of channel stability here. With the same parameters $\eta = 0.2$ and $\mu = 1.2$, the RCEE obviously reduces with larger Tc. We can summarize that, for the $\eta - \mu$ channel, the RCEE is significantly affected by the diversity order both in the time and the spatial domain, and is slightly affected by the in-phase and quadrature power ratio. The green line indicates a special case of $\eta - \mu$ channel, with $\eta = 1$, $\mu = 1.2$. According to [6], it is also the RCEE for the Nakagami-m channel with m=1.2. We can notice that, with same μ and Tc, all curves subject to $\eta - \mu$ channel fading with $\eta \neq 1$ are below the curve subject

to Nakagama-m channel fading where $m = \mu$. According to the definition of $\eta - \mu$ channel fading, when $\eta = 1$ (the Nakagami-m channel fading), two signal components carry the same power and the system can achieve the highest frequency efficient. On the contrary, when $\eta = 0$ or $\eta = \infty$, the system completely loses the in-phase or quadrature component, only a half of channel efficiency can be applied. The model of $\eta - \mu$ channel fading allow us to observe and analyse al intermediate situations.

SNR (dB)	$\eta = 0.2$ $\mu = 1.5$	$\eta = 0.2$ $\mu = 2$	$\eta = 0.5$ $\mu = 1.5$	$\eta = 0.5$ $\mu = 2$
10	202	147	162	124
20	15	11	14	10
30	7	5	6	5

Table 3.1: *Required code lengths L_r for the dual-hop AF η-μ fading SISO channel to achieve the predefined upper bound of error probabilities $P_e^r = 10^{-6}$ with $R = 1$ nats/s/Hz and $T_c = 5$.*

Table 3.1 shows the effects of parameters η and μ on the required code length of dual-hop AF SISO systems over η-μ fading channel with different SNR. The code length is estimated to achieve the predefined upper bound of error probability $P_e^{E_r} = 10^{-6}$ at the information rate $R = 1$ nats/s/Hz. The required code length $L = T_c \times \lceil N_b \rceil$ is obtained by solving the following equation involving N_b [11]

$$P_e^{E_r} = \frac{8\pi e^2 (1-\beta)^2 N_b}{T_c} \times \exp\{-N_b T_c \, E_r \, (R, T_c)\} \tag{3.21}$$

We see that, when $\eta < 1$, increasing both the parameters η and μ decreases the required code length, and the effect of μ is more significant than η. For instance, when SNR=10dB and $\eta = 0.2$, the required codeword length decreases 27.23% as μ increases from 1.5 to 2.0. However, the required codeword length only decreases 19.8% as η increases from 0.2 to 0.5 when $\mu = 1.5$.

3.3.2.3 Cutoff Rate

Corollary 3. *The cutoff rate R_0 of dual-hop AF relaying systems in η-μ fading channels is derived as*

$$R_0 = -\frac{1}{T_c}\ln\left\{\sum_{m=0}^{\infty}\sum_{n=0}^{\infty}\sum_{a=0}^{2m}\sum_{b=0}^{2n}\frac{(-1)^b 2^{7-8\mu-4m-4n}\pi\overline{\gamma}^{-1}\mu\phi^{1-2\mu-2m-2n}\psi^{2m+2n}}{\Gamma(T_c)\Gamma(\mu)^2\Gamma\left(m+\mu+\frac{1}{2}\right)\Gamma\left(n+\mu+\frac{1}{2}\right)m!n!}\right.$$
$$\left.\times\Gamma\left(m+n-\frac{a}{2}-\frac{b}{2}+\frac{1}{2}\right)G_{2,3}^{3,1}\left(\frac{16\mu\phi}{\overline{\gamma}}\middle|\begin{matrix}0, 2\mu+m+n-\frac{a}{2}-\frac{b}{2}-\frac{1}{2}\\ 2\mu-1, 4\mu+2m+2n-1, T_c-1\end{matrix}\right)\right\}. \tag{3.22}$$

It should be noticed that the parameter T_c in formula (3.22) is inversely proportional to the cutoff rate, which indicates how communication reliability impacts the information rate. This trend is presented more clearly in Figure 3.5.

Proof. Using expressions (3.6), (2.20) and the integration formula provided by [18, Eq.07.34.21.0011.01], the cutoff rate of dual-hop AF η-μ fading SISO channel (3.22) can be derived with some simple algebraic manipulations. More conveniently, We can obtain the expression of R_0 by substituting $\rho = 1$ and $\beta = 1$ into the corresponding part of (3.9). □

Corollary 4. *The simplified approximation of cutoff rate for dual-hop AF relaying systems in η-μ fading channels in the high SNR regime is given by*

$$R_0^{\infty} =$$
$$-\frac{1}{T_c}\ln\left\{\sum_{m=0}^{\infty}\sum_{n=0}^{\infty}\sum_{a=0}^{2m}\sum_{b=0}^{2n}\frac{(-1)^b 2^{7-8\mu-4m-4n}\pi\mu\psi^{2m+2n}\Gamma\left(m+n-\frac{a}{2}-\frac{b}{2}+\frac{1}{2}\right)\binom{2m}{a}\binom{2n}{b}}{m!n!\overline{\gamma}\phi^{2m+2n+2\mu-1}\Gamma(T_c)\Gamma(\mu)^2\Gamma\left(m+\mu+\frac{1}{2}\right)\Gamma(n+\mu+\frac{1}{2})}\right.$$
$$\times\left(\frac{\Gamma(2\mu+2m+2n)\Gamma(T_c-2\mu)}{\Gamma(2\mu)^{-1}\Gamma\left(m+n-\frac{a}{2}-\frac{b}{2}+\frac{1}{2}\right)}Z_3^{2\mu-1}+\frac{\Gamma(-2\mu-2m-2n)\Gamma(T_c-4\mu-2m-2n)}{\Gamma\left(-2\mu-m-n-\frac{a}{2}-\frac{b}{2}+\frac{1}{2}\right)}\right.$$
$$\left.\left.\times\Gamma(4\mu+2m+2n)Z_3^{4\mu+2m-2n-1}+\frac{\Gamma(2\mu-T_c)\Gamma(4\mu+2m+2n-T_c)\Gamma(T_c)}{\Gamma\left(2\mu+m+n-\frac{a}{2}-\frac{b}{2}-T_c\rho+\frac{1}{2}\right)}Z_3^{T_c-1}\right)\right., \tag{3.23}$$

where $Z_3 = \left(\frac{16\mu\phi}{\overline{\gamma}}\right)$.

Proof. This approximation can be derived from expression (3.23) with the help of [18, Eq.07.34.06.0006.01]. It can be obtained by directly substituting $\rho = 1$ and $\beta = 1$ into the

corresponding part of (3.15). □

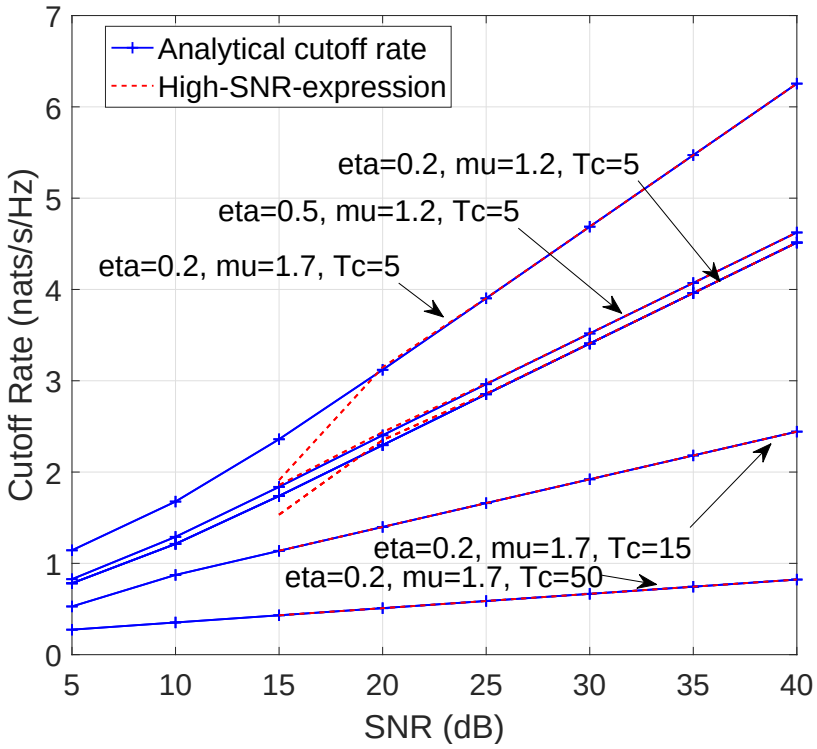

Figure 3.5: *Analytical results of the cutoff rate and high-SNR approximation of dual-hop AF η-μ fading SISO channel with selected values of η and μ.*

Figure 3.5 shows the cutoff rate R_0 with selected parameters η and μ with $T_c = 5$. It shows that the cutoff rate increases with SNR, η and μ, but the effect of μ on the value of cutoff rate is more pronounced than η. Similar to in Figure 3.4, when $\bar{\gamma} \geq 20$dB, the asymptotic expression could match the cutoff rates very accurately. Similar to the RCEE, the cutoff rates of the AF dual-hop system are significantly affected by the parameter μ but are only slightly impacted by η. In addition, the curves represent the tradeoff between information rate and reliability of block-coding communication by showing that the cutoff rate decreases with the channel coherence time T_c.

3.3.2.4 Ergodic Capacity

Corollary 5. *The ergodic capacity of dual-hop AF relaying systems in η-μ fading channels can be expressed as*

$$\langle C\rangle = \sum_{m=0}^{\infty}\sum_{n=0}^{\infty}\sum_{a=0}^{2m}\sum_{b=0}^{2n}\frac{(-1)^b 2^{6-8\mu-4m-4n}\pi\mu\psi^{2m+2n}\phi^{1-2\mu-2m-2n}\binom{2m}{a}\binom{2n}{b}}{\overline{\gamma}\Gamma(\mu)^2\Gamma\left(m+\mu+\frac{1}{2}\right)m!n!\Gamma\left(n+\mu+\frac{1}{2}\right)\Gamma\left(m+n-\frac{a}{2}-\frac{b}{2}+\frac{1}{2}\right)} \times G_{3,4}^{4,1}\left(\frac{8\mu\phi}{\overline{\gamma}}\middle|\begin{matrix}-1,0,2\mu+m+n-\frac{a}{2}-\frac{b}{2}-\frac{1}{2}\\ 2\mu-1,4\mu+2m+2n-1,-1,-1\end{matrix}\right). \tag{3.24}$$

Proof. We can express the ergodic capacity in nat as

$$\langle C\rangle \triangleq \mathbb{E}_{\gamma}[\ln(1+\gamma)], \tag{3.25}$$

where γ is the instantaneous SNR. According to [41, eq.(2.24.3.1)],
$\mathrm{G}_{1,2}^{2,2}\left(z\middle|\begin{smallmatrix}a,a\\ a,a-1\end{smallmatrix}\right) = z^{a-1}\ln(1+z)$, we represent equation (3.25) as

$$\langle C\rangle \triangleq \mathbb{E}_{\gamma}[\ln(1+\gamma)] \triangleq \mathbb{E}_{\gamma}\left\{G_{2,2}^{1,2}\left(\gamma\middle|\begin{matrix}1,1\\ 1,0\end{matrix}\right)\right\} = \int_0^{\infty} f_{\gamma_{\eta-\mu}}(x)G_{2,2}^{1,2}\left(x\middle|\begin{matrix}1,1\\ 1,0\end{matrix}\right)\mathrm{d}x. \tag{3.26}$$

Combining (3.6) and (3.26) and applying the integral formula provided by (2.47), the expression of ergodic capacity for the dual-hop AF SISO system over η-μ channel is derived. □

3.3.3 Error exponents for the κ-μ Channel

Proposition 2. *The analytical expression of RCEE of dual-hop AF relaying systems in κ-μ fading channels is given by*

$$E_r(R,T_c) = \max_{0\le\rho\le 1}\left\{\max_{0\le\beta\le 1}\left\{\mathcal{A}(\rho,\beta) - \frac{1}{T_c}\ln\left\{\sum_{m=0}^{\infty}\sum_{n=0}^{\infty}\sum_{a=0}^{m}\sum_{b=0}^{n}\frac{(-1)^{n-b}\mu^{1+m+n}}{2^{2\mu+m+n-3}\kappa^{-m-n}} \times \frac{\binom{m}{a}\binom{n}{b}(1+\kappa)\beta(1+\rho)\Gamma\left(\frac{m}{2}+\frac{n}{2}-\frac{a}{2}-\frac{b}{2}+\frac{1}{2}\right)}{m!n!\overline{\gamma}\Gamma(T_c\rho)\Gamma(m+\mu)\mathrm{e}^{2\mu\kappa}\Gamma(n+\mu)} \times G_{2,3}^{3,1}\left(\frac{4\mu(1+\kappa)\beta(1+\rho)}{\overline{\gamma}}\middle|\begin{matrix}0,\mu+\frac{m}{2}+\frac{n}{2}-\frac{a}{2}-\frac{b}{2}-\frac{1}{2}\\ \mu-1,2\mu+m+n-1,T_c\rho-1\end{matrix}\right)\right\}\right\} - \rho R\right\}. \tag{3.27}$$

Proof. With the same mathematical manipulation in Proposition 1, (3.11) is first transformed to a Meijer's G-function (3.12) according to [18, Eq.07.34.03.0271.01], shown by (3.13). The RCEE of dual-hop $\kappa-\mu$ SISO system is then derived by submitting (3.8) into (3.12) and (3.10):

$$
\begin{aligned}
&E_r(R,T_c) = \\
&\max_{0\le\rho\le1}\left\{\max_{0\le\beta\le1}\left\{\mathcal{A}(\rho,\beta)-\frac{1}{T_c}\ln\left\{\sum_{m=0}^{\infty}\sum_{n=0}^{\infty}\sum_{a=0}^{m}\sum_{b=0}^{n}\frac{(-1)^{n-b}\binom{m}{a}\binom{n}{b}}{2^{2\mu+m+n-3}\overline{\gamma}\mathrm{e}^{2\mu\kappa}m!n!}\right.\right.\right.\\
&\times\frac{\Gamma\left(\frac{m}{2}+\frac{n}{2}-\frac{a}{2}-\frac{b}{2}+\frac{1}{2}\right)\mu^{1+m+n}(1+\kappa)}{\Gamma(m+\mu)\Gamma(n+\mu)\kappa^{-m-n}\Gamma(T_c\rho)}\int_0^{\infty}G_{1,1}^{1,1}\left(\frac{x}{\beta(1+\rho)}\middle|\begin{matrix}1-T_c\rho\\0\end{matrix}\right)\\
&\left.\left.\left.\times G_{1,2}^{2,0}\left(\frac{4\mu(1+\kappa)x}{\overline{\gamma}}\middle|\begin{matrix}\mu+\frac{m}{2}+\frac{n}{2}-\frac{a}{2}-\frac{b}{2}-\frac{1}{2}\\\mu-1,2\mu+m+n-1\end{matrix}\right)\mathrm{d}x\right\}\right\}-\rho R\right\}. \qquad (3.28)
\end{aligned}
$$

Calculating the integral with the aid of [18, 07.34.21.0011.01], shown by (2.47), we finally obtain (3.27) □

Corollary 6. *The simplified approximation of expurgated error exponent of dual-hop AF relaying systems in κ-μ fading channels at high SNR regime is represented by*

$$
\begin{aligned}
E_r^{\infty}(R,T_c) = &\max_{0\le\rho\le1}\left\{\max_{0\le\beta\le1}\left\{\mathcal{A}(\rho,\beta)-\frac{1}{T_c}\ln\left\{\sum_{m=0}^{\infty}\sum_{n=0}^{\infty}\sum_{a=0}^{m}\sum_{b=0}^{n}(-1)^{n-b}\right.\right.\right.\\
&\times\frac{\mu^{1+m+n}\Gamma\left(\frac{m}{2}+\frac{n}{2}-\frac{a}{2}-\frac{b}{2}+\frac{1}{2}\right)\binom{2m}{a}\binom{n}{b}\beta(1+\rho)(1+\kappa)}{2^{2\mu+m+n-3}\kappa^{-m-n}\overline{\gamma}\Gamma(T_c\rho)\Gamma(m+\mu)\mathrm{e}^{2\mu\kappa}\Gamma(n+\mu)m!n!}\\
&\times\left(\frac{\Gamma(\mu+m+n)\Gamma(T_c\rho-\mu)Z_4^{\mu-1}}{\Gamma(\mu)^{-1}\Gamma\left(\frac{m}{2}+\frac{n}{2}-\frac{a}{2}-\frac{b}{2}+\frac{1}{2}\right)}+\frac{\Gamma(T_c\rho-2\mu-m-n)}{\Gamma\left(\frac{1}{2}-\mu-\frac{m}{2}-\frac{n}{2}-\frac{a}{2}-\frac{b}{2}\right)}\right.\\
&\times\Gamma(2\mu+m+n)\Gamma(-\mu-m-n)Z_4^{2\mu+m+n-1}\\
&\left.\left.\left.\left.+\frac{\Gamma(\mu-T_c\rho)\Gamma(\rho+2\mu+m+n-T_c)\Gamma(T_c\rho)Z_4^{2\mu+m+n-1}}{\Gamma\left(\frac{1}{2}+\frac{m}{2}+\frac{n}{2}-\frac{a}{2}-\frac{b}{2}\right)+\mu-T_c\rho}\right)\right\}\right\}\right\}, \qquad (3.29)
\end{aligned}
$$

where $Z_4=\frac{4\mu(1+\kappa)\beta(1+\rho)}{\overline{\gamma}}$.

Proof. When $\bar{\gamma}\to\infty$ at the high SNR regime, it is easy to know that $\frac{4\mu(1+\kappa)\beta(1+\rho)}{\overline{\gamma}}\to0$ in (3.27). In this scenario, the approximation (3.29) can be developed from (3.27) with the aid of [18, Eq.07.34.06.0006.01], shown in (2.46). □

3.3.3.1 Expurgated Error Exponents

Corollary 7. *The analytical expression and simplified approximation of the expurgated error exponent for dual-hop AF relaying systems in κ-μ fading channels are given by the following expressions, respectively*

$$E_{ex}(R,T_c) = \max_{\rho\geq 1}\left\{\max_{0\leq\beta\leq 1}\left\{\mathcal{A}'(\rho,\beta) - \frac{1}{T_c}\ln\left\{\sum_{m=0}^{\infty}\sum_{n=0}^{\infty}\sum_{a=0}^{m}\sum_{b=0}^{n}(-1)^{n-b} \times \frac{\mu^{1+m+n}\Gamma\left(\frac{m}{2}+\frac{n}{2}-\frac{a}{2}-\frac{b}{2}+\frac{1}{2}\right)\binom{m}{a}\binom{n}{b}\kappa^{m+n}(1+\kappa)\beta\rho}{2^{2\mu+m+n-4}\mathrm{e}^{2\mu\kappa}\Gamma(T_c\rho)\Gamma(m+\mu)\Gamma(n+\mu)m!n!\overline{\gamma}} \times G_{2,3}^{3,1}\left(\frac{8\mu(1+\kappa)\beta\rho}{\overline{\gamma}}\middle| \begin{matrix} 0,\mu+\frac{m}{2}+\frac{n}{2}-\frac{a}{2}-\frac{b}{2}-\frac{1}{2} \\ \mu-1,2\mu+m+n-1,T_c\rho-1 \end{matrix}\right)\right\}\right\} - \rho R\right\}, \tag{3.30}$$

$$\begin{aligned} E_{ex}^{\infty}(R,T_c) = \max_{\rho\geq 1}\Bigg\{\max_{0\leq\beta\leq 1}\Bigg\{\mathcal{A}'(\rho,\beta) - \frac{1}{T_c}\ln\Bigg\{\sum_{m=0}^{\infty}\sum_{n=0}^{\infty}\sum_{a=0}^{m}\sum_{b=0}^{n}(-1)^{n-b} \\ \times \frac{\mu^{1+m+n}\kappa^{m+n}\Gamma\left(\frac{m}{2}+\frac{n}{2}-\frac{a}{2}-\frac{b}{2}+\frac{1}{2}\right)}{2^{2\mu+m+n-4}\mathrm{e}^{2\mu\kappa}\overline{\gamma}\Gamma(T_c\rho)\Gamma(m+\mu)\Gamma(n+\mu)} \\ \times \frac{\binom{2m}{a}\binom{n}{b}(1+\kappa)\beta\rho}{m!n!}\Bigg(\frac{\Gamma(\mu+m+n)\Gamma(T_c\rho-\mu)Z_5^{\mu-1}}{\Gamma(\mu)^{-1}\Gamma\left(\frac{m}{2}+\frac{n}{2}-\frac{a}{2}-\frac{b}{2}+\frac{1}{2}\right)} \\ + \frac{\Gamma(-\mu-m-n)\Gamma(T_c\rho-2\mu-m-n)Z_5^{2\mu+m+n-1}}{\Gamma(2\mu+m+n)^{-1}\Gamma\left(\frac{1}{2}-\mu-\frac{m}{2}-\frac{n}{2}-\frac{a}{2}-\frac{b}{2}\right)} \\ + \frac{\Gamma(\mu-T_c\rho)\Gamma(\rho+2\mu+m+n-T_c)Z_5^{2\mu+m+n-1}}{\Gamma(T_c\rho)^{-1}\Gamma\left(\frac{1}{2}+\frac{m}{2}+\frac{n}{2}-\frac{a}{2}-\frac{b}{2}\right)-T_c\rho}\Bigg)\Bigg\}\Bigg\}\Bigg\} \end{aligned} \tag{3.31}$$

where $Z_5 = \frac{8\mu(1+\kappa)\beta\rho}{\overline{\gamma}}$.

Proof. Similar to the derivation for Proposition 2, the expression (3.30) is obtained by substituting (3.8) into (3.20) and (3.18), the integral is made according to [18, Eq.07.34.21.0011.01], shown in (2.47). The expression (3.31) is subsequently derived through the transformation guided by [18, Eq.07.34.06.0006.01], shown in (2.46). □

Figure 3.6 illustrates the RCEE and expurgated error exponent against different information rate R with $T_c = 5$ and $\bar{\gamma} = 15$dB. It is clear that both the RCEE and expurgated error exponent decline monotonically when R increases. At low information rates, 0.5 nats/s/Hz here, the

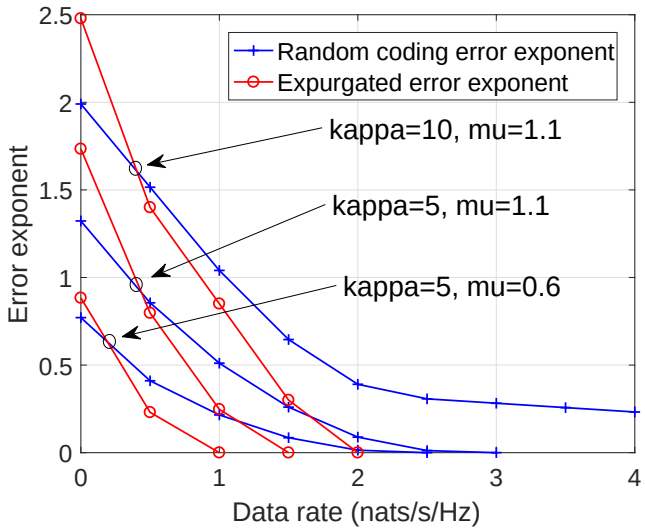

Figure 3.6: *The analytical and simulation results for the RCEE and expurgated error exponent of dual-hop AF κ-μ fading SISO channel with T_c=10 and SNR=15dB.*

SNR (dB)	$\kappa = 5$ $\mu = 1.4$	$\kappa = 5$ $\mu = 2.2$	$\kappa = 10$ $\mu = 1.4$	$\kappa = 10$ $\kappa = 2.2$
10	349	44	19	6
20	18	11	9	5
30	9	5	5	3

Table 3.2: *Required code lengths L_r for dual-hop AF κ-μ fading SISO channel to achieve the predefined upper bound of decoding error probabilities $P_e^r \leq 10^{-6}$ with $R = 1.5$ nats/s/Hz and $T_c = 5$.*

expurgated error exponent performs better than the RCEE, but performs worse than the RCEE as the data rate increases. We can see that both parameters μ and κ increase the value of error exponents as they increase. This is because that κ denotes how the power is concentrated in the distribution and μ illustrates the number of multipath clusters.

Figure 3.7 demonstrates the analytical result and high SNR approximation of RCEE as functions of end-to-end SNR with different value of κ and μ. It is clear that the RCEE of dual-hop AF κ-μ fading SISO channel increases with the SNR and the slope of the curve is determined by both κ and μ. From $\gamma = 25$dB, the high SNR approximation matches the analytical result very well. In addition, according to (3.39), we present the analytical result of the RCEE for the Nakagami-m channel with the same μ (m). It is clear that, a positive parameter κ will significantly increase the error exponent.

Table 3.2 presents the required code length to achieve the predefined upper bound error proba-

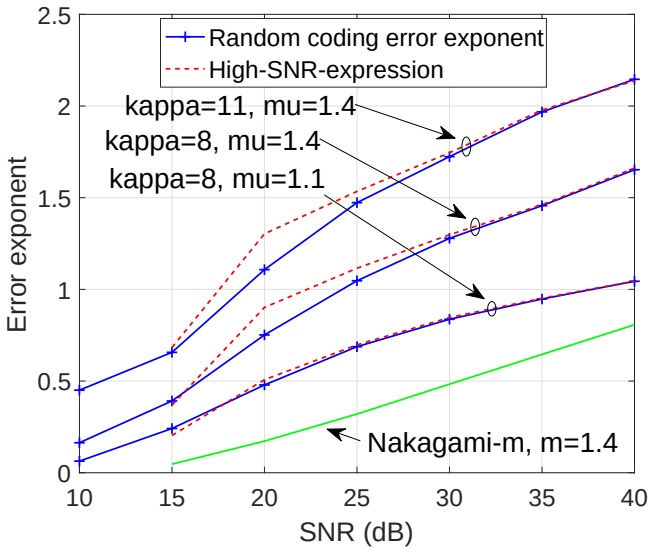

Figure 3.7: *The Analytical and high-SNR approximation of RCEE against SNR of dual-hop AF κ-μ fading SISO channel with T_c=10 and R=1.5 nats/s/Hz*

bility $P_e^{E_r} = 10^{-6}$ at a transmission rate $R = 1.5$ nats/s/Hz of dual-hop AF SISO systems over κ-μ fading channel with a fixed value $T_c = 5$. As can be seen, the increasing of both parameters κ and μ help to reduce the required code length considerably. The reduction for low-SNR regime is particularly remarkable. For example, considering with $\kappa = 5$, μ increases from 1.4 to 2.2, the required code length reduces 87.37% when SNR=10dB but it just decreases 44.44% when SNR=30dB. Similarly, when κ increases from 5 to 10, with $\mu = 2.2$, the required code length decreases 86.39% with SNR=10dB but it only declines 40% when SNR=30dB. Since error exponents always reduce with decreasing $\bar{\gamma}$, κ and μ, it is clear that the required code length will be dramatically enlarged when error exponents is very small.

3.3.3.2 Cutoff Rate

Corollary 8. *The analytical expression of cutoff rate of dual-hop AF relaying systems in κ-μ fading channels can be expressed as*

$$R_0 = -\frac{1}{T_c}\ln\left\{\sum_{m=0}^{\infty}\sum_{n=0}^{\infty}\sum_{a=0}^{m}\sum_{b=0}^{n}\frac{(-1)^{n-b}\binom{m}{a}\binom{n}{b}\mu^{1+m+n}\kappa^{m+n}(1+\kappa)\Gamma\left(\frac{m}{2}+\frac{n}{2}-\frac{a}{2}-\frac{b}{2}+\frac{1}{2}\right)}{2^{2\mu+m+n-4}m!n!\mathrm{e}^{2\mu\kappa}\bar{\gamma}\Gamma(T_c\rho)\Gamma\left(m+\mu-\frac{1}{2}\right)\Gamma\left(n+\mu-\frac{1}{2}\right)}\right.$$
$$\left.\times G_{2,3}^{3,1}\left(\frac{8\mu(1+\kappa)}{\bar{\gamma}}\middle|\begin{matrix}0,\mu+\frac{m}{2}+\frac{n}{2}-\frac{a}{2}-\frac{b}{2}-\frac{1}{2}\\ \mu-1,2\mu+m+n-1,T_c\rho-1\end{matrix}\right)\right\}. \quad (3.32)$$

Proof. Directly submitting $\rho = 1, \beta = 1$ into (3.27) , expression (3.32) is generated. □

Corollary 9. *The cutoff rate of dual-hop AF relaying systems in κ-μ fading channels at high SNR regime can be expressed as*

$$R_0^{\infty} = -\frac{1}{T_c}\ln\left\{\sum_{m=0}^{\infty}\sum_{n=0}^{\infty}\sum_{a=0}^{m}\sum_{b=0}^{n}\frac{(-1)^{n-b}\binom{m}{a}\binom{n}{b}\mu^{1+m+n}\kappa^{m+n}(1+\kappa)\Gamma\left(\frac{m}{2}+\frac{n}{2}-\frac{a}{2}-\frac{b}{2}+\frac{1}{2}\right)}{2^{2\mu+m+n-4}m!n!\mathrm{e}^{2\mu\kappa}\bar{\gamma}\Gamma(T_c\rho)\Gamma\left(m+\mu-\frac{1}{2}\right)\Gamma\left(n+\mu-\frac{1}{2}\right)}\right.$$
$$\times\left(\frac{\Gamma(\mu+m+n)\Gamma(T_c-\mu)Z_6^{\mu-1}}{\Gamma(\mu)^{-1}\Gamma\left(\frac{m}{2}+\frac{n}{2}-\frac{a}{2}-\frac{b}{2}+\frac{1}{2}\right)}+\frac{\Gamma(-\mu-m-n)\Gamma(T_c-2\mu-m-n)Z_6^{2\mu+m+n-1}}{\Gamma(2\mu+m+n)^{-1}\Gamma\left(\frac{1}{2}-\mu-\frac{m}{2}-\frac{n}{2}-\frac{a}{2}-\frac{b}{2}\right)}\right.$$
$$\left.\left.+\frac{\Gamma(\mu-T_c)\Gamma(+2\mu+m+n-T_c)\Gamma(T_c)Z_6^{2\mu+m+n-1}}{\Gamma\left(\frac{1}{2}+\frac{m}{2}+\frac{n}{2}-\frac{a}{2}-\frac{b}{2}+\mu-T_c\right)}\right)\right\} \tag{3.33}$$

where $Z_6 = \frac{4\mu(1+\kappa)\beta(1+\rho)}{\bar{\gamma}}$.

Proof. by submitting $\rho = 1, \beta = 1$ into (3.29), expression (3.33) is derived. □

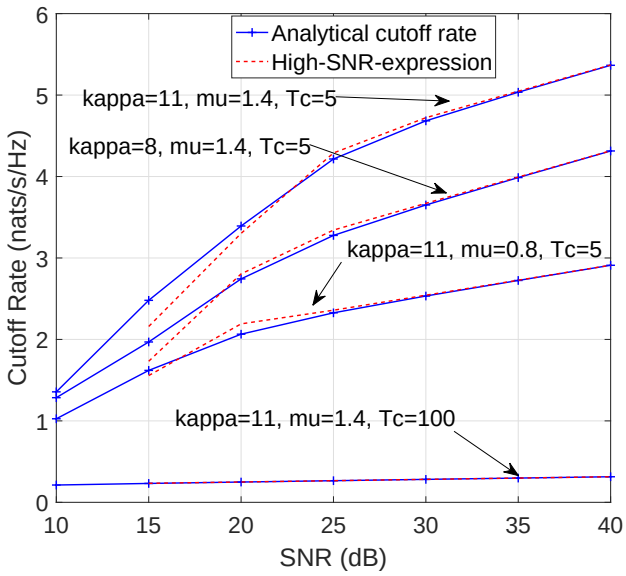

Figure 3.8: *The Analytical results and high-SNR approximation of cutoff rate against SNR of dual-hop AF κ-μ fading SISO channel with $T_c = 5$.*

Figure 3.8 depicts the analytical results and high SNR approximation of cutoff rate as a function of SNR with selected values of κ and μ. When the block length T_c is fixed, we see that the cutoff rate monotonically increase with SNR, κ and μ, respectively. The high-SNR approximation works perfectly when SNR is greater than 25dB. On the other hand, the cutoff rate decreases when T_c increases. Note that the Shannon capacity just offers the achievable information rate,

but the cutoff rate affords more insight into the tradeoff of information reliability and coding complexity in block-coding channels.

3.3.3.3 Ergodic Capacity

Corollary 10. *The ergodic capacity in nat of dual-hop AF relaying systems in κ-μ fading channels is given by*

$$\langle C\rangle = \sum_{m=0}^{\infty}\sum_{n=0}^{\infty}\sum_{a=0}^{m}\sum_{b=0}^{n}\frac{(-1)^{n-b}\binom{m}{a}\binom{n}{b}\mu^{1+m+n}\kappa^{m+n}(1+\kappa)\Gamma\left(\frac{m}{2}+\frac{n}{2}-\frac{a}{2}-\frac{b}{2}+\frac{1}{2}\right)}{2^{m+n+2\mu-3}m!n!\mathrm{e}^{2\mu\kappa\overline{\gamma}}\Gamma(m+\mu)\Gamma(n+\mu)} \times G_{3,4}^{4,1}\left(\frac{4\mu(1+\kappa)}{\overline{\gamma}}\middle|\begin{matrix}-1,0,\mu+\frac{m}{2}+\frac{n}{2}-\frac{a}{2}-\frac{b}{2}+\frac{1}{2}\\ \mu-1,2\mu+m+n-1,-1,-1\end{matrix}\right). \tag{3.34}$$

Proof. Combining (3.8) and (3.26), we have

$$\langle C\rangle = \int_0^{\infty} G_{2,2}^{1,2}\left(x\middle|\begin{matrix}1,1\\ 1,0\end{matrix}\right) f_{\gamma}^{\kappa-\mu}(x)dx. \tag{3.35}$$

Then, Corollary 10 can be obtained with the help of the integral formula provided by (2.47). □

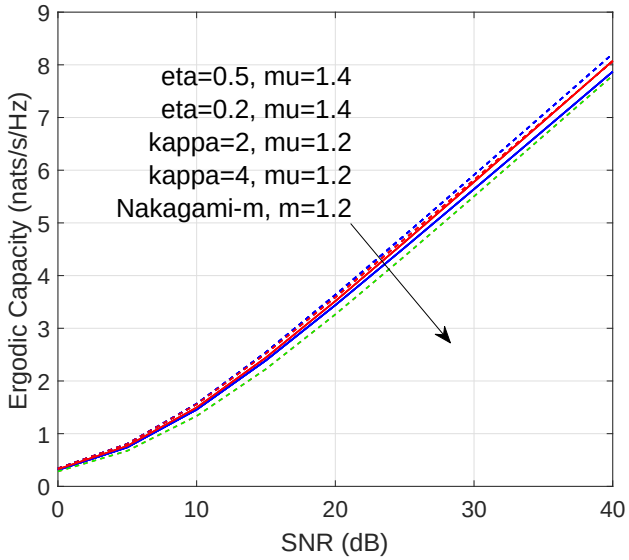

Figure 3.9: *The Analytical results for the Ergotic Capacity of dual-hop AF κ-μ fading SISO channel for selected parametersη, κ and μ.*

In Figure 3.9, the effects of parameters η, κ and μ on ergodic capacity with different SNR values are evaluated.The ergodic capacity increases with η (when $\eta < 1$), κ, μ and SNR, respectively. In addition, a special case where $\kappa \to 0$, which is related to the Nakagami-m distribution is shown as dash lines (see expression (3.41)). It should be noted that, capacities with different parameters are close to each other, however as shown above, the related error exponents are quite different, which indicate the distinguishing code lengths.

3.3.4 With Other Distributions

As mentioned above, the general η-μ and κ-μ distributions include a series of other widely studied statistical distributions as special cases, such as the Raleigh, Nakagami-m, Hoyt and Rician distributions. This subsection introduces how to derive analytical expressions of RCEE, expurgated error exponent, ergodic capacity and cutoff rate for these widely used fading channels from our analytical results. Note that all the subsequent analytical results are presented without strict mathematical proofs, because the involved mathematical manipulations are simple and straightforward.

3.3.4.1 Nakagami-m Fading

The Nakagami-m distribution is used to formulize the fading signal which consists of a bundle of multi-path clusters. It corresponds to the η-μ fading distribution with $\eta \to 1$ in Format 1 or from κ-μ distribution with $\kappa \to 0$.

Substituting $\kappa \to 0$ into Theorem 2, we can obtain the pdf of end-to-end SNR of dual-hop AF nakagami-m fading channel as

$$\lim_{\kappa\to 0} f_{\gamma}^{\kappa-\mu}(\gamma) = \lim_{\kappa\to 0} \sum_{i=0}^{\infty}\sum_{j=0}^{\infty}\sum_{a=0}^{i}\sum_{b=0}^{j} \frac{(-1)^{j-b}2^{3-i-j-2\mu}\binom{i}{a}\binom{j}{b}\mu^{1+i+j}\kappa^{i+j}(1+\kappa)}{\overline{\gamma}i!j!\Gamma(i+\mu)\Gamma(j+\mu)\Gamma\left(\frac{i}{2}+\frac{j}{2}-\frac{a}{2}-\frac{b}{2}+\frac{1}{2}\right)^{-1}} \times \mathrm{e}^{-2\mu\kappa} G_{1,2}^{2,0}\left(\frac{4\mu(1+\kappa)\gamma}{\overline{\gamma}}\middle| \begin{matrix}\mu+\frac{i}{2}+\frac{j}{2}-\frac{a}{2}-\frac{b}{2}-\frac{1}{2}\\ \mu-1, 2\mu+i+j-1\end{matrix}\right) \tag{3.36}$$

$$= 2^{3-2\mu}\mu\Gamma\left(\frac{1}{2}\right)\overline{\gamma}^{-1}\Gamma(\mu)^{-2} G_{1,2}^{2,0}\left(\frac{4\mu\gamma}{\overline{\gamma}}\middle| \begin{matrix}\mu-\frac{1}{2}\\ \mu-1, 2\mu-1\end{matrix}\right). \tag{3.37}$$

By rewriting (3.37) in terms of the hypergeometric function with the aid of [18, Eq.07.34.03.0612.01],

also shown by (A.11), and replacing the parameter μ by m because of Nakagami-m distribution, the pdf of end-to-end SNR of dual-hop AF nakagami-m fading channel is obtained as

$$f_\gamma(\gamma) = 2m^m\Gamma\left(\frac{1}{2}\right)\overline{\gamma}^{-m}\Gamma(m)^{-2}x^{m-1}U\left(\frac{1}{2}-m, 1-m, \frac{4m\gamma}{\overline{\gamma}}\right). \tag{3.38}$$

Expression (3.38) also corresponds to the result presented in [42].

Thereafter, the analytical expressions of RCEE, expurgated error exponent, cutoff rate and ergodic capacity of dual-hop AF relaying systems in Nakagami-m fading channels can be derived through the similar way by substituting $\kappa \to 0$ and $\mu = m$ into (3.27), (3.32), (3.34) and (3.30):

- RCEE

$$E_r(R,T_c) = \max_{0\le\rho\le1}\left\{\max_{0\le\beta\le1}\left\{\mathcal{A}(\rho,\beta) - \frac{1}{T_c}\ln\left\{\frac{2^{3-2m}m\Gamma\left(\frac{1}{2}\right)\beta(1+\rho)}{\overline{\gamma}\Gamma(T_c\rho)\Gamma(m)^2}\right.\right.\right.$$
$$\left.\left.\left.\times G_{2,3}^{3,1}\left(\frac{4m\beta(1+\rho)}{\overline{\gamma}}\middle|\begin{matrix}0, m-\frac{1}{2}\\ 2m-1, 4m-1, T_c\rho-1\end{matrix}\right)\right\}\right\} - \rho R\right\}; \tag{3.39}$$

- Cutoff rate

$$R_0 = -\frac{1}{T_c}\ln\left\{\frac{2^{4-2m}m\Gamma\left(-\frac{1}{2}\right)}{\overline{\gamma}\Gamma(T_c)\Gamma(m)^2}G_{2,3}^{3,1}\left(\frac{8m}{\overline{\gamma}}\middle|\begin{matrix}0, m-\frac{1}{2}\\ 2m-1, 4m-1, T_c-1\end{matrix}\right)\right\}; \tag{3.40}$$

- Ergodic capacity

$$\langle C\rangle = \frac{2^{3-2m}m}{\overline{\gamma}\Gamma(m)^2}G_{4,1}^{3,4}\left(\frac{4m}{\overline{\gamma}}\middle|\begin{matrix}-1, 0, m+\frac{1}{2}\\ m-1, 2m-1, -1, -1\end{matrix}\right); \tag{3.41}$$

- Expurgated error exponent

$$E_{ex}(R,T_c) = \max_{\rho\ge1}\left\{\max_{0\le\beta\le1}\left\{\mathcal{A}'(\rho,\beta) - \frac{1}{T_c}\ln\left\{\frac{2^{4-2m}m\Gamma\left(-\frac{1}{2}\right)\beta\rho}{\overline{\gamma}\Gamma(T_c\rho)\Gamma(m)^2}\right.\right.\right.$$
$$\left.\left.\left.\times G_{2,3}^{3,1}\left(\frac{8m\beta\rho}{\overline{\gamma}}\middle|\begin{matrix}0, m-\frac{1}{2}\\ 2m-1, 4m-1, T_c\rho-1\end{matrix}\right)\right\}\right\} - \rho R\right\}. \tag{3.42}$$

Although the expressions above are derived from κ-μ fading, we should note that the same results can be also obtained from η-μ fading. We plot the analytical results of the RCEE (3.39) and the ergodic capacity (3.41) in Figure 3.4, Figure 3.7 and Figure 3.9, respectively.

3.3.4.2 Hoyt, Rician, Rayleigh and One-Side Gaussianand Fading

Discarding the consideration of the multipath clusters, our analytical results of η-μ and κ-μ fading can also be simplified to error exponents for systems with Hoyt (Nakagami-q), Rician, Rayleigh or One-Sided Gaussian fading:

- Hoyt (Nakagami-q): By setting $\mu = 0.5$ and $\eta = q^2$ in equations (3.6), (3.9), (3.16), (3.22), and (3.24), the analytical expressions of dual-hop AF relaying systems in Hoyt fading channels are obtained.
- Rician: When $\mu = 1$ and $\kappa = K$, analytical expressions (3.8), (3.27), (3.30), (3.32) and (3.34) degenerate to equations for the dual-hop AF relaying systems in Rician fading channels. We should notice that K is the ratio between the power in the direct path and the power in the other scattered paths.
- Supposing $\kappa \to 0$ and $\mu = 1$ in expressions (3.8), (3.27), (3.30), (3.32) and (3.34), we can apply our results for dual-hop AF relaying systems in Rayleigh fading channels.
- By setting $\kappa \to 0$ and $\mu = 0.5$ in expressions (3.8), (3.27), (3.30), (3.32) and (3.34), we can obtain the analytical results for dual-hop AF relaying systems in one-sided Gaussian fading channels.

3.4 Conclusion

In this chapter, the error exponents of dual-hop AF relaying systems in generalised η-μ and κ-μ fading channels are investigated. More specifically, we first developed a new analytical expression of the pdf of the end-to-end SNR. Subsequently, new analytical expressions of RCEE, expurgated error exponent, cutoff rate and ergodic capacity were derived. Our generalised analytical results include the other common fading channels as special cases. Also, simplified and insightful approximations were provided, which were shown to be tight for the high SNR regime. Meanwhile, the required code length to achieve a certain upper bound of error probability are estimated based on our analytical expressions. The results showed that for the larger

in-phase to quadrature components ratio, a higher dominant components to scattered waves ratio and number of multipath clusters could reduce the required code length and improve the communication reliability of dual-hop AF channels.

Chapter 4
Multi-Antenna Dual-Hop AF System with Random Co-channel Interference Using Different Transferring Schemes

4.1 Introduction

4.1.1 Motivation

As more aggressive frequency reuse techniques have been employed in recent years, the impact of co-channel interference (CCI) has become an interesting research topic. There is an immense number of existing works investigating the performance of relaying networks with the effects of CCI. For single-antenna AF relaying systems, outage probability results for interference-limited destinations and/or relays were addressed in [43–47]. For multi-hop AF SISO systems, the authors of [48–50] not only derived end-to-end outage probabilities but also discussed the effects of relay selection, power allocation and system delay. The performance of dual-hop multiple-input-single-output (MISO) or single-input-multiple-output (SIMO) systems were studied by [51] and [52].

These papers are less appropriate to be used in the performance analysis for emerging heterogeneous communication systems, such as femto base station networks [53] or cognitive communications [54], because the randomness of CCI is not taken into consideration. In order to overcome this weakness, the PPP models are introduced into the analysis. It is believed that the PPP can somewhat balance the tractability of performance analysis and the randomness of location for the radio elements. Inspired by the framework in [55], significant research has been conducted considering the randomness of the networks, such as [56, 57].

For studying the performance of multi-antenna relay-aided networks with random interference, the authors gave bounds for the outage probability in a multi-hop multi-antenna interference limited system over Rayleigh fading in [58], where a spatial interference cancellation was implemented. In this chapter, we analyse the capacity over a dual-hop AF multi-antenna relaying

system by considering Rayleigh fading and co-channel interference around the relay. We obtain approximations for the capacities with different signal processing schemes at relay, i.e. MRC, ZF and MMSE receivers cooperating with an MRT transmitter.

4.1.2 Main Contribution

The main contributions are presented below:

- We evaluate the performance of a dual-hop AF relay system, in which the relay is equipped with multiple antennas and adopts MRC, ZF, and MMSE receiving schemes, co-channel interference is considered and modelled with a homogeneous PPP.
- When interferers are located in an infinite area, we derive the analytical expressions for exact end-to-end capacities for MRC/MRT, ZF/MRT and MMSE/MRT schemes. when interferers are located in a limited area, we derive the lower bounds of capacities for MRC/MRT, ZF/MRT and ZF/MRT schemes.
- Among the three relay processing schemes, the performance of the MMSE/MRT protocol is always better than other two protocols over the whole SNR range; the system with ZF/MRT scheme performs the worst in an infinite-interference-area scenario, but it performs well in the limited-interference-area scenario.
- The effect of PPP on performance analysis is presented by our numerical examinations. Comparisons of ergodic capacities are made between limited-area PPP model and the fixed-number fixed-distance interference model, Where the number of interferers in the fixed-interference scenario equals to the expectation of the number of interferers in the PPP scenario.

4.2 System Model

The dual-hop relay-assisted communication system considered in this chapter is shown in Figure 4.1. A single-antenna source transmit signals to a single-antenna destination with the aid of an multi-antenna relay. The relay is interfered by co-channel interference from mobile users, which are equipped with a single antenna. Both the relay and destination are corrupted by additive white Gaussian noise (AWGN). Through this chapter, we also consider the following

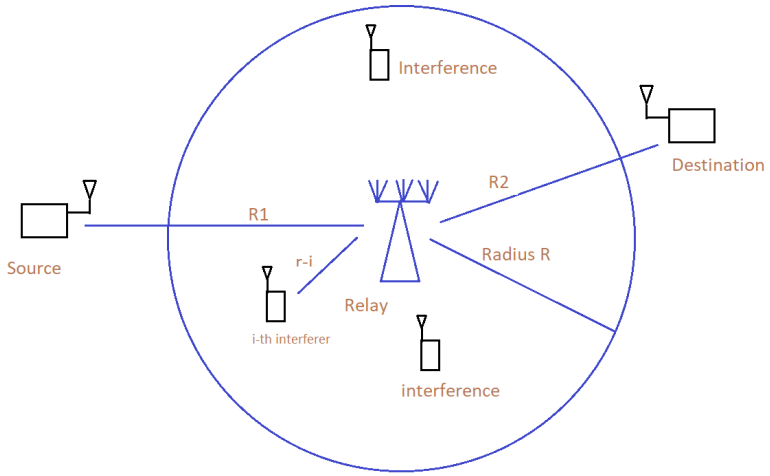

Figure 4.1: *A dual-hop AF relaying system with co-channel interference*

assumptions: (1) the source cannot directly communicate with the destination. (2) the co-channel interference is modelled by a homogeneous PPP: all interferers are randomly located in a closed round area D with external radius R. The total number and locations of interference nodes are variables characterised by the node density λ and service area D. It worth mentioning that, when making comparisons to a non-PPP model in the numerical tests, the number of interferers is given by $N_2^{noPPP} = \lambda D$ and the distance for each interference is given by $r_i = \mathbb{E}\{r\}$, rather than R. In addition to a traditional setting $R \to \infty$, we also consider the situation that D is a limited area, but assign R a large value. (3) The relay works in half-duplex mode, whose receiving and transmitting times are identical. (4) MRC, ZF, and MMSE receivers are applied at relay, working with a MRT transmitter. We assume the relay can obtain perfect knowledge of interference covariance matrix and the power level of noise.

4.2.1 System and Transformation

As mentioned, the relay works in a half-duplex mode. In the first time slot, information is transmitted from the source to relay, and the signal received by the relay can be expressed as

$$\mathbf{y}_r = l_1 \mathbf{h}_1 s_1 + \sum_{i \in \Phi} l_{I_i} \mathbf{h}_{I_i} s_{I_i} + \mathbf{n}_1, \tag{4.1}$$

where the channel coefficient between source and relay is denoted by $\mathbf{h}_1 \in \mathbb{C}^{N_1 \times 1}$, the entries follow the complex normal distribution $\mathcal{CN}(0,1)$, and are identically and independently distributed (i.i.d.). The vector $\mathbf{h}_{I_i}$ is the complex $N_1 \times 1$ channel coefficient of the i-th interfer-

ence, the entries of which follow $\mathcal{CN}(0,1)$, Φ denotes the PPP. The coefficients $l_1 = (R_1)^{-\alpha}$ and $l_{I_i} = (r_{I_i})^{-\alpha}$ denote the path-loss attenuations of the source-relay channel and the i-th interference-relay channel, respectively, where α is the exponent of path-loss attenuation, R_1 is the constant distance between source and relay, and variable r_{I_i} denotes the distance between the i-th interferer and the relay. The scalar s_1 denotes the transmitted signal with average power $\mathbb{E}\{s_1 s_1^*\} = P_s$, and the i-th interference signal is denoted by s_{I_i} with $\mathbb{E}\{s_{I_i} s_{I_i}^*\} = P_{I_i}$, where a^* is the complex conjugate of a. The symbol $\mathbf{n}_1$ is an $N_1 \times 1$ vector denoting the AWGN noise at relay, with $\mathbb{E}\{\mathbf{n}_1 \mathbf{n}_1^\dagger\} = \sigma^2 \mathbf{I}$.

The relay processes received signals with a predefined linear matrix $\mathbf{W}$ and then transmits the result to the destination in the second time slot. The signal received by the destination can be written as

$$y_d = l_2 \mathbf{h}_2^\dagger \mathbf{W} \mathbf{y}_r + n_2, \tag{4.2}$$

where $l_2 = (R_2)^{-\alpha}$ denotes the path-loss attenuation in the relay-destination transmission, R_2 is the constant distance from relay to destination, $\mathbf{h}_2 \in \mathbb{C}^{N_1 \times 1}$ is the coefficient of relay-destination channel, whose elements follow i.i.d. $\mathcal{CN}$(0,1), and n_2 is the AWGN at destination with $\mathbb{E}\{n_2 n_2^*\} = \sigma^2$. The transmission power of the relay is given by $\mathbb{E}\{||\mathbf{W}\mathbf{y}_r||_F^2\} = P_r$. The end-to-end SINR of the system can be easily derived by combining (4.1) and (4.2) as

$$\gamma_{e2e} = \frac{P_s l_1 l_2 |\mathbf{h}_2^\dagger \mathbf{W} \mathbf{h}_1|^2}{\sum\limits_{i \in \Phi} P_{I_i} l_{I_i} |\mathbf{h}_2^\dagger \mathbf{W} \mathbf{h}_{I_i}|^2 + \sigma^2 ||\mathbf{h}_2^\dagger \mathbf{W}||_F^2 + \sigma^2}. \tag{4.3}$$

Due to the difficulty to find the global optimal solution of transferring matrix $\mathbf{W}$ in (4.3) to maximise the end-to-end SINR for this system, a two-step method to design $\mathbf{W}$ proposed in [59] is adopted, which decomposes $\mathbf{W}$ into independent receiver and precoder: $\mathbf{W} = \omega \mathbf{t} \mathbf{w}_1^\dagger$, where $\mathbf{t} \in \mathbb{C}^{\mathbf{N}_1 \times 1}$ is the precoder, $\mathbf{w}_1 \in \mathbb{C}^{\mathbf{N}_1 \times 1}$ is the receiver and ω is the power constraint factor. Since in the relay-destination transmission only AWGN is considered, MRT is always used for relay transmission. The normalised MRT precoder can be written as $\mathbf{t} = \frac{\mathbf{h}_2}{||\mathbf{h}_2||_F^2}$.

4.2.2 Signal Processing Schemes at the Relay

The processing matrix applying the three classical receivers MRC, ZF and MMSE are formulated in the following.

4.2.2.1 MRC Scheme

The MRC receiver, best suited for a high-SNR scenario, maximises the received signals by multiplying the received signal with the complex conjugate of the channel at each antenna and combining them together. In our system, it can be written as $\mathbf{w}_1 = \mathbf{h}_1/||\mathbf{h}_1||_F$. Invoking the normalised MRT precoder $\mathbf{t}$, the power constraint factor is then derived as

$$\omega^2 = \frac{P_r}{l_1 P_s ||\mathbf{h}_1||_F^2 + \sum\limits_{i\in\Phi} \frac{l_{I_i} P_{I_i} |\mathbf{h}_1^\dagger \mathbf{h}_{I_i}|^2}{||\mathbf{h}_1||_F^2} + \sigma^2}, \tag{4.4}$$

and the end-to-end SINR is given by

$$\gamma_{\mathrm{MRC}} = \frac{\frac{P_s P_r ||\mathbf{h}_1||_F^2 ||\mathbf{h}_2||_F^2 l_1 l_2}{\sigma^2 + \sum\limits_{i\in\Phi} \frac{P_{I_i} l_{I_i} |\mathbf{h}_1^\dagger \mathbf{h}_{I_i}|^2}{||\mathbf{h}_1||_F^2}}}{P_r l_2 ||\mathbf{h}_2||^2 + \sigma^2 + \frac{\sigma^2 l_1 P_s ||\mathbf{h}_1||_F^2}{\sigma^2 + \sum\limits_{i\in\Phi} \frac{P_{I_i} l_{I_i} |\mathbf{h}_1^\dagger \mathbf{h}_{I_i}|^2}{||\mathbf{h}_1||_F^2}}}. \tag{4.5}$$

To give a clear picture, we rewrite (4.5) as

$$\gamma_{\mathrm{MRC}} = \frac{\gamma_1^{\mathrm{MRC}} \gamma_2^{\mathrm{MRC}}}{\gamma_1^{\mathrm{MRC}} + \gamma_2^{\mathrm{MRC}} + 1}, \tag{4.6}$$

where $\gamma_1^{\mathrm{MRC}} = P_s l_1 ||\mathbf{h}_1||_F^2 / \left(\sum\limits_{i\in\Phi} \frac{P_{I_i} l_{I_i} |\mathbf{h}_1^\dagger \mathbf{h}_{I_i}|^2}{||\mathbf{h}_1||_F^2} + \sigma^2 \right)$ is the SINR of source-relay transmission obtained after combiner $\mathbf{w}_1$ and $\gamma_2^{\mathrm{MRC}} = P_r l_2 ||\mathbf{h}_2||_F^2 / \sigma^2$ is the SNR of relay-destination transmission exploring MRT precoder $\mathbf{t}$. As is well known, the MRC combiner has advantages only for systems with weak interference, thus in the CCI-impact scenario, receivers with the function of interference elimination are more common and practical.

4.2.2.2 ZF Schemes

The ZF scheme can completely remove interference from no more than N_1 interferers, where N_1 is the number of receiving antennas at the relay. However, the number of interferers always has a non-zero probability to exceed this limit in presence of a PPP model. In this case, we introduce the strategy proposed by [58], where the filter completely eliminates interference from the nearest $N_1 - 1$ interferers and treats other interference as noise. The combiner $\mathbf{w}_1$ in

the ZF scheme can be written as

$$\mathbf{w}_1^\dagger = \frac{\mathbf{h}_1^\dagger \mathbf{P}}{\sqrt{\mathbf{h}_1^\dagger \mathbf{P} \mathbf{h}_1}}, \tag{4.7}$$

where $\mathbf{P} = \mathbf{I}_{N_1} - \mathbf{H}_I(\mathbf{H}_I^\dagger \mathbf{H}_I)^{-1}\mathbf{H}_I^\dagger$ is the null-space filter for H_I.
The matrix $\mathbf{H}_I = \left[\sqrt{\tilde{P}_{I1}\tilde{l}_{I_1}}\tilde{\mathbf{h}}_{I1}, \sqrt{\tilde{P}_{I_1}\tilde{l}_{I_1}}\tilde{\mathbf{h}}_{I_2}, \ldots, \sqrt{\tilde{P}_{I_M}\tilde{l}_{I_M}}\tilde{\mathbf{h}}_{I_1}\right]$, $\sqrt{\tilde{P}_{I_i}\tilde{l}_{I_i}}, i \in [0, M]$ are the strongest M interference power terms received by the relay, where $M = \min[N_2, N_1 - 1]$, and N_2 is the number of interferers within field D. The corresponding power constraint factor is derived as

$$\omega^2 = \frac{P_r}{P_s l_1 |\mathbf{w}_1^\dagger \mathbf{h}_1|^2 + \sigma^2} \quad N_2 < N_1, \tag{4.8a}$$

$$\omega^2 = \frac{P_r}{P_s l_1 |\mathbf{w}_1^\dagger \mathbf{h}_1|^2 + \sum\limits_{i=N_1}^{N_2} l_{I_i} P_{I_i} |\mathbf{w}_1 \mathbf{h}_{I_i}| + \sigma^2} \quad N_2 \geqslant N_1. \tag{4.8b}$$

The end-to-end SINR for the ZF/MRT processing is

$$\gamma_{\mathrm{ZF}} = \frac{\gamma_1^{\mathrm{ZF}} \gamma_2^{\mathrm{ZF}}}{\gamma_1^{\mathrm{ZF}} + \gamma_2^{\mathrm{ZF}} + 1}, \tag{4.9}$$

where $\gamma_2^{\mathrm{ZF}} = P_r l_2 ||\mathbf{h}_2||_F^2 / \sigma^2$, and γ_1^{ZF} is given by

$$\gamma_1^{\mathrm{ZF}} = \begin{cases} \frac{P_s l_1 |\mathbf{h}_1^\dagger \mathbf{P} \mathbf{h}_1|}{\sigma^2}, & N_2 < N_1 \\ \frac{P_s l_1 |\mathbf{h}_1^\dagger \mathbf{P} \mathbf{h}_1|}{\sum\limits_{i \in \Phi, i \geq N_1} P_{I_i} l_{I_i} \frac{|\mathbf{h}_1^\dagger \mathbf{P} \mathbf{h}_{I_i}|^2}{\mathbf{h}_1^\dagger \mathbf{P} \mathbf{h}} + \sigma^2}, & N_2 \geq N_1 \end{cases}.$$

.

4.2.2.3 MMSE Scheme

The MMSE combiner comprehensively considers the AWGN and CCI, and provides the optimum solution to maximise the SINR. Following the approach in [60], the MMSE combiner should be written as

$$\mathbf{w}_1^\dagger = \mathbf{h}_1^\dagger \left(\mathbf{h}_1 \mathbf{h}_1^\dagger + \mathbf{H}_I \mathbf{H}_I^\dagger + \frac{\sigma^2}{P_s l_1} \mathbf{I}_{N_2}\right)^{-1}, \tag{4.10}$$

where $\mathbf{H}_I = \left[\sqrt{\frac{P_{I_1} l_{I_1}}{P_s l_1}}\mathbf{h}_{I_1}, \ldots, \sqrt{\frac{P_{I_{N_2}} l_{I_{N_2}}}{P_s l_1}}\mathbf{h}_{I_{N_2}}\right]$. The power constraint factor is then derived as

$$\omega^2 = \frac{P_r}{P_s l_1 |\mathbf{w}_1^\dagger \mathbf{h}_1|^2 + \sum\limits_{i\in\Phi} P_{I_i} l_{I_i} |\mathbf{w}_1^\dagger \mathbf{h}_{I_i}|^2 + ||\mathbf{w}_1||_F^2}, \tag{4.11}$$

and the relevant end-to-end SINR is

$$\gamma_{\mathrm{MMSE}} = \frac{\gamma_1^{\mathrm{MMSE}} \gamma_2^{\mathrm{MMSE}}}{\gamma_1^{\mathrm{MMSE}} + \gamma_2^{\mathrm{MMSE}} + 1}, \tag{4.12}$$

where $\gamma_1^{\mathrm{MMSE}} = P_s l_1 |\mathbf{h}_1^\dagger \mathbf{R}^{-1} \mathbf{h}_1|$, $\mathbf{R} = \mathbf{H}_I \mathbf{H}_I^\dagger + (\sigma^2/(P_s l_1))\mathbf{I}_{N_2}$ and $\gamma_2^{\mathrm{MMSE}} = ||\mathbf{h}_2||_F^2 P_2 l_2 / \sigma^2$. Unlike the MRC algorithm, both the ZF and MMSE receivers require the exact CSI and CCI, which can be estimated with the aid of algorithms proposed in [61] and [62]. However, to obtain accurate CSI and CCI always implies a higher system overhead. In addition, the number of undesired source nodes in the PPP model has a probability to become very large. Therefore, when designing a relay, we should flexibly decide the number of antennas equipped at the relay and select the signal processing strategy appropriately. More specific discussion can be found in section IV.

4.3 Capacity Analysis

In this section, we investigate the capacity for our dual-hop AF relaying system implementing MRC/MRT, ZF/MRT and MMSE/MRT transferring strategies. The ergodic capacity is defined as

$$C = \frac{1}{2}\mathbb{E}\{\log_2(1+\gamma)\} \ \ \mathrm{bits/s/Hz}, \tag{4.13}$$

where γ is the end-to-end SINR and the factor $\frac{1}{2}$ is caused by the half-duplex limitation.

4.3.1 MRC/MRT Scheme

Substituting (4.6) into (4.13), the ergodic capacity undergoing MRC/MRT relaying can be written as

$$\begin{aligned} C_{\mathrm{MRC}} &= \frac{1}{2}\mathbb{E}\left\{\log_2\left(1+\frac{\gamma_1^{\mathrm{MRC}}\gamma_2^{\mathrm{MRC}}}{1+\gamma_1^{\mathrm{MRC}}+\gamma_2^{\mathrm{MRC}}}\right)\right\} \\ &= \frac{1}{2}\mathbb{E}\left\{\log_2\left(\frac{(1+\gamma_1^{\mathrm{MRC}})(1+\gamma_2^{\mathrm{MRC}})}{1+\gamma_1^{\mathrm{MRC}}+\gamma_2^{\mathrm{MRC}}}\right)\right\} \\ &= C_{\gamma_1^{\mathrm{MRC}}} + C_{\gamma_2^{\mathrm{MRC}}} - C_{\gamma_T^{\mathrm{MRC}}}, \end{aligned} \tag{4.14}$$

where

$$C_{\gamma_i^{\mathrm{MRC}}} = \frac{1}{2}\mathbb{E}\{\log_2(1+\gamma_i^{\mathrm{MRC}})\},\ \ i\in\{1,2\} \tag{4.15}$$

$$C_{\gamma_T^{\mathrm{MRC}}} = \frac{1}{2}\mathbb{E}\{\log_2(1+\gamma_T^{\mathrm{RMC}})\}.\ \gamma_T^{\mathrm{MRC}} = \gamma_1^{\mathrm{MRC}}+\gamma_2^{\mathrm{MRC}} \tag{4.16}$$

Proposition 3. *In the MRC/MRT transferring scheme, the end-to-end capacity with co-channel interference mapped in the infinite homogeneous Poisson field can be calculated by*

$$C_{\mathrm{MRC}} = C_{\gamma_1^{\mathrm{MRC}}} + C_{\gamma_2^{\mathrm{MRC}}} - C_{\gamma_T^{\mathrm{MRC}}}, \tag{4.17}$$

where

$$\begin{aligned} C_{\gamma_1^{\mathrm{MRC}}} =& \frac{1}{2\ln 2}\sum_{n=0}^{N}\frac{w_n}{1+s_n}\sum_{k=0}^{N_1-1}\frac{1}{k!}\sum_{q=0}^{k}\binom{k}{q}\sum_{l=0}^{k-q}\frac{(-1)^{k-q-l}}{l!}(I_s)^{\frac{2l}{\alpha}}(N_s)^q\pi^l\Gamma\left(1-\frac{2}{\alpha}\right)^l \\ &\times\lambda^l\Gamma\left(1+\frac{2}{\alpha}\right)^l\exp\left(-N_s s_n-\lambda\pi(I_s)^{\frac{2}{\alpha}}s_n^{\frac{2}{\alpha}}\Gamma\left(1-\frac{2}{\alpha}\right)\Gamma\left(1+\frac{2}{\alpha}\right)\right) \\ &\times\sum_{i=0}^{l}\frac{(-1)^i\binom{l}{i}\Gamma\left(1+\frac{2(l-i)}{\alpha}\right)}{1-k+q+\Gamma\left(1+\frac{2(l-i)}{\alpha}\right)}, \end{aligned} \tag{4.18}$$

$$C_{\gamma_2^{\mathrm{MRC}}} = \frac{1}{2\ln 2}\sum_{k=0}^{N_1-1}e^{N_r}(N_r)^k\Gamma(-k,Nr), \tag{4.19}$$

$$C_{\gamma_T^{\mathrm{MRC}}} = \frac{1}{2\ln 2}\sum_{n=0}^{N}\frac{w_n e^{-s_n}}{s_n}\left(1-\left(\frac{N_r}{N_r+s_n}\right)^{N_1}\left(1-s_n\sum_{k=0}^{N_1-1}\frac{1}{k!}\sum_{q=0}^{k}\binom{k}{q}\sum_{l=0}^{k-q}\frac{1}{l!}\right.\right.$$
$$\times(-1)^{k-q-l}I_s^{\frac{2}{\alpha}}(N_s)^q\pi^{l-\frac{u+v}{2}+1}\lambda^l\Gamma\left(1-\frac{2}{\alpha}\right)^l\Gamma\left(1+\frac{2}{\alpha}\right)^l\frac{u^{\frac{1}{2}}v^{q+\frac{2l}{\alpha}}+\frac{1}{2}}{2^{\frac{(u+v-2)}{2}}}$$
$$\times \mathrm{G}_{v,u}^{u,v}\left(\frac{(I_s)^{\frac{2}{\alpha}}\pi\lambda\Gamma\left(1-\frac{2}{\alpha}\right)\Gamma\left(1+\frac{2}{\alpha}\right)u^{-u}}{(N_s+s_n)v^{-v}}\middle|\begin{matrix}\mathcal{Q}(-1-q-\frac{2l}{\alpha},v)\\ \mathcal{Q}(-1,u)\end{matrix}\right)$$
$$\left.\left.\times(N_r+s_n)^{-q-\frac{2l}{\alpha}-1}\sum_{i=0}^{l}\frac{(-1)^i\binom{l}{i}\Gamma\left(\frac{2(l-i)}{\alpha}\right)}{\Gamma\left(1-k+q+\frac{2(l-i)}{\alpha}\right)}\right)\right). \tag{4.20}$$

Integers v and u can constitute a fraction satisfying $\frac{v}{u}=\frac{2}{\alpha}$. Expression $\mathcal{Q}(a,b)$ presents a list $\frac{1+a}{b},\cdots,\frac{b+a}{b}$. The parameters $N_s=\sigma^2(R_1)^\alpha/P_s$ and $I_s=P_I(R_1)^\alpha/P_s$ denote the corresponding AWGN and interference power with normalized transmitting gain of the signal-relay transmission, respectively. Similarly, for the relay-destination hop, $N_r=\sigma^2(R_2)^\alpha/P_r$. Parameters N, s_n and w_n are the number of integration points, abscissas and corresponding weights of the Gaussian-Chebyshev Quadrature (GCQ). The abscissa and weights s_n and w_n are respectively defined by

$$s_n=\tan\left(\frac{\pi}{4}\cos\left(\frac{2n-1}{2N}\pi+\frac{\pi}{4}\right)\right), \tag{4.21}$$

$$w_n=\frac{\pi^2\sin\left(\frac{2n-1}{2N}\pi\right)}{4N\cos^2\left(\frac{\pi}{4}\cos\left(\frac{2n-1}{2N}\pi+\frac{\pi}{4}\right)\right)} \tag{4.22}$$

This calculation converges steadily, and can accurately estimate the numerical result of the integral when $N\geq 100$.

Proof. See Appendix A.3. □

In the limited-area interference scenario, due to the difficulty of finding closed-form expressions of the statistics of the joint variable $\gamma_{T^{\mathrm{MRC}}}^{lim}$, we just derive the expression of the lower bound of C_{MRC}^{lim} based on:

$$C_{\gamma_T}\leq\frac{1}{2}\log_2\left(1+\mathbb{E}\{\gamma_1\}+\mathbb{E}\{\gamma_2\}\right). \tag{4.23}$$

Inequality (4.23) is obtained according to Jensen's inequality based on the fact that $\log_2(1+x_1+x_2)$ is concave. We evaluated the system performance when interferers are

located in a round area with limited radius R. This assumption can depict the circumstance that, an AF relay suffers interference from a heterogeneous network built nearby. In this case, a direct evaluation of the capacities seems intractable, because it is difficult to give the analytical expression of the pdf or moment generating function (MGF) of the variable $\gamma_{T^{\mathrm{MRT}}}^{lim} = \left(\gamma_{1^{\mathrm{MRT}}}^{lim} + \gamma_{2^{\mathrm{MRT}}}^{lim}\right)$. Therefore, we access the system performance by deriving a lower bound on the end-to-end capacity with the help of (4.23).

Proposition 4. *When co-channel interferers are mapped in a round area with radius R, the lower bound of end-to-end capacity can be accurately evaluated by*

$$C_{L_{\mathrm{MRC}}}^{lim} \simeq C_{\gamma_1^{\mathrm{MRC}}}^{lim} + C_{\gamma_2^{\mathrm{MRC}}}^{lim} - C_{\gamma_T^{\mathrm{MRC}}}^{lim}, \tag{4.24}$$

$$\begin{aligned} C_{\gamma_1^{\mathrm{MRC}}}^{lim} =& \frac{1}{2\ln 2}\sum_{n=1}^{N} w_n \left(\frac{1}{s_n} - \frac{1}{s_n(1+s_n)^{N_1}}\right) \exp\left(-\lambda\pi R^2 \left(1 - \frac{2R^\alpha}{2+\alpha}(I_r)^{-1}(s_n)^{-1}\right)\right. \\ & \left. \times\, {}_2F_1\left(1, 1+\frac{2}{\alpha}, 2+\frac{2}{\alpha}, -\frac{R^\alpha}{I_r s_n}\right)\right) e^{-N_r s_n} \end{aligned} \tag{4.25}$$

$$C_{\gamma_2^{\mathrm{MRC}}}^{lim} = \frac{1}{2\ln 2}\sum_{k=0}^{N_1-1} e^{N_r}(N_r)^k \Gamma(-k, Nr), \tag{4.26}$$

$$\begin{aligned} C_{\gamma_T^{\mathrm{MRC}}}^{lim} =& \frac{1}{2}\log_2\left(1 + \frac{N_1}{N_r} + \sum_{n=1}^{N} w_n \exp(N_r s_n) \exp\left(-\lambda\pi R^2 \left(1 - \frac{2R^\alpha}{2+\alpha}(I_r)^{-1}(s_n)^{-1}\right)\right.\right. \\ & \left.\left. \times\, {}_2F_1\left(1, 1+\frac{2}{\alpha}, 2+\frac{2}{\alpha}, -\frac{R^\alpha}{I_r s_n}\right)\right)\right). \end{aligned} \tag{4.27}$$

Proof. See Appendix A.4 □

4.3.2 ZF/MRT Scheme

According to the number of interferers N_2, the expressions of capacity for the ZF/MRT relaying system are derived considering two cases. In case 1, $N_2 < N_1$, the ZF receiver deploys N_2 dimensions to eliminate the interference and the source channel employs $(N_1 - N_2)$ degree of freedoms for the transmission. In case 2, $N_2 \geq N_1$, the ZF receiver leaves only 1 dimension of subspace to the source channel, eliminates the strongest $N_1 - 1$ interferers and treats other interference as noise. Due to the complexity, we only evaluate the lower bound of end-to-end capacity for case 1 for ZF/MRT processing scenario.

Proposition 5. *When interferers are mapped in limited area, the lower bound of end-to-end capacity in the ZF relaying scheme can be expressed as*

$$C_{L_{\mathrm{ZF}}}^{lim} = \overline{C}_{\mathrm{ZF}}^{N_2 \geq N_1} + C_{\mathrm{ZF}}^{N_2 < N_1}, \tag{4.28}$$

where $\overline{C}_{\mathrm{ZF}}^{N_2 \geq N_1}$*, given by (4.29), is the lower bound of* $C_{L_{\mathrm{ZF}}}^{lim}$ *for the condition that only part of interference can be removed by the ZF receiver, and* $C_{\mathrm{ZF}}^{N_2 < N_1}$*, given by (4.31), is the exact value of capacity for the condition that all interference can be removed.*

$$\begin{aligned}
&\overline{C}_{\mathrm{ZF}}^{N_2 \geq N_1} = \\
&\frac{1}{2\ln 2} \sum_{m_1=1}^{M} a_{m_1} e^{-\lambda\pi(b_{m_1})^2} \frac{2\left(\lambda\pi(b_{m_1})^2\right)^{N_1-1}}{b_{m_1}\Gamma\left(N_1-1\right)} \left[\sum_{n_1=1}^{N} \frac{w_{n_1} e^{N_s s_{n_1}}}{1+s_{n_1}} \left(1-\exp\left(-\lambda\pi\left(R^2-b_{m_1}^2\right)\right.\right.\right. \\
&\times \left(1-\frac{2\left(R^2-b_{m_1}^2\right)^{-1}}{\alpha+2}(I_s s_{n_1})^{-1}\left(R^{\alpha+2}\,{}_2F_1\left(1,1+\frac{2}{\alpha};2+\frac{2}{\alpha},-\frac{R^\alpha}{I_s s_{n_1}}\right)\right.\right. \\
&\left.\left.\left.\left.\left.-b_{m_1}^{\alpha+2}\,{}_2F_1\left(1,1+\frac{2}{\alpha};2+\frac{2}{\alpha},-\frac{b_{m_1}^\alpha}{I_s s_{n_1}}\right)\right)\right)\right)\right)\right] \\
&-\frac{P_{N_1-1}(R)}{2}\left[\log_2\left(1+\sum_{n_2=1}^{N}\sum_{m_2=1}^{M} a_{m_2} e^{-\lambda\pi(b_{m_2})^2} \frac{2\left(\lambda\pi(b_{m_2})^2\right)^{N_1-1}}{b_{m_2}\Gamma\left(N_1-1\right)P_{N_1-1}(R)} w_n e^{N_s s_{n_2}}\right.\right. \\
&\times \exp\left(-\lambda\pi\left(R^2-b_{m_2}^2\right)\left(1-\frac{2\left(R^2-b_{m_2}^2\right)^{-1}}{(\alpha+2)I_s s_{n_2}}\left(R^{\alpha+2}\,{}_2F_1\left(1,1+\frac{2}{\alpha};2+\frac{2}{\alpha},-\frac{R^\alpha}{I_s s_{n_2}}\right)\right.\right.\right. \\
&\left.\left.\left.\left.-b_{m_2}^{\alpha+2}\,{}_2F_1\left(1,1+\frac{2}{\alpha};2+\frac{2}{\alpha},-\frac{b_{m_2}^\alpha}{I_s s_{n_2}}\right)\right)\right)\right)+\frac{N_1}{N_r}\right)\right] \\
&+\frac{1}{2\ln 2}P_{N_1-1}(R)\left[\sum_{k=0}^{N_1-1} e^{N_r}(N_r)^k\Gamma(-k,N_r)\right]
\end{aligned} \tag{4.29}$$

where $P_{N_1-1}(R) = 1 - \frac{\Gamma(N_1-1,\lambda\pi R^2)}{\Gamma(N_1-1)}$ *is the probability that the distance from relay to the* (N_1-1)*-th interferer is smaller than* R*. The weight* a_m *and abscissa* b_m *of a typical GCQ are given by*

$$a_m = \frac{\pi R}{2M}\sqrt{1-\cos\left(\frac{(2m-1)\pi}{2M}\right)}, \tag{4.30a}$$

$$b_m = \frac{R}{2} + \frac{R}{2}\cos\left(\frac{(2m-1)\pi}{2M}\right). \tag{4.30b}$$

$$
\begin{aligned}
&C_{\mathrm{ZF}}^{N_2<N_1} = \\
&\frac{1}{2\ln 2}\sum_{N_2=0}^{N_1-1} e^{-\lambda\pi R^2}\frac{\left(\lambda\pi R^2\right)^{N_2}}{N_2!}\left[\sum_{k=0}^{N_1-N_2-1}(N_s)^k\, e^{N_s}\Gamma\left(-k,N_s\right)\right] \\
&-\left[\sum_{k_1=0}^{N_1-N_2-1}\mathrm{U}\left(1,1-k_1;N_s\right)+\sum_{k_2=0}^{N_1-1}\mathrm{U}\left(1,1-k_2;N_r\right)-\frac{1}{N_sN_r}\sum_{k_1=0}^{N_1-N_2-1}\sum_{k_2=0}^{N_1-1}\right. \\
&\left.\times \mathrm{G}_{1,1:1,0,1:1}^{1,1,1,1,1}\left(\begin{matrix}1/N_s\\1/N_r\end{matrix}\middle|\begin{matrix}2\\-k_1;-k_2\\-\\0;0\end{matrix}\right)\right]+\left[\sum_{k_3=0}^{N_1-N_2-1}(N_s)^{k_3}\, e^{N_s}\Gamma\left(-k_3,N_s\right)\right]. \qquad (4.31)
\end{aligned}
$$

Proof. See Appendix A.5 □

Due to the difficulty of finding the expression for the limit when $R \to \infty$, we can observe the infinite-area interference scenario by assigning a large value to R in equation (4.28). Meanwhile, in order to guarantee the accuracy of GCQ calculation, the integral points number M should be greater than for the small-R scenario. For instance, we can choose $M = 15$ for $R = 50$ metres, and $M = 50$ when $R = 1000$ metres.

4.3.3 MMSE/MRT Scheme

Proposition 6. *With MMSE/MRT relaying, the end-to-end system performance for the $R \to \infty$ scenario can be evaluated by*

$$C_{\mathrm{MMSE}} = C_{\gamma_1^{\mathrm{MMSE}}} + C_{\gamma_2^{\mathrm{MRC}}} - C_{\gamma_T^{\mathrm{MMSE}}}, \qquad (4.32)$$

where

$$C_{\gamma_{1\text{MMSE}}} = \sum_{i=0}^{N_1-1}\sum_{n=1}^{N} \frac{w_n\left(\lambda\Delta(I_s)^{\frac{2}{\alpha}} s_n^{\frac{2}{\alpha}} + N_s s_n\right)^i}{i!(1+s_n)} \exp\left(-\lambda\Delta(I_s)^{\frac{2}{\alpha}} s_n^{\frac{2}{\alpha}} - N_s s_n\right), \quad (4.33)$$

$$C_{\gamma_2^{\text{MMSE}}} = \frac{1}{2\ln 2}\sum_{k=0}^{N_1-1} e^{N_r}(N_r)^k \Gamma(-k, Nr), \quad (4.34)$$

$$C_{\gamma_2^{\text{MMSE}}} = \frac{1}{2\ln 2}\sum_{n=0}^{N} w_n \frac{e^{-s_n}}{s_n}\left(1 - \left(\frac{N_r}{N_r+s_n}\right)^{N_1}\left(1 - s_n\sum_{i=0}^{N_1-1}\sum_{k=0}^{i}\frac{\binom{i}{k}}{i!}\lambda^k\Delta^k(I_s)^{\frac{2k}{\alpha}}\right.\right.$$
$$\left.\left.\times\frac{(N_s)^{i-k}\, q^{\frac{1}{2}} p^{\frac{2k}{\alpha}+i-k+\frac{1}{2}}}{(2\pi)^{(p+q-2)/2}} \text{G}_{q,p}^{p,q}\left(\frac{\left(\frac{\lambda\Delta(I_s)^{\frac{2}{\alpha}}}{q}\right)^q}{\left(\frac{N_s+s_n}{p}\right)^p}\middle| \begin{matrix}\mathcal{Q}(-\frac{2k}{\alpha}-i+k-1,p)\\ \mathcal{Q}(-1,q)\end{matrix}\right)\right)\right), \quad (4.35)$$

where $\Delta = \frac{2\pi}{\alpha}\Gamma\left(\frac{2}{\alpha}\right)\Gamma\left(1-\frac{2}{\alpha}\right)$*,* s_n *and* w_n *have been defined by (4.21) and (4.22).*

Proof. See Appendix A.6. □

Proposition 7. *In the limited-R scenario, the end-to-end capacity with MMSE/MRT relaying scheme can be evaluated through the lower bound given by*

$$C_{L^{\text{MMSE}}} = C_{\gamma_1^{\text{MMSE}}}^{lim} + C_{\gamma_2^{\text{MRC}}}^{lim} - C_{\gamma_T^{\text{MMSE}}}^{lim}, \quad (4.36)$$

where

$$C_{\gamma_1^{\text{MMSE}}}^{lim} = \frac{1}{2\ln 2}\sum_{i=0}^{N_1-1}\sum_{n=1}^{N}\frac{w_n\left(\lambda\pi R^2\, {}_2F_1\left(1,\frac{2}{\alpha},1+\frac{2}{\alpha},-\frac{R^\alpha}{I_s s_n}\right)+N_s s_n\right)^i}{i!(1+s_n)}$$
$$\times\exp\left(-\lambda\pi R^2\, {}_2F_1\left(1,\frac{2}{\alpha},1+\frac{2}{\alpha},-\frac{R^\alpha}{I_s s_n}\right)-N_s s_n\right), \quad (4.37)$$

$$C_{\gamma_2^{\text{MMSE}}}^{lim} = \frac{1}{2\ln 2}\sum_{k=0}^{N_1-1} e^{N_r}(N_r)^k\Gamma(-k,Nr), \quad (4.38)$$

$$C_{\gamma_T^{\text{MMSE}}}^{lim} = \frac{1}{2}\log_2\left(1+\sum_{n=1}^{N} w_n \frac{s_n\exp\left(-N_s s_n-\lambda\pi R^2\, {}_2F_1\left(1,\frac{2}{\alpha},1+\frac{2}{\alpha},-\frac{R^\alpha}{I_s s_n}\right)\right)}{\Gamma(N_1)}\right.$$
$$\times\left(N_s+\frac{2\pi\lambda R^{\alpha+2}}{(\alpha+2)I_s s_n^2}\, {}_2F_1\left(2,1+\frac{2}{\alpha},2+\frac{2}{\alpha},-\frac{R^\alpha}{I_s s_n}\right)\right)$$
$$\left.\times\left(\lambda\pi R^2\, {}_2F_1\left(1,\frac{2}{\alpha},1+\frac{2}{\alpha},-\frac{R^\alpha}{I_s s_n}\right)+N_s s_n\right)^{N_1-1}+\frac{N_1}{N_r}\right) \quad (4.39)$$

Proof. See Appendix A.7. □

4.4 Numerical Results

In this section, the numerical results are presented to illustrate the effect of signal processing strategies, SNRs and antenna numbers on the system performance; Monte Carlo simulations are provided as well. Unless otherwise stated, all numerical experiments in this section will adopt the following set-up. The SNR is obtained at the receiver side. Without loss of generality, we assume P_s=P_r for γ_1 and γ_2 in all three signal processing schemes, (4.6), (4.9) and (4.12), therefore, the average SNR is given by SNR$= 1/N_s = 1/N_r$. Concerning the density of interferers λ, since in a well-managed LTE system, different users share orthogonal time and frequency resources, the co-channel interference is only caused by neighbouring cells (infinite-area scenario) or heterogeneous networks (limited-area scenario). Therefore, the order of magnitude of λ is set to be 10^{-4}, which guarantees that in each wireless cell, only a small number of users will disturb the desired transmission. When two cells are overlapped, the co-channel interferers could be more than one, because in a LTE system, each use could be assigned random sub channels from the whole channel resources, different sub channels could be disturbed by different users served by the other cell. We assume the transmission power $P_s = P_r = 10$, and the interference power $P_I = 0.02$. For the limited-area interference scenario, we set R=50(m), and for the infinite-area interference, we run simulations with $R = 1000$(m). Moreover, all Monte Carlo simulations are carried out through 10^5 iterations.

The system capacities applying three signal processing schemes (MRC, ZF or MMSE combined with MRT transmission) with different SNRs are depicted by Figures 4.2(a) with $\lambda = 0.0005$, $N_1 = 8$, $R \to \infty$ (R=1000(m) in simulation) and 4.2(b) with $\lambda = 0.0005$, $N_1 = 8$ R=50(m). In Figure4.2(a), the accuracy of analytical expressions for the end-to-end ergodic capacity for MRC/MRT and MMSE/MRT schemes is verified. In addition, the lower-bound expression for ZF/MRT relaying matches the simulation well, where the gap is around 0.05 bits/s/Hz. There exist only small differences between the theory result and simulation, which results from the computational limits on our Monte-Carlo simulation, the complexity of evaluating the theoretical results becomes very high if we choose large R, for example $R = 10000$(m). The comparison among the three signal processing schemes demonstrates that the highest system capacity is always achieved by the MMSE/MRT scheme, and the ZF/MRT scheme performs the worst. As expected, when the noise is relatively large, the MRC receiver performs as well

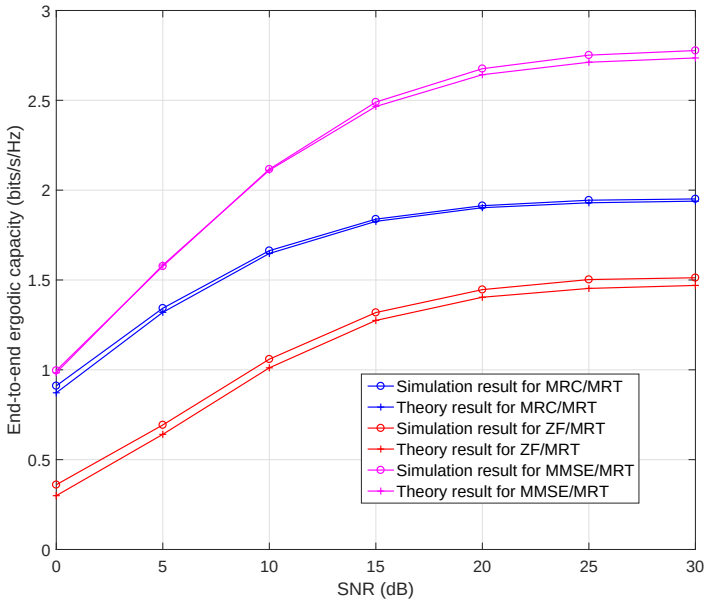

(a) $R \to \infty N1 = 8, \lambda = 0.0005$

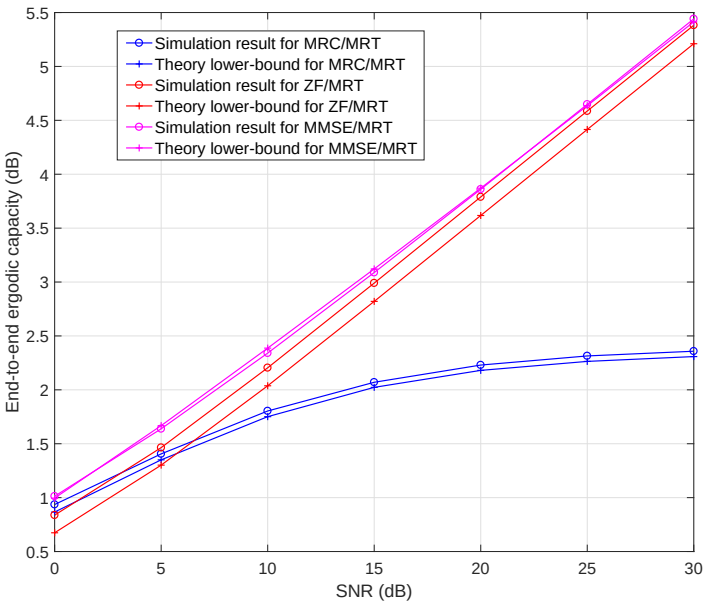

(b) $R = 50, N1 = 8, \lambda = 0.0005$

Figure 4.2: *Capacity versus SNR*

as the MMSE receiver. However, even when the system noise can be neglected, the ZF receiver cannot take advantage, because when $R \to \infty$, the number of interferers must be greater than antennas, the ZF receiver can only use 1 degree of freedom for the desired signal and use the remaining ones to try to cancel interference.

Figure 4.2(b) verifies the tightness of our expressions of the lower bounds. In the whole SNR domain, the gap between analytical expression and simulation results is less than 0.05 bits/s/Hz for MRC/MRT scheme and is less than 0.2 bits/s/Hz for ZF/MRT scheme. Comparing with Figure 4.2(a), an interesting observation is revealed by our analysis on the end-to-end capacity with interference in limited area. As the system noise declines, the performance provided by MRC receiver is obviously constrained by the interference. On the contrary, both the ZF/MRT and MMSE/MRT relaying have linearly increasing capacity results as the SNR in dB increases, and the performance of ZF/MRT relaying becomes closer to MMSE/MRT as the SNR increases. When $\lambda = 0.0005$, the average number of antennas $\mu = \lambda\pi R^2$ is around 4. That is to say, with high probability, the ZF receiver can remove all the interference by using a small number of degrees of freedom, and enhance the signal strength with the remainder. It should be emphasized that, the power of interference is not observed as a variable here, because the variance of SNR has covered different interference to noise power ratio cases.

Figure 4.3(a) and Figure 4.3(b) show the system capacity for the three signal processing strategies versus the number of antennas, where λ=0.0005, SNR=15dB. The accuracy of our exact capacity equations and the tightness of our lower-bound expressions are shown to be good, except for the ZF/MRT scheme in limited-R scenario, the gap exceeds 0.2 bits/s/Hz when $N_1 \leq 6$. In Figure 4.3(a), where R$\to \infty$, the end-to-end capacity with MMSE/MRT transferring scheme increases faster than that with MRC/MRT strategy. The performance of the ZF receiver obtains the least benefits from increasing the number of antennas. With 4 antennas at the relay, the MMSE/MRT method has a gain of a 0.4 bit/s/Hz over the MRC/MRT scheme and MRC/MRT scheme performs 0.3 bits/s/Hz better than ZF/MRT. As the antenna number increase to 16, these performance gaps grow to 0.8 bits/s/Hz and 0.8 bits/s/Hz, respectively. We can conclude that, in an infinite interference area, the diversity in transmission is more significant than the ability to removing interference.

However, in Figure 4.3(b), where the interference range R reduces to 50(m), the ZF receiver performance shows the advantage of interference cancellation in this case. As the number of antennas increases the performance of ZF/MRT scheme approaches that of MMSE/MRT, which

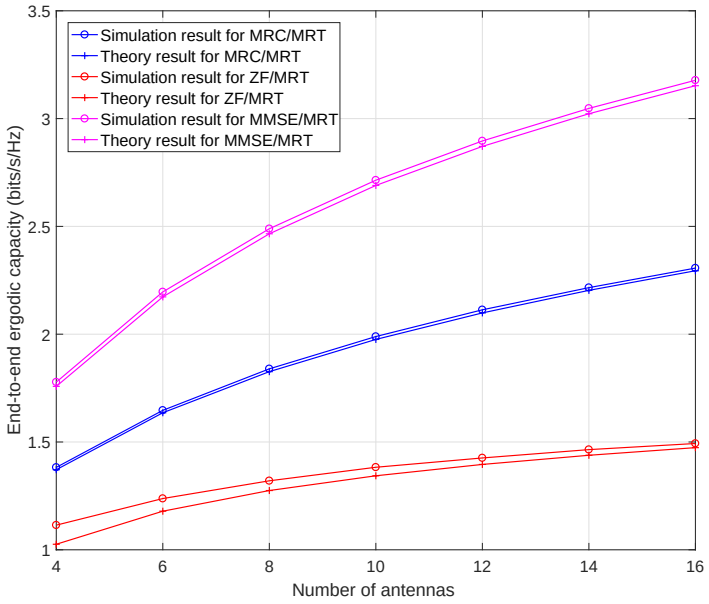

(a) $R \to \infty$, $SNR = 15\text{db}$, $\lambda = 0.0005$

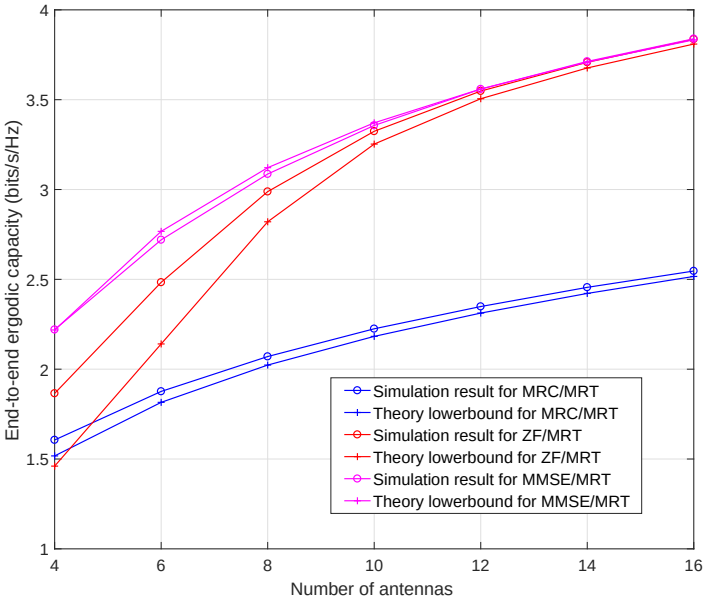

(b) $R = 50$, $\text{S}NR = 15\text{db}$, $\lambda = 0.0005$

Figure 4.3: *Capacity versus SNR*

is much better than the MRC/MRT scheme. Again, it is worth noting that, the expectation of interferer number here is around 4, when N_1=4, the ZF receiver performs in the medium of the MMSE and MRC receivers, and when N_1 is greater than double of μ, the ZF receiver performs almost as well as the MMSE one.

Figure 4.4(a) and Figure 4.4(b) present the difference of system performance between PPP interference model and fixed-number-fixed-distance interference model. Since the fixed-number-fixed-distance model is not able to depict the infinite-area interference scenario, the comparisons only concentrate on the limited-area interference scenario, with R=50(m) for the PPP model and $r_{I_i} = \mathbb{E}\{r_I\} = \frac{2R}{3}$ for the traditional model, where $i = 1, \cdots, u$, u is the number of interferers for fixed-interference model, and is the expected number of interferers ($u = \lambda\pi R^2$) for the PPP model. In this chapter, figures of the fixed-interference model are generated through Monte-Carlo simulations. In Figure 4.4(a), which plots the capacities against SNR, we set $N_1 = 8$ and $u = 3$ or $u = 8$. We can find that the gaps between our PPP-aided analysis and traditional analysis are effected strongly by the number of interferers(expected) interference number u. When $u = 3$, all interference can be eliminated by ZF and MMSE receivers in the traditional case, and have a large probability bo be completely removed in the PPP case. Therefore, the performance of the ZF/MRT and MMSE/MRT schemes is dominated by the SNR value in these two cases. Both the fixed-interference model and our PPP-aided model can evaluated the performance for ZF/MRT and MMSE/MRT schemes accurately. However the MRC receiver cannot deal with any interference, so the fixed-interference performance analysis for MRC/MRT scheme presents obvious errors when averaging the number of interferers and averaging the received interference power strength. Within the whole SNR domain, capacities obtained through fixed-interference way are around 0.4 bits/s/Hz larger than those through our PPP-aided method. With $u = 8$, traditional analysis for MRC/MRT scheme suffers a larger error, which increases from 0.4 bits/s/Hz to 0.8 bits/s/Hz as the SNR grows from 0dB to 30dB. Surprisingly, the capacities for MMSE/MRT scheme analysed by fixed-interference method do not show too much error, only when SNR is greater than 20dB, they are a little smaller than those analysed through PPP-aided model. The largest error is related to the ZF/MRT processing. When SNR is greater than 10db, traditional evaluations start to generate lower capacities than the PPP-aided evaluations. The error grows to as large as 1 bit/s/Hz at SNR=30dB.

As shown in Figure4.4(b), the number of antennas N_1 will not significantly impact the gaps between fixed-interference evaluation curves and PPP-aided evaluation curves, except for the

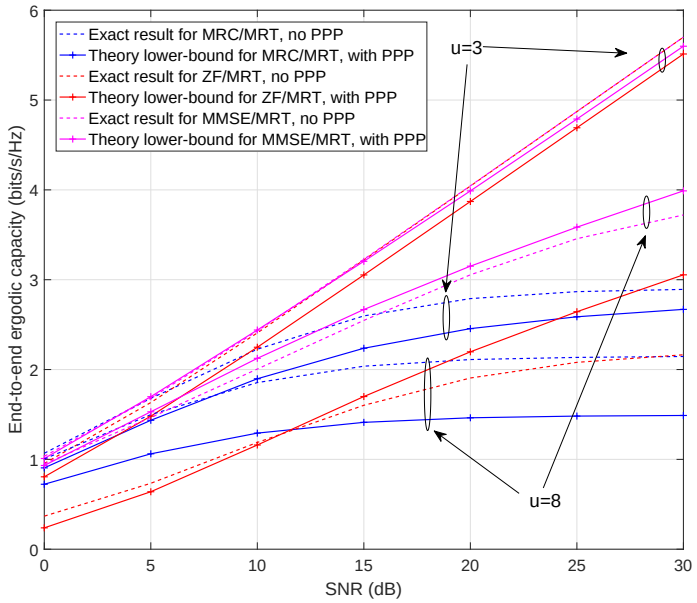

(a) $R = 50$, $N1 = 8$, $u = 3, 8$

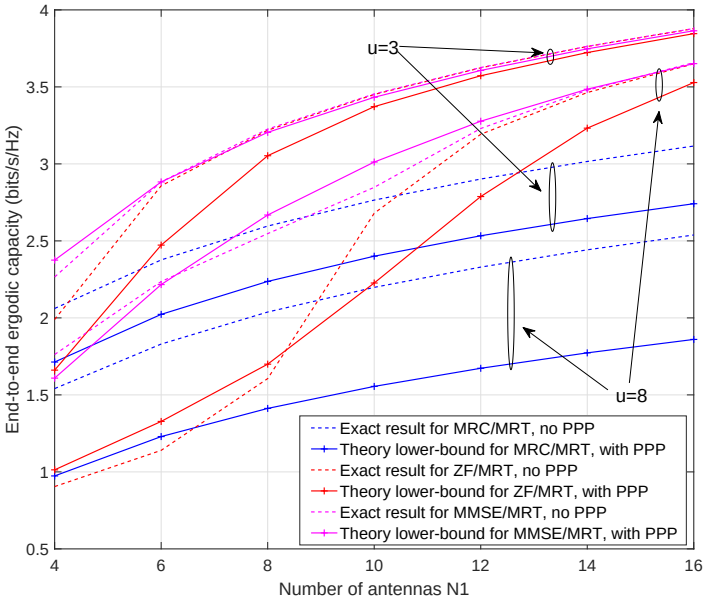

(b) $R = 50$, $SNR = 15\text{db}$, $u = 3, 8$

Figure 4.4: *PPP vs No PPP*

ZF/MRT processing scheme with large u. With $u = 8$, the capacities of ZF/MRT scheme generated by fixed-interference way are smaller than the PPP-aided evaluations when $N_1 < 8$, and when $N_1 > 8$, the fixed-interference performance analysis produce larger values than PPP-assisted evaluations. The largest error appears at $N_1 = 12$, which is around 0.5 bits/s/Hz.

In summary, fixed-interference-model analysis for the randomly-distributed-interference scenario always yields obvious errors, especially with big interference densities. For MMSE/MRT scheme, they generate smaller capacities for high-SNR cases and for MRC/MRT scheme, they produce much larger capacities. Finally, for the ZF/MRT scheme, they yield smaller capacities with small N_1 and bigger capacities with large N_1: for high SNRs, the error is dramatically enlarged.

4.5 Conclusion

In this chapter, we studied the end-to-end capacities of dual-hop multi-antenna AF relaying systems, in which the relay applies MRC/MRT, ZF/MRT and MMSE/MRT processing strategies to deal with randomly distributed co-channel interference. Two scenarios were analysed in this chapter, namely, the infinite-area-interference scenario and the limited-area-interference scenario. For the first one, we derived the analytical expressions to evaluate the exact end-to-end capacities with three transferring strategies; and for the latter one, we calculated the lower bound of the capacities. In most situations, the lower bounds match well our simulation results. Our analysis showed that the system with MMSE/MRT relaying achieved the best performance in all cases. The MRC/MRT scheme performed obviously worse than MMSE/MRT in all scenarios. Interestingly, the ZF/MRT scheme showed completely different properties in two scenarios. With infinite-area interference, it performed even worse than MRC/MRT, however with limited-area interference, especially when the the number of antennas is double that of the expected interferers, it could perform as well as the MMSE/MRT scheme. In addition, we have proved that, for a randomly-distributed interference scenario, the PPP-aided performance analysis produces quite different results from fixed-interference-model analysis, especially for ZF/MRT and MRC/MRT schemes.

Chapter 5
NOMA in Dual-hop Relaying System with Randomly Distributed Users

5.1 Introduction

The non-orthogonal multiple access technique has aroused significant attention as a promising candidate for the multiple access scheme for the upcoming 5th-generation wireless communication standard. According to the future radio access (FRA), there will be an expectation of 500 fold increase of system throughput performance. Beyond the delay-sensitive and high-volume services, a high-priority requirement for the FRA is the significant enlargement of system throughput, which is related to massive connectivity. To satisfy this exponentially enhanced demands, the NOMA technique was proposed by [63], with the purpose of cooperation with other approaches. On one hand, the proposed NOMA technique is expected to accommodate a 3-fold enhancement of frequency efficiency. On the other hand, increasing the number of connected users is hoped to be achieved by the NOMA technique. According to [64], newly proposed NOMA techniques can be divided to two dominant sorts, namely power domain NOMA and code domain NOMA. In this chapter, NOMA only denotes NOMA in power domain.

In the past few years, NOMA-assisted network has been widely investigated. A tutorial of the NOMA technique is provided by [16]. Taking a 2-user NOMA-assisted SISO system as example, this paper not only introduced the basic concepts of NOMA techniques, including superposition coding, successive interference cancellation and low-density spreading CDMA, but also discussed the effects of combining NOMA and other wireless communication concepts, such as path loss, cooperative NOMA, users paring and MIMO. The basic performance of a 2-user NOMA system for both downlink and uplink were derived and widely cited by recent research.

With respect to relay-aided networks, NOMA techniques can be easily applied in the relay-destination transmission. A simple diagram is given by Figure 5.1. The superposition coding

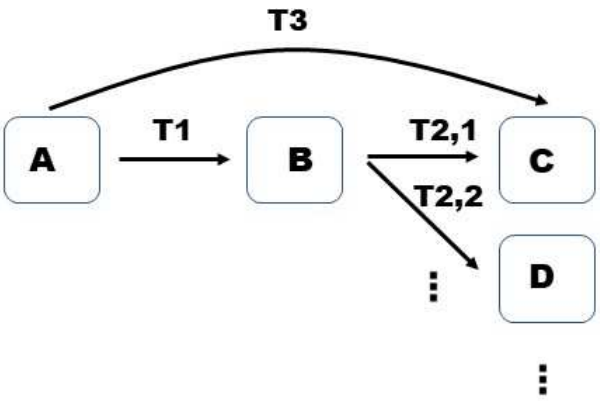

Figure 5.1: *Combining NOMA with dual-hop system*

(SC, more details of SC has been introduced in Chapter 2) is normally achieved by block A, which is the base station. However, sometimes SC is achieved by block B, such as in a DF relaying system, where block B is the relay. Some concepts combined the cooperative relaying network with NOMA, such as [65, 66]. The authors of [65] designed and evaluated a dual-hop relaying network, where the first user in the NOMA transmission played the role as a cooperative AF relay. Using Figure 5.1, block B denotes user 1, block C denotes user 2. Block A transmits SC signals to B and C at the same time. Like a cooperative AF relaying, block B immediately transmits received signals without any delaying, meanwhile it abstracts desired information at the background. The collaborative scheme in [66] constructed a 3-user NOMA network and assigned the first user as a relay. Using Diagram 5.1, block B, C and D denote user 1, 2, and 3, respectively. In order to avoid the difficulties of applying full-duplex techniques, researchers assume that the base station cannot directly communicate with user 2 and 3, so user 1 would demodulate its required signals and forward the remaining signals. Despite the advanced concepts, a great challenge is the battery life of current portable devices. Therefore, most researchers are focusing on NOMA cooperating with independent relays. The authors of [67] derived the analytical expressions of outage probability and ergodic sum rate for the dual-hop AF relaying network applying NOMA over Nakagami-m fading channels. Considering antenna selection and energy harvesting techniques, the analytical expression of the outage probability for a dual-hop NOMA network in a Nakagami-m channel was derived by [68]. For a cooperative full-duplex dual-hop network, a 1-user NOMA scenario was studied by [69], where authors provided analytical expressions of the outage probability and the ergodic capacity. Applying relay selection and power allocation techniques at the relay, a 2-user NOMA network was analysed by [70] and [71]. Considering imperfect CSI, the performance of downlink relay-assisted NOMA was investigated by [72]. A hybrid DF-AF relaying with

NOMA was proposed and evaluated by [73].

There have been many papers revealing the advantages of NOMA, however most analytical performance investigations assigned fixed path loss to different users in a NOMA cluster. From the perspective of the system level, channel fading is not the unique factor determining the power assignment for each user, the path loss is important as well. Especially, in the future 5G wireless communication, small cells will be widely applied, and the variance of positions become more significant. However, to the best of our knowledge, there is no work evaluating NOMA-aided relaying networks considering the uncertainty of user locations. The only relevant research is [74], which studied the performance of a single-hop NOMA network with randomly located users in a cell.

Motivated by this, we analyse the downlink performance of AF relaying networks over complex Gaussian channels in this chapter, where the NOMA technique in the power domain is implemented for the relay-destination transmissions. Outage probabilities of the dual-hop AF relaying system with NOMA employed in the relay-destination transmission are derived in this chapter. Besides exact analytical expressions, high-SNR approximations are given as well. Based on the upper and lower bounds for the outage probability, we can compute the diversity of NOMA-aided dual-hop AF relaying system. Subject to complex Gaussian fading, this chapter investigates both single-antenna and multi-antenna relaying systems, where the MRC/MRT scheme is applied at the relay for the multi-antenna case.

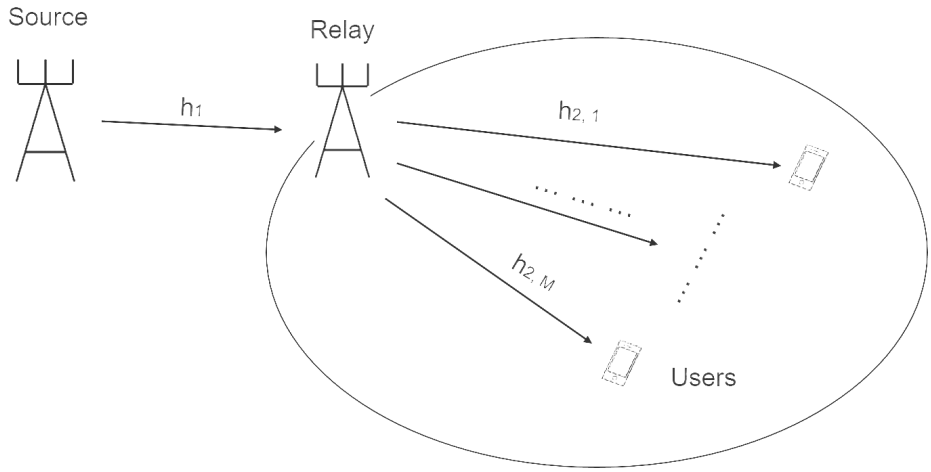

Figure 5.2: *A NOMA-aided dual-hop relaying system*

5.2 System Model

We consider a single cell downlink AF relaying system shown in Figure 5.1. The source and relay are at fixed locations with distance R_1, and mobile users served by the relay are divided into different NOMA groups. In the same NOMA group, users share the same time slots, frequency and spreading codes. In this chapter, we assume the system only supports a fixed number M of users in a particular NOMA group, these users are uniformly located in a round area $\mathcal{D}$ with radius R around the relay. Due to the limitation of mutual interference, the system works in a half-duplex mode.

In the following, the system model is first built for the single-antenna mode. In time slot one, the source transmits signals for all users to the relay, the channel coefficient is given by $h_1 = \frac{g_1}{\sqrt{1+R_1^\alpha}}$, where g_1 is the coefficient of small scale fading for the source-relay transmission, following a complex Gaussian distribution $\mathcal{CN}(0, \lambda_1)$ and $\frac{1}{1+R_1^\alpha}$ is the path-loss attenuation with exponent α. It should be emphasized that, as the lower limits of $r^{-\alpha}$, the form $\frac{1}{1+r^\alpha}$ could enable the performance evaluation for wireless communication in free space path loss environments (with $\alpha = 2$). It is practical in real applications because of the altitude intercept between the relay and users. In the second time slot, the relay transmits these signals to all M users in the same NOMA group. The channel coefficient between user U_i ($i = 1, \ldots, M$) and the relay is denoted by $h_{2,i} = \frac{g_{2,i}}{1+r_{2,i}^\alpha}$, where $g_{2,i}$ is the coefficient of small scale fading subject to a complex Gaussian distribution $\mathcal{CN}(0, \lambda_2)$ and $r_{2,i}$ is the distance between relay and the i-th nearest user. Moreover, the relay and the m-th mobile user are impacted by AWGN n_R and $n_{D,m}$, respectively. We assume $\mathbb{E}\{|n_R|^2\} = \mathbb{E}\{|n_{D,m}|^2\} = \sigma^2$, $m = 1, \cdots, M$. It should be noticed that, until here, the order of all $h_{2,i}$s are not related to the channel states, i.e. they are unordered channel coefficients.

Based on the settings above, we can write the signals received by the relay as

$$y_R = h_1 \sum_{i=1}^{M} \sqrt{a_i P_s} x_i + n_R, \tag{5.1}$$

where x_i is the signal for the i-th user with $\mathbb{E}\{xx^\dagger\} = 1$, P_s is the total transmission power at the source port, a_i is the power coefficient with $\sum_{i=1}^{M} a_i = 1$. Note that, the power allocation depends on the channel states of the relay-destiny transmissions $h_{2,i}$, $i = 1, \cdots, M$, but is only used by the source, because the relay applies a simple AF relaying scheme. Without loss of generality, we now sort the user order based on channel gains of relay-destination channels:

$|h_{2,1}|^2 \leq |h_{2,2}|^2 \leq \ldots \leq |h_{2,M}|^2$, and according to the principle of NOMA technique, we have $a_1 > a_2 > \cdots > a_M$.

The relay simply amplifies the received signal y_R and simultaneously transmits all the signals to users sharing the same time and frequency resource with each other at the second time slot. For the m-th destination D_m, $m < M$, the received signal can be expressed as

$$y_{D_m} = \sqrt{P_R}\kappa h_{2,m} h_1 \sum_{i=1}^{M} \sqrt{a_i P_S} x_i + \sqrt{P_R}\kappa h_{2,m} n_R + n_{D,m}, \tag{5.2}$$

where P_R is the transmission power of the relay, and the corresponding amplifying coefficient κ is given by $\kappa = 1/\sqrt{P_S|h_1|^2 + \sigma^2}$. By setting $P_R = P_S = P$ and denoting $\bar{\gamma} = \frac{P}{\sigma^2}$ (note that, unlike in Chapter 4, $\bar{\gamma}$ in this chapter is the average SNR at transmitter side), we can express the SINR of the m-th user as

$$\gamma_m = \frac{a_m \bar{\gamma}^2 |h_1|^2 |h_{2,m}|^2}{\bar{\gamma}^2 |h_1|^2 |h_{2,m}|^2 \sum\limits_{j=m+1}^{M} a_j + \bar{\gamma}(|h_1|^2 + |h_{2,m}|^2) + 1}. \tag{5.3}$$

In expression (5.3), the interference is the summation of signals assigned less power, which are not decoded by user m. It also implies that, (5.3) can hold only when the first $m-1$ signals have been decoded successfully. Denoting $\gamma_{i \to m}$ as the SINR when user m trying to decode the signal for user i, $(i < m)$, and $\gamma_{th,i}$ is the threshold that a user is able to decode the signal for user i, then we can say expression (5.3) holds only when the condition $\gamma_{i->m} < \gamma_{\mathrm{th},i}$ is met for all $i < m$. The SINR for the i-th $(i < m)$ signal decoded by user m is given by

$$\gamma_{i \to m} = \frac{a_i \bar{\gamma}^2 |h_1|^2 |h_{2,m}|^2}{\bar{\gamma}^2 |h_1|^2 |h_{2,m}|^2 \sum\limits_{j=i+1}^{M} a_j + \bar{\gamma}(|h_1|^2 + |h_{2,m}|^2) + 1} \tag{5.4}$$

Obviously, for user M who has best channel condition and least power assignment, the signals for all the other users should be decoded before decoding the signal for itself. Then, the desired SINR can be written as

$$\gamma_M = \frac{a_M \bar{\gamma}^2 |h_1|^2 |h_{2,M}|^2}{\bar{\gamma}(|h_1|^2 + |h_{2,M}|^2) + 1} \tag{5.5}$$

5.3 Outage Probability

The outage probability of the relaying network over a Rayleigh channel applying the NOMA technique is analysed to characterized our system. We provide the analytical expressions for both exact and asymptotic outage probabilities in this section.

5.3.1 Outage Event

Firstly, the outage event of the m-th user that fails to decode the signals for the i-th user ($i \leq m$) is defined by $E_{i\to m} = \{\gamma_{i\to m} < \gamma_{th,i}\}$, where $\gamma_{th,i}$ is the threshold of SINR for successfully decoding the signal for the i-th user. Since any failure to decode the signals for the i-th user ($i \leq m$, including decoding for itself) will result in the failure to decode the signal for the m-th user, the probability that user m cannot decode the required signal can be written as

$$Pr_m^{out} = 1 - Pr\left(E_{1\to m}^c \bigcap \cdots \bigcap E_{m\to m}^c\right), \tag{5.6}$$

where $E_{i\to m}^c$ is the complement of event $E_{i\to m}$. Based on the equation (5.4), the expression of event $E_{i\to m}^c$ is given by

$$\begin{aligned} E_{i\to m}^c &= \left\{ \frac{a_i\bar{\gamma}^2|h_1|^2|h_{2,m}|^2}{\bar{\gamma}^2|h_1|^2|h_{2,m}|^2 \sum\limits_{j=i+1}^{M} a_j + \bar{\gamma}(|h_1|^2 + |h_{2,m}|^2) + 1} > \gamma_{th,i} \right\} \\ &= \left\{ \left[\bar{\gamma}^2\left(a_i - \gamma_{th,i}\sum_{j=i+1}^{M} a_j\right)|h_{2,m}|^2 - \bar{\gamma}\gamma_{th,i}\right]|h_1|^2 > \gamma_{th,i}\left(1+\bar{\gamma}|h_{2,m}|^2\right) \right\} \\ &\overset{a}{=} \left\{ |h_{2,m}|^2 > \frac{\gamma_{th,i}}{\bar{\gamma}\left(a_i - \gamma_{th,i}\sum\limits_{j=i+1}^{M} a_j\right)} \triangleq \theta_i, |h_1|^2 > \frac{\theta_i\left(1+\bar{\gamma}|h_{2,m}|^2\right)}{\bar{\gamma}\left(|h_{2,m}|^2 - \theta_i\right)} \right\}. \end{aligned} \tag{5.7}$$

In step a, the equality holds based on the condition that $a_i > \gamma_{th,i}\sum\limits_{j=i+1}^{M} a_j$, and it is reasonable to assume that this condition is always satisfied. In addition, we present the particular case

$E^c_{M\to M}$ according to (5.5) as

$$\begin{aligned} E_{M\to M} &= \left\{ \frac{a_M\bar{\gamma}^2|h_1|^2|h_{2,M}|^2}{\bar{\gamma}(|h_1|^2+|h_{2,M}|^2)+1} > \gamma_{th,M} \right\} \\ &= \left\{ \left(a_M\bar{\gamma}|h2,M|^2 - \gamma_{th,M}\right)\bar{\gamma}|h_1|^2 > \gamma_{th,M}\left(1+\bar{\gamma}|h_{2,M}|^2\right) \right\} \\ &= \left\{ |h_{2,M}|^2 > \frac{\gamma_{th,M}}{a_M\bar{\gamma}} \triangleq \theta_M, |h_1|^2 > \frac{\theta_M\left(1+\bar{\gamma}|h_{2,M}|^2\right)}{\bar{\gamma}\left(|h_{2,M}|^2-\theta_M\right)} \right\}. \end{aligned} \tag{5.8}$$

Concerning the m-th user, although the signals to different users are transmitted through the same channel, decoding signals for different users requires different thresholds $(\theta_i, i = 1,\cdots,m)$. Since a successful transmission to user m requires user m to decode signals for all users with lower orders, we can formulate the outage probability of the m-th user according to (5.6), (5.7) and (5.8) as

$$P_m^{out} = 1 - Pr\left(|h_{2,m}|^2 > \theta^*_m, |h_1|^2 > \frac{\theta^*_m\left(1+\bar{\gamma}|h_{2,m}|^2\right)}{\bar{\gamma}\left(|h_{2,m}|^2-\theta^*_m\right)} \right), \tag{5.9}$$

where $\theta^*_m = \max(\theta_1,\cdots,\theta_m)$, $m = 1,\cdots,M$.

5.3.2 Channel Gain

5.3.2.1 Unordered Channel Gain

To find the analytical expression of outage probability for the m-th strongest channel gain, we need to find the statistical characteristics of the unordered channel gain first. Denoting $h_2 = \frac{g_2}{\sqrt{1+r^\alpha}}$ as the coefficient of channel gain for unordered relay-destination transmission, the pdf and CDF of $|h_2|^2$ can be expressed as

$$f_{|h_2|^2}(y) = \int_0^R f_{|g_2|^2}\left(y\left(1+r^\alpha\right)\right)\left(1+r^\alpha\right)\frac{2r}{R^2}\mathrm{d}r, \tag{5.10}$$

$$F_{|h_2|^2}(y) = \int_0^R f_{|g_2|^2}\left(y\left(1+r^\alpha\right)\right)\frac{2r}{R^2}\mathrm{d}r. \tag{5.11}$$

The pdf and CDF of channel fading $|g_i|^2$ $(i = 1, 2)$ are given by

$$f_{|g_i|^2}(x) = \lambda_i e^{-\lambda_i x}, \tag{5.12}$$

$$F_{|g_i|^2}(x) = 1 - e^{-\lambda_i x}. \tag{5.13}$$

When the path-loss attenuation coefficient $\alpha = 2$, the analytical expression of the pdf and CDF of $|h_2|^2$ can be easily derived. Therefore, we will start our analysis from this special case, and then study the more general case for $\alpha \neq 2$.

5.3.2.2 Ordered Channel Gain

According to order statistics [19], when variables $X_1, \cdots, X_K$ are independently and identically distributed, and denoting $X_{(1)}, \cdots, X_{(K)}$ as the sorted series with increasing order, the pdf of $X_{(k)}$ is given by

$$f_{X_{(k)}}(x) = \frac{K!}{(K-k)!(k-1)!} F_X(x)^{k-1}(1 - F_X(x))^{K-k} f_X(x), \tag{5.14}$$

where $f_X(x)$ and $F_X(x)$ are the expressions of pdf and CDF of unordered X, respectively. The pdf and CDF of the ordered channel gain of the relay-destination hop $|h_{2,m}|^2$, $m = 1, \cdots, M$ can be obtained based on this theory.

5.3.3 outage probability for α =2

For the single antenna relaying system applying the NOMA technique with path loss parameter α =2, the exact expression and asymptotic bounds for the the outage probability are given as follows.

Proposition 8. *The exact expression of the outage probability for the m-th user in the NOMA*

group with α =2 is given by

$$P_m^{out} = 1 - \frac{M!}{(M-m)!(m-1)!}\sum_{i=0}^{m-1}\left\{\binom{m-1}{i}R^{-2-2M+2m-2i}\lambda_2^{-M+m-i}\sum_{j=0}^{M-m+i}\left\{\binom{M-m+i}{j}(-1)^{i+j}\right.\right.$$
$$\left.\left.\times\sum_{t=1}^{4}\left\{\mathcal{C}_t e^{-\mathcal{B}_t\theta_m^*-\lambda_1(1+R_1^2)\theta_m^*}\int_0^{\infty}(z+\theta_m^*)^{\mathcal{A}_t}e^{-\mathcal{B}_t z}e^{-\frac{\lambda_1(1+R_1^2)\theta_m^*(1+\bar{\gamma}\theta_m^*)}{\bar{\gamma}z}}\mathrm{d}z\right\}\right\}\right\}, \tag{5.15}$$

where $\mathcal{C}_1=\lambda_2^{-1}$, $\mathcal{A}_1=-2-M+m-i$, $\mathcal{B}_1=\lambda_2(R^2j+M-m+i+1)$,
$\mathcal{C}_2=1$, $\mathcal{A}_2=-1-M+m-i$, $\mathcal{B}_2=\lambda_2(R^2j+M-m+i+1)$,
$\mathcal{C}_3=-\lambda_2$, $\mathcal{A}_3=-2-M+m-i$, $\mathcal{B}_3=\lambda_2(R^2j+M-m+i+R^2+1)$,
$\mathcal{C}_4=-(1+R^2)$, $\mathcal{A}_4=-1-M+m-i$, $\mathcal{B}_4=\lambda_2(R^2j+M-m+i+R^2+1)$.

Since $-b_t$ is negative, the integrals in formula (5.15) always converge. It is difficult to find the analytical result of the integral in equation (5.15), we can calculate with the aid of Gaussian Chebyshev Quadrature (GCQ):

$$P_m^{out} = 1 - \frac{M!}{(M-m)!(m-1)!}$$
$$\times\sum_{i=0}^{m-1}\left\{\binom{m-1}{i}R^{-2-2M+2m-2i}\lambda_2^{-M+m-i}\sum_{j=0}^{M-m+i}\left\{\binom{M-m+i}{j}(-1)^{i+j}\right.\right.$$
$$\left.\left.\times\sum_{t=1}^{4}\left\{\mathcal{C}_t e^{-(\mathcal{B}_t+\lambda_1(1+R_1^2))\theta_m^*}\sum_{n=1}^{N}w_n(s_n+\theta_m^*)^{\mathcal{A}_t}e^{-\mathcal{B}_t s_n}e^{-\frac{\lambda_1(1+R_1^2)\theta_m^*(1+\bar{\gamma}\theta_m^*)}{\bar{\gamma}s_n}}\right\}\right\}\right\}, \tag{5.16}$$

where s_n and w_n have been defined by (4.21) and (4.22), N should be greater than 50 to guarantee an accurate result.

Proof. See appendix A.8. □

Due to the complexity of the exact expression of outage probability, we propose the upper and lower bounds in high SNR regimes.

Proposition 9. *The closed-form asymptotic expressions of the upper and lower bounds for the*

outage probability for the single antenna NOMA relaying system with $\alpha = 2$ are given by

$$P_{1_m}^{out,U} = 1 - e^{-2\lambda_1(1+R_1^2)\theta_m^*} + \frac{M!}{(M-m)!(m-1)!}\sum_{i=0}^{m-1}\binom{m-1}{i}\frac{R^{-2M+2m-2i-2}}{M-m+i+1}$$
$$\times \lambda_2^{-M+m-i-1} y^{-M+m-i-1}\sum_{j=0}^{M-m+i+1}(-1)^{i+j+1}e^{-2(\lambda_1(1+R_1^2)+\lambda_2(M-m+i+jR^2+1))\theta_m^*}, \tag{5.17}$$

and

$$P_{1_m}^{out,L} = 1 - e^{-\lambda_1(1+R_1^2)\theta_m^*} + \frac{M!}{(M-m)!(m-1)!}\sum_{i=0}^{m-1}\binom{m-1}{i}\frac{R^{-2M+2m-2i-2}}{M-m+i+1}$$
$$\times \lambda_2^{-M+m-i-1} y^{-M+m-i-1}\sum_{j=0}^{M-m+i+1}(-1)^{i+j+1}e^{-(\lambda_1(1+R_1^2)+\lambda_2(M-m+i+jR^2+1))\theta_m*}. \tag{5.18}$$

Proof. The outage event of user m in (5.9) can be rewritten as

$$P_m^{out} = 1 - Pr\left\{|h_{2,m}|^2 > \theta_m^*, \frac{\bar{\gamma}|h_1|^2|h_{2,m}|^2}{\bar{\gamma}\left(|h_1|^2+|h_{2,m}|^2\right)+1} > \theta_m^*\right\}$$
$$\simeq 1 - Pr\left\{|h_{2,m}|^2 > \theta_m^*, \frac{|h_1|^2|h_{2,m}|^2}{|h_1|^2+|h_{2,m}|^2} > \theta_m^*\right\}, \tag{5.19}$$

where the approximation is made according to the fact that $\frac{x_1x_2}{x_1+x_2+1}$ is tightly bounded by $\frac{x_1x_2}{x_1+x_2}$ when x_1 or/and x_2 are large enough. This fact is widely applied in literature, such as [75] and [76]. Further, using the fact that $\frac{1}{2}\min(u,v) \leq uv/(u+v) \leq \min(u,v)$, we can give upper and lower bounds for (5.19) as

$$P_m^{out,U} = 1 - Pr\left\{|h_{2,m}|^2 > \theta_m^*, \min(|h_1|^2, |h_{2,m}|^2) > 2\theta_m^*\right\}$$
$$= 1 - Pr\left\{\min(|h_1|^2, |h_{2,m}|^2) > 2\theta_m^*\right\}$$
$$= F_{|h_1|^2}(2\theta_m^*) + F_{|h_{2,m}|^2}(2\theta_m^*) - F_{|h_1|^2}(2\theta_m^*)F_{|h_{2,m}|^2}(2\theta_m^*), \tag{5.20}$$

and

$$P_m^{out,L} = 1 - Pr\left\{|h_{2,m}|^2 > \theta_m^*, \min(|h_1|^2, |h_{2,m}|^2) > \theta_m^*\right\}$$
$$= 1 - Pr\left\{\min(|h_1|^2, |h_{2,m}|^2) > \theta_m^*\right\}$$
$$= F_{|h_1|^2}(\theta_m^*) + F_{|h_{2,m}|^2}(\theta_m^*) - F_{|h_1|^2}(\theta_m^*)F_{|h_{2,m}|^2}(\theta_m^*). \tag{5.21}$$

The upper bound is given based on the inequality $\frac{1}{2}\min(u,v) \leq uv/(u+v)$, the equality can be approached when $u = v$ [77]. Since asymptotic operation in (5.19) will be accurate only when u and/or v are large, the approximation expression in (5.20) can tightly bound the exact value just in a narrow domain of values for $|h_1|^2$ and $|h_2|^2$. Although in most situations, the upper bound is not tight, we can observe the system diversity of NOMA technique with the aid of this bound. The lower bound is obtained based on the fact that $\min(u,v) > uv/(u+v)$ [75, 78]. The asymptotic results of this bound can approach exact values when $u \gg v$ or $u \ll v$, which are common situations at dual-hop transmissions. The CDF of the ordered channel gain $|h_{2,m}|^2$ can be obtained by making indefinite integral of the corresponding pdf expression:

$$\begin{aligned} F_{|h_{2,m}|^2}(y) &= \int f_{|h_{2,m}|^2}(y)\mathrm{d}y \\ &= \frac{M!}{(M-m)!(m-1)!}\sum_{i=0}^{m-1}\binom{m-1}{i}(-1)^i \int \left(1-F_{|h_2|^2}(y)\right)^{M-m+i} f_{|h_2|^2}(y)dy \\ &= \frac{M!}{(M-m)!(m-1)!}\sum_{i=0}^{m-1}\binom{m-1}{i}(-1)^{i+1}\frac{1}{M-m+i+1}\left(1-F_{|h_2|^2}(y)\right)^{M-m+i+1}. \end{aligned} \tag{5.22}$$

Substituting (A.105) into (5.22), the CDF can be rewritten as

$$\begin{aligned} F_{|h_{2,m}|^2}(y) = \frac{M!}{(M-m)!(m-1)!}\sum_{i=0}^{m-1}\frac{\binom{m-1}{i}}{M-m+i+1}R^{-2M+2m-2i-2}\lambda_2^{-M+m-i-1} \\ \times y^{-M+m-i-1}\sum_{j=0}^{M-m+i+1}(-1)^{i+j+1}e^{-\lambda_2(M-m+i+jR^2+1)y}. \end{aligned} \tag{5.23}$$

Substituting (A.102) and (5.23) into (5.20) and (5.21), we finally obtain (5.17) and (5.18). □

In order to observe the effects of NOMA technique on system performance, we analyse the diversity gain, which will be obtained from the upper and lower bounds for the outage probability. When $\bar{\gamma} \to \infty$, $\theta_m^* \to 0$, the high-SNR approximations of the bounds for outage probability (5.20, 5.21), can be expressed as

$$\lim_{\theta_m^* \to 0} P_m^{out,U}(\theta_m^*) \simeq F_{|h_1|^2}(2\theta_m^*) + F_{|h_{2,m}|^2}(2\theta_m^*), \tag{5.24}$$

and

$$\lim_{\theta_m^* \to 0} P_m^{out,U}(\theta_m^*) \simeq F_{|h_1|^2}(\theta_m^*) + F_{|h_{2,m}|^2}(\theta_m^*). \tag{5.25}$$

For the source-relay channel, the CDF of $|h_1|^2$ has been given by (A.102). For the high-SNR domain, it is clear that

$$\lim_{y \to 0} F_{|h_1|^2}(y) = \lim_{y \to 0} 1 - e^{\lambda_1(1+R_1^2)y} \simeq \lambda_1 \left(1 + R_1^2\right) y. \tag{5.26}$$

For the relay-destination channel, we reformulate (5.22) as

$$\begin{aligned} F_{|h_{2,m}|^2}(y) &= \frac{M!}{(M-m)!(m-1)!} \sum_{i=0}^{M-m} \binom{M-m}{i} (-1)^i \int F_{|h_2|^2}(y)^{m-1+i} f_{|h_2|^2}(y) dy \\ &= \frac{M!}{(M-m)!(m-1)!} \sum_{i=0}^{M-m} \frac{\binom{M-m}{i}(-1)^i}{m+i} F_{|h_2|^2}(y)^{m+i}. \end{aligned} \tag{5.27}$$

Therefore, the high-SNR approximation of $F_{|h_{2,m}|^2}(\theta_m^*)$ is given by

$$\lim_{\theta_m^* \to 0} F_{|h_{2,m}|^2}(\theta_m^*) \simeq \lim_{\theta_m^* \to 0} \frac{M!}{(M-m)!(m-1)!} \sum_{i=0}^{M-m} \frac{\binom{M-m}{i}(-1)^i}{m+i} \left(\lim_{\theta_m^* \to 0} F_{|h_2|^2}(\theta_m^*) \right)^{m+i}. \tag{5.28}$$

From the expression (A.102), we can obtain

$$\begin{aligned} &\lim_{y \to 0} F_{|h_2|^2}(y) = \lim_{y \to 0} 1 - R^{-2}\lambda_2^{-1} y^{-1} \left(e^{-\lambda_2 y} - e^{-\lambda_2(1+R^2)y} \right) \\ &\simeq 1 - R^{-2}\lambda_2^{-1} y^{-1} \left(\left(1 - \lambda_2 y + \frac{\lambda_2^2 y^2}{2} \right) - \left(1 - \lambda_2(1+R^2)^2 y + \frac{\lambda_2^2(1+R^2)y^2}{2} \right) \right) \\ &= \frac{\lambda_2(R^2+2)y}{2}. \end{aligned} \tag{5.29}$$

Substituting (5.29) into (5.27), we have

$$\begin{aligned} \lim_{y \to 0} F_{|h_{2,m}|^2}(y) &\simeq \lim_{y \to 0} \frac{M!}{(M-m)!(m-1)!} \sum_{i=0}^{M-m} \binom{M-m}{i} (-1)^i \frac{1}{m+i} \left(\frac{\lambda_2(R^2+2)y}{2} \right)^{m+i} \\ &\simeq \frac{M!}{(M-m)!(m)!} \left(\frac{\lambda_2(R^2+2)y}{2} \right)^m. \end{aligned} \tag{5.30}$$

By substituting (5.26) and (5.30) into (5.24) and (5.25), the asymptotic expressions in high-

SNR regimes for upper and lower bounds for the outage probability are derived respectively:

$$\lim_{\theta_m^*\to 0} P_m^{out,U} = 2\lambda_1\left(R_1^2\right)\theta_m^* + \frac{M!}{(M-m)!(m)!}\left(\lambda_2(R^2+2)\theta_m^*\right)^m \propto \frac{1}{\bar{\gamma}^1}, \tag{5.31}$$

$$\lim_{\theta_m^*\to 0} P_m^{out,U} = \lambda_1\left(R_1^2\right)\theta_m^* + \frac{M!}{(M-m)!(m)!}\left(\frac{\lambda_2(R^2+2)\theta_m^*}{2}\right)^m \propto \frac{1}{\bar{\gamma}^1}. \tag{5.32}$$

By Synthesizing (5.31) and (5.32), the diversity for the SISO relaying NOMA system equals 1. However, focusing on the relay-destination transmission, the limit is proportional to $\bar{\gamma}^{-m}$, which implies that the NOMA technique are able to provide larger diversity than orthogonal SISO transmission.

5.3.4 Outage Probability for $\alpha \neq 2$

A more general expression of the outage probability for a single antenna relaying system is given bellow.

Proposition 10. *The outage probability for the NOMA assisted SISO relaying system is given by*

$$P_m^{out} = 1 - \frac{2M!}{(M-m)!(m-1)!}\sum_{j=1}^{n}\sum_{k=0}^{M-m}\binom{M-m}{k}\lambda_2 T_j(1+\Delta_j)\sum_{p=0}^{m+k-1}\{\Xi_1\}, \tag{5.33}$$

where

$$\Xi_1^{p=0} = \frac{(-1)^k\pi}{nR}e^{-\theta_m^*(\tilde{\lambda}_1+\lambda_2(1+\theta_m^*))}\left(\frac{\tilde{\lambda}_1\theta_m^*(1+\theta_m^*)}{\bar{\gamma}\lambda_2(1+\Delta_j^\alpha)}\right)^{\frac{1}{2}}K_1\left(2\sqrt{\frac{\tilde{\lambda}_1\lambda_2\theta_m^*}{\bar{\gamma}(1+\theta_m^*)^{-1}}}\right)$$

and

$$\begin{aligned}\Xi_1^{p\neq 0} =& (-1)^{p+k}\left(\frac{\pi}{nR}\right)^{p+1}\binom{m-1+k}{p}\sum_{q=0}^{n^p-1}\left\{\prod_{d1=1}^{p}\left[T_{D_{q,n,d_1}+1}\Delta_{D_{q,n,d_1}+1}\right]\right.\\ &\left.\times\, e^{-\tilde{\lambda}_1\theta_m^*-L_2}\left(\frac{\tilde{\lambda}_1\theta_m^*(1+\theta_m^*)}{\bar{\gamma}L_2}\right)^{\frac{1}{2}}K_1\left(2\sqrt{\frac{\tilde{\lambda}_1\theta_m^*(1+\theta_m^*)L_2}{\bar{\gamma}}}\right)\right\}.\end{aligned}$$

In (5.33), we set $\tilde{\lambda}_1 = (1+R_1^2)\lambda_1$ to simplify the expression, $K_\alpha(\cdot)$ is the modified Bessel function of the second kind, $L_2 = \lambda_2\left(1+\Delta_j+\sum_{d_{11}=1}^{p}(1+\Delta_{D_{q,n,d_{11}}+1})\right)$, n is the parameter controlling the trade-off between complexity and accuracy in a Gaussian-Chebyshev Quadrature. Symbols $\Delta_i = \frac{R}{2}\cos\left(\frac{2i-1}{2n}\pi\right)+\frac{R}{2}$ and $T_i = \frac{\pi}{n}\sqrt{1-\left(\cos\frac{2i-1}{2n}\pi\right)^2}$, with $\int_0^R g(r)\mathrm{d}r = \frac{R\pi}{2n}\sum_{i=1}^{n} T_i g(\Delta_i)$, which is based on the same GCQ technique with a_m and b_m in Chapter 4 [79, Ep.(25.4.39)], but with a small difference in the form, makes the expressions easier to read in this Chapter. The symbol $D_{a,b,c}$ is the number in the c-th digit of the number x, which is a b-base number transformed from the decimal number a. For example, $T = (z_1+\cdots+z_b)^n$, where n is a positive integer. Expend the expression of T, it should be a sum of elements $T = \sum_{j_1,\ldots,j_n} z_{j_1}\cdots z_{j_n}$. Without combining similar terms, there are $w = b^n$ elements. Either combining similar terms or not, it is difficult to program this expression in a software if both b and n are not fixed. Therefore, we rewrite the total number of elements w as $\hat{w}$, which is a b-based number. Now, the gather of numbers $j_1 j_2 \ldots j_n$ can be mapped to the gather $\left\{\underbrace{0\ldots0}_{\text{n digits}}, 0\ldots1, \cdots (b-1)\ldots(b-1)\right\}$, all numbers in the gather are b-based. Pick the a-th number from the gather, it can be expressed as $a_1\cdots a_c\cdots a_n$, and we denote a_c with $D_{a,b,c}$. Finally, we can express any $j_1\cdots j_n$ with $(D_{a,b,1}+1)\cdots(D_{a,b,n}+1)$.

Proof. This expression can be treated as a special case of the multi-antenna relaying NOMA system studied in the next section, and the derivation is provided in Appendix A.9. □

Proposition 11. *The upper bound and lower bound for the outage probability for the m-th user with random path-loss parameter α in the high SNR regime are given by (5.34) and (5.35) respectively.*

$$P_m^{out,U} = 2\tilde{\lambda}_1 y + \frac{2^m M!}{(M-m)!m!}(\theta_m^*)^m\left(\frac{1}{R}\sum_{i=1}^{n}\left\{\frac{\pi}{n}T_i\Delta_i(1+\Delta_i^\alpha)\lambda_2\right\}\right)^m \propto \frac{1}{\bar{\gamma}} \quad (5.34)$$

and

$$P_m^{out,L} = \tilde{\lambda}_1 y + \frac{M!}{(M-m)!m!}(\theta_m^*)^m\left(\frac{1}{R}\sum_{i=1}^{n}\left\{\frac{\pi}{n}T_i\Delta_i(1+\Delta_i^\alpha)\lambda_2\right\}\right)^m \propto \frac{1}{\bar{\gamma}}. \quad (5.35)$$

Proof. By substituting N_1=1 into (5.62) and (5.63), we can obtain (5.34) and (5.35). □

5.3.5 Outage Probability for Multi-Antenna Relaying

When the relay is equipped with $N_1 > 1$ antennas, the source-relay channel and relay-destination channels become SIMO and MISO, respectively. The source-relay channel is denoted by $\mathbf{h}_1 = \frac{\mathbf{g}_1}{1+R_1^\alpha}$, where the entries of $\mathbf{g}_1 \in \mathbb{C}^{N_1 \times 1}$ follow the complex Gaussian distribution with 0 mean and variance λ_1. The channel between the relay and the m-th user is given by $\mathbf{h}_{2,m} = \frac{\mathbf{g}_{2,m}}{1+r_2^\alpha}$, where the entries of $\mathbf{g}_{2,m} \in \mathbb{C}^{1 \times N_1}$ follow the complex Gaussian distribution with 0 mean and variance λ_2. In addition, the noise vector measured at the relay is given by $\mathbf{n}_R \in \mathbb{C}^{1 \times N_1}$ with $\mathbb{E}\{\mathbf{n}_R^\dagger \mathbf{n}_R\} = \sigma^2 \mathbf{I}_{N_1}$. The MRC receiver $\frac{\mathbf{h}_1^\dagger}{||\mathbf{h}_1||_F}$ and MRT transmitter $\frac{\mathbf{h}_{2,m}^\dagger}{||\mathbf{h}_{2,m}||_F}$ $(m = 1, \cdots, M)$ are applied at relay. Accordingly, the channel gains of the relay to destination transmission are sorted as $\mathbf{h}_{2,1}\mathbf{h}_{2,1}^\dagger < \mathbf{h}_{2,2}\mathbf{h}_{2,2}^\dagger \cdots < \mathbf{h}_{2,M}\mathbf{h}_{2,M}^\dagger$, and the assigned powers are $a_1 > a_2 \cdots > a_M$. All destinations suffer AWGN $n_{D,m}$ $(m = 1, \cdots, M)$, and for any user m, $\mathbb{E}\{|n_{D,m}|^2\} = \sigma^2$. The expressions of the received signals and the SINR at the relay and the destinations are reformulated as follows.

The received signal at relay is given by

$$\mathbf{y}_R = \mathbf{h}_1 \sum_{i=1}^{M} \sqrt{a_i P_S} x_i + \mathbf{n}_R. \tag{5.36}$$

For any user i, $\mathbb{E}\{xx^H\} = 1$. And the signal received by the m-th $(m = 1, \cdots, M)$ user is given by

$$y_{D_m} = \sqrt{P_R}\kappa_2 \mathbf{h}_{2,m}\mathbf{W}_{2,m}\mathbf{h}_1 \sum_{i=1}^{M} \sqrt{a_i P_S} x_i + \sqrt{P_R}\kappa_2 \mathbf{h}_{2,m}\mathbf{W}_{2,m}\mathbf{n}_R + n_{D-m}, \tag{5.37}$$

where $\mathbf{W}_{2,m} = \frac{\mathbf{h}_{2,m}^\dagger \mathbf{h}_1^\dagger}{||\mathbf{h}_2^\dagger||_F ||\mathbf{h}_1^\dagger||_F}$ is the signal processing matrix for user m, $\kappa_2 = \frac{1}{\sqrt{P_S||\mathbf{h}_1||_F^2 + \sigma^2}}$ denotes the power coefficient. Without loss of generality, we set $P_S = P_R = P$ and $\bar{\gamma} = \frac{P}{\sigma^2}$. Based on (5.37), the event causing outage to occur at the m-th user can be written as

$$
\begin{aligned}
E_{i\to m}^{c} &= \left\{ \frac{a_i\bar{\gamma}^2||\mathbf{h}_1||_F^2||\mathbf{h}_{2,m}||_F^2}{\bar{\gamma}^2||\mathbf{h}_1||_F^2||\mathbf{h}_{2,m}||_F^2 \sum\limits_{j=i+1}^{M} a_j + \bar{\gamma}(||\mathbf{h}_1||_F^2 + ||\mathbf{h}_{2,m}||_F^2) + 1} > \gamma_{th,i} \right\} \\
&= \left\{ \left[\bar{\gamma}^2 \left(a_i - \gamma_{th,i} \sum_{j=i+1}^{M} a_j \right) ||\mathbf{h}_{2,m}||_F^2 - \bar{\gamma}\gamma_{th,i} \right] ||\mathbf{h}_1||_F^2 > \gamma_{th,i} \left(1 + \bar{\gamma}||\mathbf{h}_{2,m}||^2 \right) \right\} \\
&= \left\{ ||\mathbf{h}_{2,m}||_F^2 > \frac{\gamma_{th,i}}{\bar{\gamma} \left(a_i - \gamma_{th,i} \sum\limits_{j=i+1}^{M} a_j \right)} \triangleq \theta_i, ||\mathbf{h}_1||_F^2 > \frac{\theta_i \left(1 + \bar{\gamma}||\mathbf{h}_{2,m}||_F^2 \right)}{\bar{\gamma} \left(||\mathbf{h}_{2,m}||_F^2 - \theta_i \right)} \right\},
\end{aligned}
\tag{5.38}
$$

for $E_{i\to m}^{c}$ $(m \neq M)$, and

$$
\begin{aligned}
E_{M\to M}^{c} &= \left\{ \frac{a_M\bar{\gamma}^2||\mathbf{h}_1||_F^2||\mathbf{h}_{2,M}||_F^2}{\bar{\gamma}(||\mathbf{h}_1||_F^2 + ||\mathbf{h}_{2,M}||_F^2) + 1} > \gamma_{th,M} \right\} \\
&= \left\{ \left(a_M\bar{\gamma}||\mathbf{h}_{2,M}||_F^2 - \gamma_{th,M} \right) \bar{\gamma}||\mathbf{h}_1||_F^2 > \gamma_{th,M} \left(1 + \bar{\gamma}||\mathbf{h}_{2,M}||_F^2 \right) \right\} \\
&= \left\{ ||\mathbf{h}_{2,M}||_F^2 > \frac{\gamma_{th,M}}{\bar{\gamma}a_M} \triangleq \theta_M, ||\mathbf{h}_1||_F^2 > \frac{\theta_i \left(1 + \bar{\gamma}||\mathbf{h}_{2,M}||_F^2 \right)}{\bar{\gamma} \left(||\mathbf{h}_{2,M}||_F^2 - \theta_M \right)} \right\}
\end{aligned}
\tag{5.39}
$$

for $E_{M\to M}$.

Consequently, the expression of the outage probability for the m-th user in a multi-antenna relaying NOMA system can be written as the complement of that for correct detections:

$$
P_m^{out} = 1 - Pr \left\{ ||\mathbf{h}_{2,m}||_F^2 > \theta_m^*, ||\mathbf{h}_1||_F^2 > \frac{\theta_m^* \left(1 + \bar{\gamma}||\mathbf{h}_{2,m}||_F^2 \right)}{\bar{\gamma} \left(||\mathbf{h}_{2,m}||_F^2 - \theta_m^* \right)} \right\}. \tag{5.40}
$$

where $\theta_m^* = \max(\theta_1, \cdots, \theta_m)$, $m = 1, \cdots, M$. Employing a MRC receiver and a MRT precoder on the relay, the small-scale channel fading of the source-relay and relay-destination transmissions are given by

$$
F_{||\mathbf{g}_i||_F^2}(x) = 1 - e^{-\bar{\lambda}_i x} \sum_{s=0}^{N_1-1} \frac{\bar{\lambda}_i^s x^s}{s!}, \tag{5.41}
$$

$$
f_{||\mathbf{g}_i||_F^2}(x) = \frac{\bar{\lambda}_i^{N_1} x^{N_1-1} e^{-\bar{\lambda}_i x}}{\Gamma(N_1)}, \tag{5.42}
$$

where $i = 1, 2$ denote the source-relay and relay-destination transmissions, respectively.

In the source-relay transmission, the path loss is fixed. Therefore, the expressions of the CDF and pdf of channel gain $||\mathbf{h}_1||_F^2$ can be expressed as

$$F_{||\mathbf{h}_1||_F^2}(y) = 1 - e^{-\tilde{\lambda}_1 y} \sum_{s=0}^{N_1-1} \frac{\tilde{\lambda}_1^s y^s}{s!}, \tag{5.43}$$

$$f_{||\mathbf{h}_1||_F^2}(y) = \frac{\tilde{\lambda}_1^{N_1} y^{N_1-1} e^{-\tilde{\lambda}_1 y}}{\Gamma(N_1)}, \tag{5.44}$$

where the parameter $\tilde{\lambda}_1 = \lambda_1(1 + R_1^\alpha)$ is obtained according to $||\mathbf{h}_1||_F^2 = ||\mathbf{g}_1||_F^2 / (1 + R_1^\alpha)$. Considering the randomness of user positions, the expressions of the CDF and pdf of the unordered channel gain for the relay-destination transmission can be given by

$$F_{||\mathbf{h}_2||_F^2}(y) = \int_0^R F_{||\mathbf{g}_2||_F^2}(y(1 + r^\alpha)) \frac{2r}{R^2} \mathrm{d}r \tag{5.45}$$

$$f_{||\mathbf{h}_2||_F^2}(y) = \int_0^R f_{||\mathbf{g}_2||_F^2}(y(1 + r^\alpha)) \frac{2r(1 + r^\alpha)}{R^2} \mathrm{d}r. \tag{5.46}$$

With the help of GCQ in (5.33), the expressions of the CDF and pdf of unordered channel gain for the relay-destination transmission are obtained as

$$F_{||\mathbf{h}_2||_F^2}(y) = 1 - \frac{1}{R} \sum_{i=1}^{n} \left\{ \frac{\pi}{n} T_i \Delta_i e^{-\lambda_2 (1+\Delta_i)^\alpha y} \sum_{s=0}^{N_1-1} \left\{ \frac{(1 + \Delta_i^\alpha)^s \lambda_2^s y^s}{s!} \right\} \right\}, \tag{5.47}$$

$$f_{||\mathbf{h}_2||_F^2}(y) = \frac{1}{R} \sum_{j=1}^{n} \left\{ \frac{\pi}{n} T_j \Delta_j \frac{\lambda_2^{N_1} (1 + \Delta_j^\alpha)^{N_1} e^{-\lambda_2 (1+\Delta_j^\alpha) y} y^{N_1-1}}{\Gamma(N_1)} \right\}. \tag{5.48}$$

Using the order statistics shown in (5.14), we can generate the analytical expression of the pdf of channel gain for the m-th user, and the outage probability can be derived accordingly.

Proposition 12. *The analytical expression of the outage probability for the m-th user in a dual-*

hop multi-antenna relaying system employing the NOMA technique is given by

$$P_{out}^{m} = 1 - \frac{2M!}{(M-m)!(m-1)!} \sum_{s_1=0}^{N_1-1} \sum_{k=0}^{M-m} \binom{M-m}{k} \frac{\tilde{\lambda}_1^{s_1}}{s_1!\Gamma(N_1)} \sum_{j=1}^{n} \Big\{ T_j \Delta_j \left(1+\Delta_j^{\alpha}\right)^{N_1} \lambda_2^{N_1} \times \sum_{p=0}^{m+k-1} \{\Xi\} \Big\}, \tag{5.49}$$

where, the expression of Ξ is determined by the value of p. For $p \neq 0$,

$$\begin{aligned}\Xi^{p\neq 0} = (-1)^{p+k} \binom{m+k-1}{p} \left(\frac{\pi}{nR_2}\right)^{p+1} \sum_{q=0}^{n^p-1} \Bigg\{ \prod_{d_1=1}^{p} \left[T_{D_{q,n,d_1}+1} \Delta_{D_{q,n,d_1}+1} \right] \\ \times \sum_{u=0}^{N_1^p-1} \Bigg\{ \prod_{d_2=1}^{p} \left[(1+\Delta_{D_{q,n,d_2}+1}^{\alpha})^{D_{u,N_1,d_2}} \lambda_2^{D_{u,N_1,d_2}} / D_{u,N_1,d_2}! \right] \\ \times \sum_{t_1=0}^{s_1} \sum_{t_2=0}^{L_1} \binom{s_1}{t_1} \binom{L_1}{t_2} \theta_m^{*s_1 - \frac{t_1}{2} + L_1 - \frac{t_2}{2} + \frac{1}{2}} \left(\frac{1+\bar{\gamma}\theta_m^*}{\bar{\gamma}} \right)^{\frac{t_1+t_2+1}{2}} \tilde{\lambda}_1^{\frac{t_2-t_1+1}{2}} \\ L_3^{\frac{t_2-t_1+1}{2}} e^{-\tilde{\lambda}_1\theta_m^* - L_3\theta_m^*} K_{t_2-t_1+1} \left(2\sqrt{\frac{\tilde{\lambda}_1 N_1 \theta_m^* (1+\bar{\gamma}\theta_m^*) L_3}{\bar{\gamma}}} \right) \Bigg\} \Bigg\}, \end{aligned} \tag{5.50}$$

where L_1 and L_3 are given by

$$\begin{aligned} L_1 &= N_1 - 1 + \sum_{d_3=1}^{p} D_{u,N_1,d_3}, \\ L_3 &= \lambda_2(1+\Delta_j^{\alpha}) + \lambda_2 \sum_{d_4=1}^{p} (1+\Delta_{D_{q,n,d_4}}^{\alpha}). \end{aligned} \tag{5.51}$$

and for $p = 0$,

$$\begin{aligned}\Xi^{p=0} = \exp\{-\tilde{\lambda} N_1 \theta_m^* (1+\bar{\gamma}\theta_m^*) - \lambda_2(1+\Delta_j^{\alpha})\theta_m^*\} \sum_{t_1=0}^{s_1} \sum_{t_2=0}^{N_1-1} \binom{s_1}{t_1} \binom{N_1-1}{t_1} \\ \times \theta_m^{*N_1+s_1-\frac{3t_1}{2}-\frac{t_2}{2}-\frac{1}{2}} \left(\frac{1+\bar{\gamma}\theta_m^*}{\bar{\gamma}} \right)^{N_1-\frac{t_1}{2}-\frac{t_2}{2}-\frac{1}{2}} \left(\frac{\tilde{\lambda}_1}{\lambda_2(1+\Delta_j^{\alpha})} \right)^{\frac{t_2-t_1+1}{2}} \\ \times K_{t_2-t_1+1} \left(\sqrt{\frac{\tilde{\lambda}_1 \lambda_2 N_1 \theta_m^* (1+\bar{\gamma}\theta_m^*)(1+\Delta_j^{\alpha})}{\bar{\gamma}}} \right). \end{aligned} \tag{5.52}$$

Proof. See Appendix A.9. □

The exact analytical expressions of the outage probabilities for this system are very complicated to study. Furthermore, the exact expressions of the upper and lower bounds are still tedious to evaluate because of the combination of Gauss-Chebyshev quadrature and order statistics. Therefore, for the multi-antenna scenario, we only provide the asymptotic expressions of upper and lower bounds for outage probabilities at high-SNR regimes, which are efficient to compute and can understand the behaviour of the NOMA system in terms of the achieved diversity gain. Rewriting (5.40), the asymptotic outage probability can be represented as

$$\begin{aligned} P_m^{out} =& 1 - Pr\left\{ ||\mathbf{h}_{2,m}||_F^2 > \theta_m^*, \frac{\bar{\gamma}||\mathbf{h}_1||_F^2||\mathbf{h}_{2,m}||_F^2}{\bar{\gamma}\left(||\mathbf{h}_1||_F^2 + ||\mathbf{h}_{2,m}||_F^2\right) + 1} > \theta_m^* \right\} \\ \simeq& 1 - Pr\left\{ ||\mathbf{h}_{2,m}||^2 > \theta_m^*, \frac{||\mathbf{h}_1||^2||\mathbf{h}_{2,m}||^2}{||\mathbf{h}_1||_F^2 + ||\mathbf{h}_{2,m}||_F^2} > \theta_m^* \right\}. \end{aligned} \tag{5.53}$$

With the same strategies employed by (5.20) and (5.21), the upper and lower bounds for the multi-antenna relaying case can be given by

$$P_m^{out,U} = F_{||\mathbf{h}_1||_F^2}(2\theta_m^*) + F_{||\mathbf{h}_{2,m}||_F^2}(2\theta_m^*) - F_{||\mathbf{h}_1||_F^2}(2\theta_m^*)F_{||\mathbf{h}_{2,m}||_F^2}(2\theta_m^*), \tag{5.54}$$

and

$$P_m^{out,L} = F_{||\mathbf{h}_1||_F^2}(\theta_m^*) + F_{||\mathbf{h}_{2,m}||_F^2}(\theta_m^*) - F_{||\mathbf{h}_1||_F^2}(\theta_m^*)F_{||\mathbf{h}_{2,m}||_F^2}(\theta_m^*). \tag{5.55}$$

In the high-SNR regimes, $\bar{\gamma} \to \infty$, $\theta_m^* \to 0$. Based on (5.43), the limit for $F_{||\mathbf{h}_1||_F^2}(y)$ as $y \to 0$ can be written as

$$\lim_{y\to 0} F_{||\mathbf{h}_1^2||}(y) = 1 - e^{-\tilde{\lambda}_1 y}\left(e^{\tilde{\lambda}_1 y} - \sum_{s=N_1}^{\infty}\frac{\tilde{\lambda}_1^s y^s}{s!}\right) \simeq \frac{\tilde{\lambda}_1^{N_1} y^{N_1}}{N_1!} \tag{5.56}$$

According to (5.14), the CDF of the relay-destination channel gain for the m-th user can be expressed as

$$F_{||\mathbf{h}_{2,m}^2||}(y) = \frac{M!}{(M-m)!(m-1)!}\sum_{k=0}^{M-m}\binom{M-m}{k}\frac{1}{m+k}(-1)^k F_{||\mathbf{h}_2||_F^2}(y)^{m+k} \tag{5.57}$$

The asymptotic expression of $F_{||\mathbf{h}_{2,m}||_F^2}(y)$ with $y \to 0$ can be written as

$$\lim_{y\to 0} F_{||\mathbf{h}_{2,m}^2||}(y) \simeq \frac{M!}{(M-m)!m!}(\lim_{y\to 0} F_{||\mathbf{h}_2||_F^2}(y))^m, \tag{5.58}$$

where

$$\lim_{y\to 0} F_{||\mathbf{h}_2^2||}(y) \simeq 1 - \frac{1}{R}\sum_{i=1}^{n}\left\{\frac{\pi}{n}T_i\Delta_i\left(1 - \frac{(1+\Delta_i^{\alpha})^{N_1}\lambda_2^{N_1}y^{N_1}}{N_1!}\right)\right\}, \tag{5.59}$$

the definitions of T_i and Δ_i are same as equation (5.33). By using the GCQ formula:

$$\frac{1}{R}\sum_{i=1}^{n}\left\{\frac{\pi}{n}T_i\Delta_i\right\} = 1, \tag{5.60}$$

therefore,

$$\lim_{y\to 0} F_{||\mathbf{h}_{2,m}^2||}(y) \simeq \frac{M!}{(M-m)!m!}y^{N_1 m}\left(\frac{1}{R}\sum_{i=1}^{n}\left\{\frac{\pi}{n}T_i\frac{\Delta_i(1+\Delta_i^{\alpha})^{N_1}\lambda_2^{N_1}}{N_1!}\right\}\right)^m. \tag{5.61}$$

By substituting (5.56) and (5.61) into (5.54) and (5.55), the asymptotic expressions of the bounds for the outage probability for such a system in high-SNR regimes are given by

$$\begin{aligned} P_m^{out,U} =& \frac{2^{N_1}\tilde{\lambda}_1^{N_1}(\theta_m^*)^{N_1}}{N_1!} + \frac{2^{mN_1}M!}{(M-m)!m!}(\theta_m^*)^{N_1 m}\left(\frac{1}{R}\sum_{i=1}^{n}\left\{\frac{\pi}{n}T_i\frac{\Delta_i(1+\Delta_i^{\alpha})^{N_1}\lambda_2^{N_1}}{N_1!}\right\}\right)^m \\ \propto& \frac{1}{\bar{\gamma}^{\min(N_1,mN_1)}} = \frac{1}{\bar{\gamma}^{N_1}}, \end{aligned} \tag{5.62}$$

and

$$\begin{aligned} P_m^{out,L} =& \frac{\tilde{\lambda}_1^{N_1}(\theta_m^*)^{N_1}}{N_1!} + \frac{M!}{(M-m)!m!}(\theta_m^*)^{N_1 m}\left(\frac{1}{R}\sum_{i=1}^{n}\left\{\frac{\pi}{n}T_i\frac{\Delta_i(1+\Delta_i^{\alpha})^{N_1}\lambda_2^{N_1}}{N_1!}\right\}\right)^m \\ \propto& \frac{1}{\bar{\gamma}^{N_1}}. \end{aligned} \tag{5.63}$$

5.4 Numerical Results

In this section, numerical results are provided to study the effect of using NOMA techniques on the performance of AF relaying systems with different SNR values and different numbers of antennas, Monte-Carlo simulations are provided to verify the accuracy of our analytical results

and the tightness of asymptotic bounds in high-SNR regimes. Unless otherwise stated, all numerical experiments in this section will adopt the following settings. The SNR is measured at the transmitter side. All Monte-Carlo simulations are carried out with 10^6 iterations. The distance between source and relay is fixed to be 5 meters, which makes $R_1 = 5$ meters in single-antenna cases and $\tilde{\lambda}_1 = 26$ with $\lambda_1 = 1$.

Figure 5.3(a) plots the outage probabilities versus the SNR at the transmitter side for a 3-user NOMA group in an AF relaying system. As mentioned above, the SNR values are for both source-relay and relay-destination transmission. The numerical results are computed based on the expressions in (5.15), (5.31) and (5.32), which indicates N_1=1 and $\alpha = 2$. In addition, we set $a_1 = 0.6$, $a_2 = 0.3$, $a_3 = 0.1$, $\gamma_{th,1} = 0.2dB$, $\gamma_{th,2} = 0.5dB$, $\gamma_{th,3} = 1.0dB$, and R=5. It is clear that the exact analytical results and the simulation results match fairly well. When the transmitting SNR is greater than 25dB, the asymptotic lower bound for the outage probability becomes tight to the analytical values. However, the upper bound is not so tight as the lower bound for most values of $\bar{\gamma}$, though it is acceptably accurate for observing the system diversity. It is worth mentioning that, the outage is close to 1 when SNR$\leq$ 20dB, because $\bar{\gamma}$ is measured at the transmitter side. With the power allocation strategy used in this figure, user 2 achieves the best performance in terms of outage probability, while users 1 and 3 have similar outage performance.

In Figure 5.3(b), we plot the curves for exact outage probabilities and the asymptotic lower bounds, with the same parameters as in Figure 5.3(a). However the computations are based on equations (5.33), (5.34) and (5.35). It is clear that both the exact analytical results and the approximate values are quite similar to those in Figure 5.3(a) with the same parameters. It verifies that the analytical expressions for different choices of α can give the correct results, and the GCQ performs accurately in our calculations. Moreover, outage probabilities with the same coefficients except the path loss parameter are observed in this figure. It can be seen that, by setting α to 3, all three users perform worse than before , due to higher path loss. The gap between two exact outage probability curves for user 1 with different values of α is stable in logarithm with increasing SNR. However, for users 2 and 3, these gaps reduce with increasing SNR.

Figure 5.3 illustrates the effect of the number of antennas equipped at relay in terms of outage probabilities with $\alpha = 2.5$, $a_1 = 0.6$, $a_2 = 0.3$, $a_3 = 0.1$, $\gamma_{th,1} = 0.2dB$, $\gamma_{th,2} = 0.5dB$, $\gamma_{th,3} = 1.0$dB, and the user range R=20 meters. For the first NOMA group, $N_1 = 1$, and for

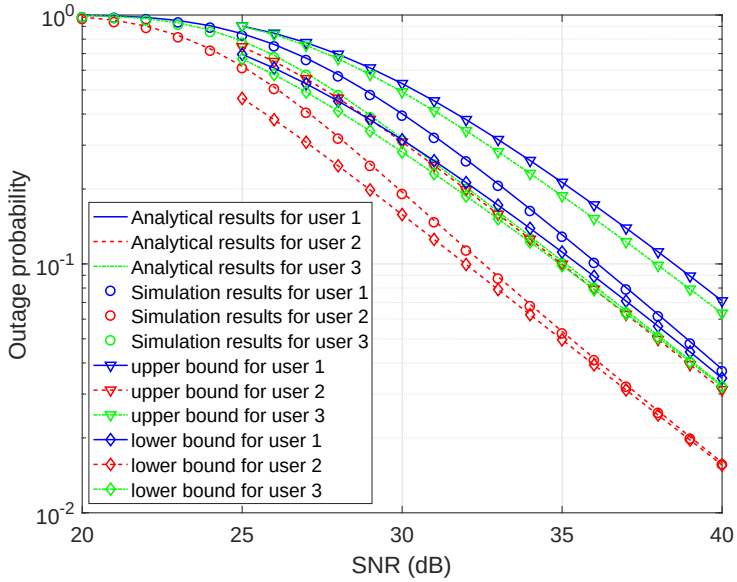

(a) $N_1 = 1, M = 3, \alpha = 2$

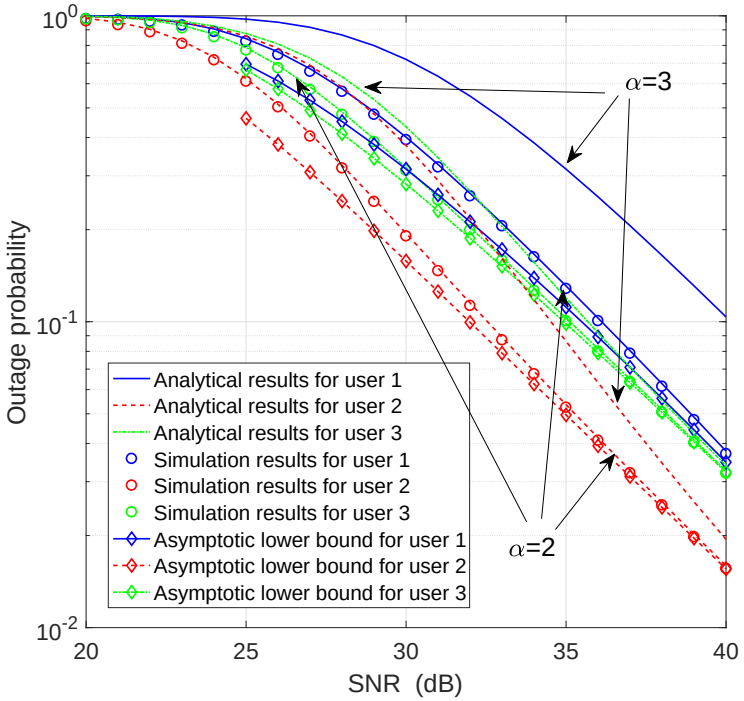

(b) $N_1 = 1, M = 3$, random α

Figure 5.3: *Outage probabilities versus transmitting SNR.*

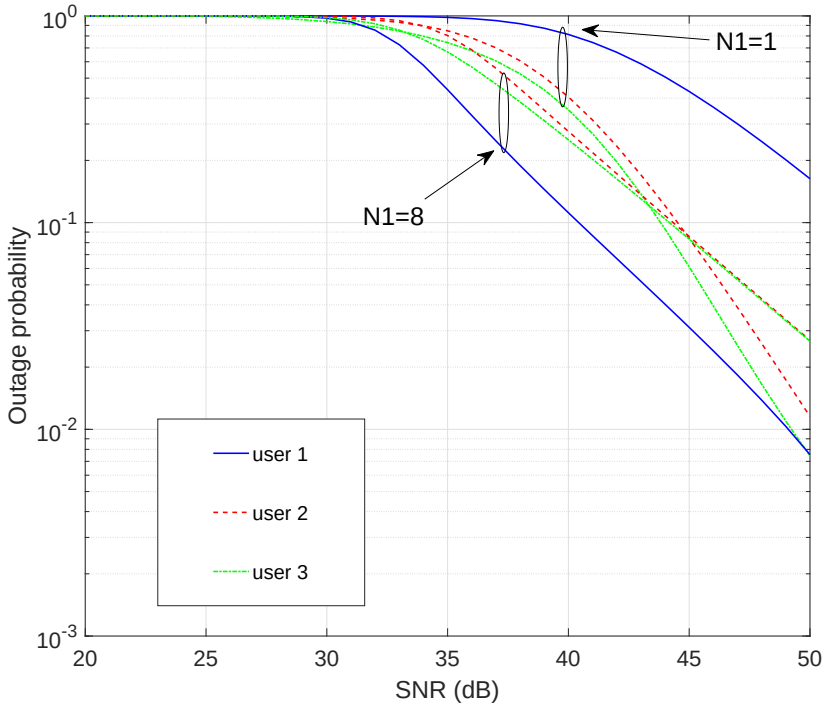

Figure 5.4: *Outage probabilities versus transmit SNR with different antenna numbers.*

the second group, $N_1 = 8$. Overall, the 8-antenna scheme shows better system performance, especially for user 1. When the SNR is below 48dB, the outage probability for user 2 with $N_1 = 8$ is better than that with $N_1 = 1$. However, user 3 receives no benefit from increasing the number of antennas. It is noticeable that, although the same power allocation schemes are applied and the same decoding thresholds are set for these two NOMA groups, the performance of all three users are not uniformly improved with the increasing number of antennas. User 1 performs the worst in the single-antenna case, however in the 8-antenna case, it has the best performance.

Figure 5.5(a) shows the outage probabilities for each user versus SNR in a 3-user NOMA system with $N_1 = 8$, $\alpha = 2.5$, $a_1 = 0.6$, $a_2 = 0.25$, $a_3 = 0.15$, $\gamma_{th,1} = 0.2dB$, $\gamma_{th,2} = 0.6dB$, $\gamma_{th,3} = 1.0dB$. With $R = 5$, user 1 performs the best, users 2 and 3 have quite similar performance in terms of outage probability. As the user range is enlarged to $R = 20$ meters, the users are expected to suffer deeper path loss and larger outage probabilities. Two features should be noticed in this figure. Firstly, unlike the number of antennas N_1, the user range R changes without affecting the rank of user performance in terms of outage probability. Secondly, in low SNR regimes, the increase of user range significantly increases the outage probabilities,

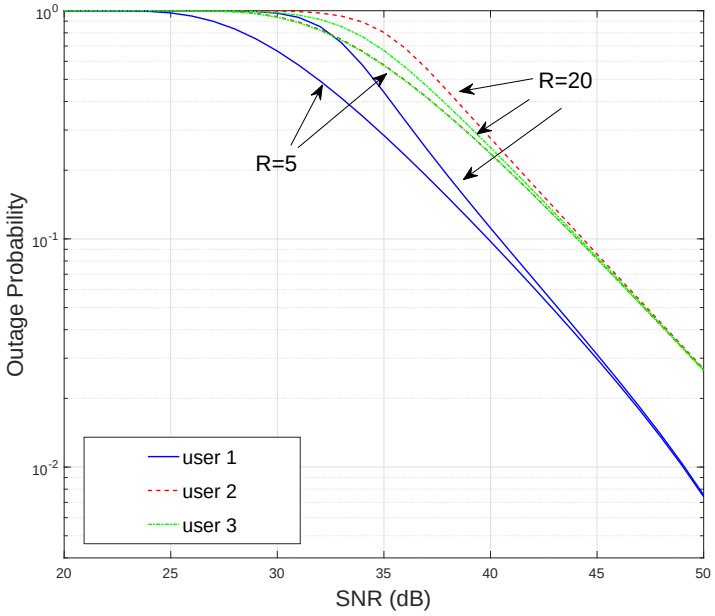

(a) $M = 3$, R=5 or 20

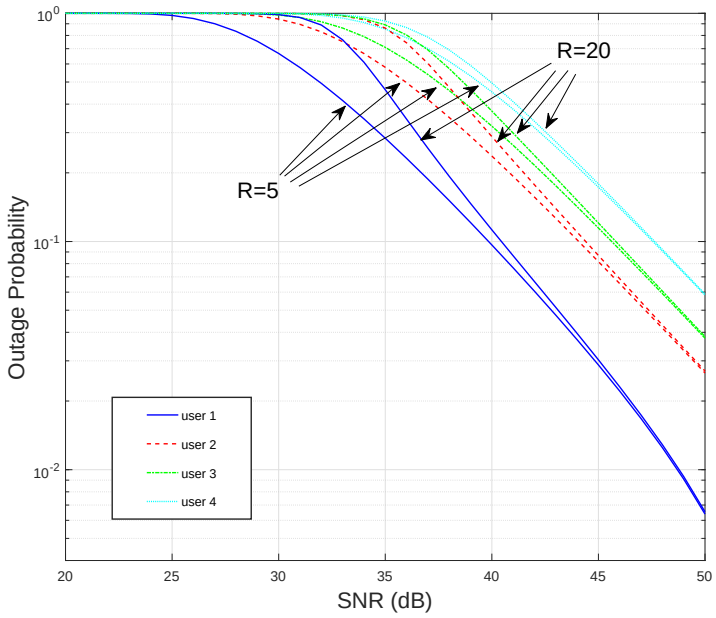

(b) $M = 4$, R=5 or 20

Figure 5.5: *Outage probabilities versus transmit SNR.*

however, these gaps shrink as the SNR value increases. Therefore, in high SNR regimes, the system performance is not significantly affected by the user range, but is significantly affected by the power assignment and the number of antennas. These two features also can be observed for parameter α in Figure 5.3(b).

Figure 5.5(b) presents the outage probabilities versus SNR in a 4-user NOMA system with $N_1 = 8, \alpha = 2.5, a_1 = 0.6, a_2 = 0.25, a_3 = 0.11, a_4 = 0.004, \gamma_{th,1} = 0.2dB, \gamma_{th,2} = 0.6dB, \gamma_{th,3} = 1.0dB, \gamma_{th,4} = 1.2dB$. In the whole range of SNR, the outage probabilities in the 4-user NOMA case perform similarly as in the 3-user NOMA case. It is worth noting that, in this figure, users 1 and 2 are assigned the same power as the 3-user case. The power of user 3 in the 3-user case is now split between by user 3 and user 4 in this figure. We can see that, users 1 and 2 in Figure 5.5(a) perform exactly the same as in Figure 5.5(b), however, the outage probabilities of both user 3 and user 4 in this case are higher than the value of user 3 in the 3-user case. It indicates that adding an extra user in a NOMA group will not significantly affect the other users whose assigned powers remain the same.

5.5 Conclusion

In this chapter, the system performance of NOMA-assisted dual-hop AF relaying systems was investigated in terms of outage probability, where users in a NOMA group were randomly located in the service area. Analytical expressions of the exact outage probabilities for both single-antenna and multi-antenna relaying systems have been derived. In order to verify the accuracy of these analytical expressions, we provided Monte-Carlo simulation results. Furthermore, the asymptotic expressions of the upper and lower bounds for the outage probabilities were provided, which significantly reduced the complexity of computation and helped to demonstrate the behaviour of NOMA techniques in terms of the achieved diversity gain.

Chapter 6
Conclusion and Future Works

6.1 Summary

In this thesis, we have investigated the performance of half-duplex (HD) amplify and forward (AF) relaying systems working in different scenarios. Exploiting information theoretic measures, we evaluated and observed the reliability of end-to-end transmission for such systems. In order to analyse the system for a wider range of channel conditions, generalized models for channel fading were utilized. The system performance in co-channel interference environments or with novel non-orthogonal multiple access (NOMA) techniques were investigated as well, in which exact or asymptotically exact analytical expressions of some information theoretic measures have been derived, such as ergodic capacities and outage probabilities. More details on our contribution and the potential future work are given in the following section.

6.2 Conclusion

In Chapter 3, the dual-hop AF relaying systems were investigated with the generalized $\kappa - \mu$ and $\eta - \mu$ distributions. The system reliabilities for single-antenna relaying systems working on block-coding models were evaluated in the form of error exponents. With a given data rate, a larger error exponent means a shorter code length or a smaller error probability. Analytical expressions for the exact random coding error exponent (RCEE), expurgated error exponents, cut-off rate and ergodic capacity were derived, and asymptotic simplifications in high SNR regimes were provided as well. In addition, we presented the shortest code length required to meet the given decoding error probabilities as examples to reveal the relationship between reliability and complexity of channel coding for such relaying systems. According to the investigation in this chapter, the following insights can be abstracted.

- Under both $\kappa - \mu$ and $\eta - \mu$ fading channels, expurgating bad codewords can significantly improve the transmission reliabilities with low data rates, but in high-speed transmissions, random coding schemes perform better in terms of the error exponent.

- The η-μ distribution is used to model the channel fading for non-line-of-sight (NLOS) transmission, where the parameter η refers to the in-phase to quadrature power ratio, the parameter μ is related to the spatial diversity orders and other transmission factors. Based on our numerical experiments, parameter μ influences the error exponent more significantly than the parameter η. Whereas, the κ-μ distribution is suitable for the line-of-sight (LOS) channels, the effect of parameter κ, which denotes the power ratio of the LOS component to the scattered components. Therefore, the parameter κ influences the error exponents more directly than η.

- The effects of parameters η, κ and μ reflected in the required code length are similar to those for error exponents. Furthermore, it is noticeable that the SNR influences the least required code length much more significantly in low-SNR regimes than in high-SNR scenarios.

Dual-hop AF relaying systems considering the effect of co-channel interference at the relay were investigated in Chapter 4. To make the system more practical, stochastic geometry was employed in modelling the interferer locations. Moreover, multiple antennas were equipped at the relay to eliminate co-channel interference. The MRC/MRT, ZF/MRT and MMSE/MRT relay processing schemes were implemented at the relay, and the corresponding ergodic capacities were derived for each processing strategy. Due to the open challenges of deriving the exact analytical expression of the pdf of the channel coefficients for multiple-antenna channels following a Poisson Point Process (PPP), asymptotic strategies were applied in the investigation. By observing the numerical results, following insights can be obtained.

- For all numbers of antennas considered, the MMSE/MRT scheme presents large advantages in terms of the end-to-end capacities. The ZF/MRT scheme performs the worst in the infinite-area interference scenario, but almost as well as the MMSE/MRT scheme in the limited-area interference regime. This is because co-channel interference always carries much more power than the noise, even when the interferers are out of the service area. In the infinite-area interference environment, the MRC/MRT scheme performs better than ZF/MRT, and achieves throughput and outage performance closer to the MMSE/MRT scheme. However in the limited-area interference regime, it performs the worst.

- In infinite-area interference regimes, the difference in performance between the MMSE/MRT scheme and the other two schemes increases with SNR; however, in the limited-area inter-

ference environment, the difference between the MMSE/MRT scheme and the ZF/MRT scheme is roughly constant with all SNR values. The difference in performance among the three processing schemes is more closely related to the number of antennas and the interference density, especially for the ZF/MRT processing scheme. Under limited-area interference environment, a suitable number of antennas could enable the ZF/MRT relay processing performs almost as well as the MMSE/MRT method.

In Chapter 5, we analysed the performance of AF relaying systems aided by the NOMA technique. The users in the NOMA group are ordered according to both the channel fading and path loss, both of which are considered as variables when we evaluate outage probabilities in our system model. We first provide analytical expressions for a single-antenna relaying system with path loss parameter $\alpha = 2$ as a special case, and then derived expressions for general α in both single-antenna and multi-antenna relaying systems. Furthermore, asymptotic expressions of the upper and lower bounds of outage probabilities are derived, which can efficiently reduce the computational complexity. The diversity order of the system can be obtained easily from the bounds. The following insights are attained from the numerical results.

- Although the implementation of multiple antennas could improve the total performance for the whole NOMA group, some users may suffer higher outage probabilities when the number of antennas increases, because the signals for other users, as the interference for this user, may obtain more benefit from these increased antennas. Among different users, the outage performance curves have no fixed order. Base stations should flexibly adjust the power allocations based on the channel state information of all users to guarantee the balance of performance among different users.

- The diversity order of different users can be changed by the order of channel states in the relay-destination transmission. However in the whole relaying system, the bottleneck of diversity order is normally the source-relay transmission. Therefore, advanced techniques applying spatial diversity should be used at both the source and relay, which can improve the system performance more significantly.

- With high transmission power, the path loss has a very limited effect on the outage performance, because in high-SNR regimes, the inter-user interference is the limiting factor on the system performance.

6.3 Future Work

Potential extensions of our research in this thesis are discussed in this section.

As regard to the performance of error exponents, our investigations of the AF relaying system with generalized κ-μ and η-μ fading channels were only for the basic AF dual-hop relaying system, which is designed with the purpose of improving the coverage of base stations. A direct extension of Chapter 3 is to evaluate error exponents for multi-hop AF relaying system or AF relaying system with relay selection techniques. Another significant aspect in wireless communications is the co-channel interference, which could be considered in the further analysis of error exponents. Moreover, observing the definitions of $\kappa - \mu$ and $\eta - \mu$ distribution, we find that they contain elements of multiple degree of freedom and power ratios in the same function. Therefore, we can guess that for SIMO and MISO systems with MRC or MRT signal processing strategies, the channel will be subject to the fading distributions with similar mathematical form to those analysed in this thesis. Currently, error exponents do not attract enough attention when novel wireless techniques are analysed. However we believe it is a very important system performance indicator, because they could determine the code length. Therefore, we are interested to extend our basic AF relaying model to more complex scenarios, such as full-duplex (FD) relaying systems and massive MIMO systems.

With respect to the stochastic geometry interference model, the exact analytical expressions of outage or ergodic capacity for MIMO systems with interference following a homogeneous PPP are still open problems. It might be tractable for a 2×2 MIMO system as a special case. Also, some approximation methods proposed in the current literature for the statistics of massive MIMO channels may help to evaluate a relay-aided massive MIMO system with PPP-modelled interference. It will be a great challenge to evaluate the AF relaying system with multiple antennas suffering non-PPP interference. However, the multi-relay situation, where the relays are modelled by PPP, could be considered in the future studies. In addition, analysis involving the full-duplex relaying mode is a valuable extension of our analysis.

With regard to NOMA techniques, our research is just a beginning of investigating the system considering randomly allocated users. Further studies at performance, such as system throughput and bit error rates are still required. In addition, with the fast-developing techniques in wireless communications, promising new techniques cooperating with NOMA need to be investigated in relaying systems, such as FD relaying, millimetre wave and massive-MIMO

techniques. Although the dominant contribution of this thesis is deriving the theoretical expression for the system performance, more realistic results should be obtained through system-level performance analysis for NOMA-assisted systems in our future studies.

Appendix A
Proofs

A.1 Proof of Theorem 1

Since the two channels before and after relay are i.i.d., we get

$$f_{\gamma_1,\gamma_2}(\gamma_1,\gamma_2) = f_{\gamma_1}(\gamma_1) f_{\gamma_2}(\gamma_2). \tag{A.1}$$

Letting $s = \gamma_1 + \gamma_2$, $t = \gamma_1\gamma_2$, and using the first Jacobian transformation, equation (A.1) can be written as

$$\begin{aligned} f_{s,t}(s,t) =& p_{\gamma_1,\gamma_2}(\gamma_1(s,t),\gamma_2(s,t))\left|\frac{\partial(\gamma_1,\gamma_2)}{\partial s,\partial t}\right| && \text{(A.2)}\\ =& \frac{4\pi\mu^{2\mu+1}\phi^{2\mu}t^{\mu-\frac{1}{2}}\mathrm{e}^{-\frac{2\mu\phi s}{\bar{\gamma}}}}{\Gamma(\mu)^2\psi^{2\mu-1}\bar{\gamma}^{2\mu+1}} I_{\mu-\frac{1}{2}}\left(\frac{\mu\psi(s+\sqrt{s^2-4t})}{\bar{\gamma}}\right)\\ & \times I_{\mu-\frac{1}{2}}\left(\frac{\mu\psi(s-\sqrt{s^2-4t})}{\bar{\gamma}}\right)\left|\frac{1}{\sqrt{s^2-4t}}\right|. && \text{(A.3)} \end{aligned}$$

Note that, since variables γ_1 and γ_2 are symmetric in expression (A.1), (A.2) keeps the same either $\gamma_1 > \gamma_2$ or $\gamma_1 < \gamma_2$. In order to manage the further derivation, we first represent the expressions of modified Bessel function of the first kind in the form of a series, based on [80, Eq.8.445]

$$I_v(z) = \sum_{k=0}^{\infty} \frac{1}{k!\Gamma(v+k+1)}\left(\frac{z}{2}\right)^{2k+v}. \tag{A.4}$$

After expanding modified Bessel functions of the first kind to the summations of infinite series and subsequently making two binomial expansions, $f_{s,t}(s,t)$ can be rewritten as

$$\begin{aligned} f_{s,t}(s,t) =& \sum_{m=0}^{\infty}\sum_{n=0}^{\infty}\sum_{a=0}^{2m}\sum_{b=0}^{2n} \frac{(-1)^b 2^{2-2m-2n}\pi\mu^{2m+2n+4\mu}\phi^{2\mu}\psi^{2m+2n}\binom{2m}{a}\binom{2n}{b}}{\bar{\gamma}^{4\mu+2}m!n!\Gamma(\mu)^2\Gamma\left(m+\mu+\frac{1}{2}\right)\Gamma\left(n+\mu+\frac{1}{2}\right)} t^{2\mu-1}\\ & \times \exp\left(-\frac{2\mu\phi s}{\bar{\gamma}}\right) s^{2m+2n-a-b}(s^2-4t)^{\frac{a}{2}+\frac{b}{2}-\frac{1}{2}} \end{aligned} \tag{A.5}$$

With another Jacobian transform, we can obtain the expression of $f_{s,x}(s,x)$ as

$$\begin{aligned} f_{s,x}(s,x) =& p_{s,t}(s,sx)|s| \\ =& \sum_{m=0}^{\infty}\sum_{n=0}^{\infty}\sum_{a=0}^{2m}\sum_{b=0}^{2n} \frac{(-1)^b 2^{2-2m-2n}\pi\mu^{2m+2n+4\mu}\phi^{2\mu}\psi^{2m+2n}\binom{2m}{a}\binom{2n}{b}}{\bar{\gamma}^{4\mu+2m+2n}m!n!\Gamma(\mu)^2\Gamma\left(m+\mu+\frac{1}{2}\right)\Gamma\left(n+\mu+\frac{1}{2}\right)} \\ & \times x^{2\mu-1}\exp\left(-\frac{2\mu\phi s}{\bar{\gamma}}\right)s^{m+n+2\mu+\frac{a}{2}+\frac{b}{2}-\frac{1}{2}}(s-4x)^{m+n-\frac{a}{2}-\frac{b}{2}-\frac{1}{2}}, \end{aligned} \tag{A.6}$$

where $x=\frac{t}{s}$. Using [81, Sec.6.2], we can further avoid variable s and derive the pdf of the joint channel:

$$\begin{aligned} f_x^{\eta-\mu}(x) =& \int_{-\infty}^{\infty} f_{s,x}(s,x)\mathrm{d}s \\ \overset{a}{=}& \sum_{m=0}^{\infty}\sum_{n=0}^{\infty}\sum_{a=0}^{2m}\sum_{b=0}^{2n} \frac{(-1)^b 2^{2-2m-2n}\pi\mu^{2m+2n+4\mu}\phi^{2\mu}\psi^{2m+2n}\binom{2m}{a}\binom{2n}{b}}{\bar{\gamma}^{4\mu+2m+2n}m!n!\Gamma(\mu)^2\Gamma\left(m+\mu+\frac{1}{2}\right)\Gamma\left(n+\mu+\frac{1}{2}\right)} \\ & \times x^{2\mu-1}\int_{4x}^{\infty}\exp\left(-\frac{2\mu\phi s}{\bar{\gamma}}\right)s^{m+n+2\mu+\frac{a}{2}+\frac{b}{2}-\frac{1}{2}}(s-4x)^{m+n-\frac{a}{2}-\frac{b}{2}-\frac{1}{2}}\mathrm{d}s \\ \overset{b}{=}& \sum_{m=0}^{\infty}\sum_{n=0}^{\infty}\sum_{a=0}^{2m}\sum_{b=0}^{2n} \frac{(-1)^b 2^{\frac{3}{2}+\mu-m-n}\pi\bar{\gamma}^{-m-n-3\mu+\frac{1}{2}}}{\mu^{\frac{1}{2}-m-n-3\mu}\phi^{\frac{1}{2}-\mu+m+n}\psi^{-2m-2n}} \\ & \times \frac{\Gamma\left(m+n-\frac{a}{2}-\frac{b}{2}+\frac{1}{2}\right)\binom{2m}{a}\binom{2n}{b}}{\Gamma\left(m+\mu+\frac{1}{2}\right)\Gamma\left(n+\mu+\frac{1}{2}\right)m!n!\Gamma(\mu)^2} \\ & \times x^{3\mu+m+n-\frac{3}{2}}\exp\left(-\frac{4\mu\phi x}{\bar{\gamma}}\right)W_{\mu+\frac{a}{2}+\frac{b}{2},-m-n-\mu}\left(\frac{8\mu\phi x}{\bar{\gamma}}\right), \end{aligned} \tag{A.7}$$

where $W_{k,\lambda}(\cdot)$ is the Whittaker-W function [17, Eq.9.222]. In step a, the range of integration is chanted, because with positive γ_1 and γ_2, $s \geq 4x$ always holds. In step b, the integral is achieved with the aid of [17, Eq.3.383.4]:

$$\int_u^{\infty} x^{v-1}(x-u)^{m-1}e^{-\beta x}\mathrm{d}x = \beta^{-\frac{\mu+v}{2}}u^{\frac{\mu+v-2}{2}}\Gamma(\mu)\exp\left(-\frac{\beta u}{2}\right)W_{\frac{v-\mu}{2},\frac{1-\mu-v}{2}}(\beta u). \tag{A.8}$$

With the help of [82, Eq.13.1.33],

$$W_{a,b}(z) = \exp\left(\frac{-z}{2}\right)z^{b+\frac{1}{2}}U\left(b-a+\frac{1}{2},1+2b;z\right), \tag{A.9}$$

equation (A.7) is reconfigured in the form of confluent hypergeometric function as

$$f_x^{\eta-\mu}(x) = \sum_{m=0}^{\infty}\sum_{n=0}^{\infty}\sum_{a=0}^{2m}\sum_{b=0}^{2n} \frac{(-1)^b 2^{3-4m-4n-2\mu}\psi^{2m+2n}\binom{2m}{a}\binom{2n}{b}\Gamma\left(m+n-\frac{a}{2}-\frac{b}{2}+\frac{1}{2}\right)}{\phi^{2m+2n}\pi^{-1}\overline{\gamma}^{2\mu}\mu^{-2\mu}\Gamma\left(n+\mu+\frac{1}{2}\right)m!n!\Gamma(\mu)^2\Gamma\left(m+\mu+\frac{1}{2}\right)} \times x^{2\mu-1}\exp\left(-\frac{8\mu\phi x}{\overline{\gamma}}\right) U_{\frac{1}{2}-2\mu-m-n-\frac{a}{2}-\frac{b}{2},1-2m-2n-2\mu}\left(\frac{8\mu\phi x}{\overline{\gamma}}\right). \tag{A.10}$$

By the end, Theorem 1 is obtained according to the relationship between confluent hypergeometric function and Meijer's G-function [18, Eq.07.34.03.0612.01]:

$$G_{1,2}^{2,0}\left(z\middle|\begin{smallmatrix}a\\b,c\end{smallmatrix}\right) = e^{-z}z^b U(a-c, b-c+1, z). \tag{A.11}$$

A.2 Proof of Theorem 2

The joint PDF of end-to-end SNR from two i.i.d. $\kappa-\mu$ channels is generated through a similar approach applied by the derivation for $\eta-\mu$ channels. Based on [17, Eq.8.445] shown in (A.4), we first replace the modified Bessel function $I_v(\cdot)$ in (3.7) by infinite series:

$$\begin{aligned} f_{\gamma_1,\gamma_2}(\gamma_1,\gamma_2) =& f(\gamma_1)f(\gamma_2) \\ =& \sum_{m=0}^{\infty}\sum_{n=0}^{\infty} \frac{\mu^{2m+2n+2\mu}\kappa^{m+n}(1+\kappa)^{m+n+2\mu}\bar{\gamma}^{-2\mu-m-n}}{e^{2\mu\kappa}m!n!\Gamma(m+\mu)\Gamma(n+\mu)} \\ & \times(\gamma_1\gamma_2)^{\mu-1}\gamma_1^m\gamma_2^n e^{-\frac{\mu(1+\kappa)(\gamma_1+\gamma_2)}{\bar{\gamma}}}. \end{aligned} \tag{A.12}$$

Setting $w=\gamma_1+\gamma_2$, $z=\gamma_1\gamma_2$, we have:

$$\begin{aligned} f_{w,z}(w,z) =& f_{\gamma_1,\gamma_2}(\gamma_1(w,z),\gamma_2(w,z))\left|\frac{\partial(\gamma_1,\gamma_2)}{\partial w,\partial z}\right| \\ =& \sum_{m=0}^{\infty}\sum_{n=0}^{\infty}\sum_{a=0}^{m}\sum_{b=0}^{n} \frac{(-1)^{n-b}2^{-m-n}\kappa^{m+n}(1+\kappa)^{m+n+2\mu}\binom{m}{a}\binom{n}{b}}{m!n!\Gamma(m+\mu)\Gamma(n+\mu)e^{2\mu\kappa}\bar{\gamma}^{2\mu+m+n}} \\ & \times w^{a+b}(w^2-4z)^{\frac{m}{2}+\frac{n}{2}-\frac{a}{2}-\frac{b}{2}-\frac{1}{2}}z^{\mu-1}e^{-\frac{\mu(1+\kappa)w}{\bar{\gamma}}}. \end{aligned} \tag{A.13}$$

Then the joint end-to-end SNR can be expressed as $x = \frac{z}{w}$, therefore we have

$$\begin{aligned} f_{w,x}(w,x) =& f_{w,z}(w, xw)|w| \\ =& \sum_{m=0}^{\infty}\sum_{n=0}^{\infty}\sum_{a=0}^{m}\sum_{b=0}^{n} \frac{(-1)^{n-b}2^{-m-n}\bar{\gamma}^{-m-n-2\mu}\mu^{2m+2n+2\mu}\kappa^{m+n}}{m!n!\Gamma(m+\mu)\Gamma(n+\mu)(1+\kappa)^{-m-n-2\mu}e^{2\mu\kappa}} \\ & \times x^{\mu-1}w^{\frac{m}{2}+\frac{n}{2}+\frac{a}{2}+\frac{b}{2}+\mu-\frac{1}{2}}(w-4x)^{\frac{m}{2}+\frac{n}{2}-\frac{a}{2}-\frac{b}{2}-\frac{1}{2}}e^{-\frac{\mu(1+\kappa)w}{\bar{\gamma}}} \end{aligned} \tag{A.14}$$

and

$$\begin{aligned} f_x(x) =& \int_0^{\infty} f_{w,x}(w,x)dw \\ =& \sum_{m=0}^{\infty}\sum_{n=0}^{\infty}\sum_{a=0}^{m}\sum_{b=0}^{n} \frac{(-1)^{n-b}\Gamma(\frac{m}{2}+\frac{n}{2}-\frac{a}{2}-\frac{b}{2}+\frac{1}{2})\binom{m}{a}\binom{n}{b}\mu^{\frac{3m}{2}+\frac{3n}{2}+\frac{3\mu}{2}-\frac{1}{2}}\kappa^{m+n}}{2^{-\mu}\bar{\gamma}^{\frac{3\mu}{2}+\frac{m}{2}+\frac{n}{2}-\frac{1}{2}}\mathrm{e}^{2\mu\kappa}m!n!\Gamma(m+\mu)\Gamma(n+\mu)(1+\kappa)^{\frac{1}{2}-\frac{3\mu}{2}-\frac{m}{2}-\frac{n}{2}}} \\ & \times x^{\frac{3\mu}{2}+\frac{m}{2}+\frac{n}{2}-\frac{3}{2}}\mathrm{e}^{-\frac{2\mu(1+\kappa)x}{\bar{\gamma}}}\mathrm{W}_{\frac{\mu}{2}+\frac{a}{2}+\frac{b}{2},-\frac{m}{2}-\frac{n}{2}-\frac{\mu}{2}}\left(\frac{4\mu(1+\kappa)x}{\bar{\gamma}}\right). \end{aligned} \tag{A.15}$$

The integral in (A.15) is achieved with the help of [17, Eq.3.383.4], shown in (A.8). Finally, we transform (A.15) to Theorem 2, which is in the form of Meijer's G-function, according to [82, Eq.13.1.33] and [18, Eq.07.34.03.0612.01], given by (A.9) and (A.11), respectively.

A.3 Proof of Proposition 3

Considering (4.14), the end-to-end ergodic capacity is in the form of:

$$C_{MRC} = C_{\gamma_1^{\mathrm{MRC}}} + C_{\gamma_2^{\mathrm{MRC}}} - C_{\gamma_T^{\mathrm{MRC}}}. \tag{A.16}$$

The three expectations $C_{\gamma_1^{\mathrm{MRC}}}$, $C_{\gamma_2^{\mathrm{MRC}}}$, and $C_{\gamma_T^{\mathrm{MRC}}}$ are separately derived in the following.

A.3.1 Calculation of $C_{\gamma_1^{\mathrm{MRC}}}$

From (4.15), it is easy to find that, $C_{\gamma_1^{\mathrm{MRC}}}$ and $C_{\gamma_2^{\mathrm{MRC}}}$ are exactly the ergodic capacity in the source-relay and relay-destination transmissions, respectively, if data is extracted by the relay. According to [83], ergodic capacity can be derived from

$$C_{er} = \frac{1}{2\ln 2}\int_0^{\infty}\frac{1-F_{\gamma}(x)}{1+x}\mathrm{d}x. \tag{A.17}$$

The CDF of γ_1^{MRC} is given by

$$F_{\gamma_1^{\mathrm{MRC}}}(\gamma) = \Pr\left(\frac{P_s R_1^{-\alpha} ||\mathbf{h}_1||_F^2}{\sum\limits_{i\in\Phi} \frac{P_{I_i} r_{I_i}^{-\alpha} |\mathbf{h}_1^\dagger \mathbf{h}_{I_i}|^2}{||\mathbf{h}_1||_F^2} + \sigma^2} < \gamma \right), \tag{A.18}$$

We can easily find that the CDF and pdf of random variable $|\mathbf{h}_1^\dagger \mathbf{h}_1|$ are given by

$$f_{|\mathbf{h}_1^\dagger \mathbf{h}_1|}(x) = \frac{x^{N_1-1} e^{-x}}{\Gamma(N_1)}, \tag{A.19a}$$

$$F_{|\mathbf{h}_1^\dagger \mathbf{h}_1|}(x) = 1 - \sum_{k=0}^{N_1-1} \frac{1}{k!} x^k e^{-x}. \tag{A.19b}$$

Since $\frac{\mathbf{h}_1}{||\mathbf{h}_1||_F}$ is independent of $\mathbf{h}_{I_i}$, for any $i \in \Phi$, the variables of $\bar{I}_i = \frac{|\mathbf{h}_1 \mathbf{h}_{I_i}|^2}{||\mathbf{h}_1||_F^2}$ follow the unit exponential distribution:

$$f_{\bar{I}}(x) = e^{-x}, \tag{A.20}$$

$$F_{\bar{I}}(x) = 1 - e^{-x}. \tag{A.21}$$

Without loss of generality, we set all $P_{I_i} = P_I$ for any , $i \in \Phi$. In order to make the expression clear, we define variable y as the aggregate interference gain, coefficients $I_s = \frac{P_I (R_1)^\alpha}{P_s}$ and $N_s = \frac{\sigma_2 (R_1)^\alpha}{P_s}$ as the power of the source and of interference signal received at the relay,respectively. The expression (A.18) is hereafter derived as:

$$F_{\gamma_1^{\mathrm{MRC}}}(\gamma) = \Pr\left[||\mathbf{h}_1||_F^2 < \gamma(I_s y + N_s) \right] = \mathbb{E}_y \{ F_{||\mathbf{h}_1||_F^2} (\gamma(I_s y + N_s)) \} \tag{A.22}$$

Pulling (A.19b) into (A.22), we get:

$$\begin{aligned} F_{\gamma_1^{\mathrm{MRC}}}(\gamma) &= 1 - \sum_{k=0}^{N_1-1} \frac{1}{k!} \mathbb{E}_y \left\{ (I_s y + N_s)^k \gamma^k e^{-(I_s y + N_s)\gamma} \right\} \\ &= 1 - \sum_{k=0}^{N_1-1} \frac{(-1)^k}{k!} \mathbb{E}_y \left\{ D_s^k \left[e^{-(I_s y + N_s)\gamma s} \right] \Big|_{s=1} \right\} \\ &= 1 - \sum_{k=0}^{N_1-1} \frac{(-1)^k}{k!} D_s^k \left[M_y(I_s y \gamma s) e^{-N_s \gamma s} \right] \Big|_{s=1}, \end{aligned} \tag{A.23}$$

where $D_s^k[y(x)] = \frac{\mathrm{d}^k y(x)}{\mathrm{d}x^k}$ denotes the k-th derivative of variable s, $M_y(\cdot)$ denotes the moment generating function (MGF) of y. With the fact that

$$D_x^k[f(x)g(x)] = \sum_{q=0}^{k} \binom{k}{q} D_x^q[f(x)] D_x^{k-q}[g(x)], \tag{A.24}$$

we can express (A.23) as

$$F_{\gamma_1^{\mathrm{MRC}}}(\gamma) = 1 - \sum_{k=0}^{N_1-1} \frac{(-1)^k}{k!} \sum_{q=0}^{k} \binom{k}{q} D_s^q \left[e^{-N_s \gamma s}\right] D_s^{k-q} \left[M_y(I_s \gamma s)\right] \Big|_{s=1}. \tag{A.25}$$

When the interferers are mapped into the infinite area, the MGF of aggregated interference gain is briefly derived in the following, more details can be found from [84, Eq.15-22], including step a and b.

$$\begin{aligned}
M_y(t) &= \lim_{R\to\infty} \sum_{v=0}^{\infty} \frac{e^{-\lambda\pi R^2} \left(\lambda\pi R^2\right)^v}{v!} \mathbb{E}_{g,r} \left\{ e^{-t \sum\limits_{u=0}^{v} g_u (r_u)^{-\alpha}} \right\} \\
&= \lim_{R\to\infty} \sum_{v=0}^{\infty} \frac{e^{-\lambda\pi R^2} \left(\lambda\pi R^2\right)^v}{v!} \mathbb{E}_{g,r} \left\{ \left(e^{-t g_1 (r_1)^{-\alpha}} \right)^v \right\} \\
&= \lim_{R\to\infty} \exp\left(-\lambda\pi R^2 \left(1 - \mathbb{E}_{r,g} \left\{ e^{-t g_1 (r_1)^{-\alpha}} \right\} \right) \right) \\
&= \exp\left(-\lambda\pi \mathbb{E}_g \left\{ \int_0^{\infty} 2r \left(1 - e^{-t g_1 (r_1)^{-\alpha}} \right) dr \right\} \right) \overset{a}{=} \exp\left(-\lambda\pi \mathbb{E}_g \left\{ \Gamma\left(1 - \frac{2}{\alpha}\right) t^{\frac{2}{\alpha}} g^{\frac{2}{\alpha}} \right\} \right) \\
&= \exp\left(-\lambda\pi \Gamma\left(1 - \frac{2}{\alpha}\right) t^{\frac{2}{\alpha}} \int_0^{\infty} e^{-g} g^{\frac{2}{\alpha}} dg \right) \overset{b}{=} \exp\left(-\lambda\pi \Gamma\left(1 - \frac{2}{\alpha}\right) \Gamma\left(1 + \frac{2}{\alpha}\right) t^{\frac{2}{\alpha}} \right),
\end{aligned} \tag{A.26}$$

where $g_i = \frac{|\mathbf{h}_1 \mathbf{h}_{I_i}|^2}{||\mathbf{h}_1||_F^2}$, whose pdf is given by (A.20).

The results of multiple-derivatives of elements $e^{-N_s\gamma s}$ and $M_y(I_s\gamma s)$ are given by

$$D_s^q\left[e^{-N_s\gamma s}\right] = (-1)^q(N_s\gamma)^q e^{-N_s\gamma s}, \tag{A.27}$$

$$\begin{aligned} D_s^{k-q}\left[M_y(I_s\gamma s)\right] = &\sum_{l=0}^{k-q}(-1)^l\left(\lambda\pi\Gamma\left(1-\frac{2}{\alpha}\right)\Gamma\left(1+\frac{2}{\alpha}\right)I_s^{\frac{2}{\alpha}}\gamma^{\frac{2}{\alpha}}\right)^l s^{\frac{2l}{\alpha}-k} \\ &\times\exp\left(\lambda\pi\Gamma\left(1-\frac{2}{\alpha}\right)\Gamma\left(1+\frac{2}{\alpha}\right)I_s^{\frac{2}{\alpha}}\gamma^{\frac{2}{\alpha}}s^{\frac{2}{\alpha}}\right) \\ &\times\sum_{i=0}^{l}(-1)^i\binom{l}{i}\frac{\Gamma\left(\frac{2}{\alpha}(l-i)+1\right)}{\Gamma\left(\frac{2}{\alpha}(l-i)-k+q+1\right)} \end{aligned} \tag{A.28}$$

where (A.28) is obtained with the help of [80, Eq.0.430.1]. By substituting (A.27) and (A.28) into (A.23), the CDF of SINR of the source-relay transmission is finally obtained as

$$\begin{aligned} F_{\gamma_1^{\mathrm{MRC}}}(\gamma) = 1- &\sum_{k=0}^{N_1-1}\frac{1}{k!}\sum_{q=0}^{k}(N_s)^q\sum_{l=0}^{k-q}(-1)^{k-q-l}\left(\lambda\pi\Gamma\left(1-\frac{2}{\alpha}\right)\Gamma\left(1+\frac{2}{\alpha}\right)I_s^{\frac{2}{\alpha}}\right)^l\gamma^{q+\frac{2l}{\alpha}} \\ &\times\exp(-N_s\gamma)\exp\left(\lambda\pi\Gamma\left(1-\frac{2}{\alpha}\right)\Gamma\left(1+\frac{2}{\alpha}\right)I_s^{\frac{2}{\alpha}}\gamma^{\frac{2}{\alpha}}\right) \\ &\times\sum_{i=0}^{l}(-1)^i\binom{l}{i}\frac{\Gamma\left(\frac{2}{\alpha}(l-i)+1\right)}{\Gamma\left(\frac{2}{\alpha}(l-i)-k+q+1\right)} \end{aligned} \tag{A.29}$$

Substituting (A.29) into (A.17) and applying the Gauss-Chybeshev quadrature, we finally get the expression of (4.18). The GCQ is operated according to [85], the author of witch applied a typical GCQ method [79, Ep.(25.4.39)], and replaced the variable γ with $\tan(\theta)$.

A.3.2 Calculation of $C_{\gamma_2^{\mathrm{MRC}}}$

Through a similar approach of $C_{\gamma_1^{\mathrm{MRC}}}$, we can derive the expression of $C_{\gamma_1^{\mathrm{MRC}}}$ by calculating the following formula:

$$C_{\gamma_2^{\mathrm{MRC}}} = \frac{1}{2\ln 2}\int_0^{\infty}\frac{1-F_{\gamma_2^{\mathrm{MRC}}}(x)}{1+x}\mathrm{d}x, \tag{A.30}$$

where $\gamma_2^{\mathrm{MRC}} = \frac{P_r||\mathbf{h}_2||_F^2(R_2)^{-\alpha}}{\sigma^2} = \frac{||\mathbf{h}_2||_F^2}{N_r}$. It is noticeable that $||\mathbf{h}_2||_F^2$ follows the same distribution as $||\mathbf{h}_1||_F^2$ shown in (A.19b), and the CDF of γ_2^{MRC} is given by

$$F_{\gamma_2^{\mathrm{MRC}}}(\gamma) = 1 - e^{-N_r\gamma}\sum_{k=0}^{N_1-1}\frac{\gamma^k(N_r)^k}{k!}, \tag{A.31}$$

Substituting (A.31) into (A.30), the expression of $C_{\gamma_2^{\mathrm{MRC}}}$ can be written as:

$$C_{\gamma_2^{\mathrm{MRC}}} = \frac{1}{2\ln 2}\sum_{k=0}^{N_1-1}\frac{(N_r)^k}{k!}\int_0^{\infty}\frac{e^{N_r\gamma}\gamma^k}{1+\gamma}\mathrm{d}\gamma = \frac{1}{2\ln 2}\sum_{k=0}^{N_1-1}e^{N_r}(N_r)^k\Gamma(-k,N_r), \tag{A.32}$$

the integration is operated with the help of [80, Eq.3.383.10]. Actually, in all scenarios, the second hop has the same average capacity

$$C_{\gamma_2} = \frac{1}{2\ln 2}\sum_{k=0}^{N_1-1}e^{N_r}(N_r)^k\Gamma(-k,N_r), \tag{A.33}$$

A.3.3 Calculation of $C_{\gamma_T^{\mathrm{MRC}}}$

Applying the expression proposed by [86]:

$$C_{\gamma_T^{\mathrm{MRC}}} = \frac{1}{2\ln 2}\int_0^{\infty}\frac{e^{-z}}{z}(1 - M_{\gamma_T^{\mathrm{MRC}}}(z))\mathrm{d}t, \tag{A.34}$$

Since $\gamma_T^{\mathrm{MRC}} = \gamma_1^{\mathrm{MRC}} + \gamma_2^{\mathrm{MRC}}$, we have

$$\begin{aligned} M_{\gamma_T^{\mathrm{MRC}}}(t) =& \int_0^{\infty}\int_0^{\infty} e^{-t\left(\gamma_1^{\mathrm{MRC}}+\gamma_2^{\mathrm{MRC}}\right)} f_{\gamma_1^{\mathrm{MRC}}}(\gamma_1)\, f_{\gamma_2^{\mathrm{MRC}}}(\gamma_2)\,\mathrm{d}\gamma_1\mathrm{d}\gamma_2 \\ =& M_{\gamma_1^{\mathrm{MRC}}}(t)M_{\gamma_2^{\mathrm{MRC}}}(t). \end{aligned} \tag{A.35}$$

In the following, $M_{\gamma_1^{\mathrm{MRC}}}(t)$ and $M_{\gamma_2^{\mathrm{MRC}}}(t)$ are derived separately. Using integral by part, the MGF can be obtained through calculating:

$$M(t) = \int_0^{\infty} e^{-tz}f(z)\mathrm{d}z = \left[e^{-tz}F(z)\right]_0^{\infty} - \int_0^{\infty} -te^{-tz}F(z)\mathrm{d}z = t\int_0^{\infty} e^{-tz}F(z)\mathrm{d}z. \tag{A.36}$$

Substituting (A.29) into (A.36), $M_{\gamma_1^{\mathrm{MRC}}}(t)$ can be expressed as

$$M_{\gamma_1^{\mathrm{MRC}}}(t) = 1 - \sum_{k=0}^{N_1-1} \frac{1}{k!} \sum_{q=0}^{k} N_s^a \sum_{l=0}^{k-q} (-1)^{k-q-l} \left(\lambda\pi\Gamma\left(1-\frac{2}{\alpha}\right)\Gamma\left(1+\frac{2}{\alpha}\right) I_s^{\frac{2}{\alpha}}\right)^l \times t \int_0^\infty \gamma^{q+\frac{2l}{\alpha}} \exp(-(N_s+t)\gamma) \exp\left(\lambda\pi\Gamma\left(1-\frac{2}{\alpha}\right)\Gamma\left(1+\frac{2}{\alpha}\right) I_s^{\frac{2}{\alpha}} \gamma^{\frac{2}{\alpha}}\right) \mathrm{d}\gamma \times \sum_{i=0}^{l} (-1)^i \binom{l}{i} \frac{\Gamma\left(\frac{2}{\alpha}(l-i)+1\right)}{\Gamma\left(\frac{2}{\alpha}(l-i)-k+q+1\right)} \tag{A.37}$$

In order to address this integral, we first express exponential elements in the form of Meijer's G-function [41, Eq.8.4.3.2]: $\exp\left[-bx^a\right] = \mathrm{G}_{0,1}^{1,0}\left(bx^a \middle| \begin{matrix} - \\ 0 \end{matrix}\right)$, the second line of(A.37) turns to be the integral of a production of one power function and two Meijer's-G functions. With arbitrary path-loss coefficient α, the integral can be solved directly and the output is a Fox-H function. However, numerical calculations for Fox-H functions are not supported by most popular software. Therefore, we attempted to make the output in the form of Meijer's G functions. Finding positive integers u and v, satisfying $\frac{v}{u} = \frac{2}{\alpha}$, the integral can be solved with the aid of [18, Eq.07.34.21.0013.01]. The MGF of γ_1^{MRC} is finally given by

$$\begin{aligned} &M_{\gamma_1^{\mathrm{MRC}}}(t) = \\ &1 - \sum_{k=0}^{N_1-1} \frac{1}{k!} \sum_{q=0}^{k} N_s^a \sum_{l=0}^{k-q} (-1)^{k-q-l} I_s^{\frac{2l}{\alpha}} (N_s)^q \pi^l \lambda^l \frac{u^{\frac{1}{2}} v^{-q-\frac{2l}{\alpha}-1}}{(2\pi)^{\frac{u+v}{2}-1}} \\ &\times \left(\Gamma\left(1-\frac{2}{\alpha}\right)\Gamma\left(1+\frac{2}{\alpha}\right)\right)^l \sum_{i=0}^{l} \frac{(-1)^i \binom{l}{i} \Gamma\left(\frac{2}{\alpha}(l-i)+1\right)}{\Gamma\left(\frac{2}{\alpha}(l-i)-k+q+1\right)} \\ &\times t(N_s+t)^{-q-\frac{2l}{\alpha}-1} \mathrm{G}_{v,u}^{u,v}\left(\frac{\left(\lambda\pi I_s^{\frac{2}{\alpha}}\Gamma\left(1-\frac{2}{\alpha}\right)\Gamma\left(1+\frac{2}{\alpha}\right)\right)^u u^{-u}}{(N_s+t)^v v^{-v}} \middle| \begin{matrix} \mathcal{Q}(-q-\frac{2l}{\alpha}-1, v) \\ \mathcal{Q}(-1, u) \end{matrix}\right) \end{aligned} \tag{A.38}$$

where $\mathcal{Q}(a,b) = \left[\frac{1+a}{b}, \frac{2+a}{b} \cdots \frac{a+b}{b}\right]$.

Since $||\mathbf{h}_2||_F^2$ obeys identical distribution with $||\mathbf{h}_1||_F^2$, the pdf of γ_2^{MRC} can be expressed as

$$f_{\gamma_2^{\mathrm{MRC}}}(\gamma) = \frac{N_r^{N_1} \gamma^{N_1-1} e^{-N_r\gamma}}{\Gamma(N_1)} \tag{A.39}$$

and the MGF of γ_2^{MRC} is given by

$$\begin{aligned} M_{\gamma_2^{\mathrm{MRC}}}(t) =& \frac{N_r^{N_1}}{\Gamma(N_1)} \int_0^{\infty} \gamma^{N_1-1} e^{-(N_r+t)\gamma} \mathrm{d}\gamma \\ =& \frac{N_r^{N_1}}{(N_r+t)^{N_1}}. \end{aligned} \tag{A.40}$$

The integral is operated according to [80, Eq.3.351.1].

Combining (A.38), (A.40), (A.35) and (A.34), and applying the GCQ technique, we finally obtain (4.20).

A.4 Proof of Proposition 4

Considering the scenario that all the interferers are mapped in a limited area with radium R, the statistics of the SINR in relay-destination transmission are the same as the infinite-range interferers scenario. $C_{\gamma_2^{\mathrm{MRC}}}^{lim} = C_{\gamma_2}$.

Focusing on the difference between the aggregate interference gain in the limited-area scenario and the infinite-area scenario, we first derive the MGF of the interference gain. Similar to (A.26), we have

$$\begin{aligned} M_{I_{\mathrm{MRC}}}^{lim}(t) =& \sum_{v=0}^{\infty} \frac{e^{-\lambda\pi R^2} \left(\lambda\pi R^2\right)^k}{v!} \mathbb{E}_{g,r} \left\{ e^{-t \sum_{u=0}^{v} g_u (r_u)^{-\alpha}} \right\} \\ =& \exp\left(-\lambda\pi R^2 \left(1 - \mathbb{E}_{r,g} \left\{ e^{-tg(r)^{-\alpha}} \right\} \right) \right) \end{aligned} \tag{A.41}$$

where $\mathbb{E}_{r,g} \left\{ e^{-tg(r)^{-\alpha}} \right\}$ is derived in the following,

$$\begin{aligned} \mathbb{E}_{r,g} \left\{ e^{-tg_1(r_1)^{-\alpha}} \right\} =& \mathbb{E}_r \left\{ \int_0^{\infty} e^{-g\left(1+tr^{-\alpha}\right)} \mathrm{d}g \right\} \\ \overset{a}{=}& \mathbb{E}_r \left\{ \frac{1}{tr^{-\alpha}+1} \right\} = \frac{2}{R^2} \int_0^{R} \frac{r}{tr^{-\alpha}+1} \mathrm{d}r. \end{aligned} \tag{A.42}$$

By setting $z = r^{-\alpha}$, we have

$$\begin{aligned}\mathbb{E}_{r,g}\left\{e^{-tg(r)^{-\alpha}}\right\} =& -\frac{2}{R^2}\int_{R^{-\alpha}}^{\infty}\frac{z^{-\frac{1}{\alpha}}}{1+tz}\mathrm{d}z^{-\frac{1}{\alpha}} = \frac{2}{\alpha R^2}\int_{R^{-\alpha}}^{\infty}\frac{z^{-\frac{2}{\alpha}-1}}{1+tz}\mathrm{d}z \\ \overset{b}{=}& \frac{2R^{\alpha}}{\alpha+2}t^{-1}\,{}_2F_1\left(1,1+\frac{2}{\alpha};2+\frac{2}{\alpha},-\frac{R^{\alpha}}{t}\right).\end{aligned} \tag{A.43}$$

The integral in step a and b are operated with the aid of [80, Eq.3.381.4] and [80, Eq.3.194.2], respectively. Substituting (A.43) into (A.41), the GMF of the limited-ranged interference can be expressed as

$$M_{I_{\mathrm{MRC}}}^{lim}(t) = \exp\left(-\lambda\pi R^2\left(1-\frac{2R^{\alpha}}{\alpha+2}t^{-1}\,{}_2F_1\left(1,1+\frac{2}{\alpha};2+\frac{2}{\alpha},-\frac{R^{\alpha}}{t}\right)\right)\right). \tag{A.44}$$

Due to the complexity of expression (A.44) for the further derivation, it is intractable to derive the CDF and MGF of the SINR in this case. As an alternative, we present the lower bound of the end-to-end capacity with the inequality (4.23), which leads to the expression

$$C_{\mathrm{MRC}}^{lim} > C_{L_{\mathrm{MRC}}}^{lim} = C_{\gamma_1^{\mathrm{MRC}}}^{lim} + C_{\gamma_2^{\mathrm{MRC}}}^{lim} - \frac{1}{2}\log_2\left(1+\mathbb{E}\{\gamma_{1^{\mathrm{MRC}}}^{lim}\}+\mathbb{E}\{\gamma_{2^{\mathrm{MRC}}}^{lim}\}\right) \tag{A.45}$$

Since $C_{\gamma_2^{\mathrm{MRC}}}^{lim} = C_{\gamma_2}$, which has been presented in formula (A.33). We only need to derive the expressions of elements $C_{\gamma_1^{\mathrm{MRC}}}^{lim}$, $\mathbb{E}\left\{\gamma_{1^{\mathrm{MRC}}}^{lim}\right\}$ and $\mathbb{E}\left\{\gamma_{2^{\mathrm{MRC}}}^{lim}\right\}$.

The expression $\mathbb{E}\left\{\frac{x}{ay+b}\right\}$, can be evaluated through the frame work [87], which was proposed for the Nakagami-m fading, where variables x and y denote the received channel gains of source and aggregated interference. Using the coefficients $a = I_s$ and $b = N_s$, which have the same definitions as in (A.22), and after a slight adjustment due to the difference between SIMO Rayleigh and Nakagami-m channels, we have:

$$\mathbb{E}_{x,y}\left\{g\left(\frac{x}{I_r y + N_r}\right)\right\} = g(0) + \int_0^{\infty} g_m(z) M_y(I_s z) e^{-N_s z}\mathrm{d}z, \tag{A.46}$$

where $g_m(z) = \frac{1}{\Gamma(m)}\frac{\mathrm{d}^m}{\mathrm{d}z^m}z^{m-1}g(z)$, m is the antenna number, or saying valid diversity of the channel, for the MRC receiver, $m = N_1$. $M_y(\cdot)$ is the MRF of interference.

A.4.1 Calculation of $\mathbb{E}\left\{C_{\gamma_{1\mathrm{MRC}}}^{lim}\right\}$

According to [87], when $g(z)=\ln(1+z)$,

$$\begin{aligned} g_{N_1}(z) =& \frac{1}{\Gamma(N_1)}\frac{\mathrm{d}^{N_1}}{\mathrm{d}z^{N_1}} z^{N_1}\ {}_2F_1\left(1,1;2,-z\right) \\ =& N_1\ {}_2F_1\left(1+N_1,1;2,-z\right) \\ =& \frac{1}{z}-\frac{1}{z(1+z)^{N_1}} \end{aligned} \tag{A.47}$$

Substituting (A.47) and (A.44) into (A.46), $C_{1\mathrm{MRC}}^{lim}$ can be calculated by

$$\begin{aligned} C_{\gamma_{1\mathrm{MRC}}}^{lim} =& \int_0^{\infty}\left(\frac{1}{z}-\frac{1}{z(1+z)^{N_1}}\right)\exp\left(-\lambda\pi R^2\left(1-\frac{2R^{\alpha}}{\alpha+2}I_s^{-1}z^{-1}\right.\right. \\ & \left.\left.\times\ {}_2F_1\left(1,1+\frac{2}{\alpha};2+\frac{2}{\alpha},-\frac{R^{\alpha}}{I_s z}\right)\right)\right)\exp(N_s z)\mathrm{d}z \end{aligned} \tag{A.48}$$

With the aid of GCQ, the expression of $C_{\gamma_{1\mathrm{MRC}}}^{lim}$, shown in (4.25), is finally obtained.

A.4.2 Calculation of $\mathbb{E}\left\{\gamma_{1\mathrm{MRC}}^{lim}\right\}$

Given by [87], when $g(z)=z$,

$$g_{N_1}(z)=\frac{1}{\Gamma(N_1)}\frac{\mathrm{d}^{N_1}}{\mathrm{d}z^{N_1}}z^{N_1}=N_1 \tag{A.49}$$

Substituting (A.49) and (A.44) into (A.46) and using GCQ, the expression of $\mathbb{E}\left\{\gamma_{1\mathrm{MRC}}^{lim}\right\}$ can be expressed as

$$\begin{aligned} \mathbb{E}\left\{\gamma_{1\mathrm{MRC}}^{lim}\right\} =& \sum_{n=1}^{N} w_n \exp(N_r s_n)\exp\left(-\lambda\pi R^2\left(1-\frac{2R^{\alpha}}{2+\alpha}I_r^{-1}(s_n)^{-1}\right)\right. \\ & \left.\times\ {}_2F_1\left(1,1+\frac{2}{\alpha},2+\frac{2}{\alpha},-\frac{R^{\alpha}}{I_r s_n}\right)\right) \end{aligned} \tag{A.50}$$

In [87], the integrals was suggested to be made with a Gaussian quadrature in another term, which can eliminate one exponential element $\exp(N_r z)$. Because in that way, the abscissa and weights are difficult to be calculated with fundamental functions, we still apply the GCQ technique in this case.

A.4.3 Calculation of $\mathbb{E}\left\{\gamma_{2^{\mathrm{MRC}}}^{lim}\right\}$

The expectation of the SINR in the second hop can be derived with a straight integral, as

$$\mathbb{E}\left\{\gamma_{2^{\mathrm{MRC}}}^{lim}\right\} = \int_0^\infty \gamma f_{\gamma_2^{\mathrm{MRC}}}(\gamma)\mathrm{d}\gamma = \int_0^\infty \frac{N_r^{N_1}\gamma^{N_1}e^{-N_r\gamma}}{\Gamma(N_1)} = \mathrm{d}\gamma = \frac{N_1}{N_r}, \tag{A.51}$$

where the integral is made with the aid of [80, Eq.3.351.3]. Since γ_2 is independent of the transferring schemes, this expression fits for all transferring schemes.

$$\mathbb{E}\left\{\gamma_2\right\} = \frac{N_1}{N_r}. \tag{A.52}$$

In the end, substituting (4.25), (4.26), (A.50) and (A.51) into (A.45), the final result is obtained.

A.5 Proof of Proposition 5

Since the range of interference is setted to be limited, there is a probability that the number of interferers N_2 is less than that of antennas N_1, the comprehensive end-to-end capacity should be the combination of capacities of two states, $N_2 < N_1$ and $N_2 > N_1$. Substituting (4.9) into (4.13), the ergodic capacity for the ZF/MRT scheme is given by

$$C_{ZF}^{A} = C_{\gamma_1^{\mathrm{ZF}}}^{A} + C_{\gamma_2^{\mathrm{ZF}}}^{A} - C_{\gamma_T^{\mathrm{ZF}}}^{A}, \tag{A.53}$$

where A denotes the states $N_2 < N_1$ or $N_2 \geq N_1$, $C_{\gamma_{i^{\mathrm{ZF}}}}^{A} = \frac{1}{2}\mathbb{E}\{\log_2(1+\gamma_{i^{\mathrm{ZF}}}^{A})\}$ $(i = 1, 2)$, $C_{\gamma_T^{\mathrm{ZF}}}^{A} = \frac{1}{2}\mathbb{E}\{\log_2(1+\gamma_{1^{\mathrm{ZF}}}^{A}+\gamma_{2^{\mathrm{ZF}}}^{A})\}$ and $\gamma_{i^{\mathrm{ZF}}}^{A}, (i = 1, 2)$ is given in the system model of this chapter.

A.5.1 Calculation of $C_{\gamma_1^{\mathrm{ZF}}}^{A}$

When the total number of interferers N_2 is less than the number of antennas N_1, all interference is filtered by the N_2-ranked null space of matrix $\mathbf{P}$, and the pdf and CDF expressions of channel

gain $|\mathbf{h}_1^\dagger \mathbf{P} \mathbf{h}_1|$ are given by [88]:

$$f_{|\mathbf{h}_1^\dagger \mathbf{P} \mathbf{h}_1|}^{N_2<N_1}(x) = \frac{x^{N_1-N_2-1}e^{-x}}{\Gamma(N_1-N_2)}, \tag{A.54a}$$

$$F_{|\mathbf{h}_1^\dagger \mathbf{P} \mathbf{h}_1|}^{N_2<N_1}(x) = 1 - \sum_{k=0}^{N_1-N_2-1} \frac{1}{k!} x^k e^{-x}. \tag{A.54b}$$

It is noticeable that the rank of null space of $\mathbf{P}$ will occupy the same diversity for channel $\mathbf{h}_1$.

Setting R_m is the distance between the relay and the (N_1-1)-th nearest interferer, the event $N_2 < N_1$ can be described by event $R_m \geq R$, vice versa. The pdf of R_m is given by [89], as

$$f_{N_1-1}(R_m) = e^{-\lambda\pi(R_m)^2} \frac{2\left(\lambda\pi(R_m)^2\right)^{N_1-1}}{R_m \Gamma\left(N_1-1\right)}. \tag{A.55}$$

When $N_2 \geq N_1$, only N_1-1 largest interference are considered, and $\mathbf{P}$ remains diversity 1 for the source channel $\mathbf{h}_1$. The corresponding pdf and CDF are given by

$$f_{|\mathbf{h}_1^\dagger \mathbf{P} \mathbf{h}_1|}^{N_2\geq N_1}(x) = e^{-x} \tag{A.56a}$$

$$F_{|\mathbf{h}_1^\dagger \mathbf{P} \mathbf{h}_1|}^{N_2\geq N_1}(x) = 1 - e^{-x}. \tag{A.56b}$$

Moreover, since the receiver vector is independent of the interference not considered, the aggregated received interference has similar statistics properties as that in MRC scheme, shown in (A.20) and (A.21).

By substituting $\gamma_{1^{\text{ZF}}}^{N_2<N_1} = \frac{x}{N_s}$ into (A.54b), where N_s has been defined in MRC scenarios, the pdf and CDF of $\gamma_{1^{\text{ZF}}}^{N_2<N_1}$ are defined by

$$f_{\gamma_1}^{N_2<N_1}(\gamma) = \frac{(N_s)^{N_1-N_2}\gamma^{N_1-N_2-1}e^{-N_s\gamma}}{\Gamma(N_1-N_2)}, \tag{A.57a}$$

$$F_{\gamma_1}^{N_2<N_1}(\gamma) = 1 - \sum_{k=0}^{N_1-N_2-1} \frac{1}{k!} (N_s)^k \gamma^k e^{-N_s\gamma}. \tag{A.57b}$$

The corresponding capacity is then derived by substituting (A.57b) into (A.17) and considering

the probability of N_2:

$$C_{\gamma_1^{\mathrm{ZF}}}^{N_2<N_1} = \sum_{N_2=0}^{N_1-1} e^{-\lambda\pi R^2} \frac{\left(\lambda\pi R^2\right)^{N_2}}{N_2!} \frac{1}{2\ln 2} \sum_{k=0}^{N_1-N_2-1} \frac{(N_s)^k}{k!} \int_0^{\infty} \frac{e^{N_s x} x^k}{1+x} \mathrm{d}x$$
$$= \frac{1}{2\ln 2} \sum_{N_2=0}^{N_1-1} e^{-\lambda\pi R^2} \frac{\left(\lambda\pi R^2\right)^{N_2}}{N_2!} \sum_{k=0}^{N_1-N_2-1} (N_s)^k e^{N_s} \Gamma\left(-k, N_s\right), \tag{A.58}$$

the integral is calculated with the aid of [80, 3.383.10].

In the following, we will concentrate on the case $N_2 \geq N_1$. As mentioned above, it is equivalent to the event $R_m \leq R$. On the condition that, the (N_1-1)-th interferer has the distance R_m, The effective interference are randomly mapped in a annular area $R_M \leq r \leq R$, with the same density λ. The system model is equivalent to a single antenna receiver effected by interferers in the annular area. The system evaluation could follow the similar approach as the limited-area MRC scenario:

$$F_{\gamma_1^{\mathrm{ZF}}}^{N_2\geq N_1}(\gamma) = \mathbb{E}_y\left\{F_x^{N_2\geq N_1}(\gamma(I_s y + N_s))\right\} = \mathbb{E}_y\left\{1 - e^{-\gamma(I_s y + N_s)}\right\}$$
$$= 1 - M_y(I_s\gamma) e^{N_s\gamma}, \tag{A.59}$$

and

$$\mathbb{E}\left\{g\left(\gamma_{1^{\mathrm{ZF}}}^{N_2\geq N_1}\right)\right\} = \mathbb{E}_{x,y}\left\{g\left(\frac{x}{I_s y + N_s}\right)\right\}$$
$$= g(0) + \int_0^{\infty} \frac{\mathrm{d}g_(z)}{\mathrm{d}z} M_y(I_s z) e^{-N_s z} \mathrm{d}z, \tag{A.60}$$

Variable x denotes the source-relay channel gain of small-scale fading for source signal. Formula (A.60) can be obtained by substituting $m = 1$ into (A.46). Variable $y = g r^{-\alpha}$ denotes the aggregated interference channel gain at relay, where g is the gain of small-scale fading. I_{ZF}, with given R_m it can be derived as:

$$M_{I_{\mathrm{ZF}}|R_m}(t) = \sum_{v=0}^{\infty} \frac{e^{-\lambda\pi\left(R^2-R_m^2\right)}\left(\lambda\pi\left(R^2-R_m^2\right)\right)^k}{v!} \mathbb{E}_{g,r|R_m}\left\{e^{-t\sum_{u=0}^{v} g_u (r_u)^{-\alpha}}\right\}$$
$$= \exp\left(-\lambda\pi\left(R^2-R_m^2\right)\left(1 - \mathbb{E}_{r,g|R_m}\left\{e^{-t g_1 (r_1)^{-\alpha}}\right\}\right)\right). \tag{A.61}$$

Following the integral techniques used by (A.42) and (A.43) we derive the expression of

$\mathbb{E}_{r,g|R_m}\left\{e^{-tg_1(r_1)^{-\alpha}}\right\}$ in the following,

$$\begin{aligned}
&\mathbb{E}_{r,g|R_m}\left\{e^{-tg_1(r_1)^{-\alpha}}\right\} = \mathbb{E}_r\left\{\int_0^{\infty} e^{-g\left(1+tr^{-\alpha}\right)}\mathrm{d}g\right\} = \mathbb{E}_r\left\{\frac{1}{tr^{-\alpha}+1}\right\} \\
&= \frac{2}{R^2-R_m^2}\int_{R_m}^{R}\frac{r}{tr^{-\alpha}+1}\mathrm{d}r = \frac{2}{R^2-R_m^2}\left(\int_0^{R}\frac{r}{tr^{-\alpha}+1}\mathrm{d}r - \int_0^{R_m}\frac{r}{tr^{-\alpha}+1}\mathrm{d}r\right) \\
&= \frac{2\left(R^2-R_m^2\right)^{-1}}{\alpha+2}t^{-1}\left(R^{\alpha+2}\,{}_2F_1\left(1,1+\frac{2}{\alpha};2+\frac{2}{\alpha},\frac{R^{\alpha}}{t}\right)\right. \\
&\quad \left.-R_m^{\alpha+2}\,{}_2F_1\left(1,1+\frac{2}{\alpha};2+\frac{2}{\alpha},\frac{R_m^{\alpha}}{t}\right)\right). \qquad \text{(A.62)}
\end{aligned}$$

Pulling (A.62) into (A.61), the expression of $M_{I_{\mathrm{ZF}}|R_m}(t)$ is then given by

$$\begin{aligned}
&M_{I_{\mathrm{ZF}}|R_m}(t) = \\
&\exp\left(-\lambda\pi\left(R^2-R_m^2\right)\left(1-\frac{2\left(R^2-R_m^2\right)^{-1}}{\alpha+2}t^{-1}\left(R^{\alpha+2}\right.\right.\right. \\
&\left.\left.\left.\times\,{}_2F_1\left(1,1+\frac{2}{\alpha};2+\frac{2}{\alpha},\frac{R^{\alpha}}{t}\right)-R_m^{\alpha+2}\,{}_2F_1\left(1,1+\frac{2}{\alpha};2+\frac{2}{\alpha},\frac{R_m^{\alpha}}{t}\right)\right)\right)\right). \qquad \text{(A.63)}
\end{aligned}$$

Substituting $g(z)=\ln(1+z)$ into (A.60) and invoking the pdf of R_m shown in (A.55), the expression of $C_{\gamma_1^{\mathrm{ZF}}}^{N_2\geq N_1}$ can be expressed as

$$\begin{aligned}
C_{\gamma_1^{\mathrm{ZF}}}^{N_2\geq N_1} &= \frac{1}{2\ln 2}\int_0^{R} e^{-\lambda\pi(R_m)^2}\frac{2\left(\lambda\pi(R_m)^2\right)^{N_1-1}}{R_m\Gamma\left(N_1-1\right)}\int_0^{\infty}\frac{e^{N_s z}}{1+z}\exp\left(-\lambda\pi\left(R^2-R_m^2\right)\right. \\
&\quad\times\left(1-\frac{2\left(R^2-R_m^2\right)^{-1}}{\alpha+2}(I_s z)^{-1}\left(R^{\alpha+2}\,{}_2F_1\left(1,1+\frac{2}{\alpha};2+\frac{2}{\alpha},-\frac{R^{\alpha}}{I_s z}\right)\right.\right. \\
&\quad\left.\left.\left.-R_m^{\alpha+2}\,{}_2F_1\left(1,1+\frac{2}{\alpha};2+\frac{2}{\alpha},-\frac{R_m^{\alpha}}{I_s z}\right)\right)\right)\right)\mathrm{d}z\mathrm{d}R_m \qquad \text{(A.64)}
\end{aligned}$$

The integral for variable z can be calculated with the transformed GCQ used by (4.18), and the

integral for variable R_m can be directly calculated by GCQ [79, Ep.(25.4.39)]. Finally we get,

$$C_{\gamma_1^{\mathrm{ZF}}}^{N_2\geq N_1} = \frac{1}{2\ln 2}\sum_{m=1}^{M} a_m e^{-\lambda\pi(b_m)^2}\frac{2\left(\lambda\pi(b_m)^2\right)^{N_1-1}}{b_m\Gamma\left(N_1-1\right)}\sum_{n=1}^{N}\frac{w_n e^{N_s s_n}}{1+s_n}\exp\left(-\lambda\pi\left(R^2-b_m^2\right)\right.$$
$$\times\left(1-\frac{2\left(R^2-b_m^2\right)^{-1}}{\alpha+2}(I_s s_n)^{-1}\left(R^{\alpha+2}\,{}_2F_1\left(1,1+\frac{2}{\alpha};2+\frac{2}{\alpha},-\frac{R^\alpha}{I_s s_n}\right)\right.\right.$$
$$\left.\left.\left.-b_m^{\alpha+2}\,{}_2F_1\left(1,1+\frac{2}{\alpha};2+\frac{2}{\alpha},-\frac{b_m^\alpha}{I_s s_n}\right)\right)\right)\right) \tag{A.65}$$

where the weights a_m and abscissas b_m have been given by (4.30a) and (4.30b).

A.5.2 Calculation of $C_{\gamma_2^{\mathrm{ZF}}}$

For all $N_2 \in \Phi$, the expression of $C_{\gamma_2^{\mathrm{ZF}}}$ equals C_{γ_2} shown in (A.33).

A.5.3 Calculation of $C^A_{\gamma_T^{\mathrm{ZF}}}$

In the scenario $N_2 < N_1$, all interference are completely removed, both $\gamma_{1^{\mathrm{ZF}}}^{N_2<N_1}$ and $\gamma_{2^{\mathrm{ZF}}}^{N_2<N_1}$ can be treated as noise-limited, but with different transmission diversities. Applying the expression proposed by [86], we have:

$$C_{\gamma_T^{\mathrm{ZF}}} = \frac{1}{2\ln 2}\int_0^\infty \frac{e^{-z}}{z}(1-\mathrm{M}_{\gamma_T^{\mathrm{ZF}}}(z))\mathrm{d}z, \tag{A.66}$$

where $\mathrm{M}_{\gamma_T^{\mathrm{ZF}}}(z)$ is the MGF of γ_T^{ZF}. The pdf of $\gamma_{1^{\mathrm{ZF}}}^{N_2<N_1}$ has been given in (A.57a), and the MGF of $\gamma_{1^{\mathrm{ZF}}}^{N_2<N_1}$ can be calculated by

$$\begin{aligned} M_{\gamma_1^{\mathrm{MRC}}}^{N_2<N_1}(t) =& \frac{N_s^{N_1-N_2}}{\Gamma\left(N_1-N_2\right)}\int_0^\infty \gamma^{N_1-N_2-1}e^{-(N_s+t)\gamma}\mathrm{d}\gamma \\ =& \frac{N_s^{N_1-N_2}}{(N_s+t)^{N_1-N_2}}. \end{aligned} \tag{A.67}$$

and the MGF of γ_2^{ZF} equals that for γ_2^{MRC}, which is given by (A.40). Since γ_1^{ZF} and γ_2^{ZF} are independent to each other, we have:

$$\mathrm{M}_{\gamma_{T^{\mathrm{ZF}}}}^{N_2<N_1}(t) = \mathrm{M}_{\gamma_{1^{\mathrm{ZF}}}}^{N_2<N_1}(t)\mathrm{M}_{\gamma_{2^{\mathrm{ZF}}}}^{N_2<N_1}(t) = \left(\frac{1}{1+\frac{t}{N_s}}\right)^{N_1-N_2}\left(\frac{1}{1+\frac{t}{N_r}}\right)^{N_1}. \tag{A.68}$$

In order to avoid the singularity problem caused by e^{-z}/z at zero in the computation of (A.66), we change the term MGFs above to

$$\mathrm{M}_{\gamma_1^{\mathrm{ZF}}}^{N_2<N_1}(t) = 1 - \frac{t}{N_s} \sum_{k=0}^{N_1-N_2-1} \left(\frac{1}{1+t/N_s} \right)^{k+1}, \tag{A.69a}$$

$$\mathrm{M}_{\gamma_2^{\mathrm{ZF}}}^{N_2<N_1}(t) = 1 - \frac{t}{N_r} \sum_{k=0}^{N_1-1} \left(\frac{1}{1+t/N_r} \right)^{k+1}, \tag{A.69b}$$

then the corresponding $\mathrm{M}_{\gamma_T^{\mathrm{ZF}}}^{N_2<N_1}(t)$ is given by

$$\begin{aligned} \mathrm{M}_{\gamma_T^{\mathrm{ZF}}}^{N_2<N_1}(t) =& 1 - \frac{t}{N_s} \sum_{k_1=0}^{N_1-N_2-1} \left(\frac{1}{1+\frac{t}{N_s}} \right)^{k_1+1} - \frac{t}{N_r} \sum_{k_2=0}^{N_1-1} \left(\frac{1}{1+\frac{t}{N_r}} \right)^{k_2+1} \\ &+ \frac{t^2}{N_s N_r} \sum_{k_1=0}^{N_1-N_2-1} \sum_{k_2=0}^{N_1-1} \left(\frac{1}{1+\frac{t}{N_s}} \right)^{k_1+1} \left(\frac{1}{1+\frac{t}{N_r}} \right)^{k_2+1}. \end{aligned} \tag{A.70}$$

Substituting (A.70) into (A.66), we can derive the $C_{\gamma_T^{\mathrm{ZF}}}$ in the condition $N_2 < N_1$:

$$C_{\gamma_T^{\mathrm{ZF}}}^{N_2<N_1} = \frac{1}{2N_s \ln 2} \sum_{k_1=0}^{N_1-N_2-1} \mathcal{I}_1 + \frac{1}{2N_r \ln 2} \sum_{k_2=0}^{N_1-1} \mathcal{I}_2 - \frac{1}{2N_s N_r \ln 2} \sum_{k_1=0}^{N_1-N_2-1} \sum_{k_2=0}^{N_1-1} \mathcal{I}_3 \tag{A.71}$$

where

$$\begin{aligned} \mathcal{I}_1 &= \int_0^\infty \left(\frac{e^{-z}}{1+\frac{z}{N_s}} \right)^{k_1+1} \mathrm{d}z = N_s \mathrm{U}\left(1, 1-k_1; N_s\right), \\ \mathcal{I}_2 &= \int_0^\infty \left(\frac{e^{-z}}{1+\frac{z}{N_r}} \right)^{k_2+1} \mathrm{d}z = N_r \mathrm{U}\left(1, 1-k_2; N_r\right), \\ \mathcal{I}_3 &= \int_0^\infty z e^{-z} \left(\frac{1}{1+\frac{z}{N_s}} \right)^{k_1+1} \left(\frac{1}{1+\frac{z}{N_r}} \right)^{k_2+1} \mathrm{d}z \\ &= \int_0^\infty z e^{-z} \mathrm{G}_{1,1}^{1,1}\left(\frac{z}{N_s} \middle| \begin{matrix} -k_1 \\ 0 \end{matrix} \right) \mathrm{G}_{1,1}^{1,1}\left(\frac{z}{N_r} \middle| \begin{matrix} -k_2 \\ 0 \end{matrix} \right) \mathrm{d}z = \mathrm{G}_{1,1:1,0,1:1}^{1,1,1,1,1}\left(\begin{matrix} 1/N_s \\ 1/N_r \end{matrix} \middle| \begin{matrix} 2 \\ -k_1;-k_2 \\ - \\ 0;0 \end{matrix} \right). \end{aligned} \tag{A.72}$$

The integrals in $\mathcal{I}_1$ and $\mathcal{I}_2$ is with the aid of [80, Eq.90211.4], and $\mathcal{I}_3$ is integrated using the formula [90, 2.6.2]. Finally, the $C_{\gamma_T^{\mathrm{ZF}}}^{N_2<N_1}$ can be written as

$$C_{\gamma_T^{\mathrm{ZF}}}^{N_2<N_1} = \frac{1}{2\ln 2}\left(\sum_{k_1=0}^{N_1-N_2-1} \mathrm{U}\left(1, 1-k_1; N_s\right) + \sum_{k_2=0}^{N_1-1} \mathrm{U}\left(1, 1-k_2; N_r\right) - \frac{1}{N_s N_r} \sum_{k_1=0}^{N_1-N_2-1} \sum_{k_2=0}^{N_1-1} \mathrm{G}_{1,1:1,0,1:1}^{1,1,1,1,1}\left(\begin{matrix} 1/N_s \\ 1/N_r \end{matrix} \middle| \begin{matrix} 2 \\ -k_1; -k_2 \\ - \\ 0; 0 \end{matrix}\right)\right). \tag{A.73}$$

In the scenario $N_2 \geq N_1$, part of the interference is treated as the noise. Therefore, we apply the same method explored by MRC/MRT to find the lower bound for $C_{\gamma_T^{\mathrm{ZF}}}^{N_2\geq N_1}$.

$$C_{\gamma_T{}^{\mathrm{ZF}}}^{N_2\geq N_1} \leq \frac{1}{2}\Pr\left(R_m < R\right)\log_2\left(1 + \mathbb{E}_{\gamma_1|R_m<R}\{\gamma_1^{\mathrm{ZF}}\} + \mathbb{E}\{\gamma_2^{\mathrm{ZF}}\}\right), \tag{A.74}$$

where

$$\mathbb{E}\{\gamma_2^{\mathrm{ZF}}\} = \mathbb{E}\{\gamma_2\} = \frac{N_1}{N_r}. \tag{A.75}$$

and

$$\mathbb{E}_{\gamma_1|R_m<R}\{\gamma_1^{\mathrm{ZF}}\} = \int_0^R f_{R_m<R}(R_m)\mathbb{E}_{\gamma_1|R_m}\{\gamma_1^{\mathrm{ZF}}\}\mathrm{d}R_m. \tag{A.76}$$

Substituting $m = 1$ and $g(z) = z$ into (A.46), we have $g_1(z) = 1$ and the expression of $\mathbb{E}_{\gamma_1|R_m}\{\gamma_1^{\mathrm{ZF}}\}$ can be expressed as

$$\begin{aligned}\mathbb{E}_{\gamma_1|R_m}\{\gamma_1^{\mathrm{ZF}}\} = &\int_0^\infty e^{-N_s z}\exp\left(-\lambda\pi\left(R^2-R_m^2\right)\left(1-\frac{2\left(R^2-R_m^2\right)^{-1}}{\alpha+2}\right.\right.\\ &\times(I_s z)^{-1}\left(R^{\alpha+2}\,{}_2F_1\left(1,1+\frac{2}{\alpha};2+\frac{2}{\alpha},\frac{R^\alpha}{I_s z}\right)\right.\\ &\left.\left.\left.-R_m^{\alpha+2}\,{}_2F_1\left(1,1+\frac{2}{\alpha};2+\frac{2}{\alpha},\frac{R_m^\alpha}{I_s z}\right)\right)\right)\right)\mathrm{d}z\\ \approx &\sum_{n=1}^{N} w_n e^{-N_s s_n}\exp\left(-\lambda\pi\left(R^2-R_m^2\right)\left(1-\frac{2\left(R^2-R_m^2\right)^{-1}}{\alpha+2}\right.\right.\\ &\times(I_s s_n)^{-1}\left(R^{\alpha+2}\,{}_2F_1\left(1,1+\frac{2}{\alpha};2+\frac{2}{\alpha},-\frac{R^\alpha}{I_s s_n}\right)\right.\\ &\left.\left.\left.-R_m^{\alpha+2}\,{}_2F_1\left(1,1+\frac{2}{\alpha};2+\frac{2}{\alpha},-\frac{R_m^\alpha}{I_s s_n}\right)\right)\right)\right),\end{aligned} \tag{A.77}$$

where s_n and w_n have been defined by (4.21) and (4.22). The pdf of R_m in the condition that $0 \le R_m \le R$ can be expressed as $f_{R_m\le R}(R_m)$. Since the corresponding CDF $F_{R_m\le R}(R_m)$ can be expressed as

$$\begin{aligned}F_{R_m\le R}(R_m) =&\Pr\left(X < R_m | X < R\right) = \frac{\Pr\left(X < \min(R_m, R)\right)}{\Pr(X<R)}\\ =&\begin{cases}\frac{F_{N_1-1}(R_m)}{F_{N_1-1}(R)}, & R_m < R\\ 1 \qquad R_m \ge R,\end{cases}\end{aligned} \tag{A.78}$$

we have

$$f_{R_m\le R}(R_m) = \frac{f_{N_1-1}(R_m)}{F_{N_1-1}(R)}, R_m \in [0, R], \tag{A.79}$$

where $f_{N_1-1}(R_m)$ is the pdf of the (N_1-1)-th nearest interferer when $R_m \in (0,\infty)$, given by (A.55). $P_{N_1-1}(R) = 1 - \frac{\Gamma(N_1-1,\lambda\pi R^2)}{\Gamma(N_1-1)}$ is the probability that the distance from relay to the (N_1-1)-th interferer is smaller than R, which is given by [89]. Substituting (A.79) into (A.76)

and applying the GCQ with a_m and b_m defined by (4.30a) and (4.30b), respectively, we have

$$\begin{aligned}\mathbb{E}_{\gamma_1|R_m<R}\{\gamma_1^{\mathrm{ZF}}\} = &\sum_{n=1}^{N}\sum_{m=1}^{M} a_m e^{-\lambda\pi(b_m)^2}\frac{2\left(\lambda\pi(b_m)^2\right)^{N_1-1}}{b_m\Gamma\left(N_1-1\right)P_{N_1-1}(R)}\\ &\times w_n e^{N_s s_n}\exp\left(-\lambda\pi\left(R^2-b_m^2\right)\left(1-\frac{2\left(R^2-b_m^2\right)^{-1}}{\alpha+2}\right.\right.\\ &\times\left(I_s s_n\right)^{-1}\left(R^{\alpha+2}\,{}_2F_1\left(1,1+\frac{2}{\alpha};2+\frac{2}{\alpha},-\frac{R^\alpha}{I_s s_n}\right)\right.\\ &\left.\left.\left.-b_m^{\alpha+2}\,{}_2F_1\left(1,1+\frac{2}{\alpha};2+\frac{2}{\alpha}-\frac{b_m^\alpha}{I_s s_n}\right)\right)\right)\right)\end{aligned} \tag{A.80}$$

Substituting (A.80), (A.75) into (A.74), , the expression of the lower bound of $C_{\gamma_T^{\mathrm{ZF}}}^{N_2}$ is given by

$$\begin{aligned}C_{\gamma_T^{\mathrm{ZF}}}^{N_2\geq N_1} \geq &\frac{P_{N_1-1}(R)}{2}\log_2\left(1+\sum_{n=1}^{N}\sum_{m=1}^{M} a_m e^{-\lambda\pi(b_m)^2}\frac{2\left(\lambda\pi(b_m)^2\right)^{N_1-1}}{b_m\Gamma\left(N_1-1\right)P_{N_1-1}(R)}\right.\\ &\times w_n e^{N_s s_n}\exp\left(-\lambda\pi\left(R^2-b_m^2\right)\left(1-\frac{2\left(R^2-b_m^2\right)^{-1}}{\alpha+2}\right.\right.\\ &\times(I_s s_n)^{-1}\left(R^{\alpha+2}\,{}_2F_1\left(1,1+\frac{2}{\alpha};2+\frac{2}{\alpha},-\frac{R^\alpha}{I_s s_n}\right)\right.\\ &\left.\left.\left.\left.-b_m^{\alpha+2}\,{}_2F_1\left(1,1+\frac{2}{\alpha};2+\frac{2}{\alpha},-\frac{b_m^\alpha}{I_s s_n}\right)\right)\right)\right)+\frac{N_1}{N_r}\right),\end{aligned} \tag{A.81}$$

Combining (A.65), (A.33)and (A.81), we get the expression of $\overline{C}_{\mathrm{ZF}}^{N_2\geq N_1}$. By combining (A.58) and (A.73), we obtain the expression of $C_{\mathrm{ZF}}^{N_2<N_1}$

A.6 Proof of Proposition 6

Substituting (4.12) into (4.13), the ergodic capacity in the MMSE/MRT scheme can be written as

$$C_{\mathrm{MMSE}} = C_{\gamma_1^{\mathrm{MRC}}} + C_{\gamma_2^{\mathrm{MMSE}}} - C_{\gamma_T^{\mathrm{MMSE}}}. \tag{A.82}$$

Since $C_{\gamma_2^{\mathrm{MMSE}}} = C_{\gamma_2}$ has been given by (A.33), we only need to find out the expressions of $C_{\gamma_1^{\mathrm{MMSE}}}$ and $C_{\gamma_T^{\mathrm{MMSE}}}$.

A.6.1 Calculation of $C_{\gamma_1^{\mathrm{MMSE}}}$

Without considering the PPP, the CDF of SINR of the MISO system with optimal combining (OP) precoder had been studied by many researchers, but was expressed in the form of a polynomial ratio in [91] for the first time.

$$F_{\gamma_1}(z) = 1 - \exp(-zN_r) \sum_{m=1}^{M} \frac{A_m(z)}{(m-1)!} (zN_r)^{m-1} \tag{A.83}$$

where

$$\mathrm{A}_m(z) = \begin{cases} 1, & N_1 \geq N_2 + m; \\ \frac{1+\sum_{i=1}^{N_1-m} C_i z^i}{\prod_{n=1}^{N_2}(1+\Gamma_n z)}, & N_1 \leq N_2 + m \end{cases}. \tag{A.84}$$

and C_i is the coefficient of z^i of function $\prod_{n=1}^{N_2}(1+\Gamma_n z)$, that is

$$C_i = \sum_{1 \leq n_1 \leq \cdots \leq n_i \leq N} \Gamma_{n_1} \Gamma_{n_2} \cdots \Gamma_{n_i}, \tag{A.85}$$

$\Gamma_i = \frac{P_i |X_i|^\alpha}{P_s}$, X_i is the position of the i-th interferer. Based on [91], the authors of [92] addressed the CDF of SINR for MISO systems considering PPP. Firstly, the authors rewrote (A.83) as:

$$F_{\gamma|N_2,\Gamma_1,\cdots\Gamma_{N_2}}(z) = 1 - \frac{\sum_{i=0}^{N_1-1} a_i z^i}{\exp(N_r z) \prod_{j=1}^{N_2} (1+\Gamma_j z)}, \tag{A.86}$$

where $a_i, i = 1, \cdots, N_2 - 1$, are the first N_2 coefficients of Taylor expansion of function $\exp(N_r z) \prod_{j=1}^{N_2} (1+\Gamma_j z)$, Γ_j has the same definition as in (A.83).

Since the definitions of $F_{\gamma|N_2,\Gamma_1,\cdots\Gamma_{N_2}}(z)$ applied in this chapter and in [92] are very similar, i.e. $\gamma = \frac{|\mathrm{w}_1^H \mathrm{h}1|^2}{I_s \sum_\phi |X_i|^{-\alpha} |\mathrm{w}_1^H \mathrm{h}_{\mathrm{I}_i}|^2 + N_s}$ in our work, where I_s and N_s have been defined in MRC and ZF scenarios, and $\gamma = \frac{R_1^\alpha |\mathrm{w}_1^H \mathrm{h}1|^2}{\sum_\phi ||X_i|^{-\alpha} \mathrm{w}_1^H \mathrm{h}_{\mathrm{I}_i}|^2 + \sigma^2}$ in [92], $F_{\gamma_1^{\mathrm{MMSE}}}(z)$ can be directly obtained

from [92, Ep.15] by replacing $|X|^{-\alpha}$ and σ^2 with $I_r|X|^{-\alpha}$ and N_r, respectively:

$$\begin{aligned}
F_{\gamma_1^{\mathrm{MMSE}}}(z) =& 1-\exp(-N_s z)\sum_{i=0}^{N_1-1}\sum_{k=0}^{i}\frac{1}{k!(i-k)!}(N_s z)^{i-k}\left(\lambda\int_{\mathbb{R}^2}\frac{|X|^{-\alpha}I_s z}{1+|X|^{-\alpha}I_s z}\mathrm{d}X\right)^k \\
&\times\exp\left(\lambda\int_{\mathbb{R}^2}\frac{-|X|^{-\alpha}I_s z\mathrm{d}X}{1+|X|^{-\alpha}I_s z}\right) \\
=& 1-\sum_{i=0}^{N_1-1}\frac{\left(\lambda\int_{\mathbb{R}^2}\frac{|X|^{-\alpha}I_s z\mathrm{d}X}{1+|X|^{-\alpha}I_s z}+N_s z\right)}{i!} \\
&\times\exp\left(-\lambda\int_{\mathbb{R}^2}\frac{|X|^{-\alpha}I_s z\mathrm{d}X}{1+|X|^{-\alpha}I_s z}-N_s z\right) \qquad \text{(A.87)} \\
=& 1-\sum_{i=0}^{N_1-1}\frac{\left(\lambda\Delta(I_s)^{\frac{2}{\alpha}}z^{\frac{2}{\alpha}}+N_s z\right)^i}{i!}\exp\left(-\lambda\Delta(I_s)^{\frac{2}{\alpha}}z^{\frac{2}{\alpha}}-N_s z\right) \qquad \text{(A.88)}
\end{aligned}$$

where $\Delta=\frac{2\pi}{\alpha}\Gamma\left(\frac{2}{\alpha}\right)\Gamma\left(1-\frac{2}{\alpha}\right)$. The integral is derived by [92, Appendix A].

By substituting (A.88) into (A.17), we have:

$$C_{\gamma_{1\mathrm{MMSE}}}=\frac{1}{2\ln 2}\sum_{i=0}^{N_1-1}\int_0^{\infty}\frac{1}{1+z}\frac{\left(\lambda\Delta(I_s)^{\frac{2}{\alpha}}z^{\frac{2}{\alpha}}+N_s z\right)^i}{i!}\exp\left(-\lambda\Delta(I_s)^{\frac{2}{\alpha}}z^{\frac{2}{\alpha}}-N_s z\right)\mathrm{d}z, \tag{A.89}$$

which can be efficiently calculated through the GCQ applied in (4.18):

$$C_{\gamma_{1\mathrm{MMSE}}}=\sum_{i=0}^{N_1-1}\sum_{n=1}^{N}\frac{w_n\left(\lambda\Delta(I_s)^{\frac{2}{\alpha}}s_n^{\frac{2}{\alpha}}+N_s s_n\right)^i}{2\ln(2)i!(1+s_n)}\exp\left(-\lambda\Delta(I_s)^{\frac{2}{\alpha}}s_n^{\frac{2}{\alpha}}-N_s s_n\right), \tag{A.90}$$

the expression of s_n and w_n have been given by (4.21) and (4.22), respectively.

A.6.2 Calculation of $C_{\gamma_T^{\mathrm{MMSE}}}$

We can calculate $C_{\gamma_T^{\mathrm{MMSE}}}$ by following the similar approach of calculating $C_{\gamma_T^{\mathrm{MRC}}}$, i.e. Applying the expression proposed by [86]:

$$C_{\gamma_T^{\mathrm{MMSE}}}=\frac{1}{2\ln 2}\int_0^{\infty}\frac{e^{-z}}{z}(1-M_{\gamma_T^{\mathrm{MMSE}}}(z))\mathrm{d}t, \tag{A.91}$$

where

$$M_{\gamma_T^{\mathrm{MMSE}}}(t) = M_{\gamma_1^{\mathrm{MMSE}}}(t) M_{\gamma_2^{\mathrm{MMSE}}}(t). \tag{A.92}$$

The expression of $M_{\gamma_1^{\mathrm{MMSE}}}(t)$ is the same as $M_{\gamma_1^{\mathrm{MRC}}}(t)$ given by (A.40). By substituting (A.88) into (A.36), we can obtain $M_{\gamma_1^{\mathrm{MMSE}}}(t)$ by calculating

$$\begin{aligned}
M_{\gamma_1^{\mathrm{MMSE}}}(t) &= t \left(\int_{z=0}^{\infty} e^{-zt} \left(1 - \sum_{i=0}^{N_1-1} \frac{\left(\lambda \Delta (I_s)^{\frac{2}{\alpha}} z^{\frac{2}{\alpha}} + N_s z \right)^i}{i!} \exp\left(-\lambda \Delta (I_s)^{\frac{2}{\alpha}} z^{\frac{2}{\alpha}} - N_s z \right) \mathrm{d}z \right) \right) \\
&= 1 - t \int_{z=0}^{\infty} e^{-zt} \sum_{i=0}^{N_1-1} \frac{\left(\lambda \Delta (I_s)^{\frac{2}{\alpha}} z^{\frac{2}{\alpha}} + N_s z \right)^i}{i!} \exp\left(-\lambda \Delta (I_s)^{\frac{2}{\alpha}} z^{\frac{2}{\alpha}} - N_s z \right) \mathrm{d}z \\
&= 1 - t \sum_{i=0}^{N_1-1} \sum_{k=0}^{i} \frac{\binom{i}{k}}{i!} \left(\lambda \Delta I_s^{\frac{2}{\alpha}} \right)^k (N_s)^{i-k} \int_0^{\infty} z^{\frac{2k}{\alpha}+i-k} e^{-(t+N_s)z} e^{-\lambda \Delta (I_s)^{\frac{2}{\alpha}} z^{\frac{2}{\alpha}}} \mathrm{d}z
\end{aligned} \tag{A.93}$$

With the fact that $\exp\left(-bx^a\right) = \mathrm{G}_{0,1}^{1,0}\left(bx^a \middle| \begin{matrix} - \\ 0 \end{matrix} \right)$, given by [41, Ep.8.4.3.2] we have

$$\begin{aligned}
M_{\gamma_1^{\mathrm{MMSE}}}(t) &= 1 - t \sum_{i=0}^{N_1-1} \sum_{k=0}^{i} \frac{\binom{i}{k}}{i!} \left(\lambda \Delta I_s^{\frac{2}{\alpha}} \right)^k (N_s)^{i-k} \\
&\qquad \times \int_0^{\infty} z^{\frac{2k}{\alpha}+i-k} \mathrm{G}_{0,1}^{1,0}\left((t+N_s)z \middle| \begin{matrix} - \\ 0 \end{matrix} \right) \mathrm{G}_{0,1}^{1,0}\left(\lambda \Delta (I_s)^{\frac{2}{\alpha}} z^{\frac{2}{\alpha}} \middle| \begin{matrix} - \\ 0 \end{matrix} \right) \mathrm{d}z \\
&\overset{b}{=} 1 - t \sum_{i=0}^{N_1-1} \sum_{k=0}^{i} \frac{\binom{i}{k}}{i!} \lambda^k \Delta^k (I_s)^{\frac{2k}{\alpha}} (N_s)^{i-k} \frac{q^{\frac{1}{2}} p^{\frac{2k}{\alpha}+i-k+\frac{1}{2}}}{(2\pi)^{(p+q-2)/2}} \\
&\qquad \times \mathrm{G}_{q,p}^{p,q}\left(\frac{\left(\frac{\lambda \Delta (I_s)^{\frac{2}{\alpha}}}{q} \right)^q}{\left(\frac{N_s+t}{p} \right)^p} \middle| \begin{matrix} \mathcal{Q}\left(-\frac{2k}{\alpha}-i+k-1, p\right) \\ \mathcal{Q}(-1, q) \end{matrix} \right)
\end{aligned} \tag{A.94}$$

the integral is made with the aid of [18, 07.34.21.0013.01], where $\mathcal{Q}(a,b)$ presents a list $\frac{1+a}{b}, \cdots, \frac{b+a}{b}$.

Combining (A.94), (A.40), (A.92) and (A.91), and use GCQ, we finally get (4.35).

A.7 Proof of Proposition 7

The lower bound of end-to-end capacity with MMSE/MRT scheme in a infinite-area interference circumstance can be expressed as

$$C_{\mathrm{MMSE}}^{lim} > C_{L_{\mathrm{MMSE}}}^{lim} = C_{\gamma_1^{\mathrm{MMSE}}}^{lim} + C_{\gamma_2^{\mathrm{MMSE}}}^{lim} - \frac{1}{2}\log_2\left(1 + \mathbb{E}\{\gamma_{1^{\mathrm{MMSE}}}^{lim}\} + \mathbb{E}\{\gamma_{2^{\mathrm{MMSE}}}^{lim}\}\right) \tag{A.95}$$

The expressions $C_{\gamma_2^{\mathrm{MMSE}}}^{lim} = C_{\gamma_2}$ and $\mathbb{E}\left\{\gamma_{2^{\mathrm{MMSE}}}^{lim}\right\} = \mathbb{E}\left\{\gamma_2\right\}$ have been presented in formula (A.33) and (A.52), respectively. We only need to derive the expressions of $C_{\gamma_1^{\mathrm{MMSE}}}^{lim}$ and $\mathbb{E}\left\{\gamma_{1^{\mathrm{MMSE}}}^{lim}\right\}$.

Recalling expression (A.87), the CDF of $\gamma_{1^{\mathrm{MMSE}}}^{lim}$ can be obtained by finding the result of integration $\int_{\mathbb{R}^2} \frac{|X|^{-\alpha} I_s z}{1+|X|^{-\alpha} I_s z} \mathrm{d}X$ in a finite area.

$$\begin{aligned}
\int_{\mathbb{R}^2} \frac{|X|^{-\alpha} I_s z}{1 + |X|^{-\alpha} I_s z} \mathrm{d}X =& \int_0^R \int_0^{2\pi} \frac{r^{1-\alpha} I_s z}{1 + |X|^{-\alpha} I_s z} \mathrm{d}\theta \mathrm{d}r \\
=& 2\pi \int_0^R \frac{r^{1-\alpha} I_s z}{1 + r^{-\alpha} I_s z} \mathrm{d}r \\
\overset{a}{=}& \frac{2\pi}{\alpha} (I_s z)^{\frac{2}{\alpha}} \int_{R^{-\alpha} I_s z}^{\infty} \frac{y^{-\frac{2}{\alpha}}}{1+y} \mathrm{d}y \\
\overset{b}{=}& \pi R^2 \, {}_2F_1\left(1, \frac{2}{\alpha}, 1 + \frac{2}{\alpha}, -\frac{R^\alpha}{I_s z}\right),
\end{aligned} \tag{A.96}$$

where step a is obtained by changing the variable to $y = r^{-\alpha} I_s z$, step b is calculated according to [80, Eq.3.194.2]. Substituting (A.96) into (A.87), the expression of CDF of $\gamma_{1^{\mathrm{MMSE}}}^{lim}$ can be expressed as

$$\begin{aligned}
F_{\gamma_1^{\mathrm{MMSE}}}^{lim}(z) =& 1 - \sum_{i=0}^{N_1 - 1} \frac{\left(\lambda \pi R^2 \, {}_2F_1\left(1, \frac{2}{\alpha}, 1 + \frac{2}{\alpha}, -\frac{R^\alpha}{I_s z}\right) + N_s z\right)^i}{i!} \\
& \times \exp\left(-\lambda \pi R^2 \, {}_2F_1\left(1, \frac{2}{\alpha}, 1 + \frac{2}{\alpha}, -\frac{R^\alpha}{I_s z}\right) - N_s z\right).
\end{aligned} \tag{A.97}$$

Substituting (A.97) into (A.17), and using GCQ to operate the integral, expression of (4.37) is finally obtained.

The expression of $\mathbb{E}\left\{\gamma_{1^{\text{MMSE}}}^{lim}\right\}$ is can be directly derived by $\mathbb{E}\left\{\gamma_{1^{\text{MMSE}}}^{lim}\right\} = \int_0^\infty z f_{\gamma_{1^{\text{MMSE}}}}^{lim}(z)\mathrm{d}z$ and $f_{\gamma_1^{\text{MMSE}}}^{lim}(z) = \frac{\mathrm{d}F_{\gamma_1^{\text{MMSE}}}^{lim}(z)}{\mathrm{d}z}$. To simplify the differentiation, we first rewrite (A.97) according to the property of incomplete gamma function $\gamma(n,x) = \Gamma(n)e^{-x}\sum_{i=0}^{n-1}\left(\frac{x^i}{i!}\right)$, n is a positive integer [82, Eq.6.5.13, Eq.6.5.1].

$$F_{\gamma_1^{\text{MMSE}}}^{lim}(z) = \frac{1}{\Gamma(N_1)}\gamma\left(N_1, N_s z + \lambda\pi R^2\, {}_2F_1\left(1, \frac{2}{\alpha}, 1+\frac{2}{\alpha}, -\frac{R^\alpha}{I_s z}\right)\right) \tag{A.98}$$

and corresponding pdf is derived in the following:

$$\begin{aligned}
f_{\gamma_1^{\text{MMSE}}}^{lim}(z) =& \frac{\mathrm{d}F_{\gamma_1^{\text{MMSE}}}^{lim}(z)}{\mathrm{d}z} \\
\overset{a}{=}& \frac{1}{\Gamma(N_1)}\left(N_s z + \lambda\pi R^2\, {}_2F_1\left(1, \frac{2}{\alpha}, 1+\frac{2}{\alpha}, -\frac{R^\alpha}{I_s z}\right)\right)^{N_1-1} \\
& \times \exp\left(-N_s z - \lambda\pi R^2\, {}_2F_1\left(1, \frac{2}{\alpha}, 1+\frac{2}{\alpha}, -\frac{R^\alpha}{I_s z}\right)\right) \\
& \times \frac{\mathrm{d}\left(N_s z + \lambda\pi R^2\, {}_2F_1\left(1, \frac{2}{\alpha}, 1+\frac{2}{\alpha}, -\frac{R^\alpha}{I_s z}\right)\right)}{\mathrm{d}z} \\
\overset{b}{=}& \frac{1}{\Gamma(N_1)}\left(N_s z + \lambda\pi R^2\, {}_2F_1\left(1, \frac{2}{\alpha}, 1+\frac{2}{\alpha}, -\frac{R^\alpha}{I_s z}\right)\right)^{N_1-1} \\
& \times \exp\left(-N_s z - \lambda\pi R^2\, {}_2F_1\left(1, \frac{2}{\alpha}, 1+\frac{2}{\alpha}, -\frac{R^\alpha}{I_s z}\right)\right) \\
& \times \left(N_s + \frac{2\lambda\pi R^{\alpha+2} I_s^{-1} z^{-2}}{\alpha+2}\, {}_2F_1\left(2, 1+\frac{2}{\alpha}, 2+\frac{2}{\alpha}, -\frac{R^\alpha}{I_s z}\right)\right)
\end{aligned} \tag{A.99}$$

where step a is with according to $\frac{\mathrm{d}\gamma(a,x)}{\mathrm{d}x} = x^{a-1}e^{-x}$ [82, Eq.6.5.25], step b is with the aid of $\frac{\mathrm{d}}{\mathrm{d}x}\,{}_2F_1\left(a,b,c,x\right) = \frac{ab}{c}\,{}_2F_1\left(a+1,b+1,c+1,x\right)$ [82, Eq.15.2.1]. Applying GCQ with s_n and w_n given in (4.21) and (4.22), the expression of $\mathbb{E}\left\{\gamma_{1^{\text{MMSE}}}^{lim}\right\}$ is obtained.

$$\begin{aligned}
\mathbb{E}\left\{\gamma_{1^{\text{MMSE}}}^{lim}\right\} =& \sum_{n=1}^{N}\frac{w_n s_n}{\Gamma(N_1)}\left(N_s s_n + \lambda\pi R^2\, {}_2F_1\left(1, \frac{2}{\alpha}, 1+\frac{2}{\alpha}, -\frac{R^\alpha}{I_s s_n}\right)\right)^{N_1-1} \\
& \times \exp\left(-N_s z - \lambda\pi R^2\, {}_2F_1\left(1, \frac{2}{\alpha}, 1+\frac{2}{\alpha}, -\frac{R^\alpha}{I_s s_n}\right)\right) \\
& \times \left(N_s + \frac{2\lambda\pi R^{\alpha+2} I_s^{-1} s_n^{-2}}{\alpha+2}\, {}_2F_1\left(2, 1+\frac{2}{\alpha}, 2+\frac{2}{\alpha}, -\frac{R^\alpha}{I_s s_n}\right)\right).
\end{aligned} \tag{A.100}$$

Finally, combining (4.37), (A.33), (A.100), (A.52) and (A.95), Proposition 7 is obtained.

A.8 Proof of Proposition 8

According to (5.9), the outage can be expressed as:

$$\begin{aligned} P_m^{out} &= 1 - \int_{\theta_m^*}^{\infty} f_{|h_{2,m}|^2}(y) \int_{\frac{\theta_m^*(1+\bar{\gamma}y)}{\bar{\gamma}(y-\theta_m^*)}}^{\infty} f_{|h_1|^2}(x)\mathrm{d}x\mathrm{d}y \\ &= 1 - \int_{\theta_m^*}^{\infty} f_{|h_{2,m}|^2}(y) \left(1 - F_{|h_1|^2}\left(\frac{\theta_m^*(1+\bar{\gamma}y)}{\bar{\gamma}(y-\theta_m^*)}\right)\right)\mathrm{d}y \\ &= F_{|h_{2,m}|^2}(\theta_m^*) + \int_{\theta_m^*}^{\infty} f_{|h_{2,m}|^2}(y) F_{|h_1|^2}\left(\frac{\theta_m^*(1+\bar{\gamma}y)}{\bar{\gamma}(y-\theta_m^*)}\right)\mathrm{d}y. \end{aligned} \tag{A.101}$$

To begin with, we should find out the expressions of $F_{|h_1|^2}(x)$ and $f_{|h_2|^2}(x)$. Since $h_1 = \frac{g_1}{\sqrt{1+R_1^2}}$, we can easily get the CDF expression of $|h_1|^2$ from (5.13):

$$F_{|h_1|^2}(x) = F_{|g_1|^2}\left(x\left(1+R_1^2\right)\right) = 1 - e^{\lambda_1(1+R_1^2)x} \tag{A.102}$$

Substituting (A.102) into (A.101), we get:

$$\begin{aligned} P_m^{out} &= F_{|h_{2,m}|^2}(\theta_m^*) + \int_{\theta_m^*}^{\infty} f_{|h_{2,m}|^2}(y)\left(1 - e^{-\lambda_1(1+R_1^2)\left(\frac{\theta_m^*(1+\bar{\gamma}y)}{\bar{\gamma}(y-\theta_m^*)}\right)}\right)\mathrm{d}y \\ &= 1 - \int_{\theta_m^*}^{\infty} f_{|h_{2,m}|^2}(y) e^{-\lambda_1(1+R_1^2)\left(\frac{\theta_m^*(1+\bar{\gamma}y)}{\bar{\gamma}(y-\theta_m^*)}\right)}\mathrm{d}y \end{aligned} \tag{A.103}$$

By combining (5.10) and (5.12), the pdf of $|h_2|^2$ can be derived as

$$\begin{aligned} f_{|h_2|^2}(y) &= \int_0^R \lambda_2 e^{-\lambda_2 y\left(1+r^2\right)}(1+r^2)\frac{2r}{R^2}\mathrm{d}r \\ &\overset{a}{=} 1 - \frac{1}{R^2}\int_1^{1+R^2} e^{-\lambda_2 y z}\mathrm{d}z \\ &\overset{b}{=} \lambda_2^{-1}R^{-2}y^{-2}\left((1+\lambda_2 y)e^{\lambda_2 y} - (1+(1+R^2)\lambda_2 y)e^{-\left(1+R^2 y\right)}\right), \end{aligned} \tag{A.104}$$

where step a is changing the variable r to $z = 1 + r^2$ and the integral in step b is completed with the help of [80, Eq.2.321,Eq.2.322]. And combining (5.11) and (5.13), the CDF of $|h_2|^2$

can be derived through the similar approach:

$$\begin{aligned} F_{|h_2|^2}(y) &= 1 - \int_0^R e^{-\lambda_2 y\left(1+r^2\right)} \frac{2r}{R^2} \mathrm{d}r \\ &= 1 - \frac{1}{R^2} \int_1^{1+R^2} e^{-\lambda_2 y z} \mathrm{d}z \\ &= 1 - R^{-2}\lambda_2^{-1} y^{-1} \left(e^{-\lambda_2 y} - e^{-\lambda_2(1+R^2)y}\right). \end{aligned} \tag{A.105}$$

When the total number of users in a NOMA group is M, according to (5.14), the channel gain of the relay-destination transmission for the m-th user (with m-th weakest channel gain) has the pdf shown in bellow.

$$f_{|h_{2,m}|^2}(y) = \frac{M!}{(M-m)!(m-1)!} \left[F_{|h_2|^2}(y)\right]^{m-1} \left[1 - F_{|h_2|^2}(y)\right]^{M-m} f_{|h_2|^2}(y). \tag{A.106}$$

For convenience of the subsequent derivation, (A.106) is rewritten as:

$$\begin{aligned} f_{|h_{2,m}|^2}(y) &= \frac{M!}{(M-m)!(m-1)!} \left(1 - \left(1 - F_{|h_2|^2}(y)\right)\right)^{m-1} \left(1 - F_{|h_2|^2}(y)\right)^{M-m} f_{|h_2|^2}(y) \\ &= \frac{M!}{(M-m)!(m-1)!} \sum_{i=0}^{m-1} \binom{m-1}{i} (-1)^i \left(1 - F_{|h_2|^2}(y)\right)^{M-m+i} f_{|h_2|^2}(y) \end{aligned} \tag{A.107}$$

By substituting (A.104) and (A.105) into (A.107), the analytical expression of pdf of $|h_{2,m}|^2$ is given by

$$\begin{aligned} f_{|h_{2,m}|^2}(y) = \frac{M!}{(M-m)!(m-1)!} &\sum_{i=0}^{m-1} \binom{m-1}{i} R^{-2-2M+2m-2i} \lambda_2^{-M+m-i} \sum_{j=0}^{M-m+i} (-1)^{i+j} \\ &\times y^{-M+m-i} e^{-\lambda_2(R^2 j + M - m + i)y} f_{|h_2|^2}(y) \\ = \frac{M!}{(M-m)!(m-1)!} &\sum_{i=0}^{m-1} \binom{m-1}{i} \frac{R^{-2-2M+2m-2i}}{\lambda_2^{M-m+i}} \sum_{j=0}^{M-m+i} (-1)^{i+j} \left(\frac{y^{-2-M+m-i}}{\lambda_2}\right. \\ &\times e^{-\lambda_2\left(R^2 j + M - m + i + 1\right)y} + y^{-1-M+m-i} e^{-\lambda_2\left(R^2 j + M - m + i + 1\right)y} - \lambda_2^{-1} y^{-2-M+m-i} \\ &\times e^{-\lambda_2\left(R^2 j + R^2 + M - m + i + 1\right)y} - \left(1 + R^2\right) y^{-1-M+m-i} e^{-\lambda_2\left(R^2 j + R^2 + M - m + i + 1\right)y} \Big) \end{aligned} \tag{A.108}$$

Combining (A.108) and (A.103) and by setting $z = y - \theta_m^*$, we can finally obtain (5.15). Although it is difficult to give the analytical expression of the integration, it is easy to get the numerical result through some software, such as Mathematica. It can be efficiently computed with the aid of GCQ as well.

A.9 Proof of Proposition 12

Similar to (A.8), the outage probability for the m-th user in the multi-antenna relaying NOMA system can be derived according to (5.40):

$$\begin{aligned} P_m^{out} &= 1 - \int_{\theta_m^*}^{\infty} f_{||\mathbf{h}_{2,m}||_F^2}(y) \int_{\frac{\theta_m^*(1+\bar{\gamma}y)}{\bar{\gamma}(y-\theta_m^*)}}^{\infty} f_{||\mathbf{h}_1||^2}(x)\mathrm{d}x\mathrm{d}y \\ &= 1 - \int_{\theta_m^*}^{\infty} f_{||\mathbf{h}_{2,m}||_F^2}(y) \left(1 - F_{||\mathbf{h}_1||^2}\left(\frac{\theta_m^*(1+\bar{\gamma}y)}{\bar{\gamma}(y-\theta_m^*)}\right)\right)\mathrm{d}y \\ &= F_{||h_{2,m}||_F^2}(\theta_m^*) + \int_{\theta_m^*}^{\infty} f_{||\mathbf{h}_{2,m}||_F^2}(y) F_{||\mathbf{h}_1||_F^2}\left(\frac{\theta_m^*(1+\bar{\gamma}y)}{\bar{\gamma}(y-\theta_m^*)}\right)\mathrm{d}y. \end{aligned} \tag{A.109}$$

Substituting (5.43) into (A.109), we can get:

$$\begin{aligned} P_m^{out} =& F_{||\mathbf{h}_{2,m}||_F^2}(\theta_m^*) + \int_{\theta_m^*}^{\infty} f_{||\mathbf{h}_{2,m}||_F^2}(y) \left(1 - e^{-\tilde{\lambda}_1 y} \sum_{s=0}^{N_1-1} \frac{\tilde{\lambda}_1^s y^s}{s!}\right)\mathrm{d}y \\ =& 1 - \int_{\theta_m^*}^{\infty} e^{-\tilde{\lambda}_1\left(\frac{\theta_m^*(1+\bar{\gamma}y)}{\bar{\gamma}(y-\theta_m^*)}\right)} \sum_{s=0}^{N_1-1} \frac{\tilde{\lambda}_1^s \left(\frac{\theta_m^*(1+\bar{\gamma}y)}{\bar{\gamma}(y-\theta_m^*)}\right)^s}{s!} f_{||\mathbf{h}_{2,m}||_F^2}(y)\mathrm{d}y \end{aligned} \tag{A.110}$$

The same as in the single-antenna relaying case, the expression of pdf for ordered user $f_{||\mathbf{h}_{2,m}||_F^2}(y)$ can be expressed as:

$$\begin{aligned} f_{||\mathbf{h}_{2,m}||_F^2}(y) &= \frac{M!}{(M-m)!(m-1)!} F_{||\mathbf{h}_2||_F^2}(y)^{m-1} \left(1 - F_{||\mathbf{h}_2||_F^2}(y)\right)^{M-m} f_{||\mathbf{h}_2||_F^2}(y) \\ &= \frac{M!}{(M-m)!(m-1)!} \sum_{k=0}^{M-m} \binom{M-m}{k} (-1)^k F_{||\mathbf{h}_2||_F^2}(y)^{m+k-1} f_{||\mathbf{h}_2||_F^2}(y). \end{aligned} \tag{A.111}$$

Pulling (5.47) and (5.48) into (A.111), we get:

$$f_{||\mathbf{h}_{2,m}||_F^2}(y) = \frac{M!}{(M-m)!(m-1)!}\sum_{k=0}^{M-m}\binom{M-m}{k}(-1)^k\frac{\pi}{nR\Gamma(N_1)}\left(\sum_{j=1}^{n}T_j\Delta_j(1+\Delta_j^{\alpha})^{N_1}\right.$$
$$\left.\times\lambda_2^{N_1}e^{-\lambda_2(1+\Delta_j^{\alpha})y}y^{N_1-1}\right)$$
$$\times\sum_{p=0}^{m+k-1}\underbrace{\binom{m+k-1}{p}\left(-\frac{\pi}{nR}\sum_{i=1}^{n}T_i\Delta_i e^{-\lambda_2(1+\Delta_i^{\alpha})y}\sum_{s_2=0}^{N_1-1}\frac{\lambda_2^{s_2}(1+\Delta_i^{\alpha})^{s_2}}{s_2!}\right)^p}_{\varpi}. \tag{A.112}$$

A tip is implemented here to express the results of $\left(\sum_{r=1}^{b}g_r\right)^c$, where c is a natural number. Since there are b^c elements for the expansion of $\left(\sum_{r=1}^{b}g_r\right)^c$, we employ a c-digit base-b system to exhibit the permutation of the decomposition. All elements are one-to-one mapped to the set of c-digit base-b numbers $[1,\cdots,b^c]$, and numbers on different digits reflect to the serial numbers of g_r, $r\in[1,\cdots,c]$. It is worthy mentioning that, this decomposition method does not unite similar terms, however it is convenient for the machine computation in terms of multi-loop programming. In addition, this expansion is available only for $c>0$. Therefore, we should discuss the $p=0$ case separately in (A.112).

$$\varpi^{p=0} = 1;$$
$$\varpi^{p\neq 0} = (-1)^p\binom{m+k-1}{p}\left(\frac{\pi}{nR_2}\right)^p\sum_{q=0}^{n^p-1}\left\{\prod_{d_1=1}^{p}\left[T_{D_{q,n,d_1}+1}\Delta_{D_{q,n,d_1}+1}\right.\right.$$
$$\left.\left.\times e^{(1+\Delta_{D_{q,n,d1}}^{\alpha})\lambda_2 y}\right]\sum_{u=0}^{N_1^p-1}\left\{\prod_{d_2=1}^{p}\left[\frac{(1+\Delta_{D_{q,n,d_2}+1}^{\alpha})^{D_{u,N_1,d_2}}\lambda_2^{D_{u,N_1,d_2}}y^{D_{u,N_1d_2}}}{D_{u,N_1,d_2}!}\right]\right\}\right\} \tag{A.113}$$

Equations in (A.113) are derived through a two-fold decomposition of the form $\left(\sum_{r=1}^{b}g_r\right)^c$, where $D_{a,b,c}$ denotes the c-th digit from left of a base-b number presenting the decimal value a.

Substituting (A.113) into (A.112), the pdf of m-th channel gain is given by

$$f_{||\mathbf{h}_{2,m}||_F^2}(y) = \frac{M!}{(M-m)!(m-1)!}\sum_{j=1}^{n}\sum_{k=0}^{M-m}\binom{M-m}{k}\lambda_2^{N_1}T_j\Delta_j(1+\Delta_j^{\alpha})^{N_1}\frac{1}{\Gamma(N_1)}\sum_{p=0}^{m+k-1}\{\varpi_1\} \tag{A.114}$$

where

$$\begin{aligned}\varpi_1^{p=0} =&(-1)^k\left(\frac{\pi}{nR}\right)e^{-\lambda_2(1+\Delta_j^{\alpha})y}y^{N_1-1}\\ \varpi_1^{p\neq 0} =& \sum_{p=0}^{m+k-1}(-1)^{p+k}\binom{m+k-1}{p}\left(\frac{\pi}{nR}\right)^{p+1}\sum_{q=0}^{n^p-1}\left\{\prod_{d_1=1}^{p}[T_{D_{q,n,d_1}+1}\Delta_{D_{q,n,d_1}+1}]\right.\\ &\times\sum_{u=0}^{N_1^p-1}\left\{\prod_{d_2=1}^{p}\left[\frac{(1+\Delta_{D_{q,n,d_2}^{\alpha}})^{D_{u,N_1,d_2}}\lambda_2^{D_{u,N_1,d_2}}}{D_{u,N_1,d_2}!}\right]\exp\left\{-(\lambda_2(1+\Delta_j^{\alpha})\right.\right.\\ &\left.\left.+\lambda_2\sum_{d_{11}=1}^{p}(1+\Delta_{D_{q,n,d_{11}}}^{\alpha}))y\right\}\times y^{N_1-1+\sum_{d_{22}=1}^{p}D_{u,N_1,d_{22}}}\right\}\right\}.\end{aligned} \tag{A.115}$$

Substituting (A.114) into (A.110), the outage probability can be written as

$$\begin{aligned}P_m^{out} =&1-\frac{M!}{(M-m)!(m-1)!}\sum_{s_1=0}^{N_1-1}\sum_{k=0}^{M-m}\binom{M-m}{k}\frac{\tilde{\lambda}_1^{s_1}}{s_1!\Gamma(N_1)}\sum_{j=1}^{n}\left\{T_j\Delta_j(1+\Delta_j^{\alpha})^{N_1}\lambda_2^{N_1}\right.\\ &\left.\times\sum_{p=0}^{m+k-1}\{\Xi\}\right\},\end{aligned} \tag{A.116}$$

where the expressions of $\Xi^{p=0}$ and $\Xi^{p\neq 0}$ are presented and calculated separately in the follow-

ing:

$$\Xi^{p\neq 0} = \sum_{p=0}^{m+k-1} (-1)^{p+k} \binom{m+k-1}{p} \left(\frac{\pi}{nR}\right)^{p+k} \sum_{q=0}^{n^p-1} \left\{ \prod_{d_2=1}^{p} [T_{D_{q,n,d_1}+1} \Delta_{D_{q,n,d_1}+1}] \right.$$
$$\times \sum_{u=0}^{N_1^p-1} \left\{ \prod_{d_2=1}^{p} \left[\frac{(1+\Delta_{D^{\alpha}_{q,n,d_2}})^{D_{u,N_1,d_2}} \lambda_2^{D_{u,N_1,d_2}}}{D_{u,N_1,d_2}!} \right] \int_{\theta_m^*}^{\infty} \exp\left\{ -(\lambda_2(1+\Delta_j^{\alpha}) \right.\right.$$
$$+\lambda_2 \sum_{d_{11}=1}^{p} (1+\Delta^{\alpha}_{D_{q,n,d_{11}}}) - \frac{\tilde{\lambda}_1 N_1 \theta_m^*(1+\bar{\gamma}y)}{\bar{\gamma}(y-\theta_m^*)}) y \left.\right\} \left(\frac{\theta_m^*(1+\bar{\gamma}y)}{\bar{\gamma}(y-\theta_m^*)} \right)^{s_1}$$
$$\left.\left. \times y^{N_1-1+\sum_{d_{22}=1}^{p} D_{u,N_1,d_{22}}} \mathrm{d}y \right\} \right\}. \tag{A.117}$$

By defining $z = y - \theta_m^*$, the expression (A.117) can be rewritten as

$$\Xi^{p\neq 0} = \sum_{p=0}^{m+k-1} (-1)^{p+k} \binom{m+k-1}{p} \left(\frac{\pi}{nR}\right)^{p+k} \sum_{q=0}^{n^p-1} \left\{ \prod_{d_2=1}^{p} [T_{D_{q,n,d_1}+1} \Delta_{D_{q,n,d_1}+1}] \right.$$
$$\times \sum_{u=0}^{N_1^p-1} \left\{ \prod_{d_2=1}^{p} \left[\frac{(1+\Delta^{\alpha}_{D_{q,n,d_2}})^{D_{u,N_1,d_2}} \lambda_2^{D_{u,N_1,d_2}}}{D_{u,N_1,d_2}!} \right] \sum_{t_1=0}^{s_1} \sum_{t_2=0}^{L_1} \binom{s_1}{t_1} \binom{L_1}{t_1} \theta_m^{*L_1-t_2+s_1-t_1} \right.$$
$$\times \left(\frac{\theta_m^*(1+\bar{\gamma}\theta_m^*)}{\bar{\gamma}} \right)^{t_1} \exp\left\{ -\tilde{\lambda}_1 \theta_m^* - (\lambda_2(1+\Delta_j^{\alpha}) + N_1 \lambda_2 \sum_{d_4=1}^{p} (1+\Delta^{\alpha}_{D_{q,n,d_4}})) \theta_m^* \right\}$$
$$\times \int_0^{\infty} \exp\left\{ -\left(\lambda_2(1+\Delta_j^{\alpha}) + \lambda_2 \sum_{d_{11}=1}^{p} (1+\Delta^{\alpha}_{D_{q,n,d_{11}}}) \right) z - \frac{\tilde{\lambda}_1 N_1 \theta_m^*(1+\bar{\gamma}z)/\bar{\gamma}}{z} \right\}$$
$$\left.\left. \times z^{t_2-t_1} \mathrm{d}z \right\} \right\}, \tag{A.118}$$

where $L_1 = N_1 - 1 + \sum_{d_3=1}^{p} D_{u,N_1,d_3}$. Completing the integral with the help of [80, Eq.3.471.9],

$$\int_0^{\infty} x^{v-1} e^{-\frac{\beta}{x} - \gamma x} \mathrm{d}x = 2 \left(\frac{\beta}{\gamma} \right)^{\frac{v}{2}} K_v \left(2\sqrt{\beta\gamma} \right) \tag{A.119}$$

the exact expression of $\Xi^{p\neq 0}$ is given by

$$\begin{aligned}\Xi^{p\neq 0} = 2(-1)^{p+k}\binom{m+k-1}{p}\left(\frac{\pi}{nR_2}\right)^{p+1}\sum_{q=0}^{n^p-1}\Bigg\{\prod_{d_1=1}^{p}\left[T_{D_{q,n,d_1}+1}\Delta_{D_{q,n,d_1}+1}\right] \\ \times\sum_{u=0}^{N_1^p-1}\Bigg\{\prod_{d_2=1}^{p}\left[(1+\Delta^{\alpha}_{D_{q,n,d_2}+1})^{D_{u,N_1,d_2}}\lambda_2^{D_{u,N_1,d_2}}/D_{u,N_1,d_2}!\right] \\ \times\sum_{t_1=0}^{s_1}\sum_{t_2=0}^{L_1}\binom{s_1}{t_1}\binom{L_1}{t_2}(\theta_m^*)^{s_1-\frac{t_1}{2}+L_1-\frac{t_2}{2}+\frac{1}{2}}\left(\frac{1+\bar{\gamma}\theta_m^*}{\bar{\gamma}}\right)^{\frac{t_1+t_2+1}{2}}\tilde{\lambda}_1^{\frac{t_2-t_1+1}{2}} \\ L_3^{\frac{t_2-t_1+1}{2}}e^{-\tilde{\lambda}_1\theta_m^*-L_3\theta_m^*}K_{t_2-t_1+1}\left(2\sqrt{\frac{\tilde{\lambda}_1 N_1\theta_m^*(1+\bar{\gamma}\theta_m^*)L_3}{\bar{\gamma}}}\right)\Bigg\}\Bigg\}, \end{aligned} \tag{A.120}$$

with $L_3 = \lambda_2(1+\Delta_j^{\alpha}) + \lambda_2\sum_{d_4=1}^{p}(1+\Delta^{\alpha}_{D_{q,n,d_4}})$. Through the same approach, the expression of $\Xi^{p\neq 0}$ is derived as follows:

$$\begin{aligned}\Xi^{p=0} &= \int_{\theta_m^*}^{\infty}\left(\frac{\theta_m^*(1+\bar{\gamma}y)}{\bar{\gamma}(y-\theta_m^*)}\right)^{s_1}y^{N_1-1}e^{-\tilde{\lambda}_1\frac{\theta_m^*(1+\bar{\gamma}y)}{\bar{\gamma}(y-\theta_m^*)}-\lambda_2(1+\Delta_j^{\alpha})\theta_m^*}\mathrm{d}y \\ &= \exp\{-\tilde{\lambda}_1\theta_m^*(1+\bar{\gamma}_m^*)-\lambda_2\theta_m^*(1+\Delta_j^{\alpha})\}(\theta_m^*)^{N_1-1-t_2+s-t_1}\left(\frac{1+\bar{\gamma}\theta_m^*}{\bar{\gamma}}\right)^{N_1-1-t_2} \\ &\quad\times\int_0^{\infty}\sum_{t_1=0}^{s_1}\sum_{t_2=0}^{N_1-1}\binom{s_1}{t_1}\binom{N_1}{t_2}z^{t_2-t_1}\exp\left\{-\frac{\tilde{\lambda}_1\theta_m^*(1+\bar{\gamma}\theta_m^*)/\bar{\gamma}}{z}-\lambda_2(1+\Delta_j^{\alpha})z\right\}\mathrm{d}z \\ &= \exp\{-\tilde{\lambda}_1\theta_m^*(1+\bar{\gamma}\theta_m^*)-\lambda_2(1+\Delta_j^{\alpha})\theta_m^*\}\sum_{t_1=0}^{s_1}\sum_{t_2=0}^{N_1-1}\binom{s_1}{t_1}\binom{N_1-1}{t_1} \\ &\quad\times(\theta_m^*)^{N_1+s_1-\frac{3t_1}{2}-\frac{t_2}{2}-\frac{1}{2}}\left(\frac{1+\bar{\gamma}\theta_m^*}{\bar{\gamma}}\right)^{N_1-\frac{t_1}{2}-\frac{t_2}{2}-\frac{1}{2}}\left(\frac{\tilde{\lambda}_1}{\lambda_2(1+\Delta_j^{\alpha})}\right)^{\frac{t_2-t_1+1}{2}} \\ &\quad\times K_{t_2-t_1+1}\left(\sqrt{\frac{\tilde{\lambda}_1\lambda_2 N_1\theta_m^*(1+\bar{\gamma}\theta_m^*)(1+\Delta_j^{\alpha})}{\bar{\gamma}}}\right). \end{aligned} \tag{A.121}$$

Finally, (5.49) is obtained by joining (A.116), (A.120) and (A.121) together.

Appendix B
Publications

B.1 Conference

1. Jiang Xue, **Yunhan Zhang**, et al. "Error exponents analysis for dual-hop η-μ fading channel with amplify-and-forward relaying." *IEEE. Wireless Communications and Networking Conference (WCNC)*, 2014.

B.2 Journal

1. **Yunhan Zhang**, et al. "Error exponents analysis of dual-hop η-μ and κ-μ fading channel with amplify-and-forward relaying." *IET Communications* vol. 9, iss. 11, pp. 1367-1379, Jul. 2015.

2. **Yunhan Zhang**, et al. "Capacity Analysis for Multi-Antenna Dual-Hop AF System with Random Co-channel Interference Using Different Transferring Schemes" *IET Communications* vol. 11, Mar. 2017.

References

[1] C. Hoymann, W. Chen, J. Montojo, A. Golitschek, C. Koutsimanis, and X. Shen, "Relaying operation in 3gpp lte: challenges and solutions," *IEEE Communications Magazine*, vol. 50, no. 2, pp. 156–162, 2012.

[2] K. Loa, C.-C. Wu, S.-T. Sheu, Y. Yuan, M. Chion, D. Huo, and L. Xu, "Imt-advanced relay standards [wimax/lte update]," *IEEE Communications Magazine*, vol. 48, no. 8, pp. 40–48, 2010.

[3] Y. Yang, H. Hu, J. Xu, and G. Mao, "Relay technologies for wimax and lte-advanced mobile systems," *IEEE Communications Magazine*, vol. 47, no. 10, pp. 100–105, 2009.

[4] F. Baccelli, M. Klein, M. Lebourges, and S. Zuyev, "Stochastic geometry and architecture of communication networks," *Telecommunication Systems*, vol. 7, no. 1-3, pp. 209–227, 1997.

[5] Y. Saito, Y. Kishiyama, A. Benjebbour, T. Nakamura, A. Li, and K. Higuchi, "Non-orthogonal multiple access (noma) for cellular future radio access," pp. 1–5, 2013.

[6] M. Yacoub, "The $\eta - \mu$ distribution and the $\kappa - \mu$ distribution," *Antennas and Propagation Magazine, IEEE*, vol. 49, pp. 68–81, Feb 2007.

[7] C. E. Shannon, "A mathematical theory of communication," *Mobile Computing and Communications Review*, vol. 5, no. 1, pp. 3–55, 2001.

[8] T. M. Cover and J. A. Thomas, *Elements of information theory*. John Wiley & Sons, 2012.

[9] R. G. Gallager, *Information Theory and Reliable Communication*. New York: Wiley, 1968.

[10] H. Shin and M. Win, "Gallager's exponent for MIMO channels: a reliability-rate tradeoff," *IEEE Trans. on Communications*, vol. 57, no. 4, pp. 972–985, April, 2009.

[11] W. K. M. Ahmed and P. J. McLane, "Random coding error exponents for two-dimensional flat fading channels with complete channel state information," *IEEE Trans. Inform. Theory*, vol. 45, pp. 1338–1346, May 1999.

[12] A. Hero and T. Marzetta, "Cutoff rate and signal design for the quasi-static Rayleigh-fading space-time channel," *IEEE Trans. Information Theory*, vol. 47, no. 6, pp. 2400–2416, Sep. 2001.

[13] J. Xue, M. Sarkar, T. Ratnarajah, and C. Zhong, "Error exponents for Rayleigh fading product MIMO channels," in *Proc. IEEE Int. Symp. on Information Theory (ISIT), Cambridge, MA*, pp. 2166–2170, July, 2012.

[14] E. C. Van Der Meulen, "Three-terminal communication channels," *Advances in applied Probability*, pp. 120–154, 1971.

[15] M. Haenggi, J. G. Andrews, F. Baccelli, O. Dousse, and M. Franceschetti, "Stochastic geometry and random graphs for the analysis and design of wireless networks," *IEEE Journal on Selected Areas in Communications*, vol. 27, no. 7, pp. 1029–1046, 2009.

[16] S. R. Islam, N. Avazov, O. A. Dobre, and K.-S. Kwak, "Power-domain non-orthogonal multiple access (noma) in 5g systems: Potentials and challenges," *IEEE Communications Surveys & Tutorials*, 2016.

[17] I. S. Gradshteyn and I. M. Ryzhik, *Table of integrals, series, and products*. New York: Academic Press, 7th ed., 2000.

[18] wolfram inc, "Wolfram function site: http://functions.wolfram.com/HypergeometricFunctions/MeijerG/," *Wolfram function*.

[19] U. Kamps, *Generalized order statistics*. Wiley Online Library, 1981.

[20] V. Merlen, "Three-terminal communication channels," *Adv. appl. Prob.*, vol. 3, pp. 120–154, 1971.

[21] T. M. Cover and A. E. Gamal, "Capacity theorems for the relay channels," *IEEE Trans. Inform. Theory*, vol. 25, no. 5, pp. 572–584, 1979.

[22] M. O. Hasna and M. S. Alouini, "End-to-end performance of transmission systems with relays over Rayleigh-fading channels," *IEEE Trans. on Wireless Communications*, vol. 2, pp. 1126–1131, Nov 2003.

[23] M. O. Hasna and M. S. Alouini, "Harmonic mean and end-to-end performance of transmission systems with relays," *IEEE Transactions on Communications*, vol. 52, pp. 130–135, Jan 2004.

[24] M. O. Hasna and M. S. Alouini, "A performance study of dual-hop transmissions with fixed gain relays," *IEEE Trans. on Wireless Communications*, vol. 3, no. 6, pp. 1963–1968, 2004.

[25] M. Hasna and M. S. Alouini, "End-to-end performance of transmission systems with relays over rayleigh-fading channels," *IEEE Transactions on Wireless Communications*, vol. 2, pp. 1126–1131, Nov 2003.

[26] G. Farhadi and N. C. Beaulieu, "On the ergodic capacity of wireless relaying systems over rayleigh fading channels," *IEEE Transactions on Wireless Communications*, vol. 7, pp. 4462–4467, November 2008.

[27] M. Torabi, D. Haccoun, and J.-F. Frigon, "On the performance of AF opportunistic relaying with adaptive transmission over Rayleigh fading channels," in *IEEE Pacific Rim Conference on Communications, Computers and Signal Processing (PacRim), Victoria, BC*, pp. 173–178, Aug. 2011.

[28] I. Trigui, S. Affes, and A. Stephenne, "Exact error analysis of dual-hop fixed-gain af relaying over arbitrary Nakagami-m fading," in *Proc. IEEE Vehicular Technology Conference (VTC Fall), Quebec City, QC*, pp. 1–5, 2012.

[29] G. Zhu, C. Zhong, H. Suraweera, Z. Zhang, C. Yuen, and R. Yin, "Ergodic capacity comparison of different relay precoding schemes in dual-hop af systems with co-channel interference," *Communications, IEEE Transactions on*, vol. 62, pp. 2314–2328, July 2014.

[30] K. Peppas, F. Lazarakis, A. Alexandridis, and K. Dangakis, "Cascaded generalised-K fading channel," *IET Commun.*, vol. 4, pp. 116–124, Jan 2010.

[31] K. Peppas, F. Lazarakis, A. Alexandridis, and K. Dangakis, "Moments-based analysis of dual-hop amplify-and-forward relaying communications systems over generalised fading channels," *IET Communications*, vol. 6, no. 13, pp. 2040–2047, Nov. 2012.

[32] K. Peppas, G. Alexandropoulos, and P. Mathiopoulos, "Performance analysis of dual-hop af relaying systems over mixed η-μ and κ-μ fading channels," *Vehicular Technology, IEEE Transactions on*, vol. 62, pp. 3149–3163, Sept 2013.

[33] E. Malkamaki and H. Leib, "Coded diversity on block-fading channels," *IEEE Trans. Information Theory*, vol. 45, no. 2, pp. 771–781, Mar. 1999.

[34] W. Ahmed and P. J. Mclane, "On the error exponent for memoryless flat fading channels with channel-state-information feedback," *IEEE Commun. Lett.*, vol. 3, no. 2, pp. 49–51, Feb. 1999.

[35] J. Xue, M. Sarkar, C. Zhong, and T. Ratnarajah, "Error exponents for orthogonal STBC in generalized-K fading MIMO channels," in *Proc. IEEE Wireless Communications and Networking Conference (WCNC), Shanghai, China*, pp. 1925–1929, April, 2012.

[36] J. Zhang, M. Matthaiou, G. Karagiannidis, H. Wang, and Z. Tan, "Gallager's exponent analysis of STBC MIMO systems over η-μ and κ-μ fading channels," *IEEE Transactions on Communications*, vol. 61, pp. 1028–1039, Mar 2013.

[37] J. Xue, M. Sarkar, and T. Ratnarajah, "Error exponents for Nakagami-m fading channels," *Problems of Information Transmission*, vol. 50, no. 2, pp. 144–170, Apr. 2014.

[38] J. Xue, T. Ratnarajah, C. Zhong, and C. Wen, "Reliability analysis for large MIMO systems," in *IEEE Wireless Communications Letters*, Sep. 2014.

[39] B. Barua, M. Abolhasan, F. Safaei, and D. Franklin, "On the error exponent of amplify and forward relay networks," *IEEE Commun. Lett.*, vol. 15, no. 10, pp. 1047–1049, Aug. 2011.

[40] H. Q. Ngo, T. Q. Quek, and H. Shin, "Random coding error exponent for dual-hop Nakagami-m fading channels with amplify-and-forward relaying," *IEEE Commun. Lett.*, vol. 13, pp. 823–825, Nov 2009.

[41] A. P. Prudnikow, Y. A. Brychkov, and O. I. Marchev, *Integrals and Series*. Gordon and Breach Science Publishers, 1990.

[42] H. Q. Ngo, T. Quek, and H. Shin, "Random coding error exponent for dual-hop Nakagami-m fading channels with amplify-and-forward relaying," *IEEE Commun. Letts.*, pp. 823–825, Nov 2009.

[43] C. Zhong, S. Jin, and K. K. Wong, "Dual-hop systems with noisy relay and interference-limited destination," *IEEE Transactions on Communications*, vol. 58, pp. 764–768, March 2010.

[44] D. Lee and J. H. Lee, "Outage probability for dual-hop relaying systems with multiple interferers over rayleigh fading channels," *IEEE Transactions on Vehicular Technology*, vol. 60, pp. 333–338, Jan 2011.

[45] F. S. Al-Qahtani, T. Q. Duong, C. Zhong, K. A. Qaraqe, and H. Alnuweiri, "Performance analysis of dual-hop af systems with interference in nakagami- m fading channels," *IEEE Signal Processing Letters*, vol. 18, pp. 454–457, Aug 2011.

[46] F. S. Al-Qahtani, J. Yang, R. M. Radaydeh, C. Zhong, and H. Alnuweiri, "Exact outage analysis of dual-hop fixed-gain af relaying with cci under dissimilar nakagami-m fading," *IEEE Communications Letters*, vol. 16, pp. 1756–1759, November 2012.

[47] H. A. Suraweera, D. S. Michalopoulos, and C. Yuen, "Performance analysis of fixed gain relay systems with a single interferer in nakagami- m fading channels," *IEEE Transactions on Vehicular Technology*, vol. 61, pp. 1457–1463, March 2012.

[48] S. S. Ikki and S. Aissa, "Multihop wireless relaying systems in the presence of cochannel interferences: Performance analysis and design optimization," *IEEE Transactions on Vehicular Technology*, vol. 61, pp. 566–573, Feb 2012.

[49] T. Soithong, V. A. Aalo, G. P. Efthymoglou, and C. Chayawan, "Outage analysis of multihop relay systems in interference-limited nakagami- m fading channels," *IEEE Transactions on Vehicular Technology*, vol. 61, pp. 1451–1457, March 2012.

[50] K. T. Hemachandra and N. C. Beaulieu, "Outage analysis of opportunistic scheduling in dual-hop multiuser relay networks in the presence of interference," *IEEE Transactions on Communications*, vol. 61, pp. 1786–1796, May 2013.

[51] Y. Huang, F. Al-Qahtani, C. Zhong, Q. Wu, J. Wang, and H. Alnuweiri, "Performance analysis of multiuser multiple antenna relaying networks with co-channel interference and feedback delay," *IEEE Transactions on Communications*, vol. 62, pp. 59–73, January 2014.

[52] C. Zhong, H. A. Suraweera, A. Huang, Z. Zhang, and C. Yuen, "Outage probability of dual-hop multiple antenna af relaying systems with interference," *IEEE Transactions on Communications*, vol. 61, pp. 108–119, January 2013.

[53] J. G. Andrews, H. Claussen, M. Dohler, S. Rangan, and M. C. Reed, "Femtocells: Past, present, and future," *IEEE Journal on Selected Areas in Communications*, vol. 30, pp. 497–508, April 2012.

[54] A. Rabbachin, T. Q. S. Quek, H. Shin, and M. Z. Win, "Cognitive network interference," *IEEE Journal on Selected Areas in Communications*, vol. 29, pp. 480–493, February 2011.

[55] M. Haenggi, *Stochastic geometry for wireless networks*. Cambridge University Press, 2012.

[56] F. A. Khan, H. He, J. Xue, and T. Ratnarajah, "Performance analysis of cloud radio access networks with distributed multiple antenna remote radio heads," *IEEE Transactions on Signal Processing*, vol. 63, pp. 4784–4799, Sept 2015.

[57] H. He, J. Xue, T. Ratnarajah, F. A. Khan, and C. B. Papadias, "Modeling and analysis of cloud radio access networks using matérn hard-core point processes," *IEEE Transactions on Wireless Communications*, vol. 15, no. 6, pp. 4074–4087, 2016.

[58] K. Huang, J. G. Andrews, D. Guo, R. W. Heath, and R. A. Berry, "Spatial interference cancellation for multiantenna mobile ad hoc networks," *IEEE Transactions on Information Theory*, vol. 58, pp. 1660–1676, March 2012.

[59] W. Guo and T. O'Farrell, "Relay deployment in cellular networks: Planning and optimization," *IEEE Journal on Selected Areas in Communications*, vol. 31, pp. 1597–1606, August 2013.

[60] H. Gao, P. J. Smith, and M. V. Clark, "Theoretical reliability of mmse linear diversity combining in rayleigh-fading additive interference channels," *IEEE Transactions on Communications*, vol. 46, pp. 666–672, May 1998.

[61] D. Katselis, "On estimating the number of co-channel interferers in mimo cellular systems," *IEEE Signal Processing Letters*, vol. 18, pp. 379–382, June 2011.

[62] R. Narasimhan and S. Cheng, "Channel estimation and co-channel interference rejection for lte-advanced mimo uplink," in *Wireless Communications and Networking Conference (WCNC), 2012 IEEE*, pp. 416–420, April 2012.

[63] A. Benjebbour, Y. Saito, Y. Kishiyama, A. Li, A. Harada, and T. Nakamura, "Concept and practical considerations of non-orthogonal multiple access (noma) for future radio access," in *Intelligent Signal Processing and Communications Systems (ISPACS), 2013 International Symposium on*, pp. 770–774, IEEE, 2013.

[64] L. Dai, B. Wang, Y. Yuan, S. Han, I. Chih-Lin, and Z. Wang, "Non-orthogonal multiple access for 5g: solutions, challenges, opportunities, and future research trends," *IEEE Communications Magazine*, vol. 53, no. 9, pp. 74–81, 2015.

[65] J. So and Y. Sung, "Improving non-orthogonal multiple access by forming relaying broadcast channels," *IEEE Communications Letters*, vol. 20, no. 9, pp. 1816–1819, 2016.

[66] X. Liu and X. Wang, "Outage probability and capacity analysis of the collaborative noma assisted relaying system in 5g," in *Communications in China (ICCC), 2016 IEEE/CIC International Conference on*, pp. 1–5, IEEE, 2016.

[67] J. Men, J. Ge, and C. Zhang, "Performance analysis of non-orthogonal multiple access for relaying networks over nakagami-m fading channels," *IEEE Transactions on Vehicular Technology*, 2016.

[68] W. Han, J. Ge, and J. Men, "Performance analysis for noma energy harvesting relaying networks with transmit antenna selection and maximal-ratio combining over nakagami-m fading," *IET Communications*, vol. 10, no. 18, pp. 2687–2693, 2016.

[69] C. Zhong and Z. Zhang, "Non-orthogonal multiple access with cooperative full-duplex relaying," *IEEE Communications Letters*, vol. 20, no. 12, pp. 2478–2481, 2016.

[70] J.-B. Kim and I.-H. Lee, "Capacity analysis of cooperative relaying systems using non-orthogonal multiple access," *IEEE Communications Letters*, vol. 19, no. 11, pp. 1949–1952, 2015.

[71] J.-B. Kim, M. S. Song, and I.-H. Lee, "Achievable rate of best relay selection for non-orthogonal multiple access-based cooperative relaying systems," in *Information and Communication Technology Convergence (ICTC), 2016 International Conference on*, pp. 960–962, IEEE, 2016.

[72] J. Men, J. Ge, and C. Zhang, "Performance analysis for downlink relaying aided non-orthogonal multiple access networks with imperfect csi over nakagami-m fading," *IEEE Access*, 2016.

[73] Y. Liu, G. Pan, H. Zhang, and M. Song, "Hybrid decode-forward & amplify-forward relaying with non-orthogonal multiple access," *IEEE Access*, vol. 4, pp. 4912–4921, 2016.

[74] Z. Ding, Z. Yang, P. Fan, and H. V. Poor, "On the performance of non-orthogonal multiple access in 5g systems with randomly deployed users," *IEEE Signal Processing Letters*, vol. 21, no. 12, pp. 1501–1505, 2014.

[75] A. Almradi and K. A. Hamdi, "Mimo full-duplex relaying in the presence of co-channel interference," *IEEE Transactions on Vehicular Technology*, vol. 66, pp. 4874–4885, June 2017.

[76] M. O. Hasna and M. . Alouini, "End-to-end performance of transmission systems with relays over rayleigh-fading channels," *IEEE Transactions on Wireless Communications*, vol. 2, pp. 1126–1131, Nov 2003.

[77] P. A. Anghel and M. Kaveh, "Exact symbol error probability of a cooperative network in a rayleigh-fading environment," *IEEE Transactions on Wireless Communications*, vol. 3, pp. 1416–1421, Sept 2004.

[78] S. S. Ikki and S. Aissa, "Performance analysis of two-way amplify-and-forward relaying in the presence of co-channel interferences," *IEEE Transactions on Communications*, vol. 60, pp. 933–939, April 2012.

[79] M. A. I. A. Stegun, *Handbook of Mathematical Functions with Formulas Graphs and Mathematical Tables*. New York : Dover Publications, 1972.

[80] I.S.Gradshteyn and I.M.Ryzhik, *Table of Integrals Series, and Products*. Academic Press, it is an imprint of Elsevier, 2007.

[81] S. P. A. Papoulis, *Probability, random variables, and stochastic processes*. Boston;London: McGraw-Hill, 2002.

[82] M. Abramowitz and I. A. Stegun, *Handbook of Mathematical Functions With Formulas, Graphs, and Mathematical tables*. New York: Dover, 1970.

[83] H. A. Suraweera, P. J. Smith, and M. Shafi, "Capacity limits and performance analysis of cognitive radio with imperfect channel knowledge," *IEEE Transactions on Vehicular Technology*, vol. 59, pp. 1811–1822, May 2010.

[84] Y. M. Shobowale and K. A. Hamdi, "A unified model for interference analysis in unlicensed frequency bands," *IEEE Transactions on Wireless Communications*, vol. 8, no. 8, pp. 4004–4013, 2009.

[85] F. Yilmaz and M. Alouini, "An mgf-based capacity analysis of equal gain combining over fading channels," in *21st Annual IEEE International Symposium on Personal, Indoor and Mobile Radio Communications*, pp. 945–950, Sept 2010.

[86] K. A. Hamdi, "Capacity of mrc on correlated rician fading channels," *IEEE Transactions on Communications*, vol. 56, pp. 708–711, May 2008.

[87] K. Hamdi, "A useful technique for interference analysis in nakagami fading," *IEEE Transactions on Communications*, vol. 55, pp. 1120–1124, June 2007.

[88] Z. Ding, K. K. Leung, D. L. Goeckel, and D. Towsley, "On the application of cooperative transmission to secrecy communications," *IEEE Journal on Selected Areas in Communications*, vol. 30, pp. 359–368, February 2012.

[89] M. Haenggi, "On distances in uniformly random networks," *IEEE Transactions on Information Theory*, vol. 51, pp. 3584–3586, Oct 2005.

[90] M. A. M. and R. K. Saxena, *The H-function with Applications in Statistics and Other Disciplines*. New Delhi, 1978.

[91] H. Gao, P. J. Smith, and M. V. Clark, "Theoretical reliability of MMSE linear diversity combining in Rayleigh fading additive interference channels," *IEEE Trans. on Wireless Communications*, vol. 46, pp. 666–672, May 1998.

[92] O. B. S. Ali, C. Cardinal, and F. Gagnon, "Performance of optimum combining in a poisson field of interferers and rayleigh fading channels," *IEEE Transactions on Wireless Communications*, vol. 9, pp. 2461–2467, August 2010.